Simulation of Interconnections in High-Speed Integrated Circuits

Bruce Howard Parker

A thesis submitted in partial fulfilment of the requirements of Sheffield Hallam University for the degree of Doctor of Philosophy

October 1994

Acknowledgements

Firstly I would like to acknowledge the support given to me by the Engineering and Physical Sciences Research Council (EPSRC), and the School of Engineering Information Technology, for providing the necessary equipment to make this work possible.

Many thanks are due to my director of studies, Prof. A. K. Ray, for giving me complete freedom whilst undertaking the research documented in this thesis. Much credit is also due to my second supervisors, Prof. C. A. Hogarth, Dr. C. Johnston and Dr. Z. Ghassemlooy, for many fruitful discussions.

I would also like to take the opportunity to thank all my fellow researchers in the Electronics Research Group for all their help and support. Special thanks is also due to Barbara Siek for all her support and encouragement and for providing answers to many difficult questions. Last but not least I thank my parents for all their help and encouragement.

Abstract

The rapid development of high-speed, high-density integrated circuits has brought about a situation where the delay times and distortion of signals transmitted on the interconnections (microstrip lines) within these packages are now comparable with those of the devices in the circuit. Hence when designing high-speed digital systems the effect of signal delay, distortion, and attenuation, on these interconnections has now become a necessary part of integrated circuit design. Therefore accurate modelling and simulation of interconnects is a very important subject for research.

These interconnections can create a number of problems such as signal delay, distortion, attenuation, and crosstalk between lines of close proximity. These microstrip lines have the same behaviour as exhibited by transmission lines and can therefore be described using the well-known Telegrapher's equations.

A quasi-distributed equivalent circuit model describing the behaviour of such microstrip lines is implemented into the SPICE circuit simulator. This allows an investigation into lossless and lossy line characteristics and illustrates the importance of choosing the correct impedances for both the lines and devices within the integrated circuit package. The model is then extended to include crosstalk between neighbouring lines, by means of a transformation network. This study of crosstalk illustrates that logic functions lying in an intervening space between the pulse-activated lines are found to be affected more than the outside lines.

The MATHEMATICA package is used for the calculation of capacitance, inductance, impedance, time delay and transformation network control parameters for any set of microstrip lines of a given geometry. The results obtained from these calculations are then used for further simulation runs using the SPICE software for different line configurations.

The results obtained are seen to be consistent with all previous work conducted on coupled three line structures, and give good verification of both the Mathematica program and the SPICE equivalent circuit model.

Declaration

I hereby declare that whilst registered as a candidate for the degree of Doctor of Philosophy with Sheffield Hallam University, I have not been a registered candidate or enrolled student for any other award of the University, CNAA or other academic or professional organisation.

Table of Contents

1.0 : Introduction

The rapid development of high-speed, high-density integrated circuits has brought about a situation where the delay times and distortion of signals transmitted on the interconnections (microstrip lines) within these packages are now comparable with those of the devices in the circuit. Hence when designing high-speed digital systems the effect of signal delay, distortion, and attenuation, on these interconnections have now become a necessary part of integrated circuit design. Therefore accurate modelling and simulation of interconnects is a very important subject for research.

For the development of high-velocity logic circuits with a large scale integration, it is necessary to characterise the effects of interconnections, in the time domain, for signals having a rise time of about 10ps. These interconnections are microstrip conducting lines because they are compatible with a planar technology and the VLSI. The distortion of the signals are essentially due to losses (in the conductors and the substrate), to impedance discontinuities (at the line endings, at the changes of section or level, when the lines are crossing), and to coupling effects between the different lines.

To allow a comparison of results and verification of the method used, with those from previously published work, an example of an eight line bus has been chosen (Chilo and Arnaud 1984), which is depicted in figure 1.1. The eigenmodes (characteristic impedance and time delay) for each of the eight lines are given in table 1.1. This particular example was chosen because it can be used to evaluate the development of the coupled line equivalent circuit model, and for the investigation of the effects of rise time, upon coupled line configurations.

The thesis is organised into seven chapters, the contents of which are detailed briefly in the rest of this chapter. Chapter 2 contains a literature review giving the current state of research in the field of computer modelling and characterisation, of microstrip transmission lines. The review discusses single and coupled lines, and the methods by

which the electrical parameters (impedance and propagation velocity) can be calculated, and how different loss mechanisms (dielectric loss and skin effect) may be employed into the method. Different types of time domain and frequency domain modelling techniques (circuit simulators and numerical methods) are reviewed.

All the relevant background mathematics necessary for the calculation of impedance and time delay for a single line and a pair of coupled microstrip lines, are discussed in chapter 3. A generalised method for the calculation of the impedance and time delay for n coupled parallel microstrips is also developed.

A detailed study of ideal transmission lines is given in chapter 4, discussing how the time delay and impedance of the lines are related to the capacitance and inductance of the transmission line. Reflection diagrams are used to explain by the use of appropriate examples, the behaviour of various types of discontinuities which may be encountered in the design of microstrips within a high-speed IC.

Chapter 5 illustrates the development of a SPICE equivalent circuit model for the simulation of a lossless transmission line and its further development into a lossy line model. The coupling between a set of parallel microstrips is then considered. An appropriate transformation network is used in the development of an equivalent circuit model for the simulation of coupling between any set of n transmission lines. An investigation into crosstalk and the effect of rise time upon the coupling between lines, using the example given above, is also presented. The lossy equivalent circuit model is then modified for the study of the skin effect.

The results obtained from the program developed using Mathematica, from the equations outlined in chapter 3, for calculating the impedance and time delays for single and coupled lines are presented in chapter 6. The whole emphasis of the chapter concentrates on the results obtained using the program, rather than any details of the workings of Mathematica or the development of the program. An example of a three line bus

(Belahrach 1990) is used for the evaluation of these calculations. The results obtained are then used for SPICE simulations to in order to validate the generalised method for n coupled transmission lines.

The conclusions reached from the work undertaken in this thesis are detailed in chapter 7. Areas for possible further work, that could be undertaken in the future, are also outlined.

Line Number	Impedance (Ω)	Time Delay (ps/mm)
1	62	8.53
2	63	8.53
3	109	8.53
4	116	8.53
5	159	8.53
6	160	8.53
7	316	8.53
8	715	8.53

Table 1.1 : Eigenmode characteristics for the eight line bus example.

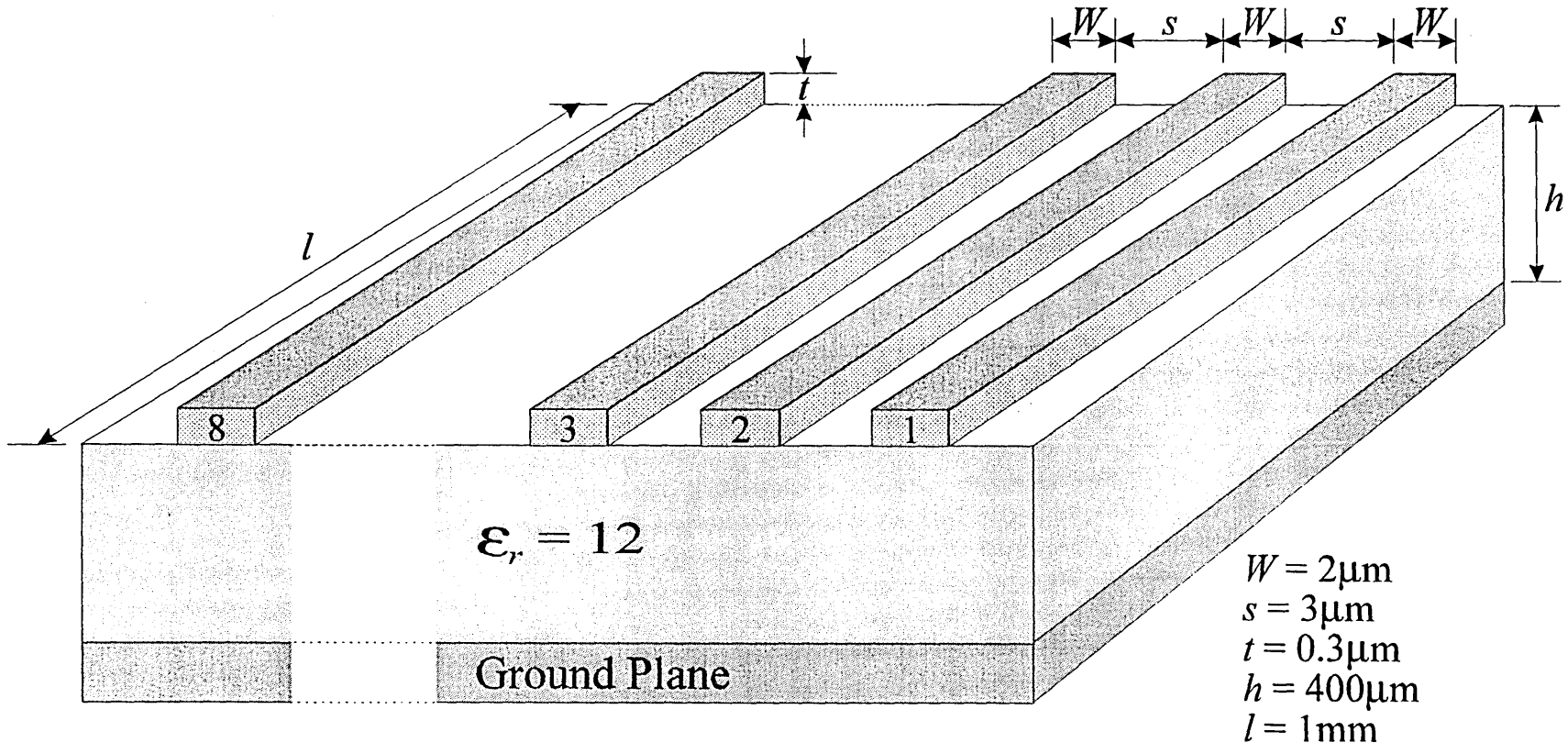

Figure 1.1 : Eight line bus configuration.

2.0 : Introduction

During the seventies an important shift took place in the design of hardware with the advent of smaller and denser integrated circuits and packages. Previously, the hardware components consisted of both physically and electrically large discrete components. Stray elements and coupling among the components were small in most cases and the interconnections between the components were electrically insignificant. The corresponding electrical network models were therefore highly decoupled with sparse network analysis matrices. This led to simple analysis models and techniques for the electrical performance of these systems.

Modern technology has however shown an increasing trend towards faster circuits, shorter rise times, and smaller pulse widths (Schutt-Aine and Mittra 1989, Deutsch *et al* 1990). At the same time, the physical dimensions of modern integrated circuits and packages are becoming ever increasingly smaller (Ruehli 1979, Deutsch *et al* 1990). This technology has resulted in very high speeds such that the behaviour of the interconnections can no longer be neglected. These integrated circuits now have delay times that are comparable with the delays of the interconnections used in packaging these circuits. This means that the transmission line properties of these interconnects need to be taken into account.

Furthermore, due to the resistive nature of the interconnections used in some of these devices, the transmitted signal pulses can exhibit attenuation and distortion of considerable magnitude (Groudis 1979, Liao *et al* 1990). Hence when designing high speed digital systems, both the components and their interconnections must be considered or the system performance may be impaired. This has led to accurate modelling and simulation of propagation delays and signal distortion apparent on interconnection lines becoming increasingly more important in the design of high speed integrated circuits.

The advances being made in circuit density and speed, both at the chip and package level, are placing increasing demands on the performance of interconnection technologies. Designers are reducing the wiring cross-sections and trying to pack the lines closer together, whilst at the same time the propagated signals are being switched with faster rise times. The proximity of the lines to each other may result in a significant amount of cross coupling (Palusinski and Lee 1989, Van Deventer *et al* 1994) between the different lines, for which accurate modelling and simulation are also necessary.

The losses and coupling among a group of physically close transmission lines are important factors, especially when high density IC interconnects are considered. The combination of these two parameters gives rise to four basic models (Chowdhury *et al* 1992) for simulating transmission lines:

1. uncoupled lossless.
2. coupled lossless.
3. uncoupled lossy.
4. coupled lossy.

These models offer various degrees of complexity in terms of interfacing transmission lines with non-linear active devices and computing the transient response of the IC circuit as a whole. Frequency dependent transmission line behaviour, such as skin effect (Wheeler 1942) adds to the complexities already encountered in the basic models.

Considering the losses apparent on a transmission line poses many problems (Pucel *et al* 1968, Schneider 1969, Deutsch *et al* 1990). The inclusion of loss renders some transmission line parameters, such as the characteristic impedance, to become dependent upon the signal frequency (Krage and Haddad 1972). Thus analysing the transmission lines in the frequency domain would seem to be the appropriate method. The transient response of integrated circuits is however usually easier to obtain in the time domain, than it is in the frequency domain (Griffith and Nakhla 1990).

A general description of the electrical properties of an interconnection line (assuming transmission line characteristics), requires four parameters (Yaun *et al*, 1982):

1. line capacitance.
2. line inductance.
3. series resistance.
4. shunt conductance.

In integrated circuits, where only high quality insulators are used, the component of shunt conductance can generally be neglected without losing generality (Deutsch *et al* 1990). The series resistance can however be of significant importance as it is determined by the material from which the interconnection is manufactured. Hence, only the capacitance and the inductance reflect the properties of the substrate on which the interconnects have been fabricated.

For guidance in the design of integrated circuit components, data are required on the parameters of coupled pairs of microstrip transmission lines. The parameters needed to characterise such a structure are the characteristic impedance and propagation velocity of the two normal propagation modes; transverse electric and transverse magnetic (Djordjevic *et al* 1987). It is also necessary to know how the characteristic impedance, phase velocity and attenuation of the dominant microstrip mode depends on geometrical factors, electrical properties of the substrate and conductors, and on the frequency.

2.1 : Microstrip Transmission Lines

The term "microstrip" is a nickname for a microwave circuit configuration that is constructed by printed circuit techniques, modified where necessary to reduce loss, reflections, and spurious coupling, but retaining advantages in size, simplicity, and reliability (Schneider 1969). The microstrip however shares some of the troublesome

properties of dispersive waveguides, in that conductor dimensions influence not only characteristic impedance, but also the velocity of propagation (Pucel *et al* 1968, Gupta *et al* 1979).

Microstrip transmission lines, consisting of a conductive ribbon attached to a dielectric sheet with conductive backing, are widely used in both microwave and computer technology. During the 1960's the design of equipment employing microstrip lines was, however, hampered by the lack of ability to predict the electrical transmission properties of such lines, especially their characteristic impedance and wave propagation velocity. Therefore it became essential to consider the geometry of the microstrip lines in order that the electrical properties can be modelled as accurately as possible.

Given a single line or set of coupled lines, (e.g., a set of microstrips on a printed circuit board or in an integrated device) capacitance and inductance matrices can be numerically computed once the geometries of the lines and the dielectric constant of the inhomogeneous coupling material are given and the transverse electromagnetic (TEM) mode of signal propagation is assumed. Algorithms to compute these parameters, and those concerning the impedance and propagation delay, are well known with many articles having been published on the subject (Gupta *et al* 1979, Silvester 1968).

A microstrip line is a parallel, two-conductor line that is made of at least one flat strip of small thickness. For mechanical stability the strip is deposited on a dielectric substrate which is usually supported by a metal ground plane (Long and Butner 1990). The basic configuration is shown in Figure 2.1.

The dielectric parameters of a microstrip required for circuit design are impedance, attenuation, unloaded Q (quality factor) (Schneider 1969, Gupta *et al* 1979), wavelength, and propagation constant. These parameters are interrelated when the following assumptions apply:

(1) The propagating mode is a transverse electromagnetic (TEM) mode, or it can be approximated by a TEM mode.

(2) Conductor losses in the metal strips are predominant, which means dielectric losses can be neglected.

(3) The relative magnetic permeability of the substrate material is $\mu_r = 1$.

In order to describe the propagation of electromagnetic waves along any transmission structure, it is necessary to specify both, the characteristic impedance, Z_0, and the propagation coefficient of the structure. At a first approximation perfect conductors are assumed, so that the propagation coefficient is uniquely specified by the velocity of propagation v_p. The characteristic impedance is related to v_p by

$$Z_0 = \frac{1}{v_p C} \tag{2.1}$$

where C is the electrostatic capacitance per unit length of the transmission line.

In order to determine the characteristic impedance and propagation velocity of the line, it is also important to note that

$$v_p = \sqrt{\left(\frac{C_0}{C}\right)}\, c \tag{2.2}$$

From equations (2.1) and (2.2) it follows that

$$Z_0 = \frac{1}{\sqrt{C_0 C}\, c} \tag{2.3}$$

where C_0 is the capacitance that the line would exhibit if the dielectric possessed unit relative permittivity (i.e. air suspended line) and c represents the speed of light in a

vacuum.

In Figure 2.2 the conductor geometry is assumed to be defined by a strip width W, a ground plane spacing h, and a small strip thickness t. It is also assumed that this is an air line with a characteristic impedance Z_0, a wavelength λ_0, an attenuation per unit length α_0, and an unloaded Q_0. For the line shown in Figure 2.1 with a dielectric support material having a relative dielectric constant ε_r, the new line parameters are given by

$$Z = \frac{Z_0}{\sqrt{\varepsilon_{re}}} \quad \Omega \tag{2.4}$$

$$\lambda = \frac{\lambda_0}{\sqrt{\varepsilon_{re}}} \quad \text{m} \tag{2.5}$$

$$\alpha = \alpha_0 \sqrt{\varepsilon_{re}} \quad \text{dB} \tag{2.6}$$

$$Q = Q_0 = \frac{20\pi}{\ln(10)} \frac{1}{\alpha_0 \lambda_0} \tag{2.7}$$

The effective dielectric constant ε_{re} has to be measured or computed as in equation (2.8) (Ross and Howes 1976, Bahl and Garg 1977).

$$\varepsilon_{re} = \frac{\varepsilon_r + 1}{2} + \frac{\varepsilon_r - 1}{2} \left(1 + \frac{10\,h}{W}\right)^{-1/2} \tag{2.8}$$

It is also found that the effective dielectric constant is related to the capacitance (John and Arlett 1974) of the microstrip line as follows (Schneider 1969):

$$\varepsilon_{re} = \frac{C}{C_0} \tag{2.9}$$

From equations (2.2) and (2.9) the velocity of propagation in a single microstrip line is given by

$$v_p = \frac{c}{\sqrt{\varepsilon_{re}}} \tag{2.10}$$

For a very narrow strip ($W \ll h$) and a very wide strip ($W \gg h$) the characteristic impedance is given by (Schneider 1969)

$$Z_0 = 60 \ln\left(\frac{8h}{W}\right) \quad \Omega \quad (W \ll h) \tag{2.11}$$

$$Z_0 = \frac{120\pi h}{W} \quad \Omega \quad (W \gg h) \tag{2.12}$$

Useful expressions given in terms of rational functions or series expansions can be obtained by generalisations of equations (2.11) and (2.12) as follows

$$Z_0 = 60 \ln \sum_{n=1}^{-\infty} a_n \left(\frac{h}{W}\right)^n \quad \Omega \quad (W \leq h) \tag{2.13}$$

$$Z_0 = \frac{120\pi}{\sum_{n=1}^{-\infty} b_n \left(\frac{W}{h}\right)^n} \quad \Omega \quad (W \geq h) \tag{2.14}$$

where a_n and b_n are terms of the series expansion. The number of terms used in the series determines the accuracy of the approximations. Equations (2.15) and (2.16) give an accuracy of ± 0.25 per cent for $0 \leq W/h \leq 10$, this being the range of importance for most engineering applications (Gupta *et al* 1979).

$$Z_0 = 60 \ln\left(\frac{8h}{W} + \frac{W}{4h}\right)\Omega \qquad \frac{W}{h} \leq 1 \qquad (2.15)$$

$$Z_0 = \frac{120\pi}{\frac{W}{h} + 2.42 - 0.44\frac{h}{W} + \left(1 - \frac{h}{W}\right)^6}\Omega \qquad \frac{W}{h} \geq 1 \qquad (2.16)$$

This is however based on the assumption that the microstrip line is of zero thickness. The inclusion of strip thickness into the calculation is important, having the effect of lowering the impedance of the line. This phenomenon can be taken into account by adding an extra term to the expression for the effective permittivity (Ross and Howes 1977).

$$\varepsilon_{re} = \frac{\varepsilon_r + 1}{2} + \frac{\varepsilon_r - 1}{2}\left(1 + \frac{10h}{W}\right)^{-\frac{1}{2}} + 0.468\left(\frac{\varepsilon_r + 0.5}{1.5}\right)\sqrt{\frac{t}{W}} \qquad (W/h \leq 2) \qquad (2.17)$$

$$\varepsilon_{re} = \frac{\varepsilon_r + 1}{2} + \frac{\varepsilon_r - 1}{2}\left(1 + \frac{10h}{W}\right)^{-\frac{1}{2}} \qquad (W/h \geq 2) \qquad (2.18)$$

As the line thickness increases so the impedance of the line decreases and has been recognised in several publications (Gunston and Weale 1969, Bahl and Garg 1977).

A large number of investigations have been carried out in order to study the characteristic impedance of a microstrip line, using numerical methods. One such method is based on the application of Fourier and variational techniques (Yamashita and Mittra 1968, Yamashita 1968). It is has been shown that the impedance, velocity, and attenuation can be determined by calculating the field distribution surrounding a microstrip line bounded by a shielding wall (Stinehelfer 1968, Krage and Haddad 1970). Two other methods used for calculating the impedance of a microstrip line are the method of moments (Farrar and Adams 1970 & 1971) and the method of lines (Nam *et*

al 1989).

The Green's function (Collin 1960, Rickayzen 1980, Ishimaru 1991) has been used in several publications for the calculation of the impedance (Bryant and Weiss 1968, Silvester 1968, Hill *et al* 1969, Gladwell and Coen 1975, Cheng and Everard 1991) of a microstrip and the capacitance (Kammler 1968, Weeks 1970, Patel 1971, Silvester and Benedek 1972(a) & 1972(b), Balaban 1973, Benedek 1976, Vu Dinh *et al* 1992) associated with a microstrip structure.

2.2 : Computer Aided Analysis

The type of analysis required for a particular system depends on its performance and purpose. The electrical analysis may be a very simple one for low speed and low frequency circuits since the reactance of the capacitances is high and the inductances may be assumed to be short circuits. For this a simple analysis may suffice involving only the key capacitances, resistances, or inductances. In contrast, complex models are required to represent high speed and high performance systems, where the analysis may involve a large number of components.

The signal transitions in very low speed digital systems may be in the micro- or even millisecond range. Conversely at the other end of the spectrum, we may be concerned with the analysis of a very high speed logic circuit where the signal transitions may be in the picosecond range (Chilo and Arnaud 1984, Hasegawa and Seki 1984, Seki and Hasegawa 1984, Schutt-Aine and Mittra 1989, Qian and Yamashita 1993, Son *et al* 1994).

A rigorous analysis of multiconductor transmission lines is very involved, especially if the response at high frequencies is to be properly evaluated (Krage and Haddad 1972, Djordjevic *et al* 1987). First a real multiconductor transmission line is most frequently

embedded in an inhomogeneous medium, and thus the waves propagating along the line are not of a transverse electromagnetic (TEM) nature. However even if the medium is homogeneous, due to losses in the conductor, the line is unable support TEM waves (Pucel *et al* 1968, Zysman and Johnson 1969, Djordjevic *et al* 1987).

At very high frequencies (in the microwave region), the cross sectional dimensions of the line become comparable to the wavelength of the propagating signal, allowing higher order (non TEM) modes to propagate (Djordjevic *et al* 1987). Secondly the analysis becomes complicated further if the influence of discontinuities (Tripathi and Bucolo 1987, Chen and Gao 1989, Orhanovic *et al* 1990, Zheng and Chang 1990, Sabban and Gupta 1992) (present at line ends, bends, crossovers, etc.), or nonuniformity of microstrips (Palusinski and Lee 1989, Mao and Li 1991, Dhaene and De Zutter 1992, Schutt-Aine 1992) (e.g. tapered) are to be included. Finally to evaluate the response of a transmission line terminated by arbitrary networks, which are generally non-linear (e.g. active components) with memory (i.e. contain capacitors and inductors), it is necessary to consider every part of the system simultaneously.

A survey of computer-aided electrical analysis of integrated circuit interconnections has been published (Ruehli 1979) providing a comprehensive analysis of techniques being employed to simulate microstrip interconnects. Although microstrip lines do not support signals of a TEM nature, they are generally simulated using TEM waveforms, which give a very good approximation. This is known as the quasi-TEM wave approximation (Gladwell and Coen 1975, Paul 1975, Chowdhury *et al* 1992).

2.3 : Single Microstrip Line

Consider a single microstrip line with its resistance, inductance, capacitance and conductance per-unit-length defined as R, L, C, and G respectively (Yaun *et al* 1982, Zhang *et al* 1992). Under the quasi-TEM wave approximation, the microstrip line can be described by the well known *Telegrapher's equations*; the following partial differential

equations can be used to describe n uniform transmission lines (Paul 1973).

$$\frac{\partial v(x,t)}{\partial x} = [\mathrm{R}]i(x,t) - [\mathrm{L}]\frac{\partial i(x,t)}{\partial t} \tag{2.19}$$

and

$$\frac{\partial i(x,t)}{\partial x} = [\mathrm{G}]v(x,t) - [\mathrm{C}]\frac{\partial v(x,t)}{\partial t} \tag{2.20}$$

where $v(x,t)$ and $i(x,t)$ are the voltage and current respectively at each point x along the line at a time t.

The method of characteristics has been used (Branin 1967) to provide a simple analytic solution for the transient analysis of a uniform lossless transmission line. For solving these equations the method of characteristics is based on a transformation in the x-t plane which accomplishes the conversion of the telegraph equations (2.19) and (2.20) into a pair of ordinary differential equations. The transformation uses the equations:

$$\frac{dx}{dt} = \pm\frac{1}{\sqrt{\mathrm{LC}}} \tag{2.21}$$

which define the characteristic curves for the forward and backward waves. When L and C are constant the characteristic curves are straight lines and the phase velocity $1/\sqrt{\mathrm{LC}}$ is constant. By appropriately combining these relations with equations (2.19) and (2.20), the differential equations (2.22) and (2.23) may be derived. The forward characteristic of the line being:

$$\sqrt{\frac{\mathrm{L}}{\mathrm{C}}}di + \left(\mathrm{R}i + \sqrt{\frac{\mathrm{L}}{\mathrm{C}}}\mathrm{G}v\right)dx + dv = 0 \tag{2.22}$$

and the backwards characteristic given by

$$-\sqrt{\frac{L}{C}}di+\left(Ri-\sqrt{\frac{L}{C}}Gv\right)dx+dv=0 \qquad (2.23)$$

Equations (2.22) and (2.23) hold true along different families of characteristic curves in the *x-t* plane; one family corresponding to the forward or incident wave and the other to the backward or reflected wave. It is not possible for these equations to be directly integrated (Branin 1967). However if these equations are used for the case of the lossless transmission line, where R = 0 (i.e. no resistive loss in the conductor) and G = 0 (i.e. no conductance between the microstrip and the ground plane), these equations can be directly integrated, yielding exact solutions of the form $\Delta v=+Z_0\ \Delta i$ and $\Delta v=-Z_0\ \Delta i$, where the characteristic impedance of the line $Z_0 = \sqrt{L/C}$. This leads to an efficient algorithm that yields not only the input and output responses but also the incident and reflected waves.

Many papers have been published concerning the analysis of a single lossy line in the time domain where the series resistance of the conductor is taken into account (Schreyer *et al* 1988). The conductance may also be taken into consideration (Chang 1990), but is not essential for an accurate lossy line model. The transient response of uniform RLC transmission lines has been studied (Cases and Quinn 1980), where the case of a general RLC transmission line was investigated, with specific reference to a line with low total series resistance.

An MIS (metal-insulator-semiconductor) microstrip line model has been used to analyse the interconnection delay on very high speed LSI/VLSI chips (Hasegawa and Seki 1984). An MIS is a microstrip formed on a surface passivated semiconductor substrate with a metallised back. Given an interconnection geometry, the equivalent circuit parameters were calculated. By substituting these into the analytic expressions for the characteristic impedance and propagation constants based on the equivalent circuit, waveforms under arbitrary excitation and termination conditions are calculated by inverse Laplace transformation.

A lossy transmission line model (Groudis 1979) has been developed for implementation into the source code of the SPICE circuit simulator (Sussman-Fort and Hantgan 1988).

The scattering matrix representation (Schutt-Aine and Mittra 1988, 1989) was used for the time domain simulation of transient signals on dispersive, lossy and non-linear, transmission lines terminated with active devices. Any linear two-port network can be described as a set of scattering parameters which relate incident and reflected voltage waves. These waves are variables which depend on the total voltages and currents at each end of the two-port.

Recently the method of lines has been used (Chen and Li 1991) for the analysis of a planar transmission line with discontinuity. If a pulsed signal is considered in a structure, the time-domain method of lines is useful not only for obtaining the characteristics of a uniform transmission line and for calculating the scattering parameters of its discontinuities for a wide range of frequencies, but also for studying the behaviour of a pulsed signal in a structure such as a high-speed digital circuit. The fast Fourier transform (FFT) technique is also used in order to greatly reduce the calculating time (c.f. Nam *et al* 1989) when the number of points is large.

To a large extent the analysis of a single line in the frequency domain has been neglected. However, a waveform relaxation method was proposed for the analysis of the single lossy transmission line (Chang 1990, 1991). The idea of simulating a transmission line by iteration originates from the observation that the voltage (current) waveform at each transmission line terminal is composed of an infinite sequence of incident and reflected waves.

2.4 : Coupled Microstrip Lines

To study the coupling effects experienced on a set of n parallel transmission lines, we start with the self and mutual, inductance and capacitance along the lines (Sato and Cristal 1970, Schutt-Aine and Mittra 1985). These parameters characterise the coupling in the vector form of the telegrapher's equations (2.19) and (2.20), where e and i are replaced by n × 1 voltage and current vectors. R, G, L, and C become $n \times n$ series resistance, shunt conductance, inductance, and capacitance per unit length matrices, respectively.

The study of coupled lines is of significant importance, as the proximity of interconnection lines has brought about conditions where the coupling effects between the lines could cause an error in the logic states on inactive lines within a logic bus. Initially, as for the case of the single transmission line it is easiest to consider a set of n coupled lossless transmission lines (Ho 1973).

Use has been made of the method of characteristics to produce the distributed parameters, and the trapezoidal rule of integration for the lumped parameters, in order to formulate a *nodal admittance matrix* method (Dommel 1969). Numerically this leads to the solution of a system of linear (nodal) equations in each time step. This method was used for the analysis of electromagnetic transients in arbitrary single and multiphase networks with lumped and distributed parameters. It is also suggested that resistive lines can be represented by several sections of an ideal transmission line with a resistor between each ideal line section.

The normal mode method (Chang 1970) has been used to solve the problem of a coupled lossless transmission line system. To derive the computational algorithm, an equivalent circuit consisting of n decoupled transmission lines in conjunction with two congruence transformers was constructed and converted into two disjointed resistive n-ports; the transformer parameters being calculated from the capacitance per unit length matrix.

This model was further modified by using the method of characteristics for both lossless (Tripathi and Rettig 1985, Ho 1973) and lossy (Groudis and Chang 1981, Orhanovic *et al* 1990) lines, and has also been applied to the case of interconnections in high speed digital circuits that are best represented as coupled transmission lines (Yaun *et al* 1982, Seki and Hasegawa 1984). All these models are mathematically identical in that they all represent the exact solution of the coupled transmission line equations.

An investigation was carried out to look at the time domain behaviour of an eight line interconnection bus in a high speed GaAs logic circuit (Chilo and Arnaud 1984) for high velocity logic signals with a 10 ps rise time. Emphasis was given to the coupling effects and distortion of signals in the time domain. For this an analogic simulator was used to evaluate the performance of the bus. To do this a modal expansion was required, which assumes that the set of lines are characterised by the [L] and [C] matrices representing the magnetic and electric couplings.

These [L] and [C] matrices for different line structures were obtained by use of the magnetic and electric Green's functions (Collin 1960, Coen 1975, Rickayzen 1980). The results obtained by this method (Chilo and Arnaud 1984) show how crosstalk could be a possible cause of logic errors. The paper goes on to discuss two methods for reducing the amount of crosstalk present in the eight line bus.

The first method introduces shield lines, by grounding the input and output ends of alternate microstrip lines. This has the effect of greatly reducing the amount of crosstalk seen on the adjacent signal lines but, does however reduce the wiring capacity by a factor of two and introduces further distortion. This implies that the shield lines react with the active signal lines.

The second method involves the introduction of a second ground plane above the microstrips. This reduces the level of crosstalk, but has an extremely detrimental effect

upon the distortion of the signal seen at the output end of the line. This increase in distortion is brought about because the characteristic impedance of each line is considerably reduced by the addition of the second ground plane, therefore making the lines prone to a considerably higher level of distortion.

Decoupling of the transmission line equations by writing the solution in the form of a perturbational series (Yang *et al*, 1985), instead of numerically integrating the coupled equations, has been proposed.

A coupled transmission line system can be decoupled into a set of independent transmission line equations by linear transformation (Chang 1970, Tripathi and Rettig 1985, Romeo and Santomauro 1987, Gao *et al* 1990, Parker *et al* 1994). A distributed characteristic wave model can be used to represent the transmission effects in the time domain. The solution of the decoupled Telegraph equations can then be represented by a set of time varying equivalent circuits. This type of model can then be implemented into a general purpose circuit simulator; e.g. SPICE (Sussman-Fort 1988, Banzhaf 1989, Rashid 1990, Wirth 1990, Huang and Wing 1991), ASTAP (Weeks *et al* 1973, Groudis and Chang 1981), iSMILE (Gao *et al* 1990).

To allow simulation of lossy transmission lines with a circuit simulator, it may require the characteristic solutions of the Telegraph equations to be modelled by equivalent current sources and impedances using the integral method (Gao *et al* 1990). Each terminal voltage waveform of a transmission line is approximated by piecewise linear function time, allowing easy evaluation of the convolution integral. The conventional multistep integral method could not be applied to the convolution integral and therefore the convolution is done directly, producing an approximated summation of nodal voltages.

2.5 : Skin Effect

When a signal of low frequency is transmitted along a wire, the current is distributed uniformly throughout the cross-section of the conducting medium. However as the frequency of the transmitted signal is increased, the current is redistributed, with a tendency to crowd towards the surface of the conductor until, at very high frequencies, it is effectively confined to a thin skin just inside the surface of the conductor. The determination of such a current density as a function of frequency is a major problem.

The "skin effect" (Wheeler *et al* 1942) is the tendency for high frequency alternating currents and magnetic flux to penetrate into the surface of a conductor only to a limited depth. The "depth of penetration" is a useful dimension, dependent upon the signal frequency and the properties of the conducting material (i.e. conductivity and permeability). If the thickness of the conductor is much greater than the depth of penetration, its behaviour toward high frequency alternating currents becomes a surface phenomenon rather than a volume phenomenon. Its "surface resistivity" is the resistance of a conducting surface of equal length and width, and has simply the dimension of resistance per square. In the case of a straight wire this width is the circumference of the wire.

The depth of penetration δ is defined as the depth at which the current density (or magnetic flux) is attenuated by 1 Neper (in the ratio 1/e = 1/2.72, -8.7 decibels) (Wheeler *et al* 1942). At this depth, there is a phase lag of 1 radian, so δ is $1/2\pi$ wavelength or 1 radian length in terms of the wave propagation in the conductor. The depth of penetration, by this definition, is (Wheeler *et al* 1942, Djordjevic and Sarkar 1994)

$$\delta = \frac{1}{\sqrt{\pi f \mu \sigma}} \quad \text{metres.} \tag{2.24}$$

where f is the frequency of the AC signal, μ is the permeability of the medium, and σ is

the conductivity of the conducting wire.

The interconnection lengths, rather than the device speed, have become one of the main limitations to very high-speed digital system performance because of the development of very high-speed semiconductor devices. The long interconnects are responsible for the delay and deformation of digital pulses. The standard approach of scaling down their physical size is limited by the increasing line resistance because of the finite resistivity of the conductors.

The loss calculations for interconnect structures typical for digital applications have been primarily based on the DC resistance. This assumption holds only at low frequencies. At high frequencies and especially in integrated microwave circuits, Wheeler's incremental inductance rule (Wheeler 1942, Pucel *et al* 1968) has been successfully applied, taking into account the skin effect. The requirement for Wheeler's theory to be applicable is that the cross-sectional dimensions of the conductor are large compared with the skin depth of penetration, δ; say about four times the skin depth of penetration. The whole frequency spectrum of very high-speed digital pulses often includes, in addition to the above-mentioned ranges, an intermediate frequency range where the skin depth of penetration is in the order of the transversal conductor geometry and thus neither the DC assumption nor Wheeler's theory hold (Wlodarczyk and Besch 1990).

The formulae concerning skin effect in a circular conductor have been well documented (Wheeler 1942) and extended for investigation into the resistive and inductive skin effect apparent in rectangular conductors (Weeks *et al* 1979) which can then be applied to the case of a microstrip transmission line system.

Brenan and Ruehli (1978) proposed a time domain skin effect model using only resistors and lossless transmission lines, which leads to efficient simulation due to the simplicity of the circuit; all capacitances and inductances have been discarded.

The skin effect has been extensively studied, firstly on coaxial lines by approximating the line series impedance by use of the function $A + B\sqrt{s}$ (Nahman and Holt 1972), where A and B represent a resistance along the line and s is a Laplace frequency domain function. This function was used to investigate the frequency dependence of transient signals being transmitted along coaxial cables. This method was further extended to include arbitrary resistive terminations (Calvez and Le Bihan 1986).

A comprehensive study of the time domain transient analysis of lossy transmission lines has been presented (Yen *et al* 1982). A skin effect equivalent circuit consisting of resistors and inductors is derived from the skin effect differential equations for simulating the loss on a transmission line. This involved dividing the line into N sections. These sections of cable are further subdivided into M rings to represent the change in current density between the surface of the conductor and its centre. Deriving directly from the skin effect differential equations, an equivalent circuit consisting of M resistors and M-1 inductors was constructed, to allow the simulation of skin effect loss.

An accurate equivalent circuit for modelling the skin effect apparent in a microstrip line has been proposed (Vu Dinh *et al* 1990(a)). The method uses no specific approximation to the frequency behaviour therefore making it applicable for any microstrip line geometry. This method is of more appropriate use when the thickness of the line is greater than its width. The investigation into the frequency dependent parameters of a microstrip transmission line using this method was carried out with the SPICE circuit simulator.

This method divides the line into a series of elementary bars so as to allow for the difference in current density from one portion of the line to another. The dimensions of the bars at the outside of the line are smaller than those of the bars in the centre, to allow for any increase in current density closer to the surface of the line. The method however assumes that the ground plane is a perfect conductor. In reality, because of the returning current in the ground plane, there is always a resistive loss and a perturbation in the field

of the dielectric film, especially at high frequencies.

This method was then extended (Vu Dinh *et al* 1990(b)) to account for loss due to the returning current in a resistive ground plane. Because the currents flowing into the strip and the ground plane are in opposite senses, the mutual inductances are negative. Due to proximity and fringe effects, the current density concentrates in regions of the ground plane located underneath the strip and at the edges of the plane. The attenuation constant is found to increase when losses in the ground plane are taken into account.

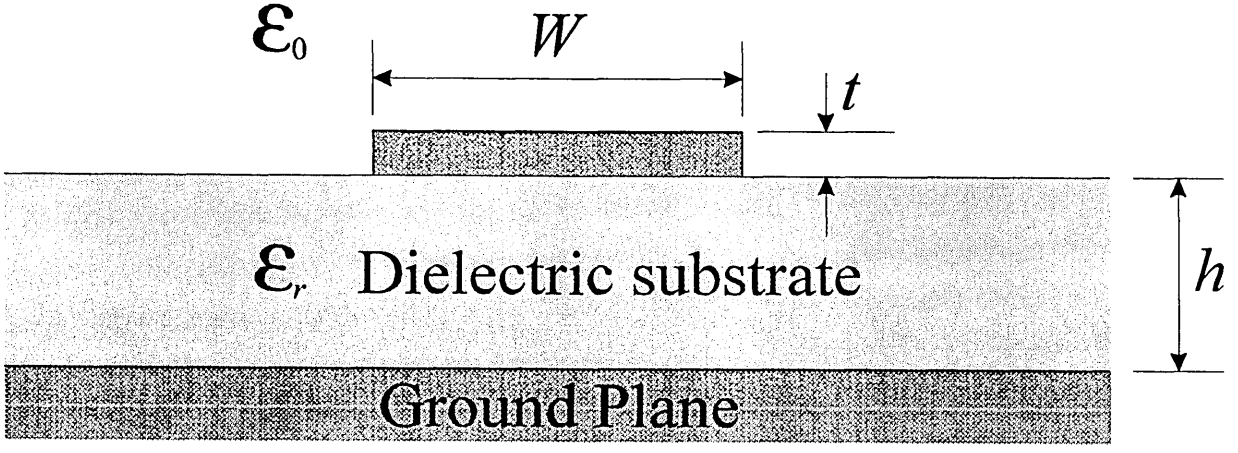

Figure 2.1 : Basic configuration of a microstrip line.

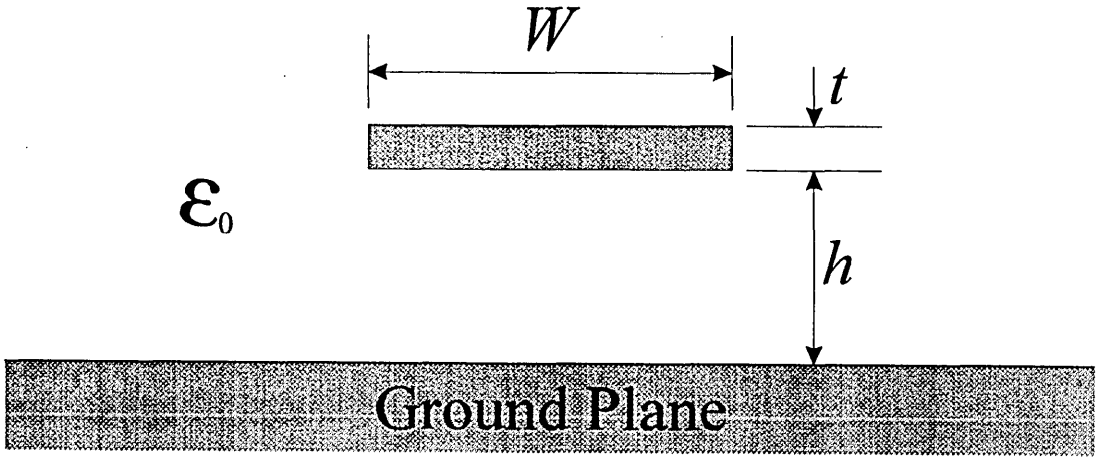

Figure 2.2 : Configuration of an air microstrip line.

3.0 : Introduction

This chapter describes all the relevant background mathematics required for the calculation of the parameters relating to microstrip interconnections, and are used later in chapter 6.

3.1 : Impedance of a Single Microstrip Line

The closed form expressions for the impedance, Z_{om}, of a single microstrip line and effective dielectric constant, ε_{re}, can be described in terms of the width, W, of the microstrip and its height, h, above the ground plane. The following closed form expressions (3.1)-(3.4) for Z_{om} and ε_{re} (Hammerstad 1975) are based on the work of Wheeler (1965) and Schneider (1968).

$$Z_{om} = \frac{60}{\sqrt{\varepsilon_{re}}} \ln\left(\frac{8h}{W} + 0.25\frac{W}{h}\right) \qquad \left(\frac{W}{h} \le 1\right) \qquad (3.1)$$

$$Z_{om} = \frac{120\pi}{\sqrt{\varepsilon_{re}}} \left[\frac{W}{h} + 1.393 + 0.667 \ln\left(\frac{W}{h} + 1.444\right)\right]^{-1} \qquad \left(\frac{W}{h} \ge 1\right) \qquad (3.2)$$

$$\varepsilon_{re} = \frac{\varepsilon_r + 1}{2} + \frac{\varepsilon_r - 1}{2} F(W/h) \qquad (3.3)$$

$$F(W/h) = \begin{cases} (1 + 12h/W)^{-1/2} + 0.04(1 - W/h)^2 & (W/h \le 1) \\ (1 + 12h/W)^{-1/2} & (W/h \le 1) \end{cases} \qquad (3.4)$$

3.2 : Capacitance Calculations

Design equations for coupled microstrip lines should relate even and odd mode

impedances and effective dielectric constants to the coupled line geometry; i.e. strip width, W, spacing between the strips, S, dielectric thickness, h, and relative dielectric constant, ε_r (Gupta *et al* 1979). Design equations for these characteristics may be written in terms of the parameters of coupled lines. Alternatively, static capacitances for the coupled line geometry may be used as an intermediate step. The latter approach yields simpler design equations. Therefore even and odd mode characteristics will be described in terms of static capacitances.

3.2.1 : Even mode capacitance

The even mode capacitance, C_{even}, where the lines are separated by a magnetic wall (figure 3.1) is given by (Gupta *et al* 1979):

$$C_{even} = C_p + C_f + C_f' \tag{3.5}$$

where C_p is the parallel plate capacitance between the microstrip and the ground plane:

$$C_p = \varepsilon_0 \varepsilon_r \frac{W}{h} \tag{3.6}$$

and C_f is the fringe capacitance between the outside edge (no neighbouring line) of the microstrip and the ground plane:

$$C_f = \frac{1}{2}\left\{\frac{\sqrt{\varepsilon_{re}}}{c Z_{om}} - \varepsilon_0 \varepsilon_r \frac{W}{h}\right\} \tag{3.7}$$

and C_f' is the modified fringe capacitance between a line edge neighbouring another and the ground plane:

$$C_f' = \frac{C_f}{1 + A\left(\frac{h}{S}\right)\tanh\left(10\frac{S}{h}\right)}\sqrt{\frac{\varepsilon_r}{\varepsilon_{re}}} \tag{3.8}$$

$$A = \exp\left[-0.1\exp\left(2.33 - 2.53\frac{W}{h}\right)\right] \tag{3.9}$$

3.2.2 : Odd mode capacitance

The odd mode capacitance, C_{odd}, where the microstrips are partitioned by an electric wall (figure 3.2), is given by (Gupta *et al* 1979):

$$C_{odd} = C_p + C_f + C_{gd} + C_{ga} \tag{3.10}$$

where C_{gd} is the capacitance between two lines through the dielectric medium:

$$C_{gd} = \frac{\varepsilon_0\,\varepsilon_r}{\pi}\ln\left[\coth\left(\frac{\pi S}{4h}\right)\right] + 0.65C_f\left[\frac{0.02}{S/h}\sqrt{\varepsilon_r} + \left(1 - \frac{1}{\varepsilon_r^{\,2}}\right)\right] \tag{3.11}$$

and C_{ga} (Owyang and Wu 1958) is the air gap capacitance given in terms of elliptic functions, where k and k' are defined in equations (3.13) and (3.14)

$$C_{ga} = \frac{\varepsilon_0}{2}\frac{K(k')}{K(k)} \tag{3.12}$$

$$k = \frac{S/h}{S/h + 2W/h} \tag{3.13}$$

$$k' = \sqrt{1 - k^2} \tag{3.14}$$

3.3 : Parameters of a Coupled Microstrip Pair

Coupled microstrips are characterised by the characteristic impedances and phase velocities for the two modes. When two or more parallel microstrip lines are considered the self and mutual inductances and capacitances must be taken into account in order that the coupling parameters can be determined. The impedances and signal propagation velocity may be calculated in terms of the odd and even capacitances, C_{odd} and C_{even} respectively.

3.3.1 : Evaluation of self and mutual capacitance

The self capacitance per unit length, C_0, of each line is defined as the average of the odd and even mode capacitances thus (Krage and Haddad 1970):

$$C_0 = \frac{1}{2}\left[C_{odd}(\varepsilon_r) + C_{even}(\varepsilon_r)\right] \tag{3.15}$$

The mutual capacitance per unit length, C_m, between the two lines under consideration is given by half the difference of the odd and even mode capacitances:

$$C_m = \frac{1}{2}\left[C_{odd}(\varepsilon_r) - C_{even}(\varepsilon_r)\right] \tag{3.16}$$

3.3.2 : Calculation of self and mutual inductance

Calculation of the self and mutual inductances, L_0 and L_m respectively, requires the odd and even mode capacitance to be determined for a microstrip structure with no dielectric substrate (i.e. air suspended line), where $\varepsilon_r = 1 = \varepsilon_0$ (Krage and Haddad 1970).

$$L_0 = \frac{\mu_0 \varepsilon_0}{2}\left\{\frac{1}{C_{odd}(\varepsilon_0)} + \frac{1}{C_{even}(\varepsilon_0)}\right\} \tag{3.17}$$

$$L_m = \frac{\mu_0 \varepsilon_0}{2}\left\{\frac{1}{C_{even}(\varepsilon_0)} - \frac{1}{C_{odd}(\varepsilon_0)}\right\} \tag{3.18}$$

3.3.3 : Evaluation of impedance

Determination of the even mode impedance, Z_{0even}, and the odd mode impedance, Z_{0odd}, require both the even and odd mode capacitances respectively, for the lines with and without a dielectric substrate as follows:

$$Z_{0even} = \sqrt{\frac{\mu_0 \varepsilon_0}{C_{even}(\varepsilon_0) C_{even}(\varepsilon_r)}} \tag{3.19}$$

$$Z_{0odd} = \sqrt{\frac{\mu_0 \varepsilon_0}{C_{odd}(\varepsilon_0) C_{odd}(\varepsilon_r)}} \tag{3.20}$$

The total impedance of each line can then be determined using the odd and even mode impedances thus (Gupta *et al* 1979):

$$Z_0 = \sqrt{Z_{0even} Z_{0odd}} \tag{3.21}$$

The above set of equations (3.15)-(3.21) can however only be used for calculating the parameters appertaining to a pair of parallel microstrip lines of equal width.

3.4 : Inclusion of Strip Thickness

The closed form expressions (3.1)-(3.4) assume a zero line thickness (i.e. $t = 0$), and therefore contain inherent inaccuracies. It is therefore important that the thickness of the line, t, be taken into account, in order to reduce the magnitude of any errors that are contained within these empirical formulae. The effect of strip thickness on Z_{om} and ε_{re} of microstrip lines has been reported by a number of investigators (Wheeler 1965, Kaupp 1967, Gunston and Weale 1969, Silvester 1968, Stinehelfer 1968, Yamashita and Mittra 1968, Schneider 1969, John and Arlett 1974, Kumar *et al* 1976, Ross and Howes 1976, Bahl and Garg 1977).

3.4.1 : Evaluation of impedance

The effect that t has upon the calculation of line impedance, can be incorporated into the calculations by means of defining an effective width, W_e, which is dependent upon the thickness of the line as follows (Bahl and Garg 1977):

$$\frac{W_e}{h} = \frac{W}{h} + \frac{1.25}{\pi}\frac{t}{h}\left(1 + \ln\left[\frac{4\pi W}{t}\right]\right) \qquad \left(\frac{W}{h} \leq \frac{1}{2\pi}\right) \qquad (3.22)$$

$$\frac{W_e}{h} = \frac{W}{h} + \frac{1.25}{\pi}\frac{t}{h}\left(1 + \ln\left[\frac{2h}{t}\right]\right) \qquad \left(\frac{W}{h} \geq \frac{1}{2\pi}\right) \qquad (3.23)$$

The effective width, W_e, can then be substituted back into the single line impedance equations, (3.1) and (3.2), to give the following:

$$Z_{om} = \frac{60}{\sqrt{\varepsilon_{re}}} \ln\left(\frac{8h}{W_e} + 0.25\frac{W_e}{h}\right) \qquad \left(\frac{W}{h} \le 1\right) \qquad (3.24)$$

$$Z_{om} = \frac{120\pi}{\sqrt{\varepsilon_{re}}}\left[\frac{W_e}{h} + 1.393 + 0.667\ln\left(\frac{W_e}{h} + 1.444\right)\right]^{-1} \qquad \left(\frac{W}{h} \ge 1\right) \qquad (3.25)$$

3.4.2 : Calculation of effective dielectric

The effective dielectric constant, ε_{re}, has a further correction term, E, added to account for a finite line thickness (Bahl and Garg 1977).

$$\varepsilon_{re} = \frac{\varepsilon_r + 1}{2} + \frac{\varepsilon_r - 1}{2} F(W/h) - E \qquad (3.26)$$

where

$$E = \frac{\varepsilon_r - 1}{4.6} \frac{t/h}{\sqrt{W/h}} \qquad (3.27)$$

It can be observed that the effect of thickness on Z_{om} and ε_{re} is insignificant for small values of t/h. This agrees with the experimental results reported by Gunston and Weale (1968) for $t/h \le 0.005$, $2 \le \varepsilon_r \le 10$ and $W/h \ge 0.1$. However, the effect of strip thickness is significant on conductor loss in the microstrip line.

3.4.3 : Effect upon odd mode capacitance

The inclusion of a finite line thickness, t, also introduces a further capacitance term, C_{gt} (Gupta *et al* 1979):

$$C_{gt} = 2\varepsilon_0 \frac{t}{S} \tag{3.28}$$

which is added to the odd mode capacitance, C_{odd} (equation (3.10)), thus:

$$C_{odd} = C_p + C_f + C_{gd} + C_{ga} + C_{gt} \tag{3.29}$$

Due to the increase in even and odd mode capacitances with finite strip thickness, the even and odd mode impedances are expected to decrease.

3.5 : Impedance and Time Delay of *n* Microstrips

Now let us consider a set of n coupled lossless transmission lines. If we assume the transverse electromagnetic (TEM) mode of wave propagation, the distribution of voltages and currents along the lines is given by the generalised telegraphists' equations (Magnusson 1970):

$$\begin{bmatrix} \mathbf{v}^x(x,t) \\ \mathbf{i}^x(x,t) \end{bmatrix} = -\begin{bmatrix} 0 & \mathbf{L} \\ \mathbf{C} & 0 \end{bmatrix} \begin{bmatrix} \mathbf{v}^t(x,t) \\ \mathbf{i}^t(x,t) \end{bmatrix} \tag{3.30}$$

where the vectors $\mathbf{v}(x, t)$ and $\mathbf{i}(x, t)$ denote voltages and currents respectively. The superscripts x and t denote differentiation of the signals with respect to space and time, respectively, $\mathbf{L}$ is the per-unit length (PUL) inductance matrix and $\mathbf{C}$ is the per-unit length (PUL) capacitance matrix.

3.5.1 : Capacitance matrix calculation

The per-unit length capacitance matrix **C** is given by

$$\mathbf{C} = \begin{bmatrix} C_{1,1} & -C_{1,2} & \cdots & -C_{1,n} \\ -C_{2,1} & C_{2,2} & & \vdots \\ \vdots & & \ddots & \vdots \\ -C_{n,1} & -C_{n,2} & \cdots & C_{n,n} \end{bmatrix} \tag{3.31}$$

The matrix **C** is symmetric, diagonally dominant, and positive definite (Pease 1965, Schwarz *et al* 1973) such that the diagonal elements are given by (Paul 1973):

$$C_{i,i} = c_{i,0} + \sum_{\substack{j=1 \\ j \neq i}}^{n} c_{i,j} \tag{3.32}$$

where $c_{i,0}$ is the capacitance PUL of line i with respect to ground, and $c_{i,j}$ is the capacitance PUL between line i and line j. The off diagonal elements of the matrix are given by:

$$C_{i,j} = -c_{i,j} \tag{3.33}$$

The capacitance PUL of line i, $c_{i,0}$, can be calculated in the following way, using the odd and even mode capacitances of a single microstrip line, thus:

$$c_{i,0} = \frac{1}{2}[C_{even} + C_{odd}] \tag{3.34}$$

and simplifies to the following in terms of parallel plate capacitance, C_p, and the fringe capacitance, C_f, shown below in equation (3.35).

$$c_{i,0} = C_p + 2C_f \tag{3.35}$$

The off diagonal elements, $c_{i,j}$, are equal to the mutual capacitance, $C_{m(i,j)}$, between line i and line j which is given in terms of static capacitances in equation (3.36).

$$c_{i,j} = C_{m(i,j)} = \frac{1}{2}\left[C_{ga} + C_{gd} + C_{gt} - C_f{}'\right] \tag{3.36}$$

3.5.2 : Calculation of inductance matrix

Given a set of coupled lines, e.g., a set of microstrips on a printed circuit board, the entries of matrices **L** and **C** can be numerically computed once the geometries of the lines and the dielectric constant of the inhomogeneous coupling material are given and the TEM mode is assumed. Algorithms to compute these parameters are well known and documented above in this chapter.

In the cases of common interest, e.g., connections on printed circuit boards, the nature of the media in which the transmission lines are embedded is such that the magnetic properties are not dependent on the type of dielectric used and are equivalent to those obtained when the dielectric is replace by a vacuum (Romeo and Santomauro 1987). Bearing this in mind, the values of the entries of matrix **L** are computed by means of the relation (Chang 1970, Yaun *et al* 1982):

$$\mathbf{L} = \mathbf{L}_0 = \mu_0 \varepsilon_0 \left[\mathbf{C}(\varepsilon_0)\right]^{-1} \tag{3.37}$$

where $\mathbf{C}(\varepsilon_0)$ is the capacitance matrix for the same set of transmission lines with the dielectric replaced by a vacuum.

3.5.3 : Matrix diagonalisation

Let us now consider the following change of basis for $\mathbf{v}$ tó $\mathbf{v}_d$ and from $\mathbf{i}$ and $\mathbf{i}_d$:

$$\mathbf{v} = \mathbf{M}_v \mathbf{v}_d \tag{3.38}$$

$$\mathbf{i} = \mathbf{M}_I \mathbf{i}_d \tag{3.39}$$

where $\mathbf{M}_I$ and $\mathbf{M}_V$ are n by n constant matrices. Substituting equations (3.38) and (3.39) into equation (3.30), we obtain (Romeo and Santomauro 1987):

$$\begin{bmatrix} \mathbf{v}_d^x(x,t) \\ \mathbf{i}_d^x(x,t) \end{bmatrix} = -\begin{bmatrix} 0 & \mathbf{L}_d \\ \mathbf{C}_d & 0 \end{bmatrix} \begin{bmatrix} \mathbf{v}_d^t(x,t) \\ \mathbf{i}_d^t(x,t) \end{bmatrix} \tag{3.40}$$

where $\mathbf{L}_d$ and $\mathbf{C}_d$ are given by Chilo and Arnaud (1984):

$$\mathbf{L}_d = \mathbf{M}_v^{-1} \mathbf{L} \mathbf{M}_I \tag{3.41}$$

$$\mathbf{C}_d = \mathbf{M}_I^{-1} \mathbf{C} \mathbf{M}_v \tag{3.42}$$

Due to the particular nature of the physical problem, a number of results can be proven. The first proposition is that the matrices $\mathbf{LC}$ and $\mathbf{CL}$ share the same eigenvalues $\lambda_i (i = 1, 2, \ldots, n)$. Secondly the corresponding right eigenvector matrices, $\mathbf{M}_V$ and $\mathbf{M}_I$, satisfy the following equation (Chang 1970):

$$\mathbf{M}_I^{-1} = \mathbf{M}_v^T \tag{3.43}$$

Matrices $\mathbf{C}_d$, $\mathbf{L}_d$, $(\mathbf{LC})_d$ and $(\mathbf{CL})_d$ given by (Romeo and Santomauro 1987):

$$\mathbf{C}_d = \mathbf{M}_v^T \mathbf{C} \mathbf{M}_v \tag{3.44}$$

$$\mathbf{L}_d = \mathbf{M}_v^{-1} \mathbf{L} \left[\mathbf{M}_v^{-1}\right]^T \tag{3.45}$$

$$(\mathbf{LC})_d = \mathbf{M}_V^{-1}\mathbf{L}\left[\mathbf{M}_V^{-1}\right]^T \mathbf{M}_V^T\mathbf{C}\mathbf{M}_V = \mathbf{L}_d\mathbf{C}_d \tag{3.46}$$

$$(\mathbf{CL})_d = \mathbf{M}_V^T\mathbf{C}\mathbf{M}_V\mathbf{M}_V^{-1}\mathbf{L}\left[\mathbf{M}_V^{-1}\right]^T = \mathbf{C}_d\mathbf{L}_d \tag{3.47}$$

and are diagonal in the new basis obtained by equations (3.38) and (3.39).

3.5.4 : Determination of time delay and impedance

The change of basis represented by equations (3.38) and (3.39) is the generalisation of the even mode and odd mode decomposition to the case in which n coupled lines are considered. Equation (3.40) represents a set of n decoupled lines. Each line propagates one and only one of the n propagation modes of the system in equation (3.30) (Romeo and Santomauro 1987). The time delay matrix, $\mathbf{T}_d$, is given by

$$\mathbf{T}_d = \sqrt{(\mathbf{L}_d \mathbf{C}_d)} \tag{3.48}$$

while the characteristic impedance matrix, $\mathbf{Z}_d$, is given by

$$\mathbf{Z}_d = \sqrt{(\mathbf{L}_d \mathbf{C}_d)}\, \mathbf{C}_d^{-1} \tag{3.49}$$

All matrices in equations (3.48) and (3.49) are diagonal and this makes the computation of square roots and inverses trivial. Moreover, since both $\mathbf{T}_d$ and $\mathbf{Z}_d$ are diagonal matrices, the set of n coupled lines can be represented by n single lines with parameters $\mathbf{T}_{di}$ and $\mathbf{Z}_{di}$ and simulated using an equivalent circuit model in the SPICE circuit simulator.

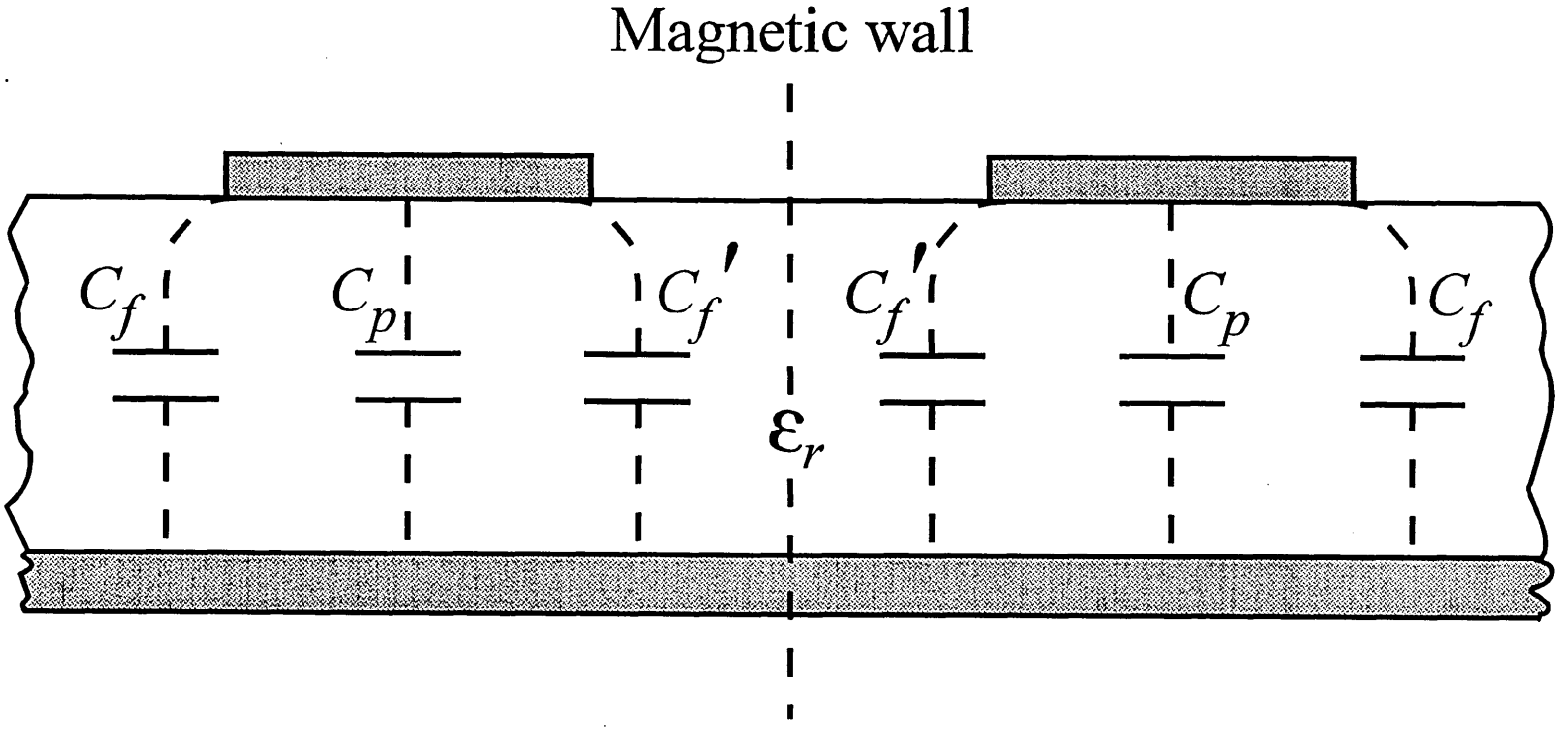

Figure 3.1 : Even mode capacitances for a pair of microstrip lines.

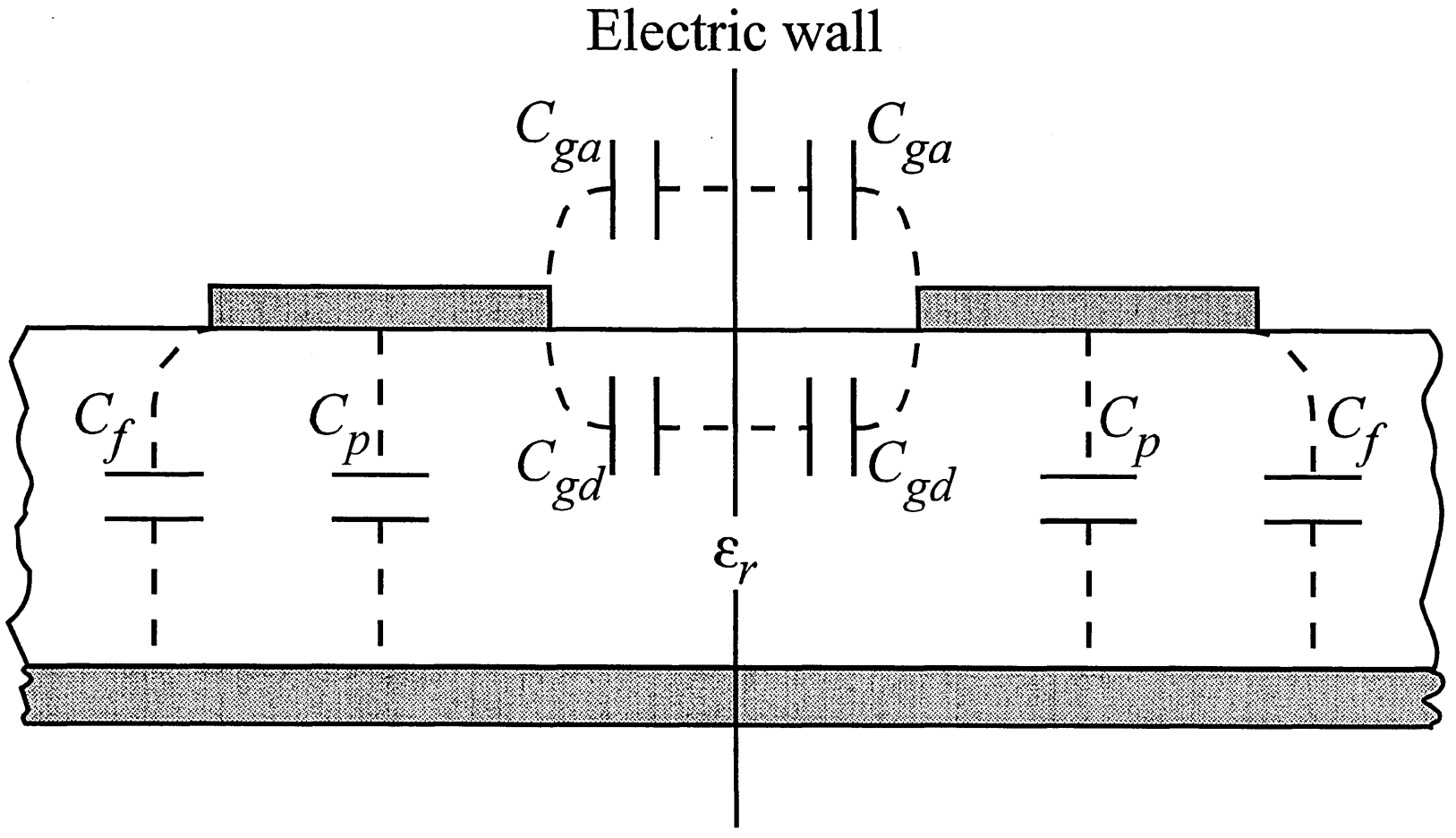

Figure 3.2 : Odd mode capacitances for a pair of microstrip lines.

4.0 : Introduction

An ideal transmission line is a line through which a signal can be sent without undergoing any attenuation or distortion (Rashid 1990). As a first approximation transmission lines are generally thought of as ideal. This chapter looks at the theory of the ideal transmission line, and how it can be related to microstrip line circuits.

4.1 : Electrical Characteristics of Transmission Lines

4.1.1 : Two-wire transmission line

The end of a two-wire transmission line that is connected to a source is ordinarily called the generator end or the input end. The other end of the line, if connected to a load, is called the load end or the receiving end.

The electrical characteristics of two-wire transmission lines are dependent primarily on the construction of the line. Since two-wire line is nothing more than a long capacitor, the change in its capacitative reactance will be noticeable as the frequency applied to it is changed (Duffin 1965). Since long conductors will have a magnetic field about them when electrical energy is being passed through them, the properties of inductance will also be observed (Duffin 1965). The values of the inductance and capacitance present are dependent on various physical factors, and the effect on the line's associated reactances will be dependent upon the frequency applied. Since no dielectric is perfect (electrons will manage to move from one conductor to the other through the dielectric), there will be a conductance value for each type of two-wire transmission line (Deutsch *et al* 1990). This conductance value will represent the value of current flow that may be expected through the insulation. If the line is uniform (all values equal at each unit length), one small section of the line may be represented as shown in figure 4.1 (Miller 1983).

4.1.2 : Equivalent circuit

If given, values of resistance, capacitance, inductance, and conductance in the circuit (figure 4.1) would represent lumped values. It is convenient to analyse one section of the line at a time. To do this adequately, the values should be significant. This type of analysis is valid because at some operating frequency, these values will become highly significant and an integral part of either the output circuit of a stage or part of the input circuit of the next stage (Miller 1983). These values can cause decreased gain, distortion, and undesirable phase shifts (Sinnema 1979). To prevent these undesirable effects, the lumped values may be incorporated into the circuit as usable components, compensated for, or simply tolerated. However, it is important to know their effects to be able to understand the circuits that employ these values as usable components.

In many applications, the values of conductance and resistance are insignificant and may be neglected (Chilo and Arnaud 1984). If they are neglected, the circuit will appear as shown in figure 4.2 (Miller 1983). Notice that this network is terminated with a resistance that represents the impedance of the infinite number of sections exactly the same as the section of line under consideration. The termination is considered to be a load connected to the line.

4.1.3 : Characteristic impedance

A line infinitely long can be considered to be composed of an infinite number of inductors and capacitors. If a voltage is applied to the input terminals of the line, current will begin to flow. It will continue to flow as long as the capacitors and inductors were able to assume a charge. Since there are an infinite number of these sections of line, the current will flow indefinitely. If the infinite line were uniform, the impedance of each section will be the same as the impedance offered to the circuit by any other section of line of the same unit length. Therefore, the current would be of some finite value. If the

current flowing in the line and the voltage applied across it are known, the impedance of the infinite line can be determined using Ohm's law. This impedance is called the characteristic impedance, Z_0, of the line. If by some means the characteristic impedance of the line were measured at any point on the line away from the ends, it would be found that the characteristic impedance would be the same (Blake 1993) and is also sometimes called the surge impedance.

In figure 4.2 (Miller 1983) the distributed inductance of the line is divided equally into two parts in the horizontal arms of the T. The distributed capacitance is lumped and shown connected in the central leg of the T. The line is terminated in a resistance equal to that of the characteristic impedance of the line as seen across terminals A and B. Since the circuit in figure 4.2 is nothing more than a series-parallel LCR circuit, the impedance of the network may be determined by the formula that will now be developed. The impedance, Z_0, looking into terminals AB of figure 4.2 is

$$Z_0 = \frac{Z_1}{2} + \frac{Z_2\left[(Z_1/2) + Z_0\right]}{Z_2 + (Z_1/2) + Z_0} \tag{4.1}$$

Simplifying gives:

$$Z_0 = \frac{Z_1}{2} + \frac{(Z_1Z_2/2) + Z_0Z_2}{Z_2 + (Z_1/2) + Z_0} \tag{4.2}$$

Expressing the right-hand side in terms of the lowest common denominator leads to:

$$Z_0 = \frac{Z_1Z_2 + (Z_1^2/2) + Z_1Z_0 + (2Z_1Z_2/2) + 2Z_0Z_2}{2\left[Z_2 + (Z_1/2) + Z_0\right]} \tag{4.3}$$

Multiplying both sides of this equation by the denominator of the right-hand side, the

result obtained is:

$$2Z_0Z_2 + Z_0Z_1 + 2Z_0^2 = Z_1Z_2 + (Z_1^2/2) + Z_1Z_0 + (2Z_1Z_2/2) + 2Z_0Z_2 \qquad (4.4)$$

Simplifying to:

$$2Z_0^2 = 2Z_1Z_2 + \frac{Z_1^2}{2} \qquad (4.5)$$

or

$$Z_0^2 = Z_1Z_2 + \left(\frac{Z_1}{2}\right)^2 \qquad (4.6)$$

If the transmission line is to be accurately represented by an equivalent network, the T-network section of figure 4.2 must be replaced by an infinite number of similar sections (Miller 1983). Thus, the distributed inductance in the line will be divided into n sections, instead of the number (2) as indicated in the last term of equation (4.6). As the number of sections approaches infinity, the last term Z_1/n will approach zero. Therefore:

$$Z_0 = \sqrt{Z_1Z_2} \qquad (4.7)$$

Since the term Z_1 represents the inductive reactance and the term Z_2 represents the capacitative reactance:

$$Z_0 = \sqrt{2\pi fL\frac{1}{2\pi fC}} \qquad (4.8)$$

and therefore:

$$Z_0 = \sqrt{\frac{L}{C}} \qquad (4.9)$$

The derivation resulting in equation (4.9) shows that an ideal transmission line's characteristic impedance is dependent upon its inductance and capacitance.

4.2 : Propagation of DC Voltage Along a Transmission Line

4.2.1 : Physical explanation of propagation

To better understand the characteristics of a transmission line with an AC voltage applied, the infinitely long transmission line will first be analysed with a DC voltage applied. This will be accomplished using the circuit shown in figure 4.3 (Miller 1983). In this circuit the resistance of the line is not shown, and therefore the line will be assumed to be loss-free; i.e. lossless.

Considering only the capacitor C_1 and the inductor L_1 as a series circuit, when voltage is applied to the network, capacitor C_1 will have the ability to charge through inductor L_1. It is characteristic of an inductor that at the first instant of time when voltage is applied, a maximum voltage is developed across it and minimum current is permitted to flow through it (Duffin 1965). At the same time, the capacitor will have a minimum of voltage across it and a tendency to pass a maximum current (Duffin 1965). The maximum current is not permitted to flow at the first instant because of the action of the inductor, which is in the charge path of the capacitor. At this time the voltage across points *c* and *d* is zero. Since the remaining portion of the line is connected to points *c* and *d*, there will be 0V developed across it at the first instant of time. The voltage across the rest of the line is dependent on the charging action of the capacitor, C_1. It will require some finite time for capacitor C_1 to charge through inductor L_1. As capacitor C_1 is charging, the ammeter records the changing current. When C_1 charges to a voltage which is near to the

value of the applied voltage, capacitor C_2 will begin to charge through inductors L_1 and L_2. The charging of capacitor C_2 will again require time. In fact the time required for the voltage to reach points *e* and *f* from points *c* and *d* will be the same time as was necessary for the original voltage to reach points *c* and *d*. This is true because the line is uniform, and the values of the reactive components are the same throughout its entire length. This action will continue in the same manner until all of the capacitors in the line are charged. Since the number of capacitors in an infinite line is infinite, the time required to charge the entire line would be an infinite amount of time. It is important to note that current is flowing continuously in the line and that it has some finite value.

4.2.2 : Velocity of propagation

When an electromagnetic field is moving down the line, its associated electric and magnetic fields are said to be propagated down the line (Blake 1993). It was found and mentioned previously that time was required to charge each unit section of the line, and if that line were infinitely long, the line would require an infinitely long time to charge. The time for a field to be propagated from one point on a line to another may be computed, for if the time and the length of the line are known, the velocity of propagation may be determined. The network shown in figure 4.4 (Miller 1983) will be used to compute the time required for the voltage wavefront to pass a section of line of specified length. The total charge (Q) in coulombs on capacitor C_1 is determined by the relationship:

$$Q = CE \tag{4.10}$$

Since the charge on the capacitor in the line has its source at the battery, the total amount of charge removed from the battery will be equal to:

$$Q = IT \tag{4.11}$$

Because these charges are equal, they may be equated thus:

$$CE = IT \tag{4.12}$$

As the capacitor C_1 charges, capacitor C_2 contains a zero charge. Since capacitor C_1's voltage is distributed across C_2 and L_2, at the same time the charge on C_2 is practically zero, the voltage across C_1 (points *c* and *d*) must be, by Kirchoff's law, entirely across L_2. The value of the voltage across the inductor is given by:

$$e = L\frac{\Delta i}{\Delta t} \tag{4.13}$$

Since current and time start at zero, the change in time and the change in current are equal to the final current and the final time. Equation (4.13) becomes:

$$ET = LI \tag{4.14}$$

Solving the equation for I:

$$I = \frac{ET}{L} \tag{4.15}$$

Solving equation (4.12), that was a statement of the equivalency of the charges, for current gives:

$$I = \frac{CE}{T} \tag{4.16}$$

Equating both of these expressions gives:

$$\frac{ET}{L} = \frac{CE}{T} \tag{4.17}$$

Solving the equation for T:

$$T^2 = LC \tag{4.18}$$

or

$$T = \sqrt{LC} \tag{4.19}$$

Since velocity is both a function of time and distance, the formula for computing propagation velocity is:

$$V_p = \frac{D}{\sqrt{LC}} \tag{4.20}$$

where V_p is the velocity of propagation, and D is the distance of travel.

It should again be noted that the time required for a wave to traverse a transmission line segment will depend on the value of L and C and that these values will be different, depending on the type of transmission line considered.

4.3 : Loading of the Line

4.3.1 : Maximum power transfer

Up to this point, only transmission lines that are terminated in a resistive load equal to the characteristic impedance of the line have been considered. This is the ideal case and

certainly the target condition, but other load conditions are found that are less than ideal. Maximum power transfer occurs when the load is resistive and equal to the characteristic impedance of the line and, furthermore, when the line impedance is equal to the source impedance. Under these arrangements, the highest percentage of transmitter output power will appear across the line-terminating impedance (Sinnema 1979).

4.3.2 : Nonresonant lines

The conditions for maximum power transfer describe a transmission line that is termed nonresonant. The load is resistive and matches the characteristic impedance of the line. All of the power put into the line by the transmitter will move down the line and appear across the load resistance (minus some small conductor losses) (Deutsch *et al* 1990).

4.3.3 : Resonant lines

The transmission line is termed resonant when the load impedance does not match the line impedance or is not purely resistive. The load impedance may be either larger or smaller than the characteristic impedance of the line and may also be resistive and reactive. The energy sent down the line by the transmitter is not all absorbed by the load (Djordevic et al 1987). The quantity of energy not absorbed, is reflected back up the line to the transmitter. There are now two energy waves moving through the line at the same time, but in opposite directions. The incident wave is the wavefront moving from the source to the load, and the reflected wavefront moves in the opposite direction, along the line from the load back toward the source. Both waves are continuous in nature; that is to say, for an AC signal, there are two sinewaves moving through the line in opposite directions at the same time (Blake 1993). There will be moments in time when the waves will be in phase or antiphase.

Although the incident wave and the reflected wave are constantly in motion along the line, the positions along the line where the waves add together and cancel each other do not move at all. This creates a standing wave of voltage along the line that is stationary. The minimum value of the standing wave voltage may go to 0V, and the crest of the standing voltage wave will reach a maximum of twice the source peak voltage ($2V_s$). Figure 4.5 shows the basic configuration used for simulating a resonant transmission line.

4.3.4 : Reflection Coefficient (ρ)

The lower-case Greek letter rho (ρ) is used as a symbol for the reflection coefficient. The value itself is a decimal number used to represent the percentage of energy coming down the line that is not absorbed by the load, in other words, the percentage of reflected energy. The coefficient can be determined by any of several standard ratios (Sinnema 1979):

$$\rho = \begin{cases} \dfrac{E_{reflected}}{E_{applied}} \\ \dfrac{E_{max} - E_{min}}{E_{max} + E_{min}} \\ \dfrac{Z_L - Z_0}{Z_L + Z_0} \end{cases} \tag{4.21}$$

This is depicted in figure 4.5 where:

$$V_{in} = \frac{Z_0}{Z_0 + Z_{in}} V_S \tag{4.22}$$

$$V_{out} = V_{in}(1 + \rho_{out}) \tag{4.23}$$

$$\rho_{out} = \frac{Z_L - Z_0}{Z_L + Z_0} \tag{4.24}$$

The reflection coefficient at the input end, ρ_{in}, is given by:

$$\rho_{in} = \frac{Z_{in} - Z_0}{Z_{in} + Z_0} \tag{4.25}$$

4.4 : Limits of Load Impedance

The load impedance is ideal when it is equal to the characteristic line impedance. In reality, the load impedance could be any value between zero and infinity. There are only a few occasions when the load would be open circuit ($Z_L = \infty$) or when the load would be short circuited ($Z_L = 0$), but it be easy to see and understand that these are the extreme limits. In practice, it would be unusual to find the load impedance different from the line impedance by more than a factor of 5.

4.5.1 : Open circuit load impedance

When the load impedance is removed, the output end of the transmission line becomes an open circuit and therefore an infinite impedance. A train of waves moving through the transmission line from the source will reach the open end of the line and encounter an impedance that will absorb no energy at all; the wave is therefore completely reflected back up the line to the source (Sinnema 1979).

Since there is no current through an open circuit, the voltage at the open circuit terminals is at a maximum, and equal to twice the peak source voltage. Looking at the voltage as it moves back up the line toward the source, we can see that the incident wave and the

reflected wave start to add and cancel at points along the line.

For an open circuit line, at the load end, ρ_{out}, is given by

$$\rho_{out} = \frac{\infty - Z_0}{\infty + Z_0} = \frac{\infty}{\infty} = 1 \qquad (4.26)$$

Figure 4.6 shows the basic configuration used for simulating a transmission line with an open circuit load. Using the reflection coefficients, at the input and output ends of the line a reflection diagram may be constructed which gives an accurate analysis of the voltages, seen at the sending and receiving ends for an ideal transmission line.

For simulation of a line with an open circuit load the following parameters were used; Z_{in} = 100Ω, Z_0 = 200Ω, and time delay, T_d = 10 (arbitrary units). The mismatch at the sending end of the line is used otherwise the resulting reflection diagram would be of little interest. The reflection diagram obtained is shown in figure 4.7, where the voltage values in the boxes represent the voltage at particular points along the line; both at the sending and receiving ends of the line. This voltage, V_{sum}, is given by

$$V_{sum} = V_{prev} + V^+ + V^+.\rho \qquad (4.27)$$

where V_{prev} is the previous voltage apparent at that point on the line, V^+ is the transmission voltage moving towards the end of the line, ρ is the reflection coefficient for that end of the line, and V_{sum} is the new voltage apparent after the voltage wavefront has reached the end of the line.

The transient response of the open circuit is given in figure 4.8, where the received signal has undergone many multilevel transitions.

4.5.2 : Short circuit load impedance

The same general conditions apply to the short circuit load. That is, the source still feeds a train of pulses down the line, and the short circuit load, reflects the total energy back toward the source. The reflected wave, however, is not the same as for the open circuit load conditions, because here Z_L is equal to zero. The current through zero resistance is at its maximum value, while the voltage drop across the short circuit is at its minimum (or zero).

For a short circuit load, the reflection coefficient at the receiving end, is given by:

$$\rho_{out} = \frac{0 - Z_0}{0 + Z_0} = -1 \qquad (4.28)$$

Figure 4.9 shows the basic configuration used for the simulation of transmission lines with a short circuit load, where the output end of the line is connected directly to ground. A single transmission line would not however be used in this configuration, but may be used in other configurations for shaping of a signal received on a line adjacent to the short circuited line (Long and Butner 1990).

For simulation of the line with a short circuit load, the same line parameters are used as for the case of an open circuit line; Z_{in} = 100Ω, Z_0 = 200Ω, T_d = 10 (arbitrary units). Figure 4.10 shows the reflection diagram obtained using these parameters and the transient representation is displayed in figure 4.11. The short circuit load has a severely detrimental effect upon the signal at the input end of the line, with the signal becoming significantly negative after the falling edge of the input pulse.

4.5 : Discontinuities

A discontinuity is a point on a line at which the impedance changes (Chen and Gao 1989, Nam *et al* 1989, Orhanovic *et al* 1990, Oh and Schutt-Aine 1993). This may be caused by a change in line width, a bend in the line, or the intersection of three or more lines at the same point.

4.5.1 : Effect of a step change in line width

If two lines of different impedances are joined together (figure 4.12(a)) (e.g. a line joined to a connection pad of a larger size) (Chen and Li 1991) the reflection coefficient at the intersection of the lines for a signal travelling in the forward direction will be different from that for a signal travelling in the backward direction.

The forward reflection coefficient, ρ_{for}, is given by:

$$\rho_{for} = \frac{Z_2 - Z_1}{Z_1 + Z_2} \tag{4.29}$$

with the backward reflection coefficient, ρ_{back}, is given by:

$$\rho_{back} = \frac{Z_1 - Z_2}{Z_1 + Z_2} \tag{4.30}$$

From the above two equations it can be seen that:

$$\rho_{back} = -\rho_{for} \tag{4.31}$$

The configuration shown in figure 4.12(b) is used for simulating the effect of a step

change in the impedance of a microstrip transmission line. For the simulation carried out, the following load parameters are used; $Z_{in} = 50\Omega$, $Z_L = 400\Omega$, $Z_1 = 100\Omega$, $Z_2 = 200\Omega$. These parameters give rise to the following set of reflection coefficients (referred to in figure 4.13), $\rho_{in} = -1/3$, $\rho_{for} = 1/3$, $\rho_{back} = -1/3$, $\rho_{out} = 1/3$. The results of the simulation using these parameters is given in figure 4.13; whereas before the voltage values at the sending and receiving ends of the lines are in boxes and calculated using equation (4.27). The reflected voltage, $V_{reflect}$, is shown in smaller typeface next to the boxes showing the voltages at the points on the line. The voltage at the intersection of the two lines, V_{inter} (also in boxes), is calculated by:

$$V_{inter} = V_{prev} + V_{for} + V_{for} \cdot \rho_{for} + V_{back} + V_{back} \cdot \rho_{back} \qquad (4.32)$$

where V_{for} is the voltage travelling in the forward direction, and V_{back} is the voltage front travelling in the backwards direction. The voltage travelling away from the intersection in the forward direction, V_{intfor}, is given by:

$$V_{intfor} = V_{for} + V_{for} \cdot \rho_{for} + V_{back} \cdot \rho_{back} \qquad (4.33)$$

and the voltage travelling away from the intersection in the backward direction, $V_{intback}$, is given by:

$$V_{intback} = V_{back} + V_{back} \cdot \rho_{back} + V_{for} \cdot \rho_{for} \qquad (4.34)$$

The transient representation of the results is given in figure 4.14 where it is seen that the output pulse undergoes some distortion, but the overall shape of the pulse is preserved. This output pulse would probably be good enough for use within a logic circuit, without any possibility of an error in logic occuring.

4.5.2 : Bent microstrip line

A bend in a microstrip line introduces a different problem, in that the section of the line making up the corner will almost certainly have a different impedance from that of the two adjoining parts of the line. Figure 4.15(a) shows a schematic representation of a bend in a microstrip line, and how the line may be split into separate lines of differing impedances.

The configuration shown in figure 4.15(b) can be used to simulate a discontinuity such as a bend in a microstrip line (Zheng and Chang 1990, Huang and Wing 1991, Sabban and Gupta 1992, Harms and Mittra 1993) where the impedance Z_2 represents the corner section of the bend, which would be different from that of the two adjoining lines. This configuration will lead to multiple reflections thus introducing distortion to the signal (Huang and Wing 1991). With this type of discontinuity the impedances Z_1 and Z_3 will generally be equal.

Figure 4.16 shows the reflection diagram for the simulation of a bent microstrip line with the following parameters; $Z_{in} = 50\Omega$, $Z_1 = Z_3 = 100\Omega$, $Z_2 = 200\Omega$, $Z_L = 1000\Omega$, and the time delay of all lines being 10 (arbitrary units). These parameters give rise to the following set of reflection coefficients (shown in figure 4.16); $\rho_{in} = -1/3$, $\rho_{afor} = 1/3$, $\rho_{aback} = -1/3$, $\rho_{bfor} = -1/3$, $\rho_{bback} = 1/3$, $\rho_{out} = 0.818$. The voltages at the sending and receiving ends of the line are calculated using equation (4.27), and the voltages at points a and b, the intersections at the bend in the line, are calculated using equation (4.32).

Figure 4.17 shows the transient analysis results from the simulation carried upon the bent microstrip. The signal received at the output end still retains the essential pulse shape, although the top of the pulse has become distorted. A bend within a microstrip would appear not to be as detrimental to the received signal, as may at first be thought.

4.5.3 : Multiple line intersections

Another type of discontinuity which may occur is when more than two lines intersect at the same point (figure 4.18(a)) (Blood 1988). Within a high speed logic circuit it may be required to connect the output of an IC, which may act a source to more than one device, and therefore a microstrip may be branched several times in order that this may be achieved (Blood 1988). Within some microwave circuits it is necessary to introduce stub interconnections in order to give a transmission line the correct characteristics (Sinnema 1979).

For a forward travelling signal going from line 1 into lines 2 and 3 (figure 4.18(b)), the reflection coefficient, ρ_{inter}, is given by:

$$\rho_{inter} = \frac{Z_L - Z_1}{Z_L + Z_1} \tag{4.35}$$

where

$$Z_L = \frac{Z_2 Z_3}{Z_2 + Z_3} \tag{4.36}$$

If $Z_1 = Z_2 = Z_3 = Z_0$ (the simplified case) the following can be calculated from equations (4.35) and (4.36).

$$Z_L = \frac{1}{2} Z_0 \tag{4.37}$$

$$\rho_{inter} = \frac{\frac{1}{2}Z_0 - Z_0}{\frac{1}{2}Z_0 + Z_0}$$

$$= -\frac{\frac{1}{2}Z_0}{\frac{3}{2}Z_0} \qquad (4.38)$$

$$= -\frac{1}{3}$$

For the purposes of simplicity the following parameters were chosen; $Z_1 = Z_2 = Z_3 = 100\Omega$, $R_{in} = 100\Omega$, $R_{L1} = 1000\Omega$, $R_{L2} = 100\Omega$. These parameters were chosen so that there would be no reflections produced at the input end of line 1, and no reflections produced at the output end of the stub section of line. This is to make the calculation of voltages travelling away from the intersection easier. With more than one voltage wavefront meeting at an intersection at the same time the calculation would become very cumbersome and difficult to carry out by hand.

The resulting reflection diagram is shown in figure 4.19. For a given voltage, V_{intin}, entering the intersection from one of the three lines, the voltage that travels down the other two lines, V_{intout}, is given by:

$$V_{intout} = V_{intin} + V_{intin} \cdot \rho_{inter} \qquad (4.39)$$

where, V_{intin} is the voltage wavefront travelling towards the intersection of the lines, and ρ_{inter} is the reflection coefficient of the intersection.

The transient analysis results are displayed in figure 4.20, from which it can be seen that the signal seen at output end 1, may not be of the required magnitude for a logic circuit, but has preserved its overall pulse shape better than the output signals seen for both a microstrip with a step width change and that for a bent microstrip. However the output signal seen at output end 2 (matched load), would definitely not be adequate for use in a logic circuit.

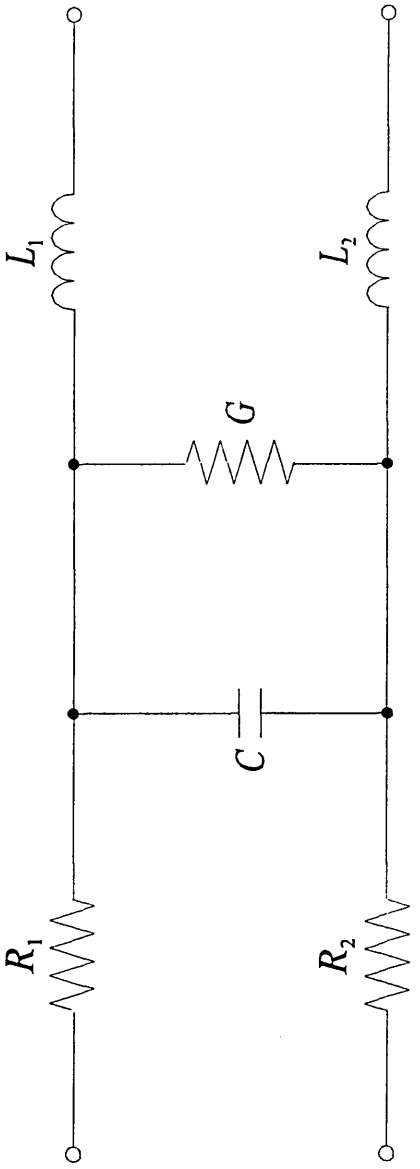

Figure 4.1 : Equivalent circuit for a two wire transmission line.

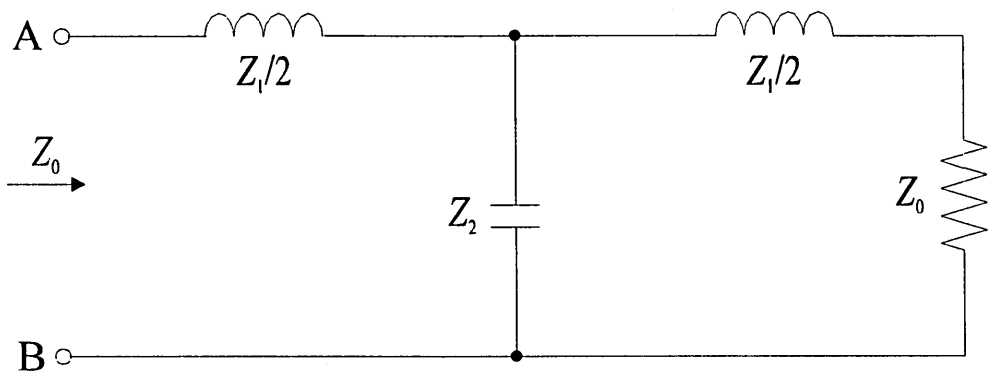

Figure 4.2 : Simplified circuit terminated with its characteristic impedance.

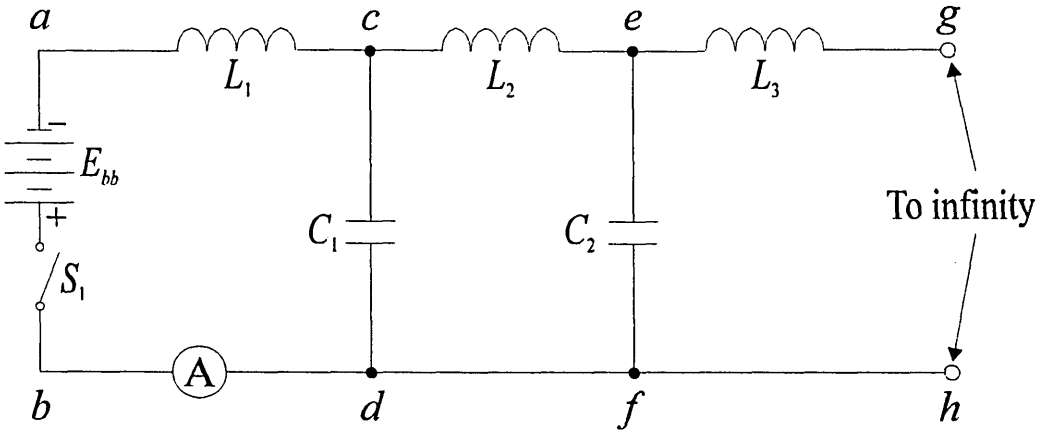

Figure 4.3: D.C. voltage applied to a transmission line.

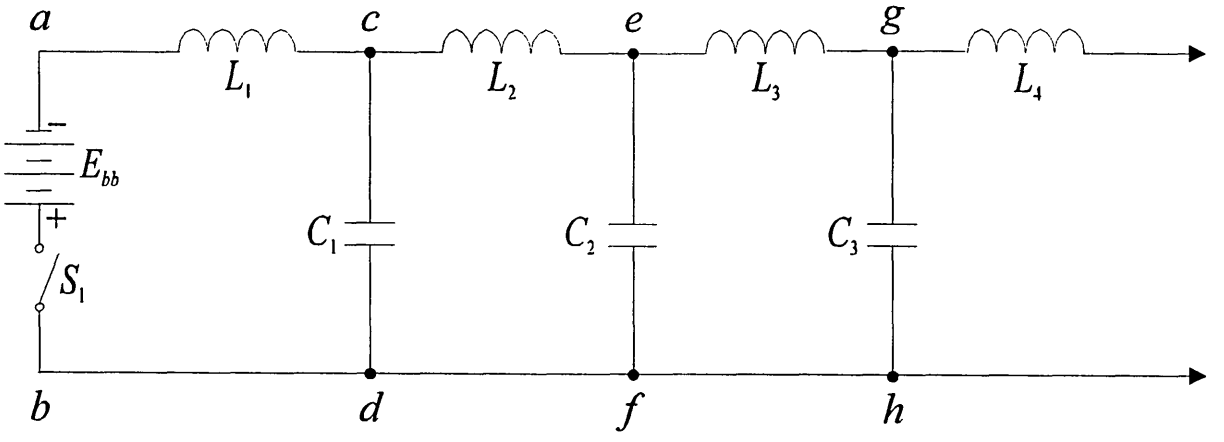

Figure 4.4: Circuit for computing the time of travel.

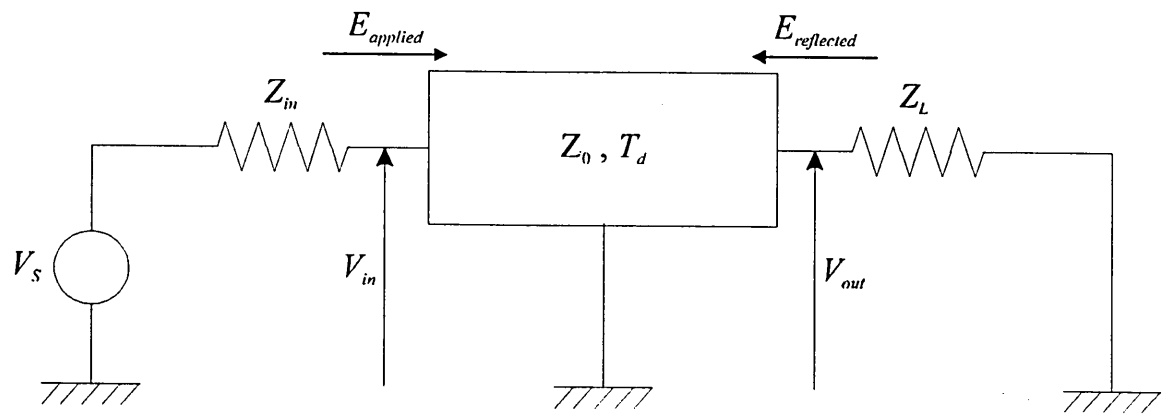

Figure 4.5: Basic transmission line configuration.

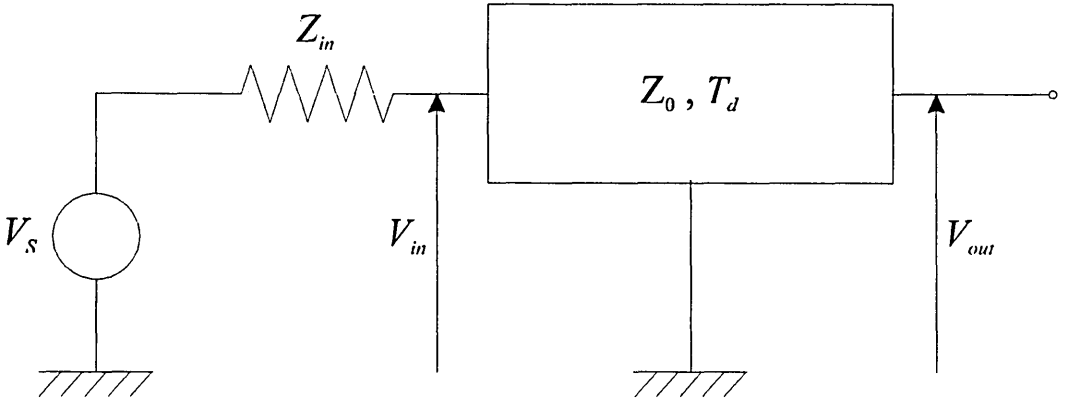

Figure 4.6: Basic configuration for open circuit load.

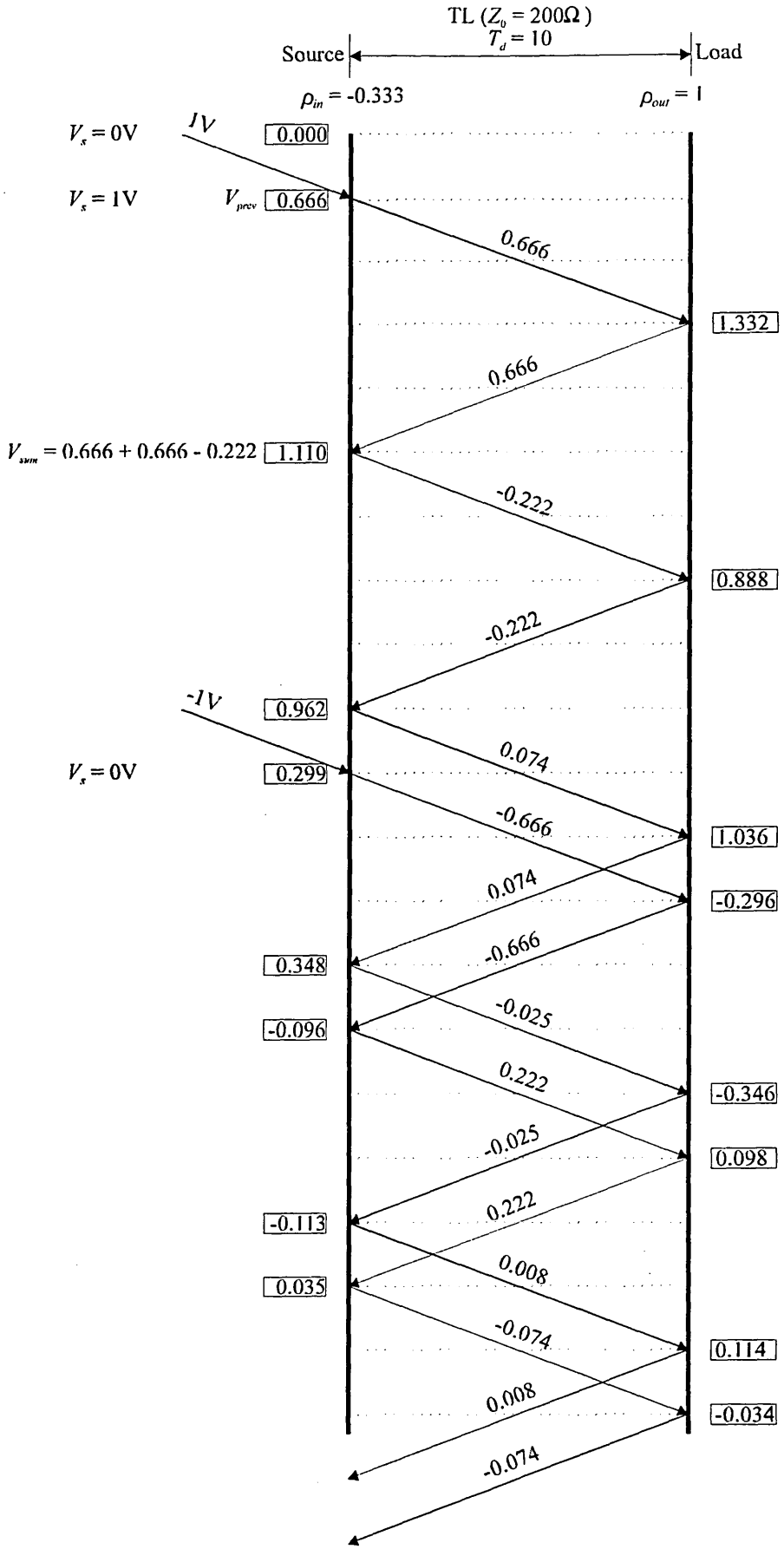

Figure 4.7: Reflection diagram for an open circuit load, Z_{in} = 100Ω, Z_0 = 200Ω.

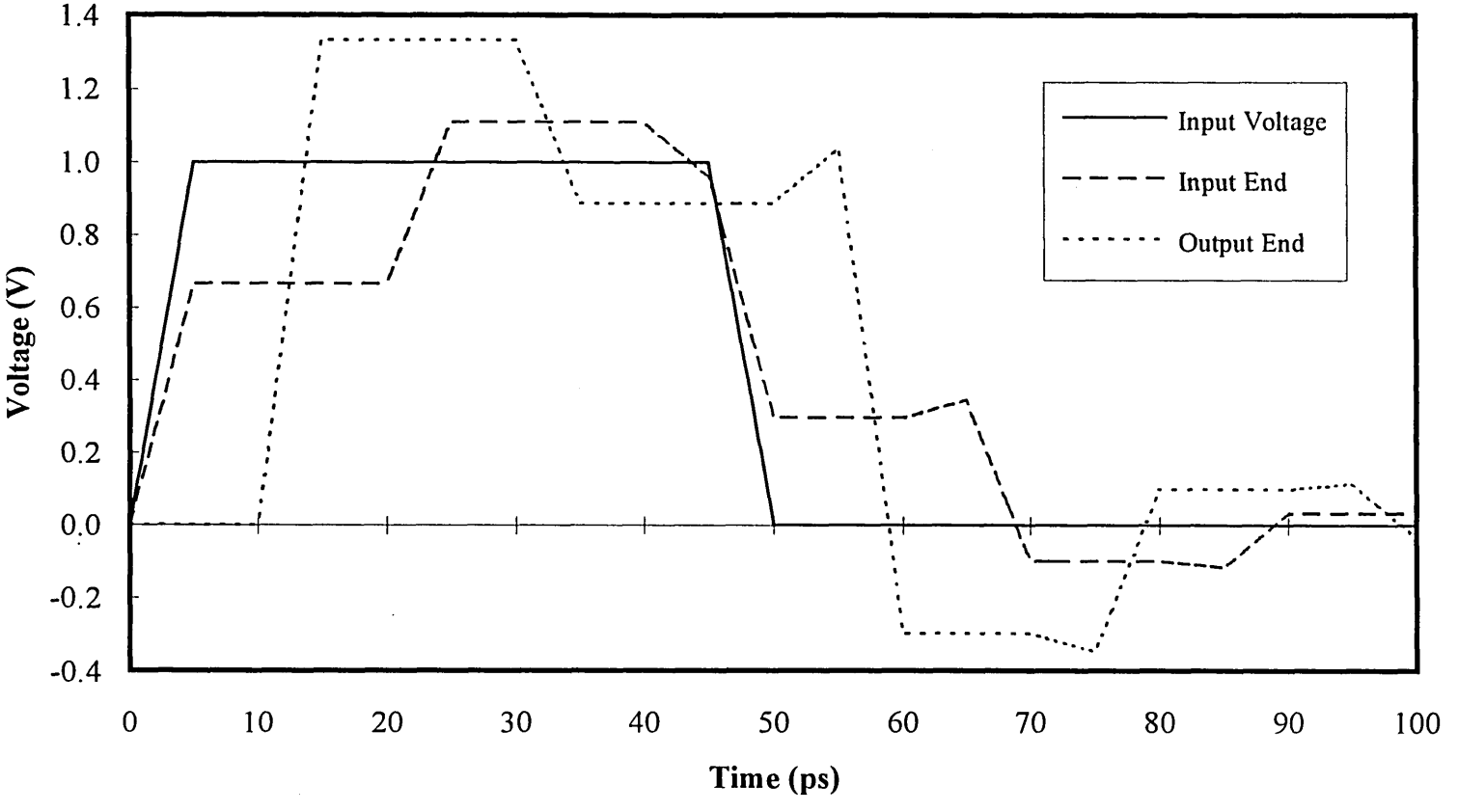

Figure 4.8 : Transient representation of signals for a line with an open circuit load.

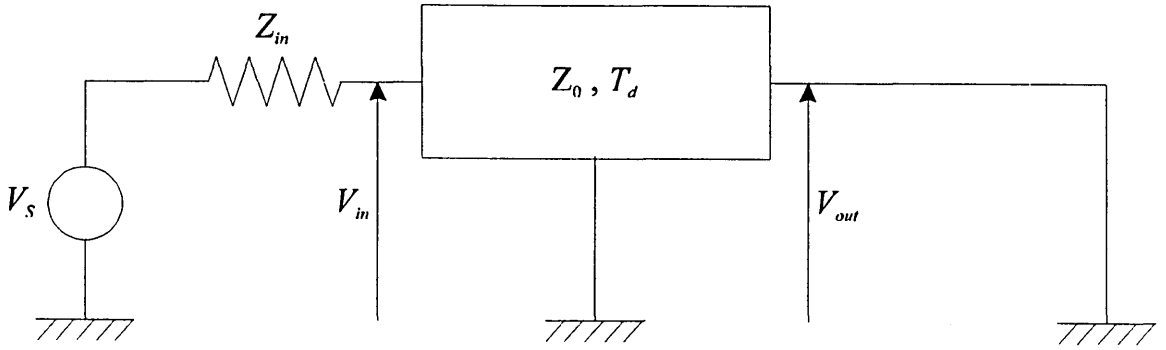

Figure 4.9: Configuration of a short circuit load.

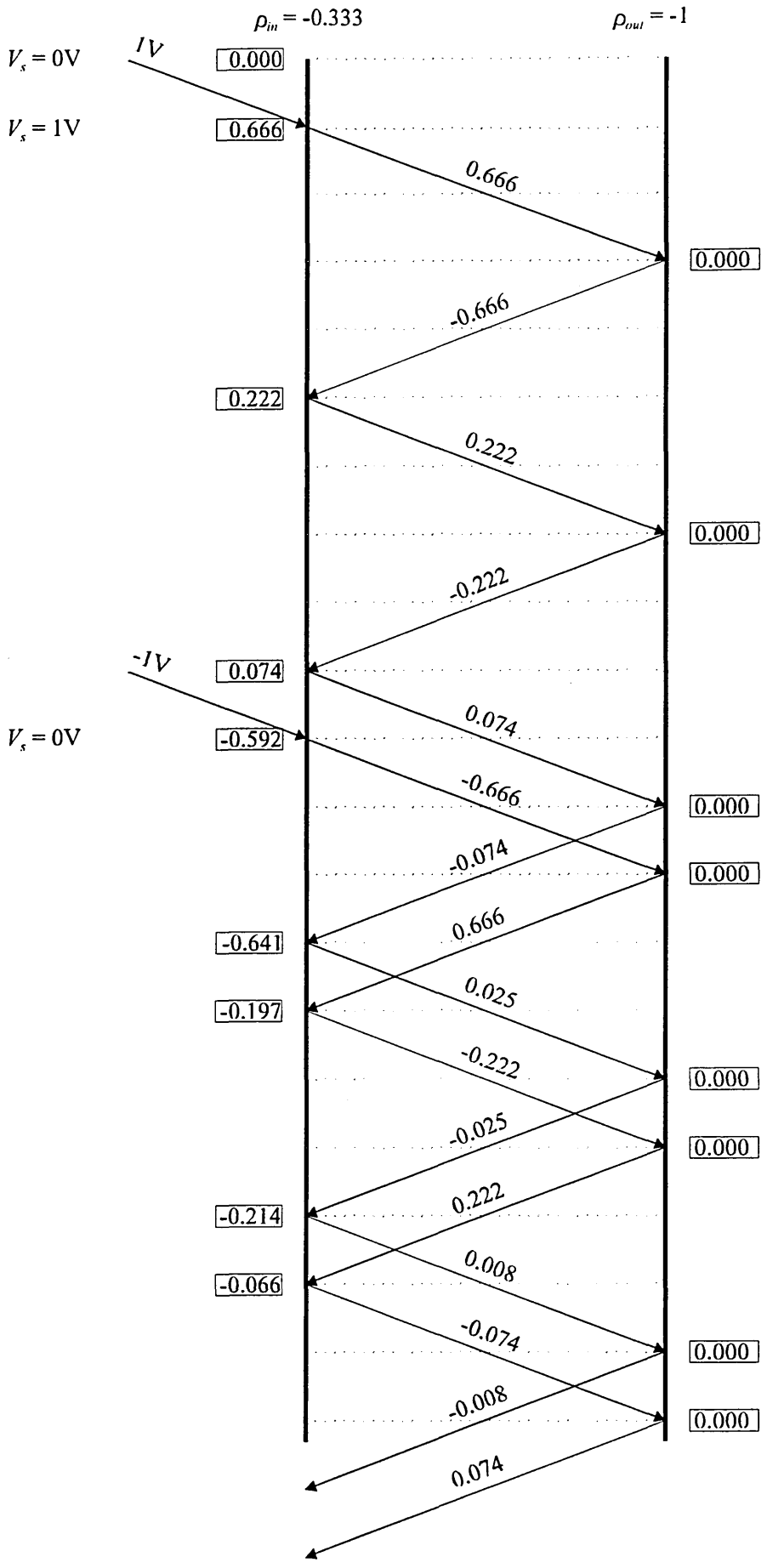

Figure 4.10 : Reflection diagram for short circuit load, Z_{in} = 100Ω, Z_0 = 200Ω.

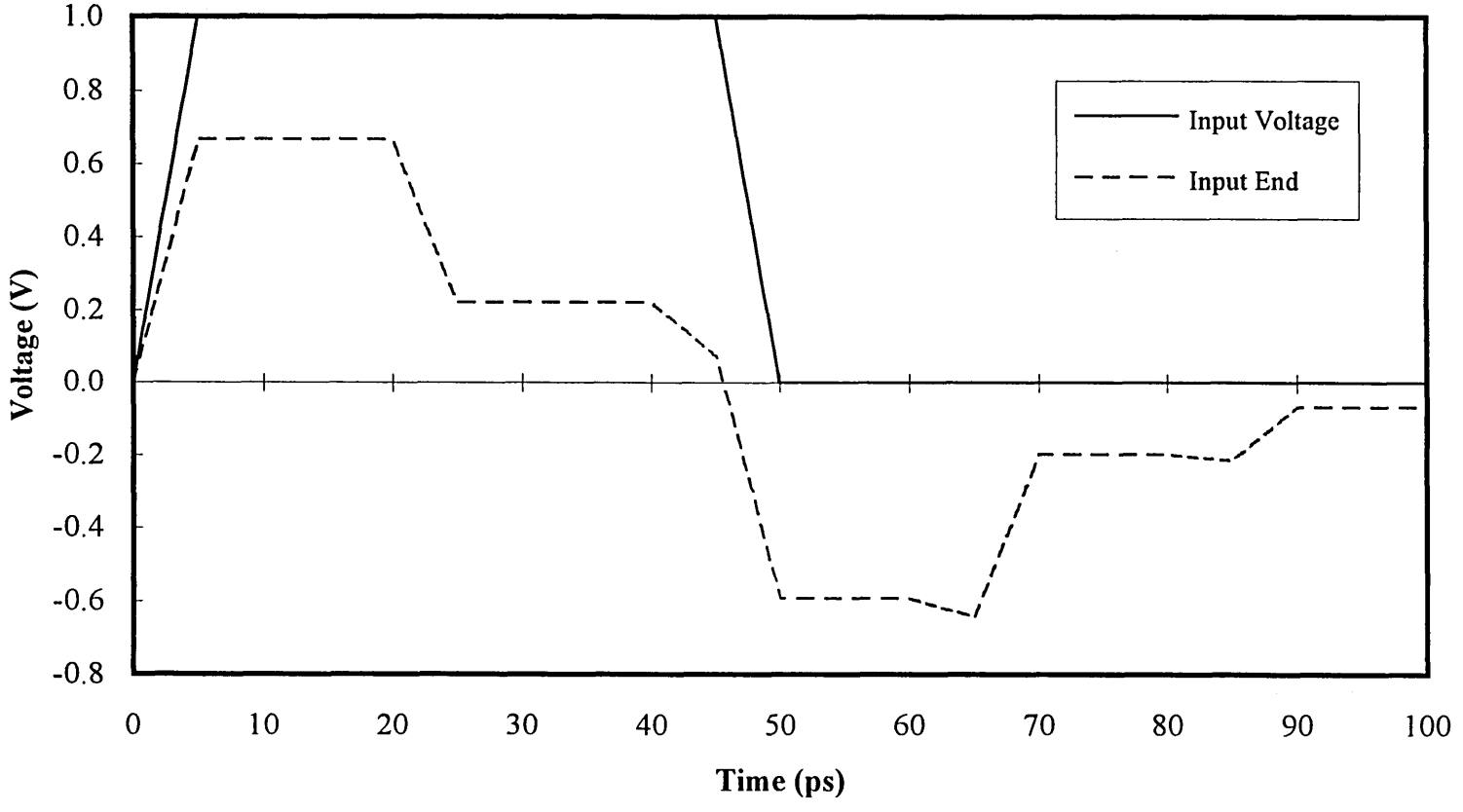

Figure 4.11 : Transient representation of a line with a short circuit load.

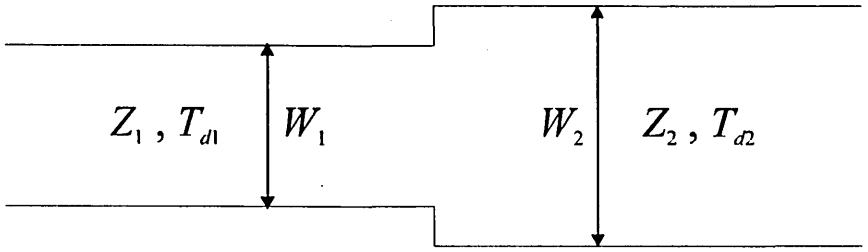

(a)

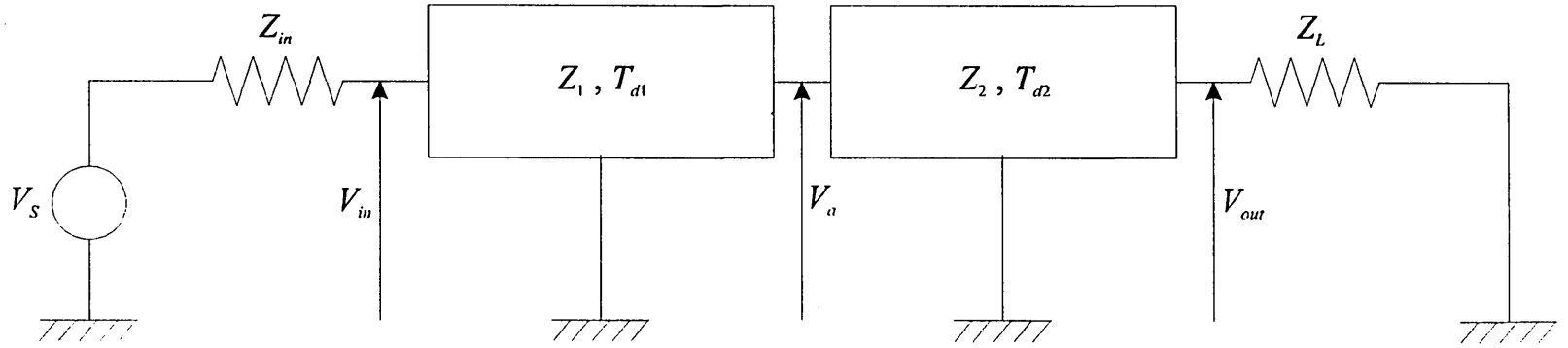

(b)

Figure 4.12: (a) Representation of intersection between two lines. (b) Basic equivalent circuit for intersection of two lines.

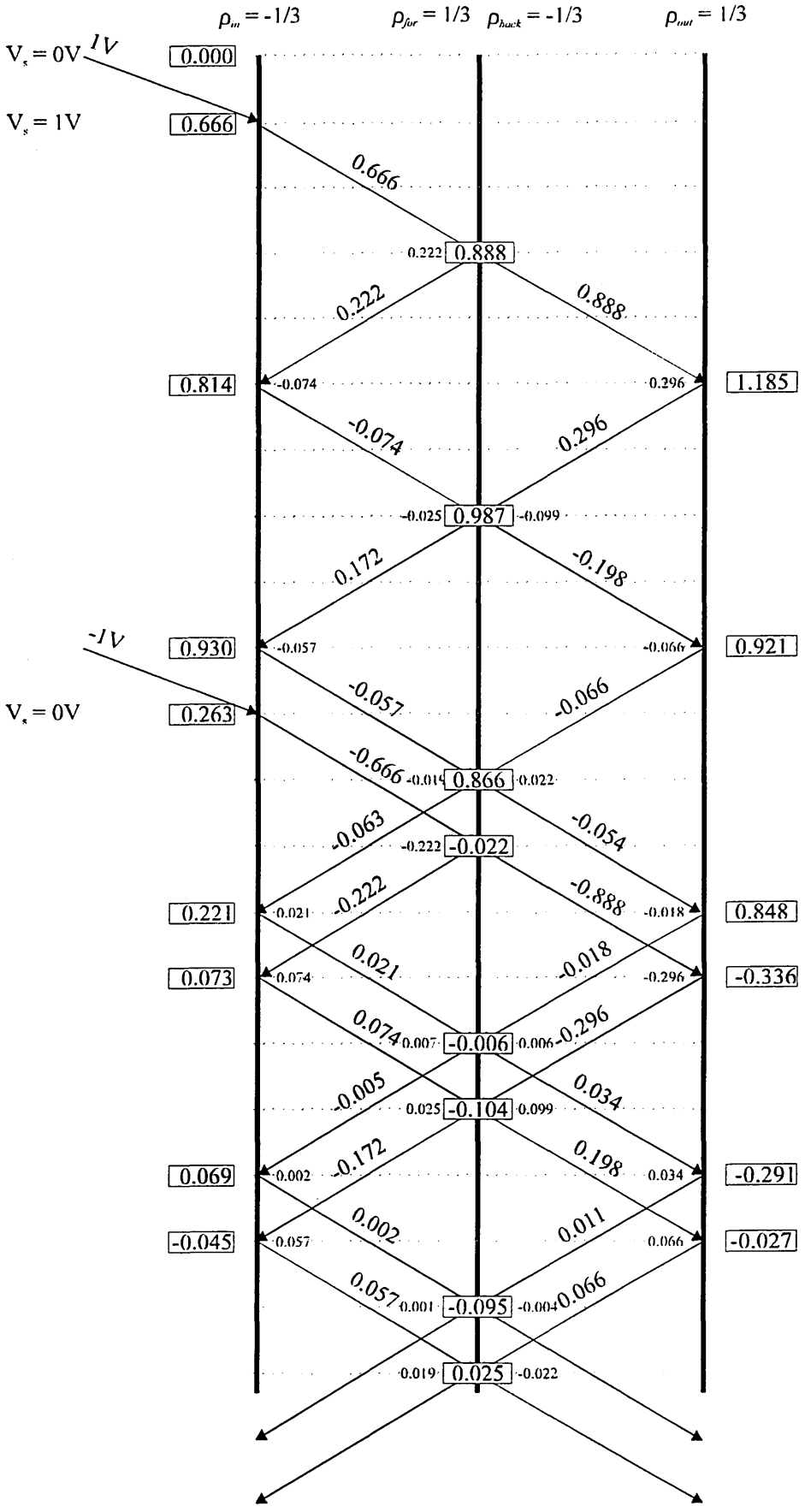

Figure 4.13: Reflection diagram for intersection of two lines, Z_{in} = 50Ω, Z_L = 400Ω, Z_1 = 100Ω, Z_2 = 200Ω.

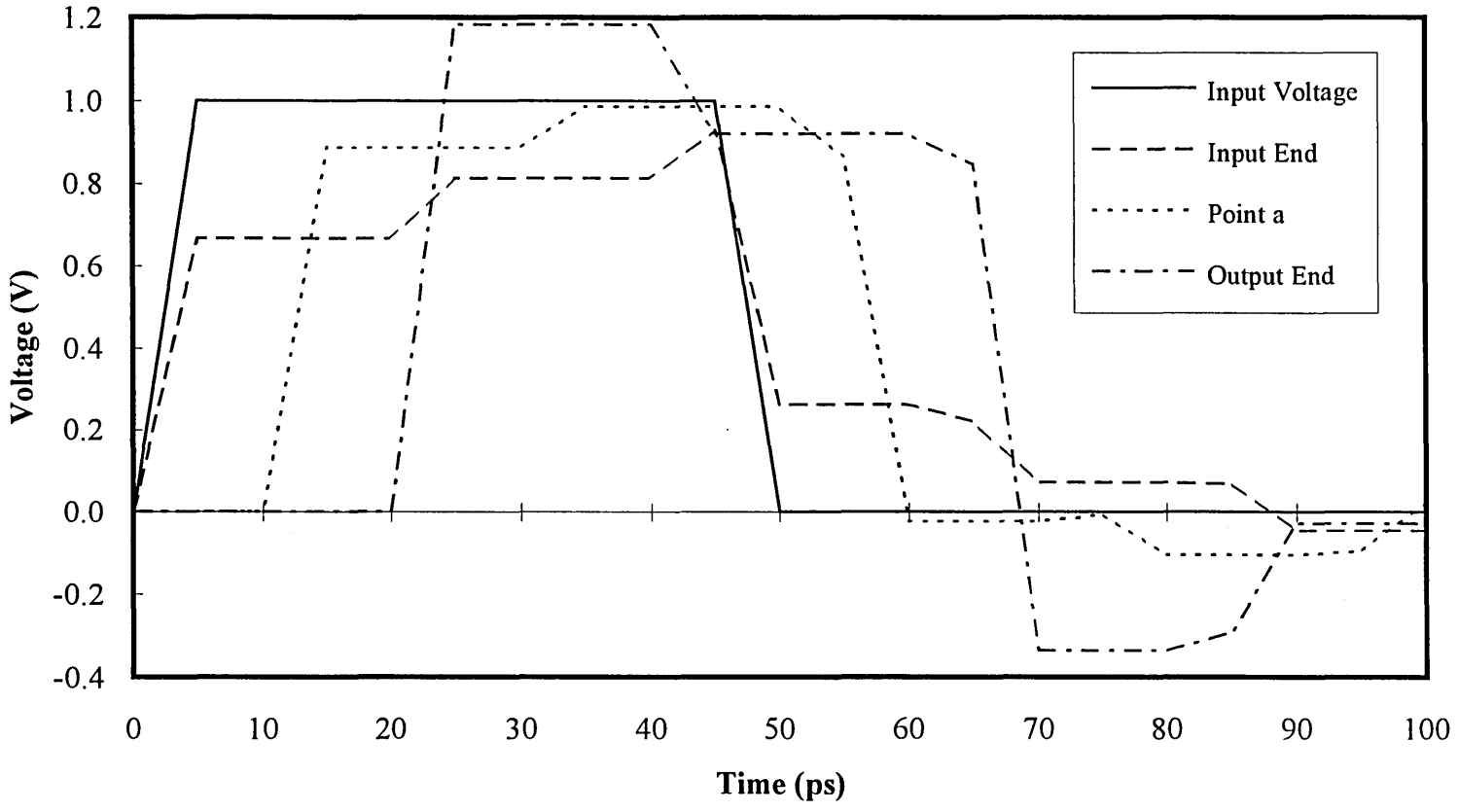

Figure 4.14 : Transient results for line with a step change in impedance.

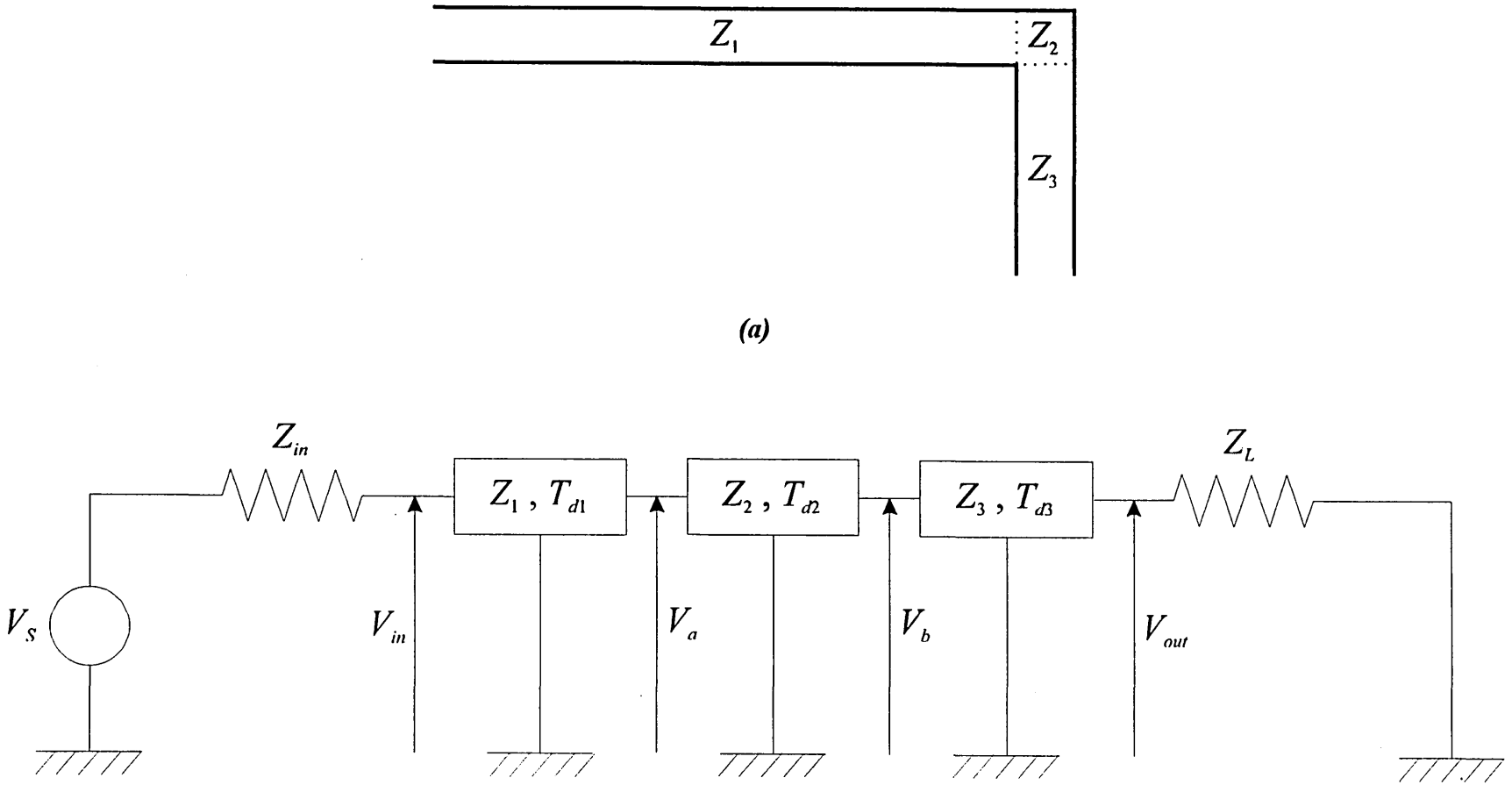

Figure 4.15: (a) Schematic representation of a microstrip bend. (b) Basic equivalent circuit for a microstrip bend.

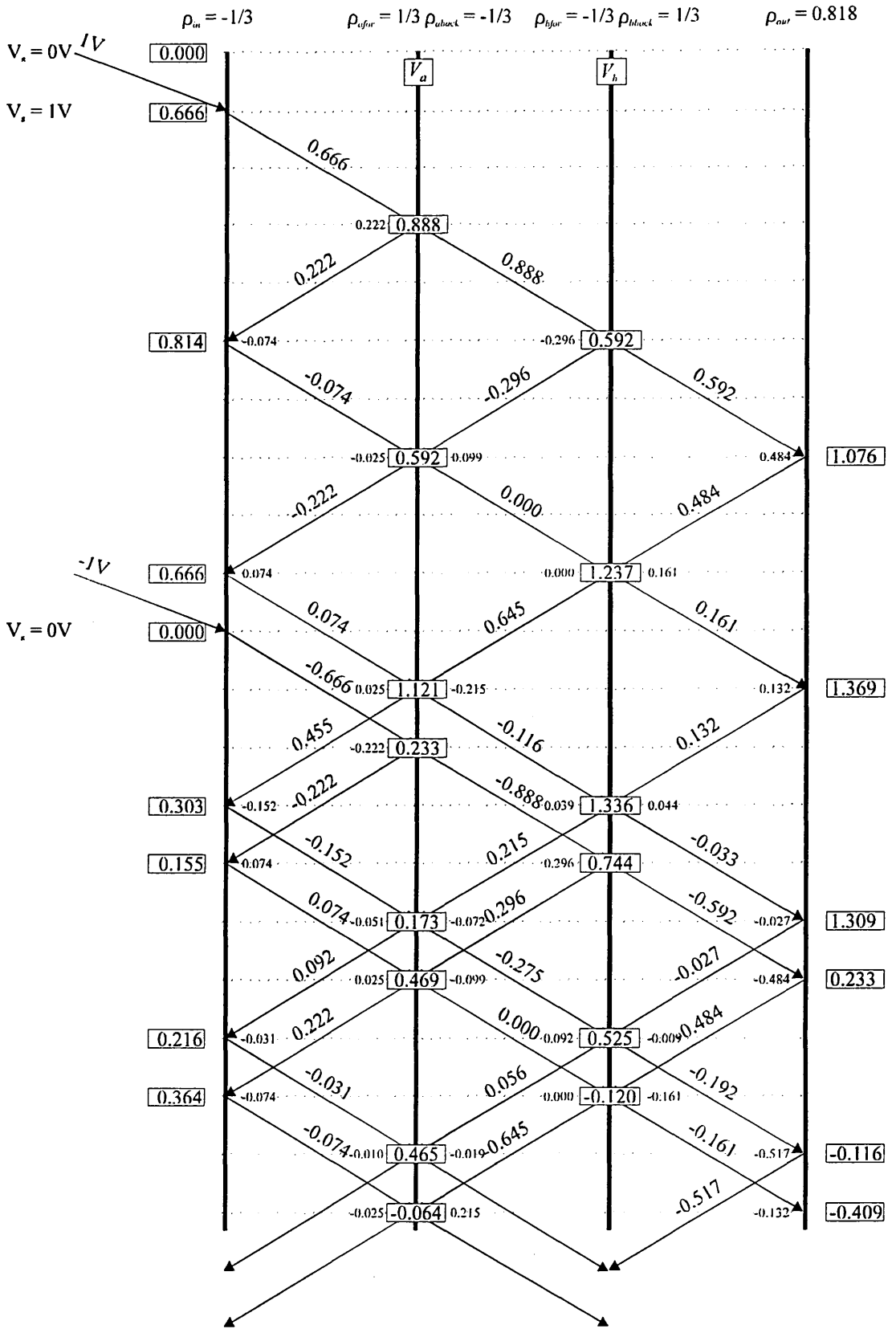

Figure 4.16: Reflection diagram for a microstrip bend.

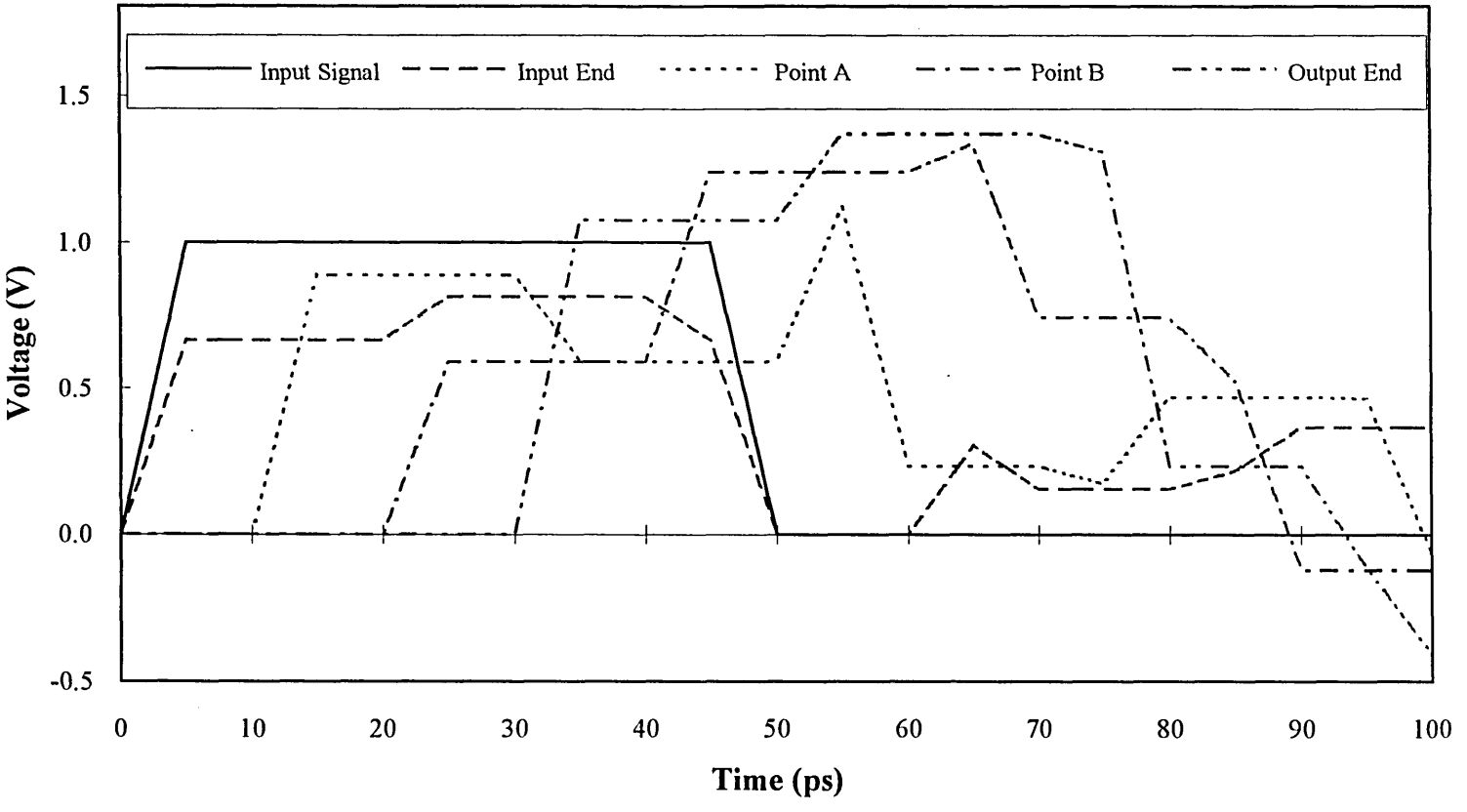

Figure 4.17 : Transient signal analysis for a bent microstrip line

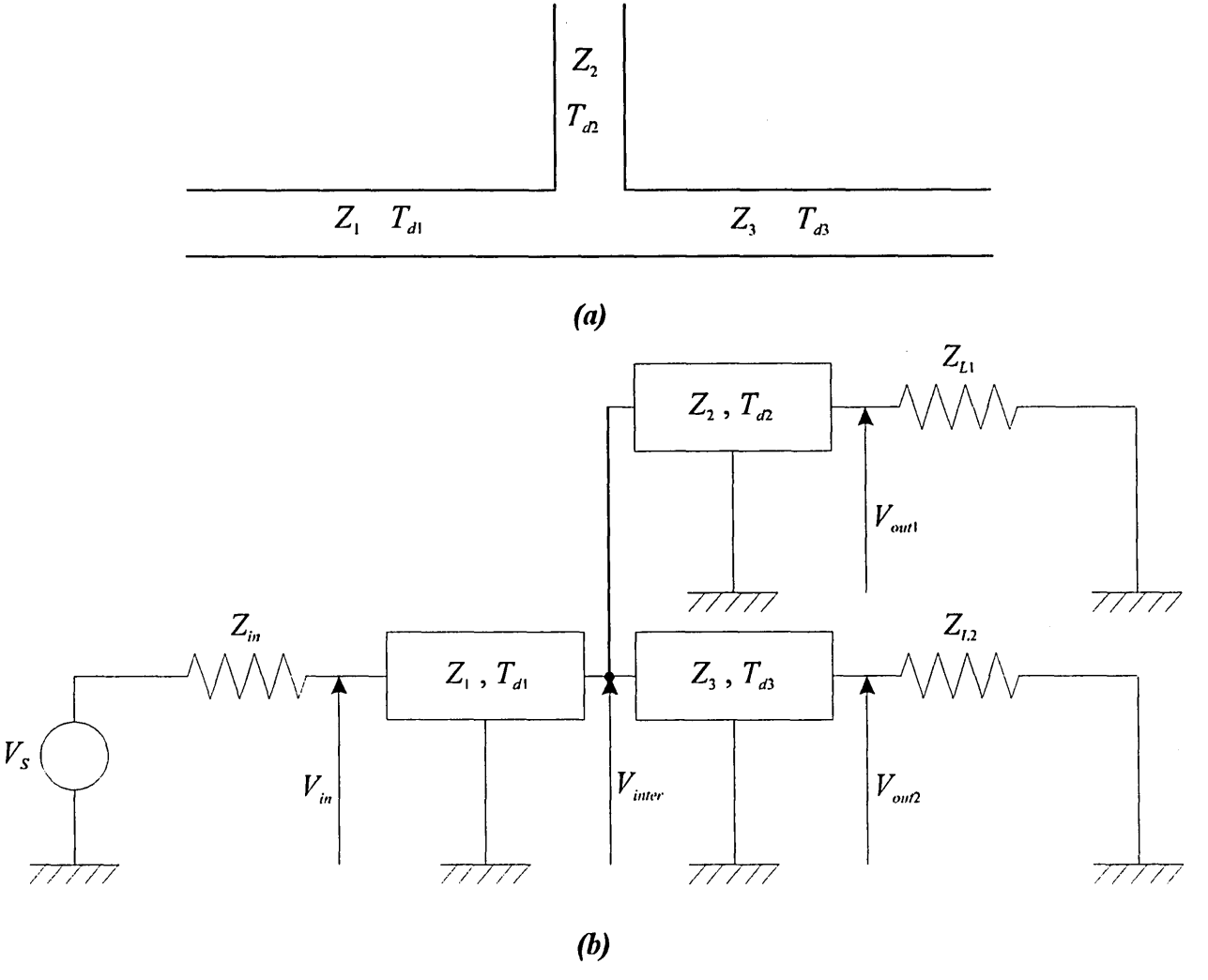

Figure 4.18 : (a) Schematic example of line intersection. (b) Equivalent circuit for simulation of intersection.

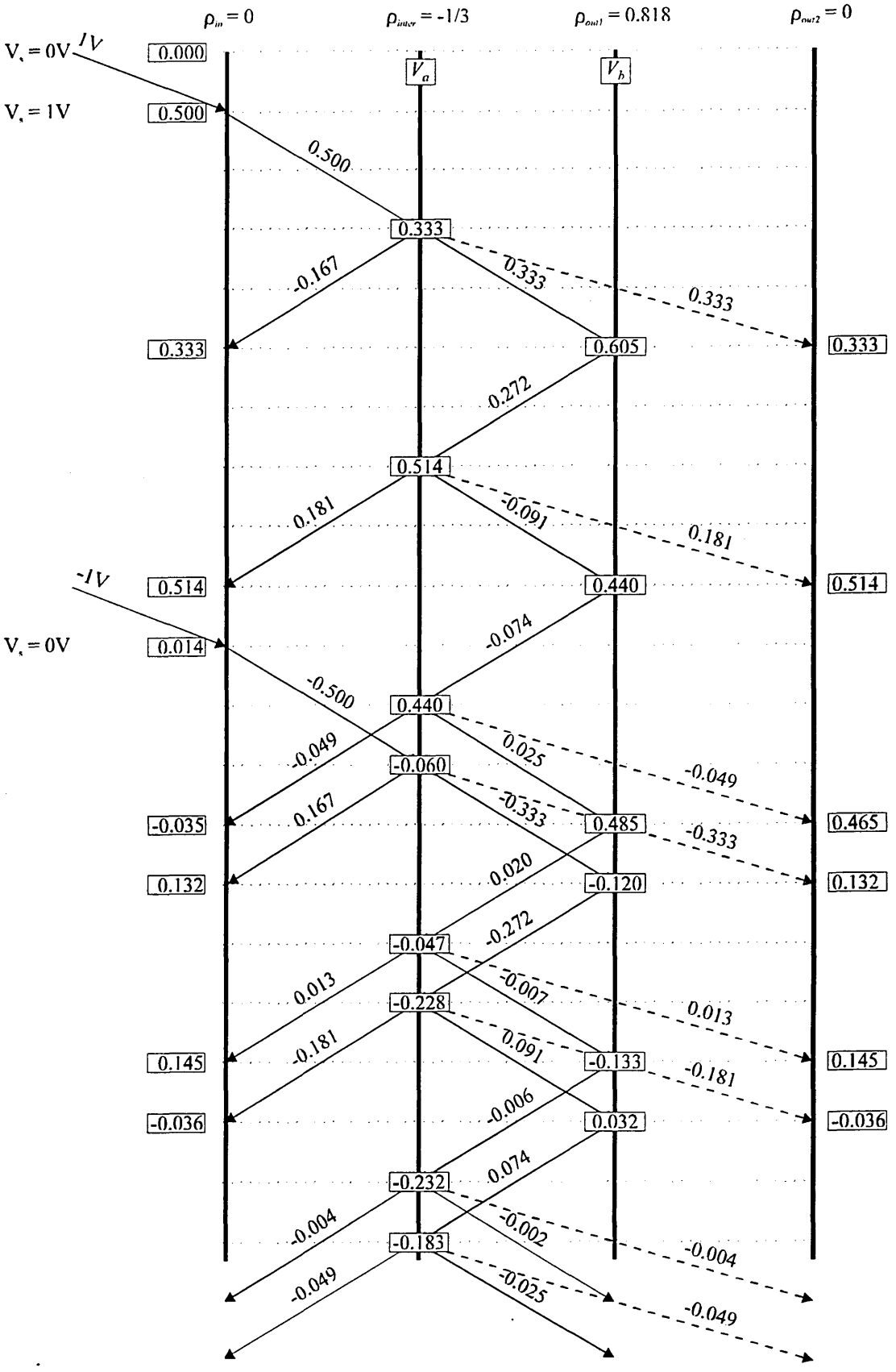

Figure 4.19 : Reflection diagram for multiple line intersection.

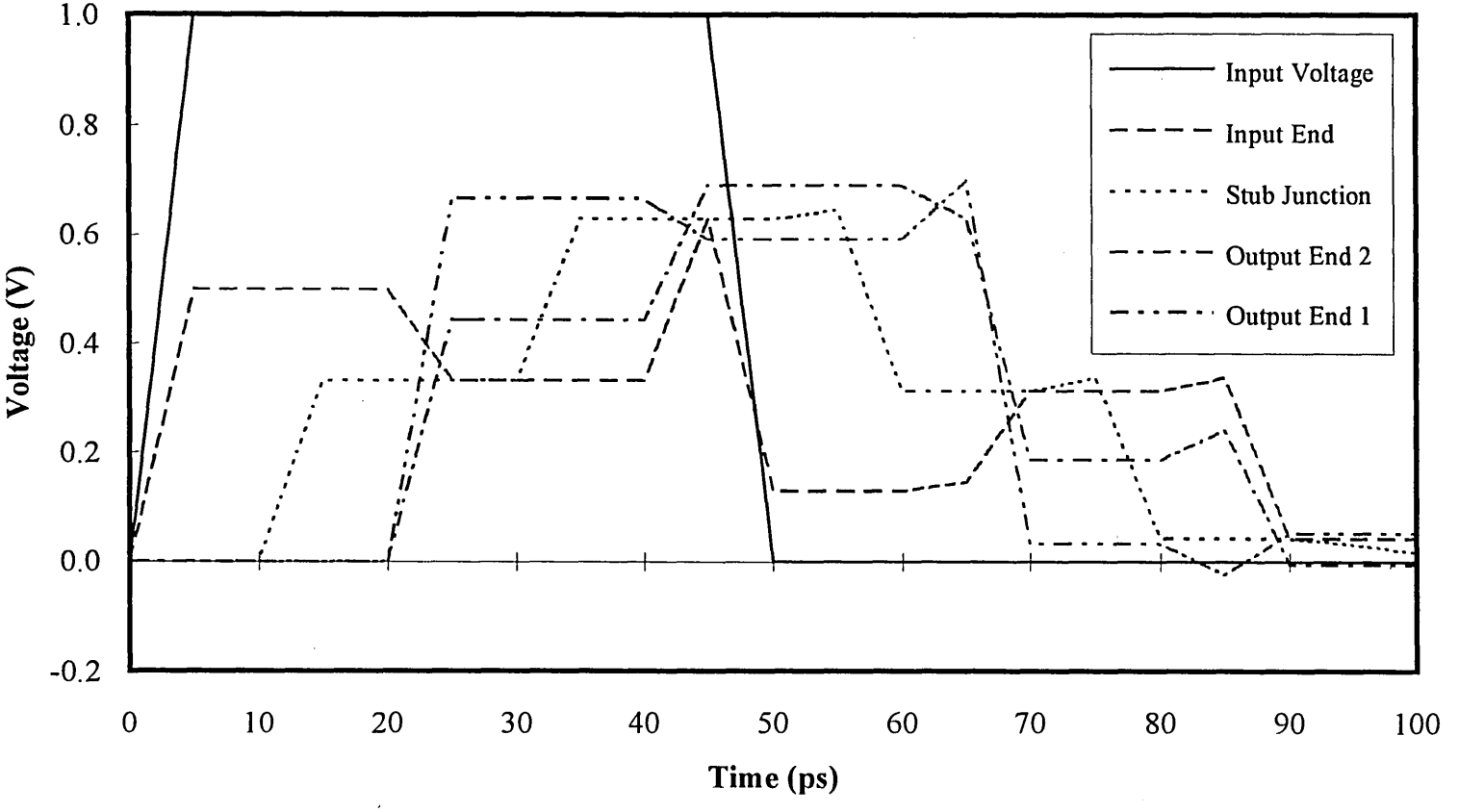

Figure 4.20 : Transient analysis for a matched load impedance stub line.

Chapter 5

SPICE Equivalent Circuit Modelling

5.0 : Introduction

Due to the increase in the packing density of interconnects and the increase in signal speed, simulation of an interconnect structure has become a very important part of integrated circuit design. This can be done using numerical methods or by using an equivalent circuit model implemented in a circuit analysis program such as SPICE (Rashid 1990). An equivalent circuit model can be used to simulate signal propagation on lossless and lossy transmission lines either coupled or uncoupled (Chowdhury *et al* 1992).

A circuit simulation program such as SPICE provides a transmission line model that is considered to be lossless (Rashid 1990). This is considered reasonable for a circuit analysis program with integrated circuit emphasis, since transmission lines within an integrated circuit (probably stripline or microstrip) are going to be very short, both physically and electrically. The loss in a short transmission line is normally quite small (a fraction of a dB) and can be considered negligible for most purposes (Chilo and Arnaud 1984).

The lossless transmission line is therefore a good first approximation, to the problem of simulating a microstrip line or interconnect within an integrated circuit package. This does not however take into account the problems of dielectric loss (increases with line length) (Pucel *et al* 1968, Deutsch *et al* 1990) and skin effect (significant at high frequencies) (Wheeler 1942, Weeks *et al* 1979, Wlodarczyk and Besch 1990). The rapid development of high-density, high-speed integrated circuits has caused the effects of dielectric loss and skin effect to become highly significant. The high-density of such devices also leads to interconnection lines becoming closer together (Yaun *et al* 1982), and has therefore given rise to the problem of crosstalk (Palusinski and Lee 1989, Van Deventer *et al* 1994) between neighbouring lines to become a very important part of integrated circuit design. This has led to the simulation of both single and coupled lines becoming a necessary part of integrated circuit design (Ruehli 1979).

5.1 : Ideal and Lossless Transmission Line Model

An ideal or lossless transmission line is a line through which a signal can be sent without undergoing attenuation or becoming distorted (Branin 1967). This does not however happen in a practical case, but is a useful reference point for further simulation. A lossless transmission line can be simulated mathematically; e.g. method of lines (Branin, 1967), or by the use of an equivalent circuit model implemented in a circuit simulator such as SPICE.

By definition a lossless line will transmit a signal without it undergoing any attenuation. Such a line would not therefore contain any resistive or conductive elements, these being the major causes of attenuation and distortion to a transmitted signal. A lossless transmission line can be considered to be made up of capacitative and inductive elements (Groudis 1979), thereby neglecting any attenuation or distortion caused by dielectric loss or skin effect.

5.1.1 : Equivalent circuit model

An equivalent circuit model can therefore be constructed using capacitors and inductors as shown in figure 5.1 (Ho 1973). The line shown in figure 5.1, is constructed from, n, number of LC filter sections. Given the impedance, Z_0, and the time delay, T_d, of the transmission line to be simulated, the values of each C_i, and L_i, component may be calculated using the following equations:

$$Z_0 = \sqrt{\frac{L_i}{C_i}} \qquad (5.1)$$

$$T_d = \sqrt{L_i C_i} \tag{5.2}$$

Equations (5.1) and (5.2) may be rearranged to give the following two equations for C_i, and L_i:

$$L_i = T_d Z_0 \tag{5.3}$$

$$C_i = \frac{T_d}{Z_0} \tag{5.4}$$

Equations (5.3) and (5.4) thus allow any line of a given impedance, Z_0, and time delay, T_d, to be constructed, from capacitors and inductors alone as shown in figure 5.1. The configuration used for the simulation of the equivalent circuit model is shown in figure 5.2.

Due to the maximum power theory when the input impedance, R_{in}, and the output impedance, R_L, match the line impedance, Z_0, the output voltage, V_{out}, will be $\frac{1}{2}V_s$, where V_s in the input voltage. Because of the impedance matching there will not be any reflected waveforms from the receiving end of the line. Reflections are a major cause of signal distortion, and are therefore of great concern when designing input and output impedances of the components connected to the line. However to receive only half of the input voltage, is not always desirable, and therefore due attention is required to find the correct loads, which will give a signal of the required magnitude with the minimum of distortion occurring on the received signal.

5.1.2 : Comparison with SPICE ideal line model

Figure 5.3 shows the input pulse, (V_s), and the voltage waveforms present at the input and output ends of the line, V_{in}, and V_{out} respectively, for the ideal lossless transmission line model available in the SPICE circuit simulation program. The parameters used during the simulation were, Z_0 = 100Ω, T_d = 10ps, R_{in} = 100Ω, R_L = 100Ω. The input pulse, V_s, used was of 50ps duration with rise and fall times of 15ps.

Figure 5.4 shows the same simulation carried out using the LC filter equivalent circuit model, given in figure 5.1. The number of LC filter sections used for this simulation was fifty. It is seen that the output waveform in figure 5.4 closely resembles that of the output waveform in figure 5.3, with the exception of some slight ringing before the voltage settles to a steady value. This ringing is due to the passive nature of the components used in the circuit model but is not of a significant magnitude to render the simulation invalid.

5.1.3 : Input and output load mismatches

Further tests were carried out to check the effect of varying the number of LC filter sections used in the equivalent circuit model when simulating a lossless transmission line, the number of sections used being varied between five and ninety.

Figures 5.5-5.8 show the output voltage pulses obtained by using different numbers of sections to simulate the line; these being 5, 10, 20, and 50 respectively. All other parameters were kept constant where Z_0 = 100Ω, T_d = 10ps, R_{in} = 100Ω, R_L = 100Ω. The input pulse, V_s, used was again of 50ps duration with rise and fall times of 15ps.

Figures 5.5-5.8 illustrate how as the number of sections used is increased, the ringing seen at the top of the output pulse becomes better defined. It is however found that there is negligible difference in the signal shape when using twenty or fifty sections for the

simulation. There is however an increase in the simulation time required for the larger number of sections; from about 20 seconds for 10 sections to over 6 minutes for 90 sections.

All the above tests were carried out using a time delay of ten picoseconds, and as such the model is only confirmed for use when transmitting high speed signals. Further tests are therefore required in order to validate the model for lines with a longer time delay of up to one millisecond. Figures 5.9-5.11 shows a set of simulations carried out using time delays of 1 ms, 1 μs, and 1 ns respectively. These simulations give confirmation that the equivalent circuit model is just as valid for signals with a delay time of one millisecond as it is for the high speed signals.

Figures 5.12-5.14 show further simulations carried out on the equivalent circuit model, with varying load impedance, R_L, whilst keeping the input impedance, R_{in}, line impedance, Z_0, time delay, T_d, and input pulse, V_s, at the same values as used for the above simulations shown in figures 5.3 and 5.4. The load impedance, R_L, used in figures 5.12, 5.13 and 5.14 were 200Ω, 400Ω, and 800Ω respectively. These graphs show how when the input impedance, R_{in}, is matched to the line impedance, Z_0, the output signal increases in magnitude, but does not become distorted from its original shape. The signal at the input end of the line does however become increasingly distorted but is of no importance to the received signal due to the impedance matching between the line and the input resistor, R_{in}.

The variation in magnitude of the output signal can be given by

$$V_{out} = \frac{R_L}{R_L + R_{in}} V_s \tag{5.5}$$

which is only valid when $R_{in} = Z_0$. However when $R_{in} \neq Z_0$, and $R_L \neq Z_0$, reflections from both ends of the line will cause a severe amount of distortion to be observed in the

received signal.

Figures 5.15-5.18 show the simulations carried out when R_{in} = 50Ω, and R_L is varied through 100Ω, 200Ω, 300Ω, and 500Ω respectively. Figure 5.15 illustrates that when the output load is matched to the line impedance, Z_0, there are no reflections, and therefore no distortion occurs to either the input or output signals. However due to the mismatch in impedance between the input load, R_{in}, and that of the line, the magnitudes of the signals seen at both ends of the line are increased when compared to those seen in figure 5.4.

When the output impedance is increased so as to be greater than the line impedance, the signals undergo a further increase in magnitude. However the signals exhibit distortion, (figures 5.16-5.18), which only occurs when the output impedance, R_L, does not match the line impedance, Z_0. This mismatch at the receiving end of the line causes a signal to be reflected back to the sending end of the line. When this reflected signal reaches the sending end of the line, the signal will become distorted, thereby altering its shape. The time at which the signal is distorted from its original shape is called a break point.

If the input impedance, R_{in}, is also not matched to the line impedance, Z_0, then a signal will be reflected back again to the receiving end of the line. At the point when this signal reaches the other end a further break point will occur. These signals will be reflected back and forth along the line causing further distortion every time a break point occurs. Due to the time delay, T_d, being ten picoseconds for the above simulations, each break point will occur, 10ps after a change in signal shape at the other end of the line.

From figure 5.16 we find that the voltage levels at which the first break point occurs at both the sending and receiving ends of the line, are greater than those seen in figure 5.12, due to R_{in} being smaller for the simulations carried out in figures 5.15-5.18.

When the input resistance is increased to 200Ω (figures 5.19 and 5.20), where R_L is

200Ω, and 400Ω respectively, the voltages at which the break points occur are lower than those seen in figures 5.12 and 5.13, where the input resistance, and line impedance are the same.

5.2 : Lossy Transmission Line Model

A lossy transmission line causes signal attenuation to become apparent due to the internal line resistance, this being independent of the line impedance (Deutsch *et al* 1990). This line resistance can be added to the transmission line model by means of resistors placed between each LC filter section used for the lossless line model. This creates an RLC 'T' section, which is the basis of a lossy transmission line and is used to form a quasi-distributed circuit model (figure 5.21).

The total series line resistance, R_{TOT}, is given by

$$R_{TOT} = \sum_{i=1}^{n} R_i \qquad (5.6)$$

where R_i is the line resistance in each section, n is the number of RLC 'T' sections used to simulate the line.

5.2.1 : Lossy line simulation results

Figures 5.22 and 5.23 (Z_0 = 100Ω and Z_0 = 200Ω respectively) show how as the line resistance, R_{TOT}, is increased, the level of attenuation of the signal at the output end, V_{out}, becomes greater. The conditions used for each simulation are T_d = 10ps, R_{in} = 100Ω, R_L = 100Ω and the input pulse, V_s, used was of 50ps duration with rise and fall times of 15ps.

The attenuation, α, in dB of the output signal, V_{out}, is defined as

$$\alpha = 20\log_{10}\left[\frac{V_{out}(R)}{V_{out}(0)}\right] \tag{5.7}$$

where $V_{out}(R)$ is the voltage at the output end of a lossy line and $V_{out}(0)$ is the output voltage on a lossless line ($R = 0$) at a time, t = 35ps, this being the midpoint of the output waveform for the current simulation. Figure 5.24 shows a plot of line resistance to line impedance ratio against attenuation in dB confirming that as the line resistance increases the attenuation becomes greater.

5.3 : Coupled Line Models

Coupling between lines that are physically close is of great importance when designing interconnections within high-speed integrated devices, such as logic circuits (Crozat *et al* 1988, Gilb and Balanis 1990, Qian and Yamashita 1993). The study of crosstalk between the interconnection lines on high-speed digital circuits is necessary because this phenomenon may lead to the distortion of the desired logic functions (Chilo and Arnaud 1984). This coupling also leads to the attenuation of signals and may lead to unwanted signals being seen on neighbouring lines. These signals if of a significant magnitude, may lead to the possibility of an error in logic occurring.

On-chip interconnects in high-speed digital circuits are regarded as being transmission lines (Gao *et al* 1990). For n coupled lossy lines, the TEM analysis is given in terms of a set of coupled equations connecting ($n \times n$) symmetric [**L**] and [**C**] matrices to ($n \times 1$) voltage [**V**] and current [**I**] vectors (Chang 1970).

5.3.1 : Development of coupling network

Using values of the characteristics of the eigenmodes $[\mathbf{Z}_d]$ and $[\mathbf{T}_d]$ for a set of, N, interconnection lines of a given geometry, a FORTRAN program is developed to calculate values of individual components $L_{i,j}$, $C_{i,j}$ and $R_{i,j}$ using the following equations:

$$L_{i,j} = T_{di} Z_{di} \tag{5.8}$$

$$C_{i,j} = \frac{Z_{di}}{T_{di}} \tag{5.9}$$

$$R_{i,j} = \frac{R_{TOT}}{n} \tag{5.10}$$

where i is the i^{th} line, j is the j^{th} section used, n is the number of sections, and R_{TOT} is the series line resistance of line i.

These values are then stored in an input file for the SPICE package (Banzhaf 1989). For the implementation of crosstalk, the transformation network (Romeo and Santomauro 1987) is described by means of voltage controlled voltage sources (VCVS) $E_i(x)$ and current controlled current sources (CCCS) $F_i(x)$ as shown in figure 5.25. The controlling parameters for each $E_i(x)$ and $F_i(x)$ can be calculated by using the following set of equations:

$$E_i(x) = \sum_{j=1}^{N} M_{i,j} V_j(x) - V_i(x) \tag{5.11}$$

$$F_i(x) = \sum_{j=1}^{N} M_{i,j} I_j(x) - I_i(x) \tag{5.12}$$

where summation extends over all N lines. Assuming the coupling is between adjacent lines only and to be independent of line length and impedance, the matrix elements $M_{i,j}$ are calculated according to a simplified model (Romeo and Santomauro 1987). The transform network depends upon the number of coupled lines but not on their electrical parameters.

5.3.2 : Application of coupled line model

Using values of the characteristics of the eigenmodes $[\mathbf{Z}_d]$ and $[\mathbf{T}_d]$ for an eight line bus with the geometries and dimensions (Chilo and Arnaud 1984), as described in chapter 1, the FORTRAN program is used to calculate values of individual components $L_{i,j}$, $C_{i,j}$ and $R_{i,j}$ for each line using Equations (5.8)-(5.10). Figure 5.26 shows the schematic diagram of an eight line bus in a high-speed GaAs logic device. Each line is 1mm long , 2μm wide and 0.3μm high. Inter-line separation is taken to be 3μm thick. Logic pulses of 1V and 5V are input to one or two chosen lines. The characteristics logic signals are 50ps long including rise and fall times of only 10ps.

5.3.3 : Simulation results

The simulation is initially run using ten sections of the RLC "T" circuit for each line, passing a one volt logic pulse along the first line with the other seven lines inactivated. It is seen that the use of unmatched loads results in severe distortion of the transmitted signal due to the reflected waveform (figure 5.27). The line capacitance causes a slight ripple in the output signal, with the series resistance bringing about a small amount of attenuation. The induced signals on the nearest neighbouring lines are often large enough to introduce possible errors in logic level. The simulation is also repeated by using twenty and fifty sections for each line. Although no significant changes in the waveforms have been noticed, the overall simulation time increases from three minutes for ten

sections to six minutes for fifty sections.

Figures 5.27 to 5.34 show the waveforms present at the input and output ends of the eight line bus under consideration, and illustrate the way in which crosstalk is transmitted from one line to another. If V_i is the voltage at time t on an inactivated line i, the crosstalk (ξ) in dB at a particular position on the line is defined as:

$$\xi = 20\log_{10}\left[\frac{V_i(t)}{V_a(t)}\right] \tag{5.13}$$

where V_a is the voltage on the activated line at the same time t. In our present investigations, ξ is calculated at both input and output ends at the time t = 25ps corresponding to the mid-point of the logic pulse. Four curves shown in Figures 5.35 to 5.38 illustrates the crosstalk between adjacent lines under different operating conditions. As shown in Figures 5.35 and 5.36 the crosstalk decays gradually in a non-linear fashion with increasing distance from the activated lines.

When signals are applied to the third and sixth lines, large crosstalk is observed for the fourth and fifth lines due to the superposition effect (vide Figure 5.37). The value is in the order of 6dB at their input ends is approximately 2dB higher than those for the second and seventh lines.

Referring to Figure 5.38, the crosstalk for line 3 remains at almost the same level whether line 4 is activated on its own or along with line 5. When the voltage pulse input is increased to 5V, voltage levels of transmitted and reflected waveforms are found to be now much higher than before but their essential features remain the same, implying that the effect on crosstalk is independent of ECL (emitter coupled logic) and TTL (transistor-transistor logic) inputs.

Further analysis (Chilo and Arnaud 1984) shows that with the use of the second ground plane at a distance of 5μm above the bus, the decrease in crosstalk is not significant enough to compensate for associated increases in signal distortions.

5.4 : Risetime Effects

The risetime of a signal travelling along a transmission line is a very important factor to consider (Son *et al* 1993, Qian and Yamashita 1993). The faster the risetime the more ringing and distortion to the output signal will occur. It is therefore important that the fastest possible risetime is calculated, so that the line can be evaluated for its suitability in a particular application, such as a high-speed digital circuit, where excess ringing may introduce severe signal distortion and induce an error in logic on a neighbouring line (Qian and Yamashita 1993).

All simulations in this section are carried out using the example described in chapter 1 (Chilo and Arnaud 1984), either upon a single line of the given dimensions or in the case of coupling the eight line bus is used. The lossy line model and coupling network, developed in sections, 5.2 and 5.3 respectively are used for the analysis of risetime effects.

5.4.1 : Step input analysis

The circuit used for simulating changes in risetime is the lossy line equivalent circuit developed in figure 5.21 where $R_L = Z_0$, so that there are no reflections back from the receiving end of the line. This allows the evaluation of percentage overshoot and settling time for any signal with a particular risetime, as illustrated by figure 5.39.

Figures 5.40-5.47 show the transient response of a line, where $Z_0 = 100\Omega$ and $T_d = 10$ps, when the input signal risetime is varied from 30ps down to 1ps respectively. It is seen that the percentage overshoot, η, increases as the risetime decreases; η, is given by

$$\eta = \frac{V_{over} - V_{settle}}{V_{settle}} \times 100\% \qquad (5.14)$$

where, V_{settle}, is the final steady state voltage the output signal attains and, V_{over}, is the maximum voltage of the first peak in the output signal.

In figure 5.48 a graph of risetime against percentage overshoot, η, is given and from this we see that as the risetime is decreased from 30ps down to 5ps the change in percentage overshoot is of a linear fashion. Below 5ps the overshoot becomes very large rising to over 25% for a risetime of 1ps. This graph (figure 5.48), would suggest that about 5ps is the fastest viable risetime for a signal being sent along this particular transmission line.

Figure 5.49 shows how the settling time for a step input varies with the signal risetime. The settling time, t_{settle}, is defined as the difference between, the time at which the signal first rises to 90% of its final steady state voltage, V_{settle}, and the time when the signal settles to within ±1% of V_{settle} (figure 5.39).

The graph in figure 5.49 shows how as the signal risetime is reduced the time taken for the signal to settle to within ±1% of V_{settle}, increases quite sharply below 5ps. For the signal with a risetime of 1ps (figure 5.47) the signal does not settle to within ±1% of V_{settle} over the duration of the simulation (100ps).

5.4.2 : Effect upon pulse shape

Excess ringing may cause a logic error in the received signal as the voltage level may

pass through the critical logic voltage levels more than once in a single pulse. Distortion to the signal shape may also be detrimental as the length of the pulse may either become shorter or longer. If a series of pulses are sent and their width becomes lengthened, errors in timing could occur and become propagated further on through the system until it no longer resembles the original signal.

Figure 5.50 shows the output waveforms for pulses of width 50ps, with rise and fall times varying between 1ps and 10ps. This illustrates that as the risetime is decreased the level of ringing increases. It also however displays how as the risetime is increased the shape of the pulses become smoothed out.

This phenomenon is even better displayed in figure 5.51 where the width of the pulses used is 25ps, again varying the rise and fall times between 1ps and 10ps. When the rise and fall time is 10ps the output pulse does not display a flat plateau region, as is seen at the top of the output pulse in figure 5.50 for a signal of the same rise and fall time, but twice the overall pulse width. This would suggest that to be able sustain the pulse shape the width of the top of the pulse must be longer than the rise and fall time of the pulse.

Figure 5.52 shows the output obtained when a pair of pulses of overall width of 25ps separated by a 25ps space are sent along a microstrip with various rise and fall times. There is however little or no difference seen in the shape of the second pulse, when compared with the first pulse and that shown in figure 5.51. A shorter space would probably cause a difference to be seen but still not of a significant nature.

In figure 5.53 it can be seen that although the risetime of the input signal is 1ps the risetime of the output takes a far greater time. From this graph (figure 5.53) we see that as the pulse width is increased the risetime of the output signal increases. The overall width of the pulse becomes broadened; in the case of input pulse widths of 5ps and 10ps the overall width is increased by about 1ps. In addition to this is the time taken for the output to settle back to the zero level.

Of great concern is what happens to the output signal when a continuous train of pulses is sent along the transmission line. A continuous pulse train with rise and fall times of 1ps and overall pulse width of 10ps, with a space of 10ps, is used with the results presented in figure 5.54. The first pulse received at the output is seen to be smaller than all the subsequent pulses by about 0.5 volts. For example, the first pulse is of a high enough voltage level for a logic level of 1 to be obtained, where the threshold voltage required for a high logic signal, on an HCMOS device, is 3.15V (Fairchild 1987). The width of the output pulses may however be of a smaller width than the originally transmitted pulses. This is due to the very fast rise time of the pulse train used.

5.4.3 : Coupled line effects

When coupled lines are under consideration it is important to know what effect changing the risetime will have upon the level of crosstalk between a set of lines. If the signal induced on another line were to cause an error in logic, due to a change in risetime this would set a limiting factor upon the speed of the risetime transition.

In this section three different line activation configurations are carried out in order to make a study of risetime upon the level of crosstalk. The example chosen, is again the eight line bus described in chapter 1. For each different configuration of activated lines, simulations are carried out using pulse signals of width 50ps and risetimes varying from 1ps to 20ps.

Figure 5.55 shows a 3D plot of the peak voltage for each line against the signal risetime for only line 1 activated. It can be seen that for all different risetime values chosen, there are none which could possibly cause an error in logic to occur.

Figure 5.56 shows a 3D plot of the peak voltage for each line against the signal risetime

where lines 3 and 6 have been activated. It can be seen that for all different risetime values chosen that the signals on lines 4 and 5 may possibly cause an error in logic to occur, especially for a very fast riestime (e.g. 1 ps).

Figure 5.57 shows a 3D plot of the peak voltage for each line against the signal risetime for lines 4 and 5 having been activated. It can be seen that for all different risetime values chosen, the voltage levels seen on the neighbouring lines (3 and 6) would not cause an error in logic to occur.

It is also noted that, for all three line activation configurations (figures 5.55-5.57), as the risetime is increased so the voltage level seen on all lines decreases, and that the further away from the activated line, the less effect that a change in the signal risetime has upon the voltage level seen on the inactive line under consideration.

5.5 : Skin Effect Model

In practice a transmission line acts in the same way as a low pass filter, and therefore signals of a frequency higher than that of the cutoff will be attenuated. This is however a simplistic view of the behaviour of a transmission line. The filter-like behaviour is due to the skin effect and for high frequency signals the current distribution becomes nonuniform over the cross-section of the transmission line or microstrip. For very high frequencies the current becomes confined to a skin around the surface of the conductor, thereby attenuating the signal (Yen *et al* 1982).

Figure 5.58 gives a representation of how, when a high frequency signal is transmitted along a circular conductor, the current distribution is non-uniform (Wheeler 1942, Gordon 1992). Figure 5.59 shows how for an air suspended microstrip as the frequency increases, the current is drawn to the outside of the conductor, and then at even higher

frequencies the current is drawn down towards the ground plane (Hwang and Turlik 1992). The higher the frequency of the signal the smaller is the depth of penetration of the skin into the conductor and the greater is the attenuation of the signal produced. The lossless and lossy transmission lines, developed in sections 5.1 and 5.2 respectively, do not however display this characteristic satisfactorily (results of AC analysis given below) and therefore a suitable equivalent circuit model must be developed in order to accurately simulate the behaviour of such a line.

5.5.1 : Development of skin effect equivalent circuit model

Due to the nonuniform nature of the current density within the conductor it is important to find a means of simulating this without disturbing the characteristic impedance and time delay of the line, and thereby altering the transmission characteristics of the line. One method suggested is using a network consisting of a resistor in series with an inductor, and then having several of these in parallel to each other (Vu Dinh *et al* 1990(a), 1990(b)). However, it is not mentioned how the values of the components are chosen. This is also the method chosen here for simulating the skin effect with the equivalent circuit model shown in figure 5.60.

Due to the time delay and impedance of the line being dependent upon the inductance and capacitance in each section of the line, it is necessary that both of these are unchanged. This requires that the overall inductance, L_{PAR}, and resistance, R_{PAR}, of the sections in parallel, must be equal to L_n and R_1 respectively. For an infinite number of sections in parallel the following holds true:

$$\frac{1}{R_{PAR}} = \frac{1}{2R_{PAR}} + \frac{1}{4R_{PAR}} + \frac{1}{8R_{PAR}} + \ldots\ldots + \frac{1}{1024R_{PAR}} + \ldots\ldots$$
$$= \sum_{j=1}^{\infty} \frac{1}{2^j R_{PAR}} \tag{5.15}$$

$$\frac{1}{L_{PAR}} = \frac{1}{2L_{PAR}} + \frac{1}{4L_{PAR}} + \frac{1}{8L_{PAR}} + \ldots\ldots + \frac{1}{1024L_{PAR}} + \ldots\ldots$$
$$= \sum_{j=1}^{\infty} \frac{1}{2^j L_{PAR}} \tag{5.16}$$

Referring to figure 5.59 the following relationship is true:

$$R_{i,j} = 2^j R_{PAR} \tag{5.17}$$

and

$$L_{i,j} = 2^j L_{PAR} \tag{5.18}$$

However for accurate modelling of skin effect the number of sections required can be reduced due the rapid convergence of the series in equations (5.15) and (5.16). The actual number of parallel sections, m, that are sufficient can only however be determined by investigation of the results obtained carrying out simulations with various equivalent circuit set-ups; i.e. varying the number of parallel RL sections.

5.5.2 : Analysis of results

All simulations in this section are carried out upon a single microstrip line of the given

dimensions as described in chapter 1 (Chilo and Arnaud 1984). The following load parameters are used throughout all the skin effect simulations: $R_{in} = 200\Omega$, $Z_0 = 166\Omega$, $R_L = 2000\Omega$, and V_s is a 1V AC signal.

Figure 5.61 shows the frequency response plot obtained using the lossy line model developed in section 5.2, using 20 lossy line sections. It is observed that the frequency plot obtained is not however smooth, with many spikes at the roll-off point. It is for this reason that a viable equivalent circuit model for simulating the skin effect is required. Figure 5.62 shows the transient response for a pulse input with rise and fall times of 10ps and total pulse width of 50ps.

Figures 5.63 and 5.64, show the frequency response results obtained from using 10 and 20 parallel RL sections respectively, for a line with 10 skin effect sections in series, with a negligible amount of difference between the two. It is however noticed that these plots also suffer from spikes at the roll-off point, and that the frequency at which the roll-off begins is lower than for the lossy line model (figure 5.61).

Figure 5.64 shows the transient response obtained from the skin effect model, using 10 series sections of line and 10 parallel RL sections, with the same pulse parameters as used for the transient response analysis for the lossy line model (figure 5.62). It is clearly seen that there is very little difference between the transient responses obtained using the lossy line model (figure 5.62) and the skin effect model (figure 5.64). Further transient analysis on the skin effect model with varying number of skin effect sections in series and RL sections in parallel displayed no further change in the transient response. Therefore the skin effect model developed is also a good lossy line equivalent circuit, but the lossy line model developed in section 5.2 would be preferred over the skin effect model as it is much simpler and therefore leads to much faster simulation times.

Further frequency analysis was carried for lines with 20 and 30 skin effect sections, and for each of these, a further two analyses was carried out using 10 and 20 RL sections in

parallel (Figures 5.66-5.69). Comparing the results of figures 5.66 and 5.67 with those of figures 5.63 and 5.64 it can be seen that the position of the roll-off frequency has increased and is in fact very similar that seen for the lossy line with 20 sections (figure 5.61). For the simulations using 30 skin effect sections, the roll-off frequency is yet further increased. This alteration of the roll-off frequency with the number of sections used in the simulation is very undesirable and is most probably due to the way in which SPICE sets up the mathematical equations used for each individual simulation. This can also be used to explain the problems of the unstable frequency analysis, where proper convergence of the results can not be obtained. The use of a more recent version of SPICE may allow the correct convergence of the results.

However smoothing of the frequency response for each simulation was attempted with results also displayed on the same set of graphs (figures 5.63-5.69). From these smoothed curves it is possible to obtain an approximate value for the 3dB cut-off point for each simulation. The 3dB cut-off frequency varies from 214 GHz, 420 GHz and 626 GHz, for 10, 20 and 30 skin effect sections respectively. This confirms the link between the cut-off frequency and the number of sections used.

5.6 : Summary

This chapter illustrates the development of the quasi-distributed equivalent circuit model, and its implementation into the SPICE circuit simulator. This equivalent circuit model is then used for the simulation of lossless transmission lines, and modified for the simulation of lossy transmission lines.

The simulations carried out demonstrate the importance of choosing the correct input and output impedances, in order to minimise the distortion inherent when unmatched loads are used. The effect of attenuation due to series line resistance of a lossy

transmission line is investigated showing how it is independent of the line impedance.

A time domain study of crosstalk between the interconnection lines on high-speed digital circuits using the SPICE circuit simulator is presented. This analysis shows that for the case of two activated lines, an increase in crosstalk is seen on the lines between them, but little or no change is seen on the other lines, when compared to the case of a single activated line. These results are seen to be consistent with those obtained from previous work.

The lossy line model is then used to investigate the effect that the risetime of a signal travelling along it, has upon the received signal. This is done using a step input with varying risetimes and pulses of varying risetime and width. Studies of the effect of risetime upon coupling is also carried out and show that under certain conditions may induce an error in logic to occur.

An equivalent circuit model for simulating the skin effect is developed, and used to investigate the frequency response of the line. It is however found that SPICE does not provide a set of satisfactory results and changing the number of sections used in the simulation alters the cut-off frequency. This is due to the nature of way in which SPICE sets up the mathematical equations used for analysing such a circuit.

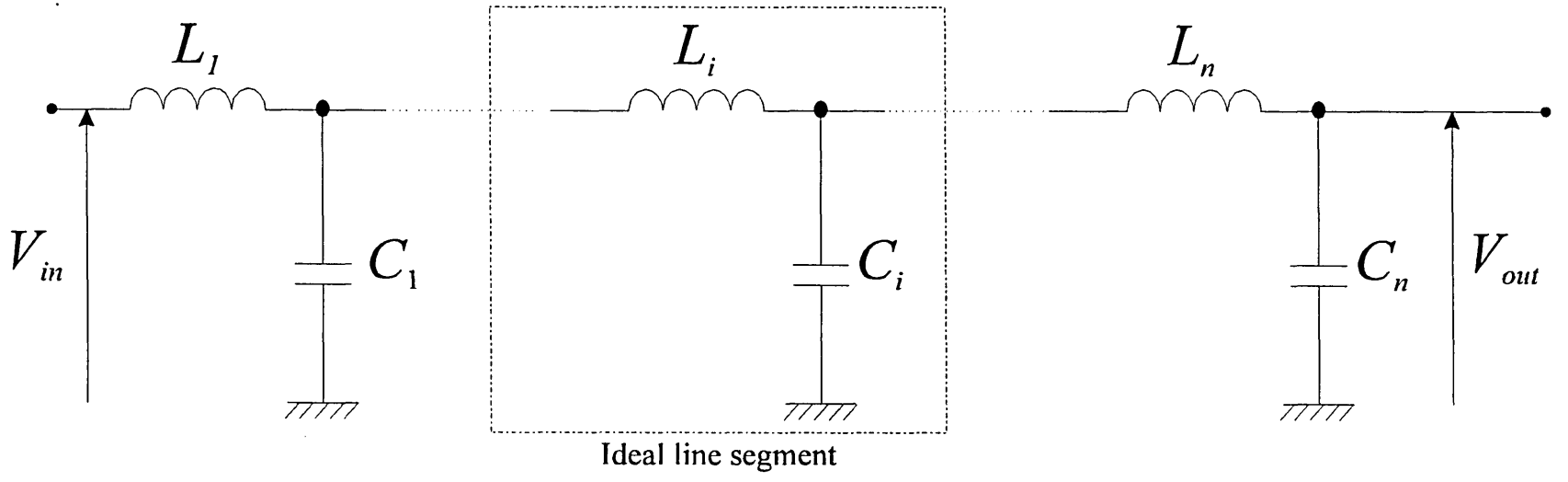

Figure 5.1 : Schematic diagram of an ideal transmission line equivalent circuit.

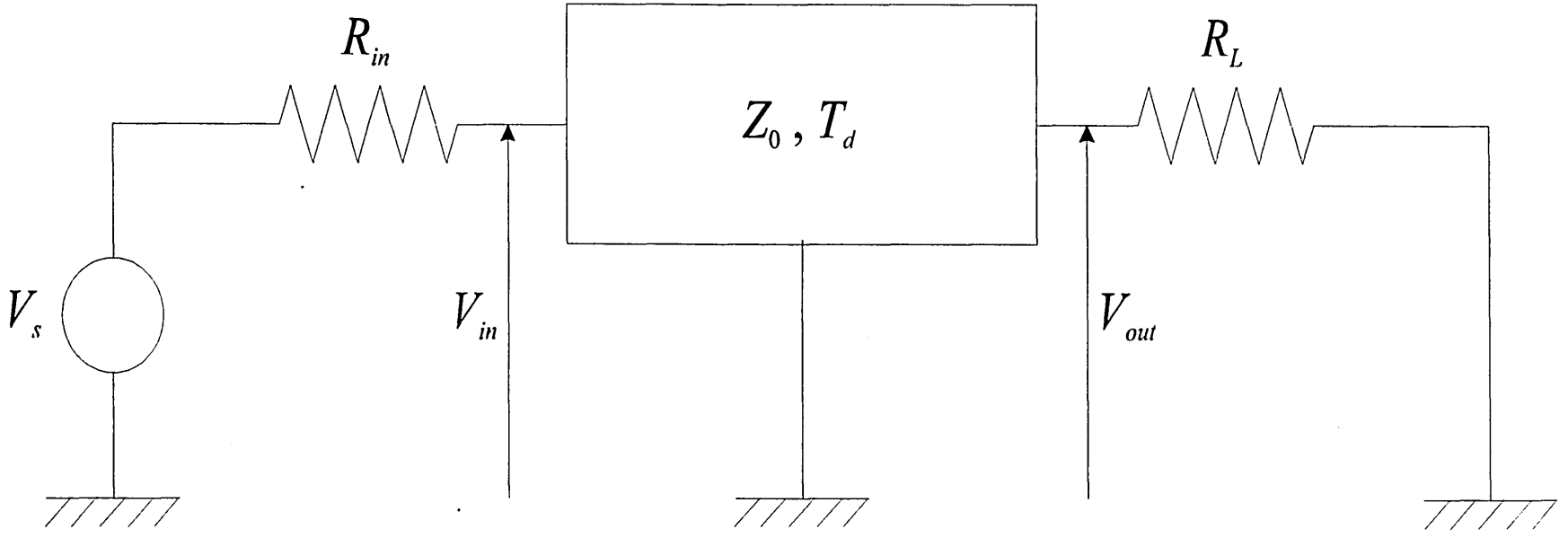

Figure 5.2 : Configuration used for simulating a single microstrip line.

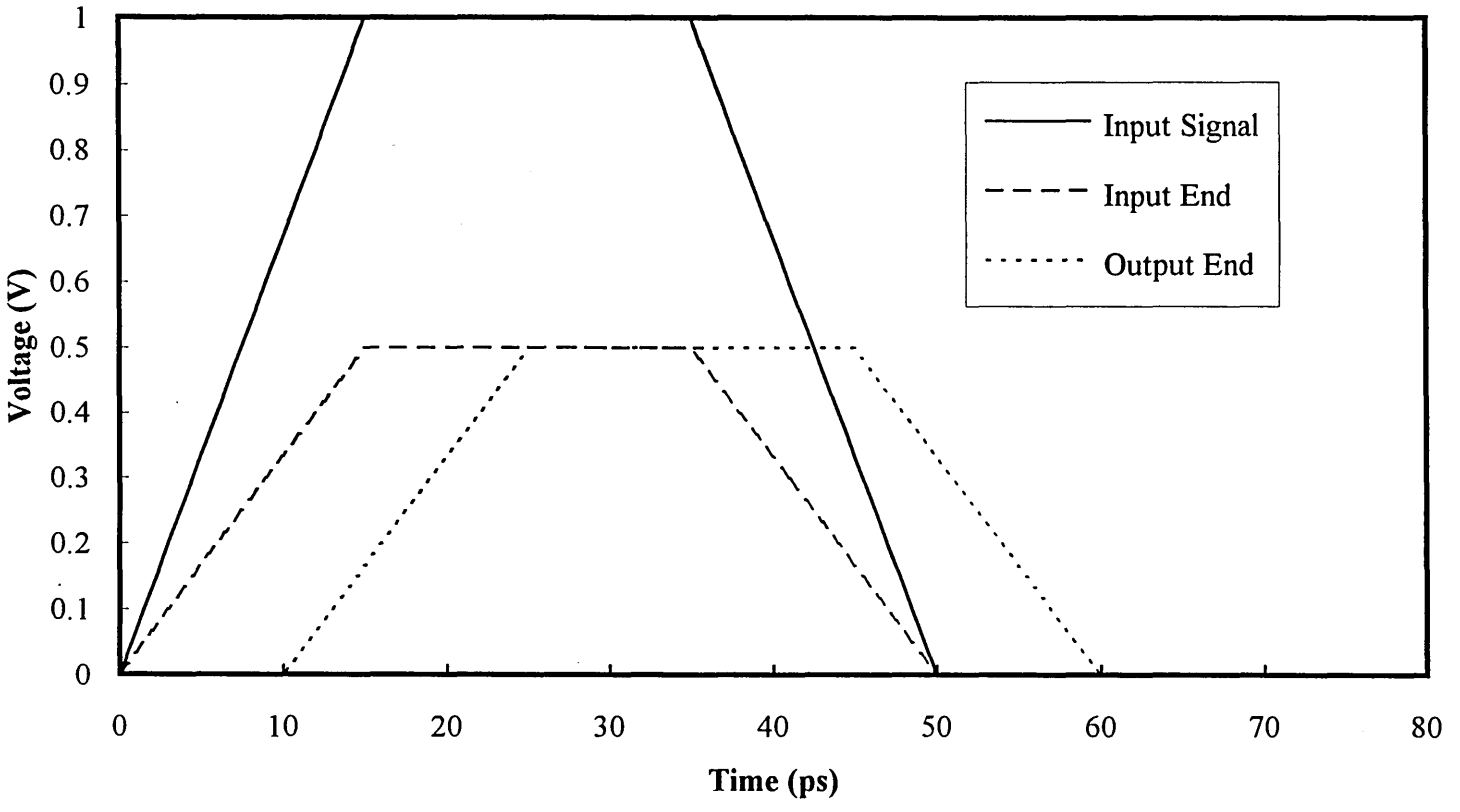

Figure 5.3 : Simulation carried out using the ideal transmission line model available in SPICE.

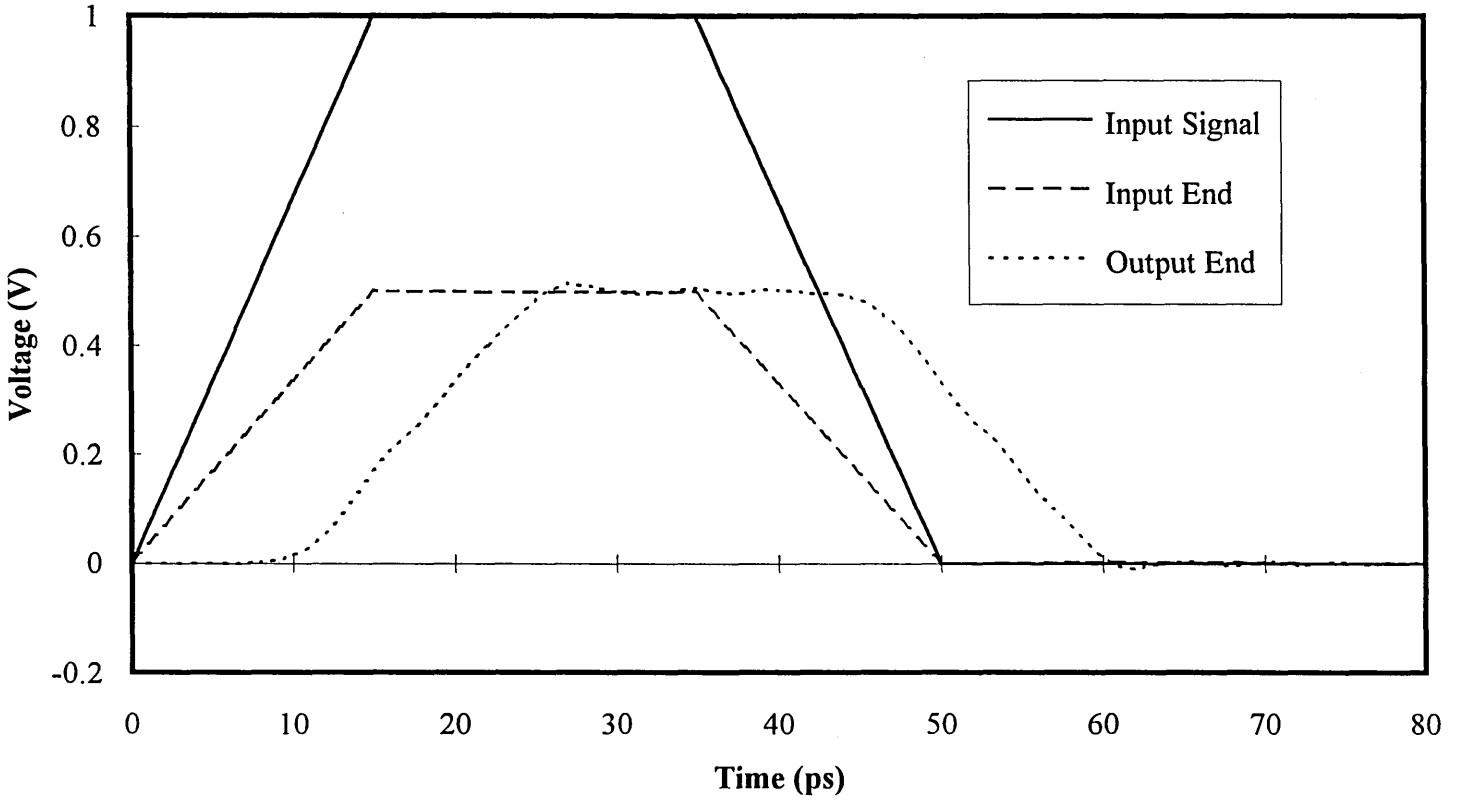

Figure 5.4 : Simulation carried out using the equivalent circuit model shown in figure 5.1.

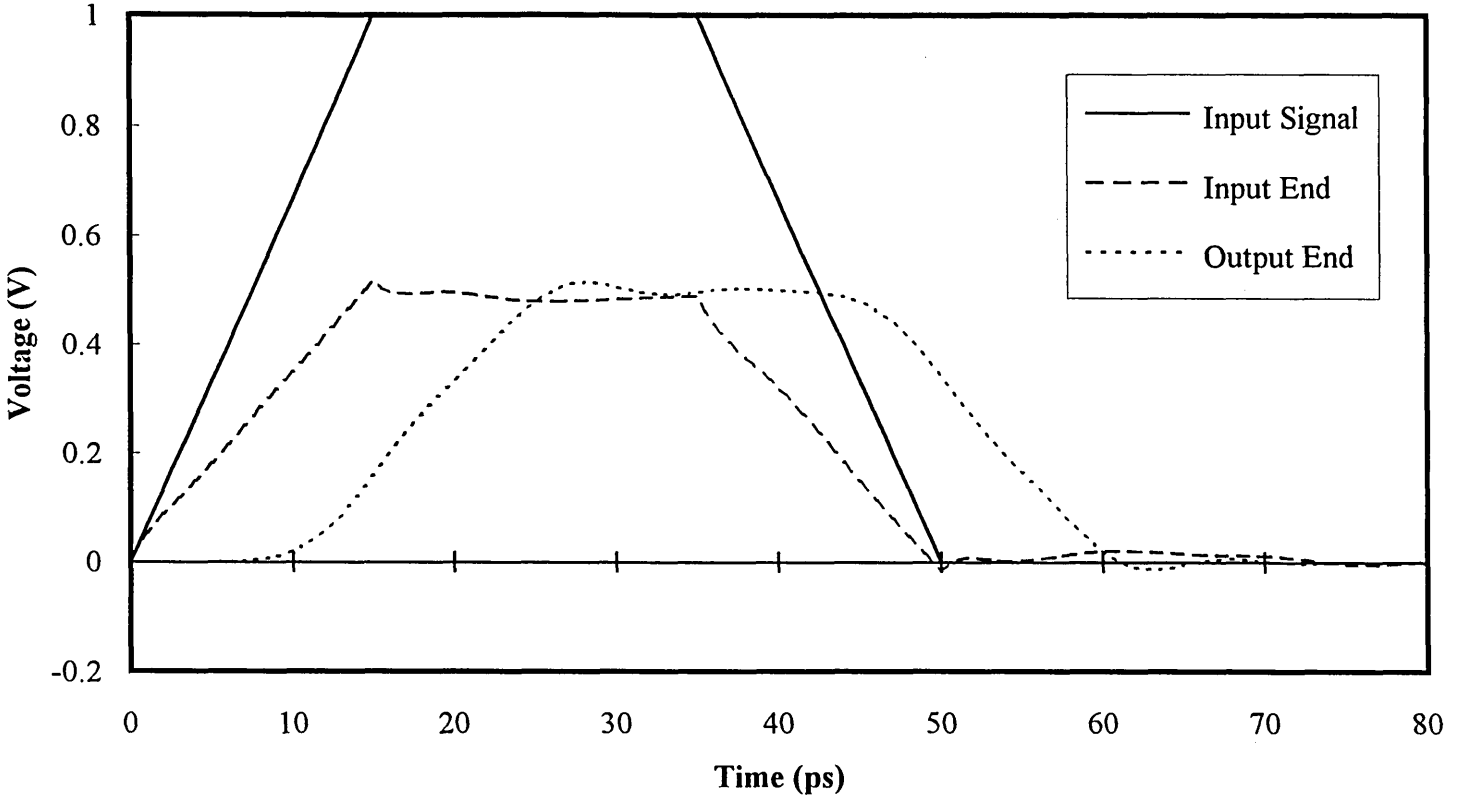

Figure 5.5 : Lossless line; 5 LC Sections used; $R_{in} = Z_0 = R_L = 100\Omega$

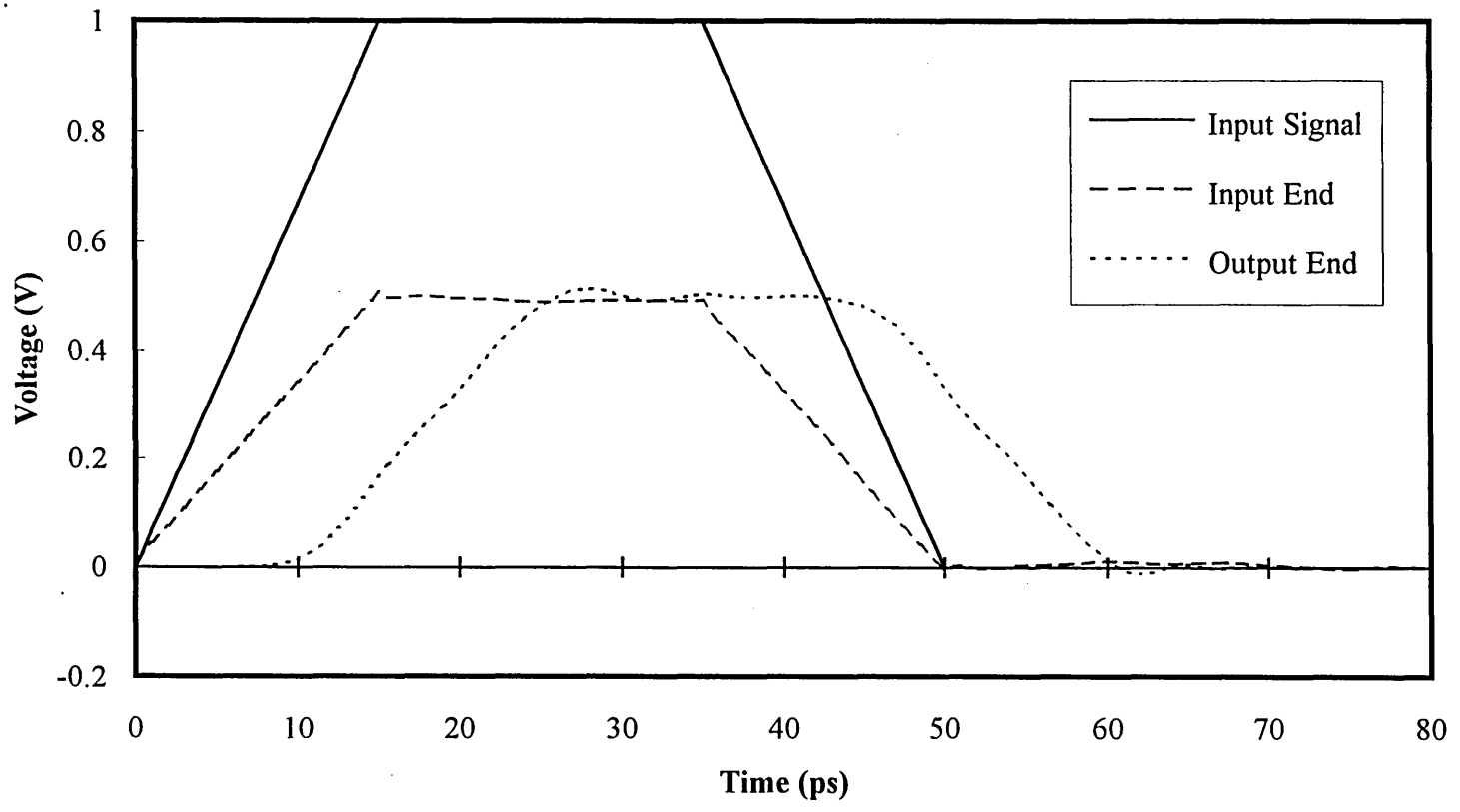

Figure 5.6 : Lossless line; 10 LC Sections used; $R_{in} = Z_0 = R_L = 100\Omega$

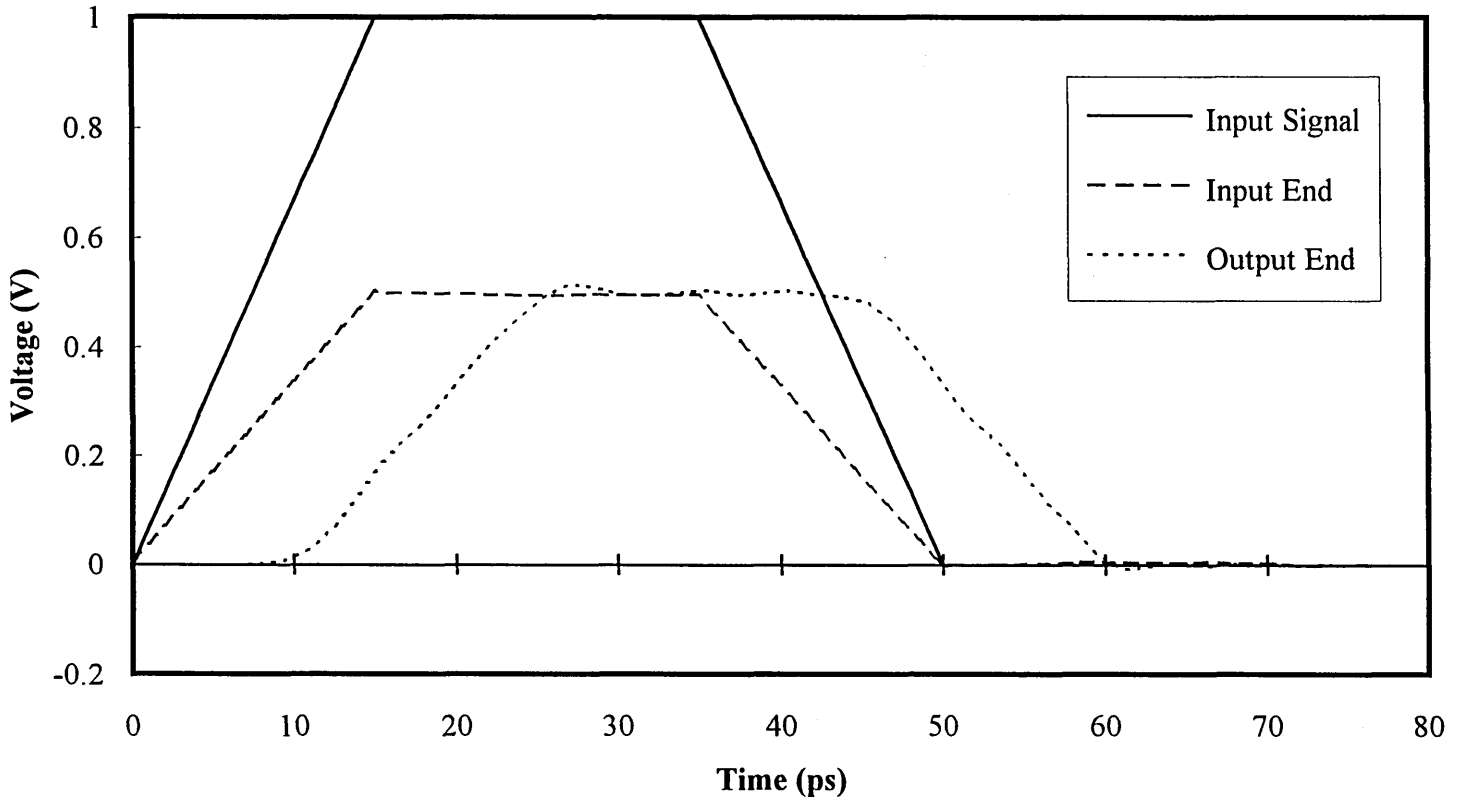

Figure 5.7 : Lossless line; 20 LC Sections used; $R_{in} = Z_0 = R_L = 100\Omega$

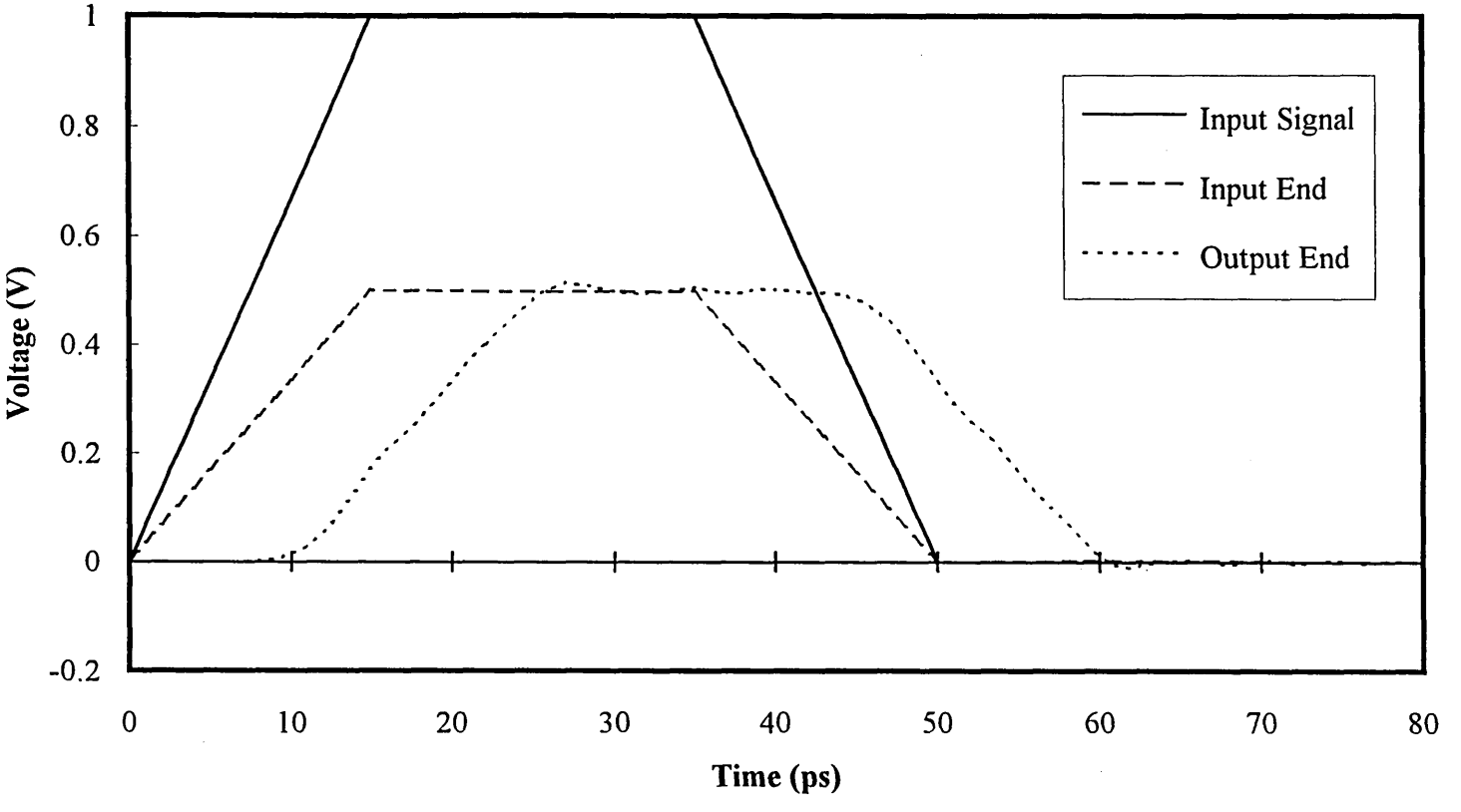

Figure 5.8 : Lossless line; 50 LC Sections used; $R_{in} = Z_0 = R_L = 100\Omega$

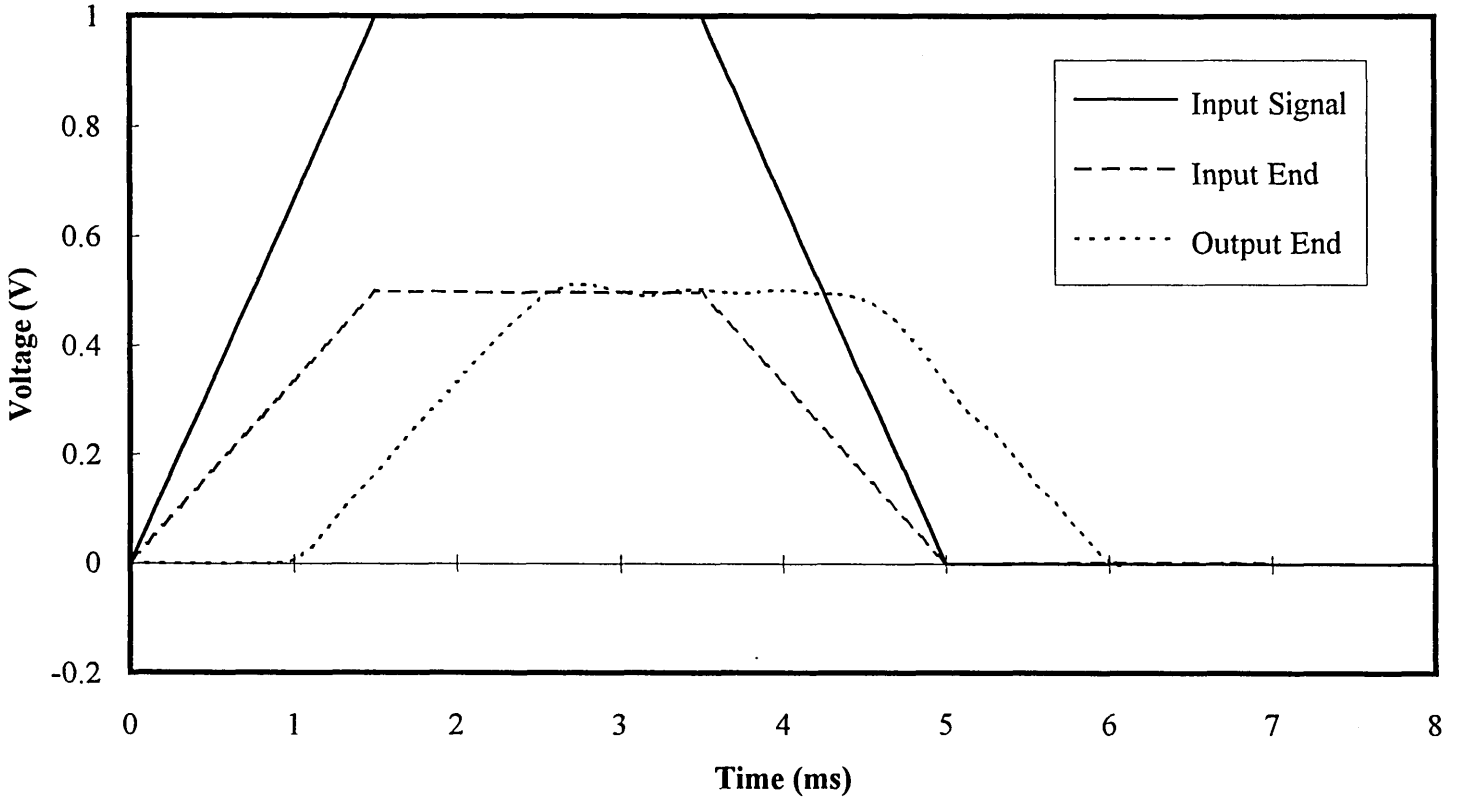

Figure 5.9 : Time delay of line 1ms, with matched loads.

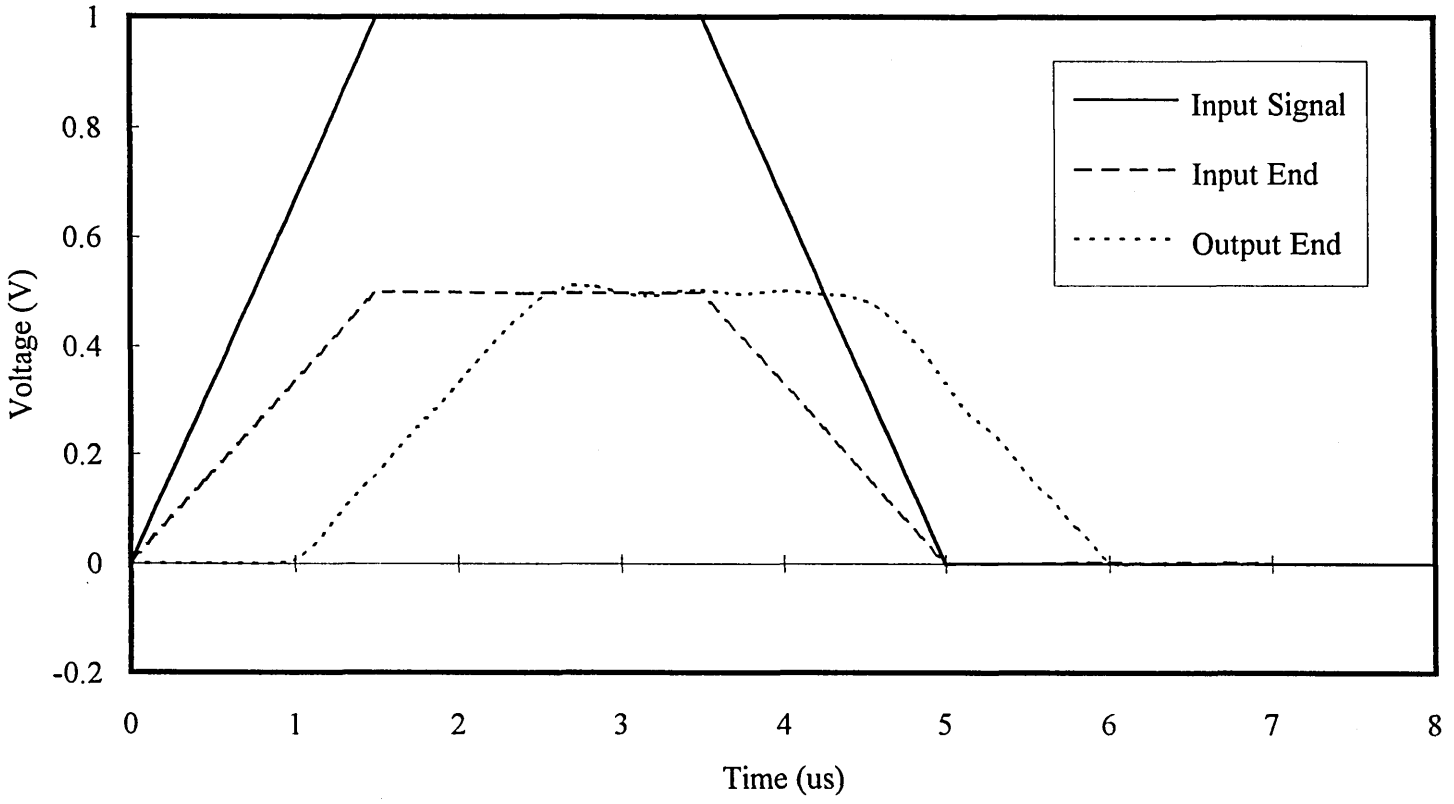

Figure 5.10 : Time delay of line 1μs, with matched loads.

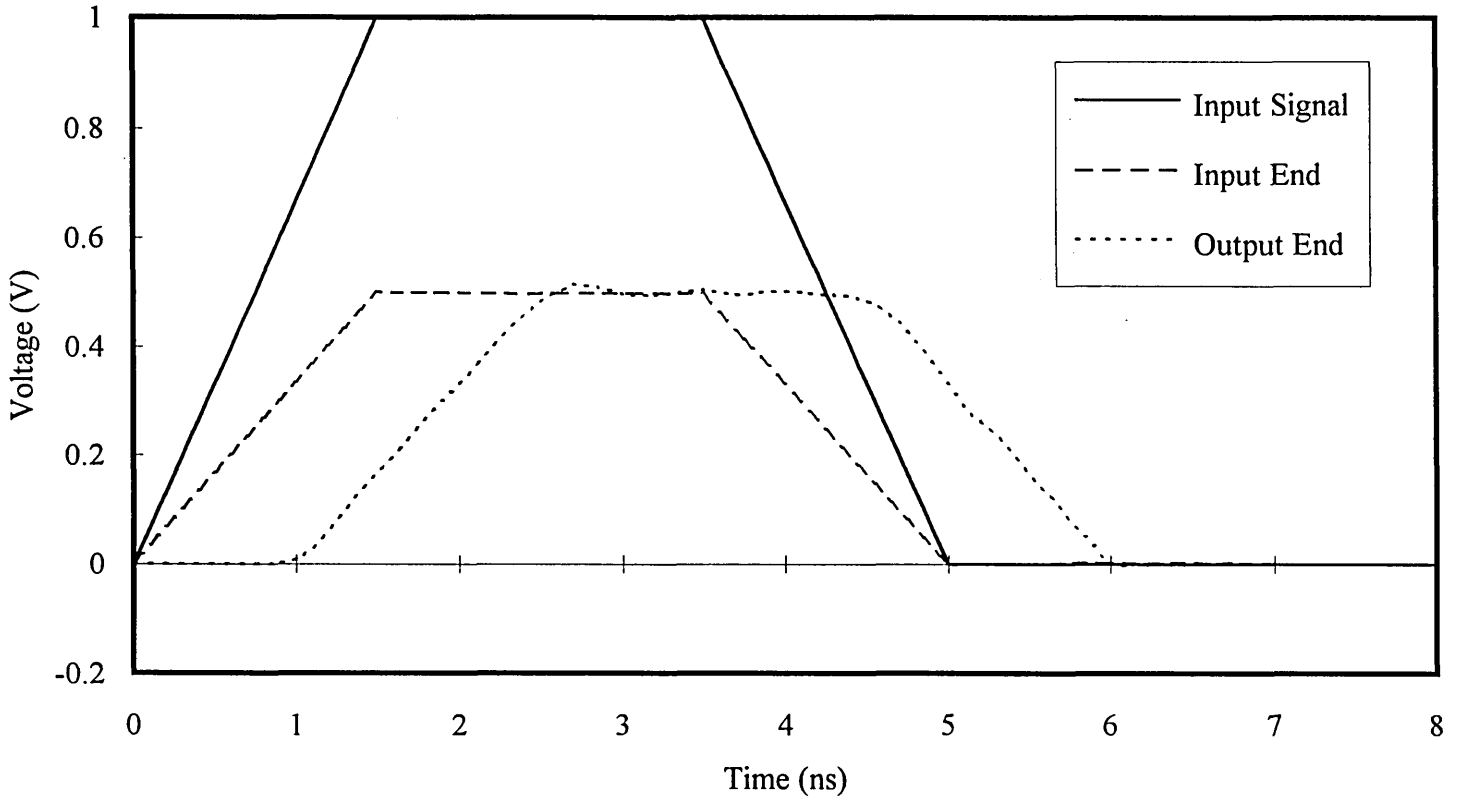

Figure 5.11 : Time delay of line 1ns, with matched loads.

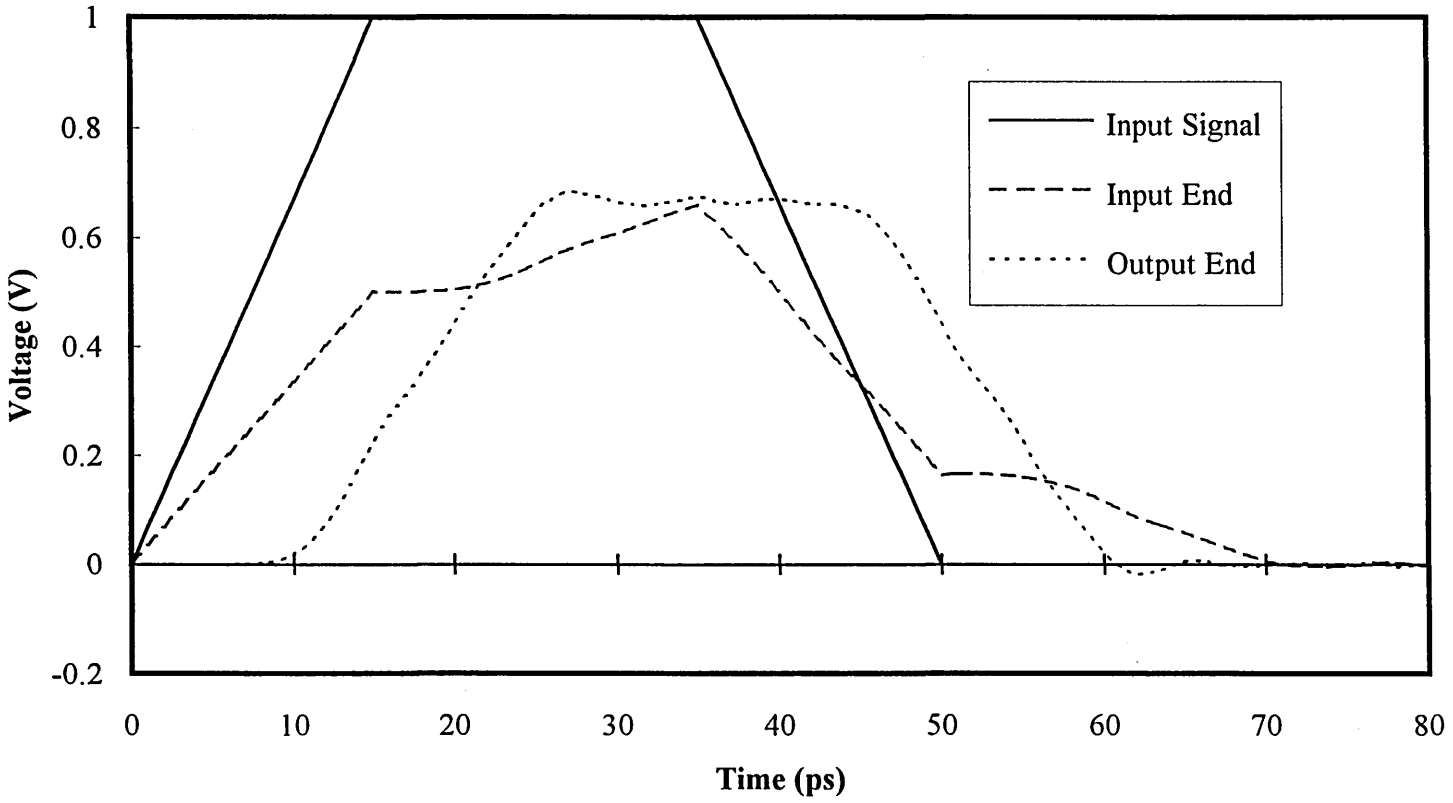

Figure 5.12 : Lossless line; $R_{in} = 100\Omega$, $Z_0 = 100\Omega$, $R_L = 200\Omega$

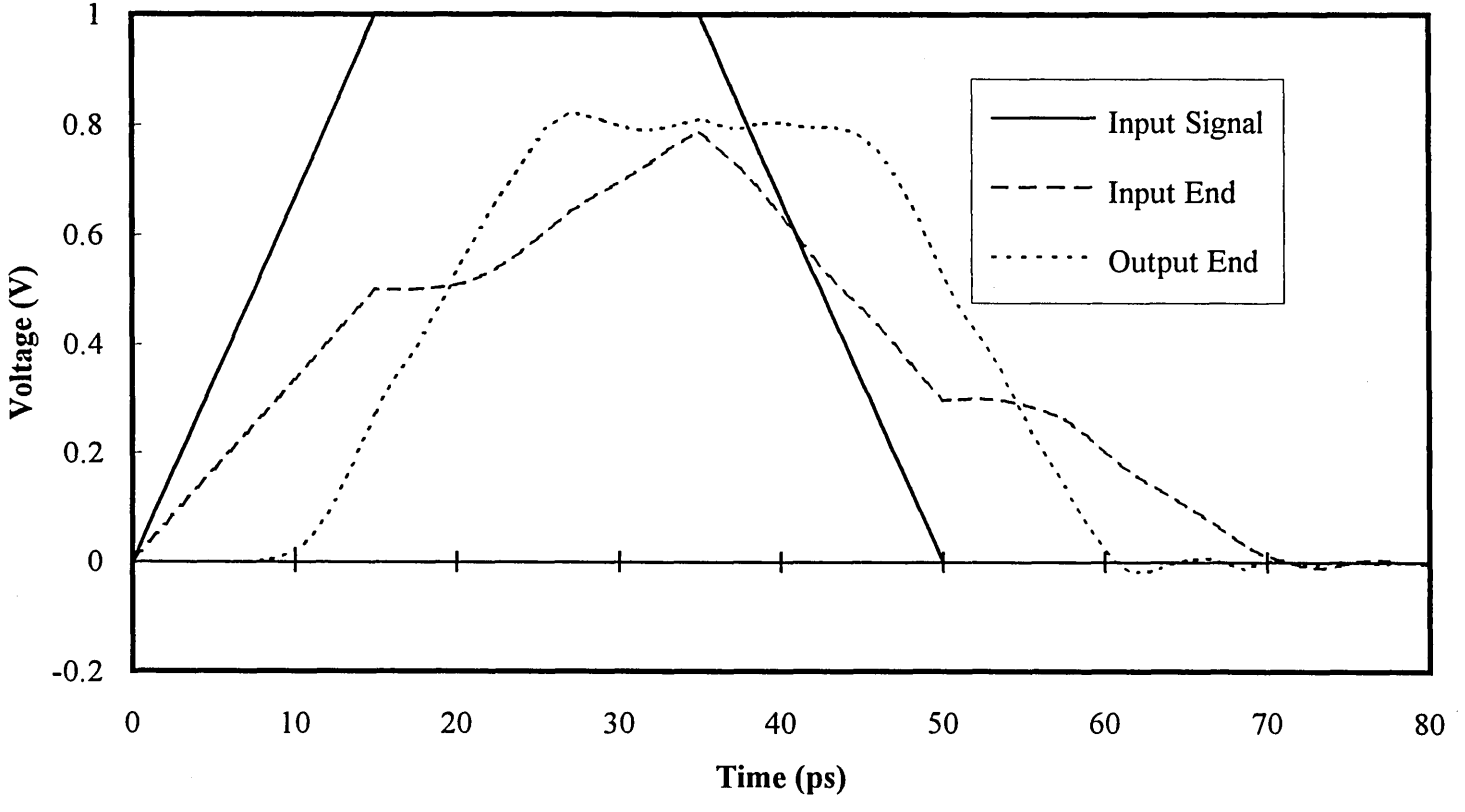

Figure 5.13 : Lossless line; $R_{in} = 100\Omega$, $Z_0 = 100\Omega$, $R_L = 400\Omega$

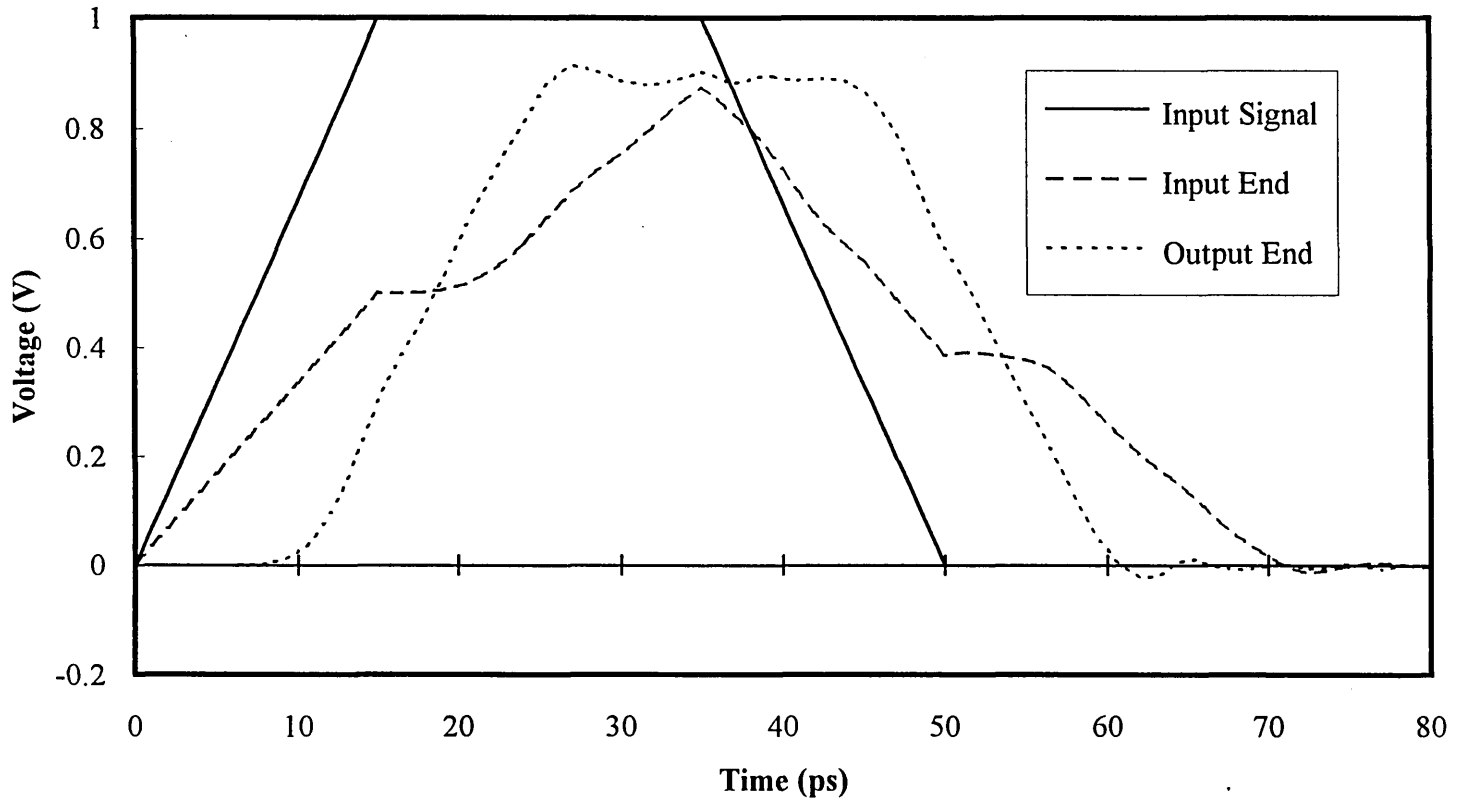

Figure 5.14 : Lossless line; $R_{in} = 100\Omega$, $Z_0 = 100\Omega$, $R_L = 800\Omega$

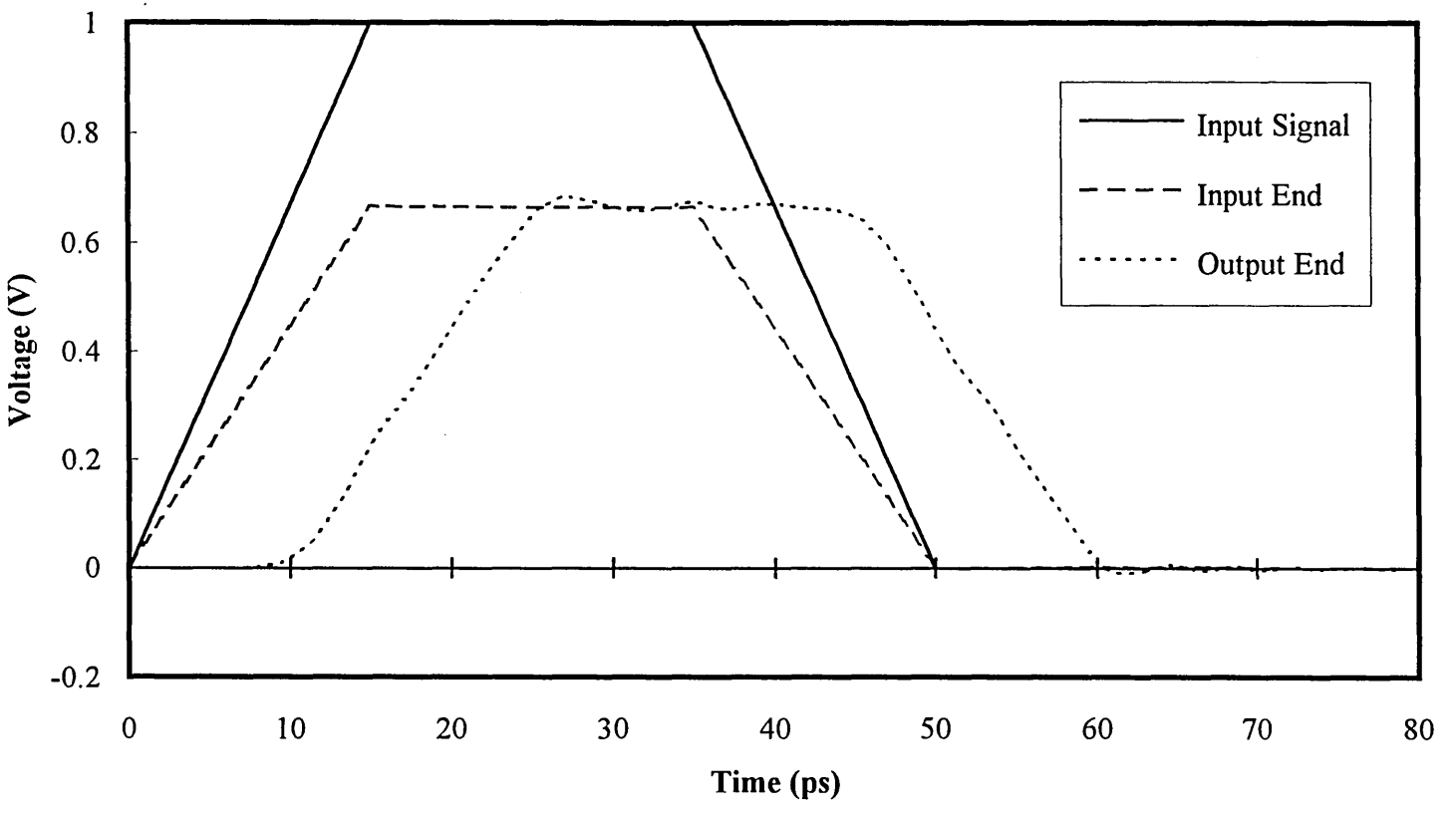

Figure 5.15 : Lossless line; R_{in} = 50Ω, Z0 = 100Ω, R_L = 100Ω.

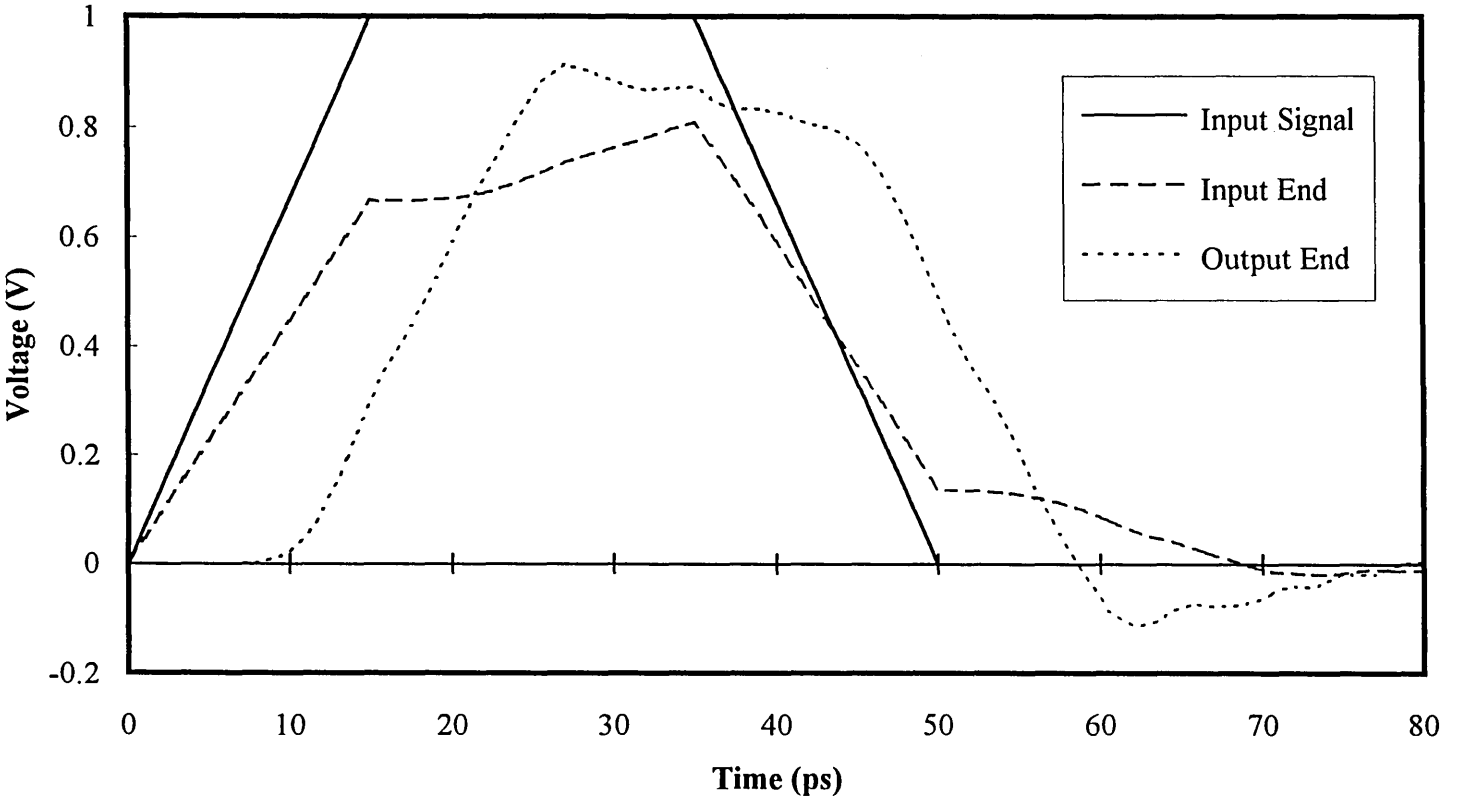

Figure 5.16 : Lossless line; $R_{in} = 50\Omega$, $Z_0 = 100\Omega$, $R_L = 200\Omega$

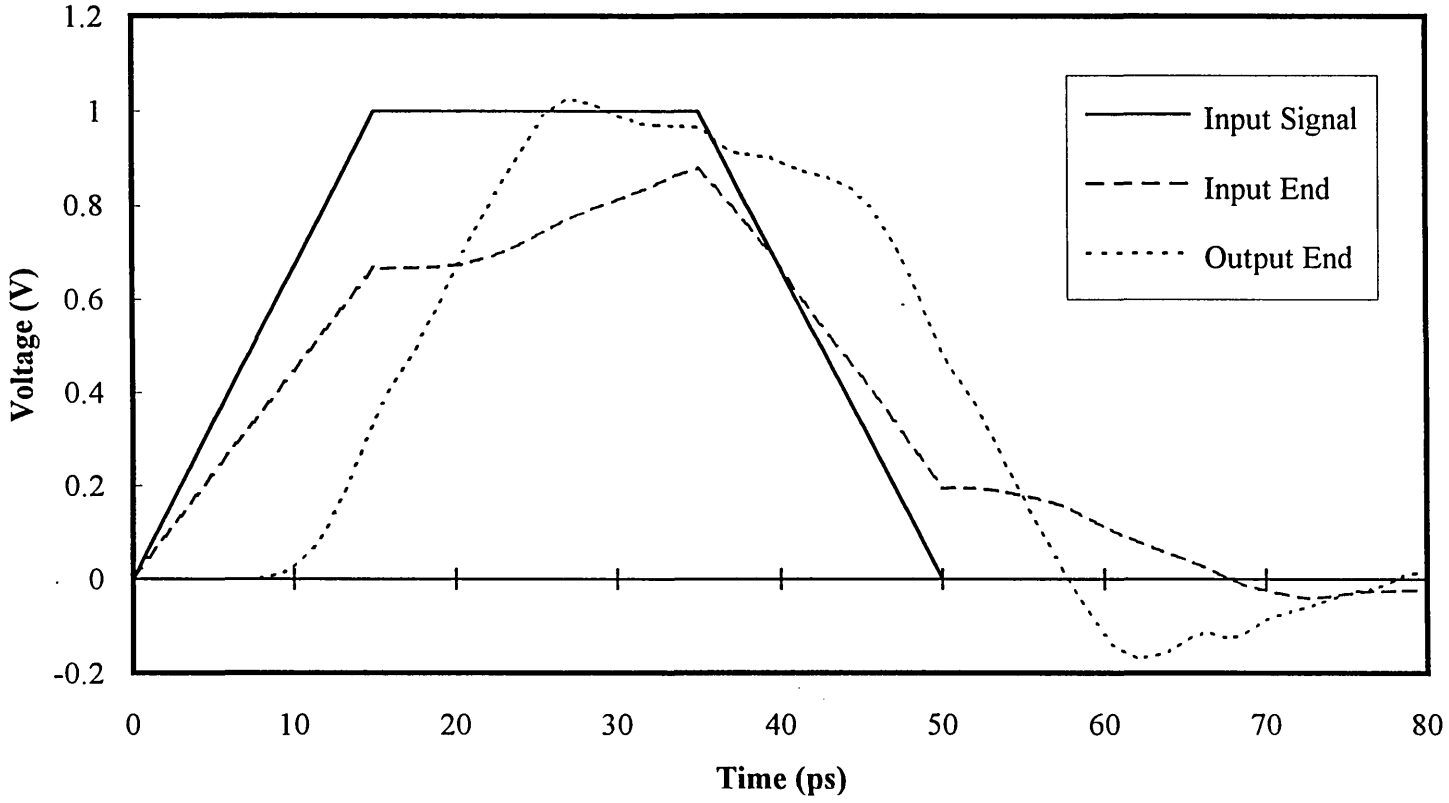

Figure 5.17 : Lossless line; $R_{in} = 50\Omega$, $Z_0 = 100\Omega$, $R_L = 300\Omega$

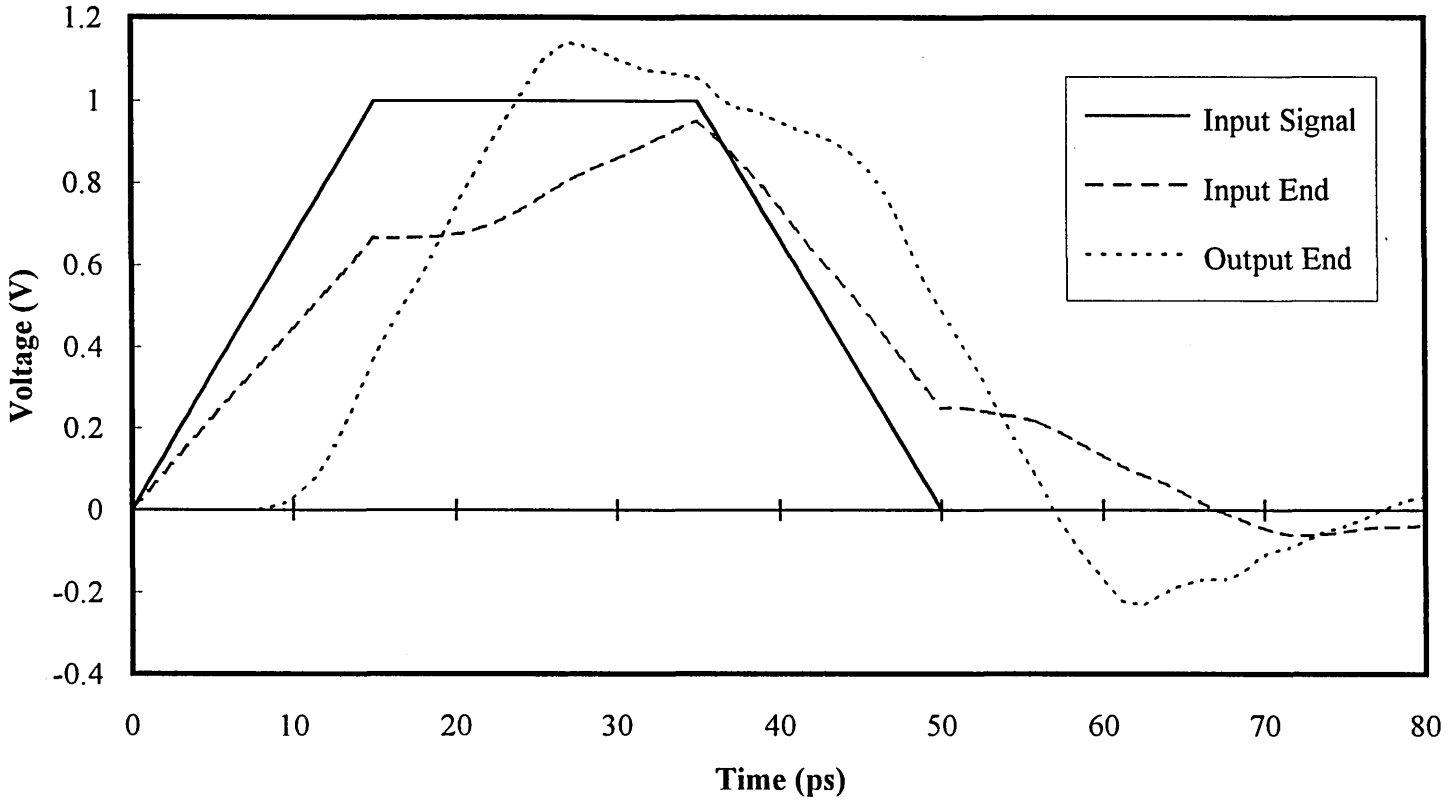

Figure 5.18 : Lossless line; $R_{in} = 50\Omega$, $Z_0 = 100\Omega$, $R_L = 500\Omega$

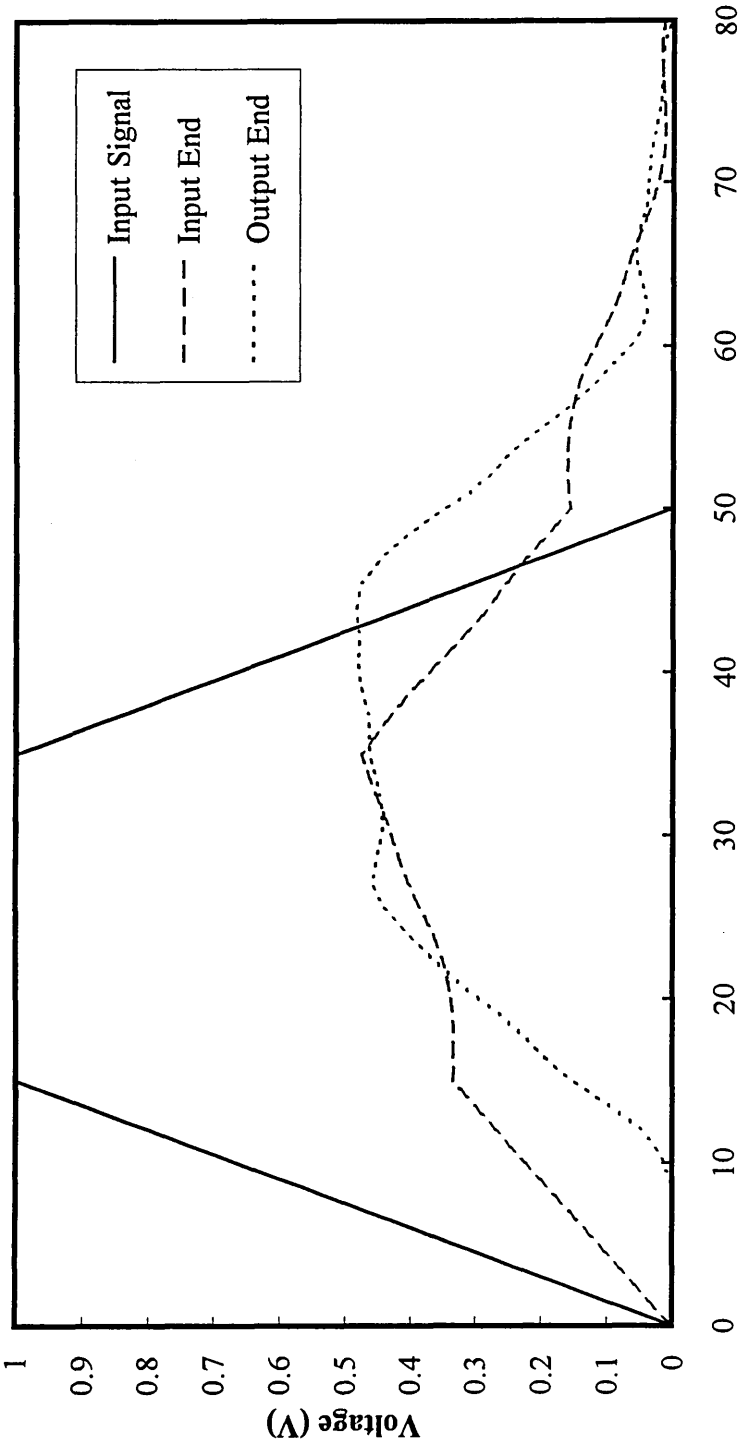

Figure 5.19 : Lossless line; $R_{in} = 200\Omega$, $Z_0 = 100\Omega$, $R_L = 200\Omega$

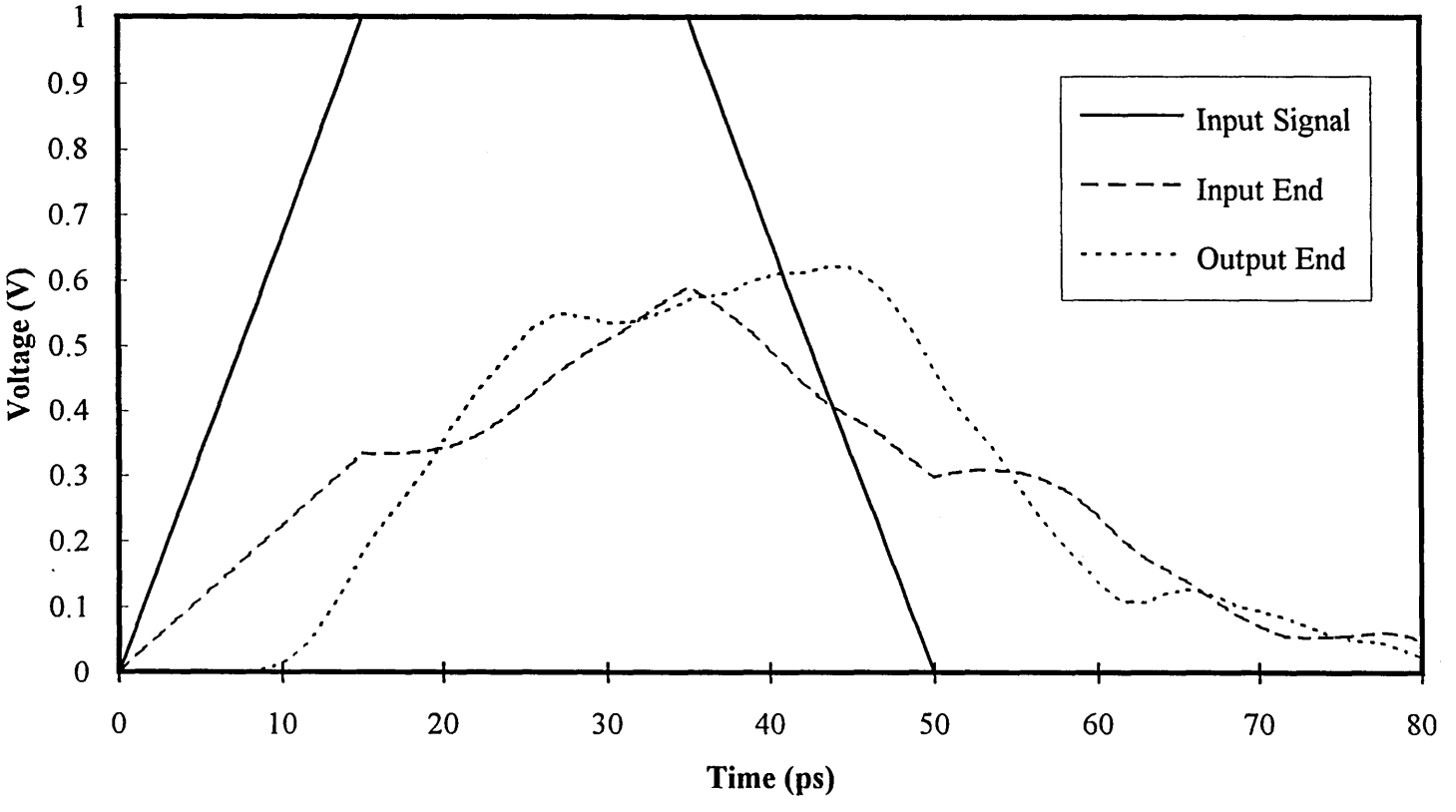

Figure 5.20 : Lossless line; $R_{in} = 200\Omega$, $Z_0 = 100\Omega$, $R_L = 400\Omega$

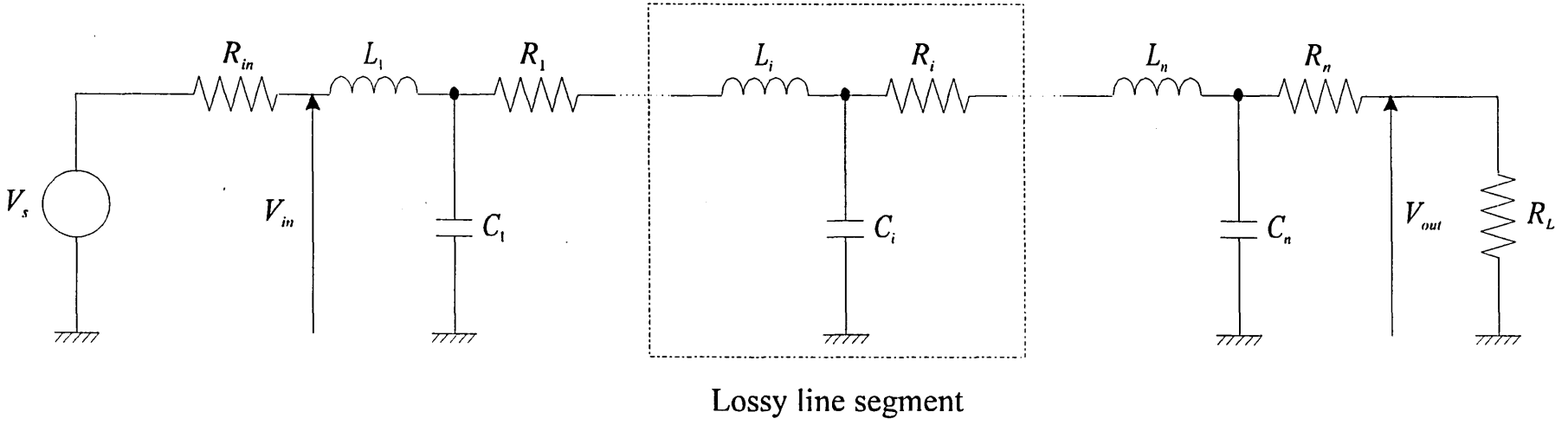

Figure 5.21 : Schematic diagram of a lossy transmission line equivalent circuit.

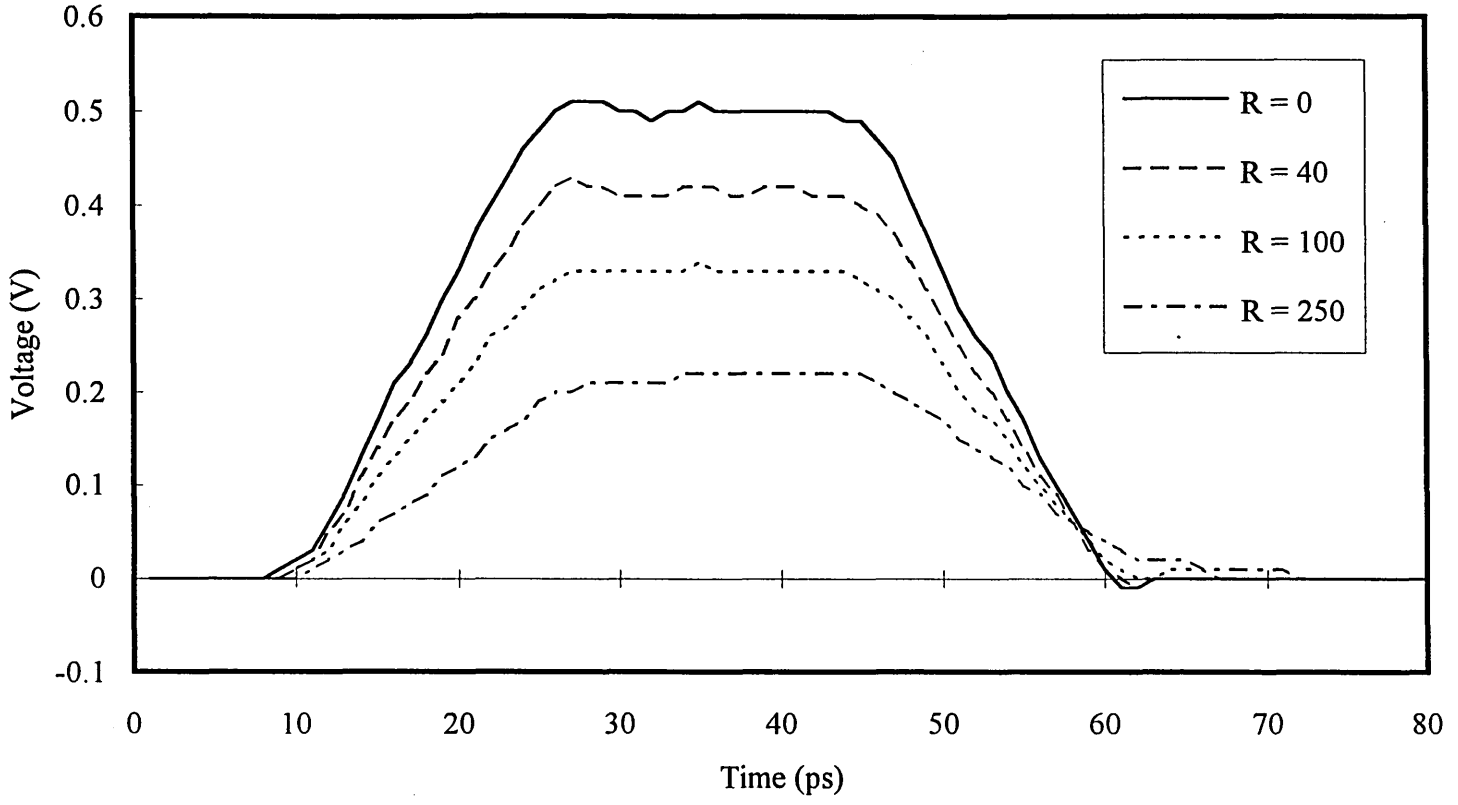

Figure 5.22 : Graph of varying R_i for $Z_0 = 100\Omega$.

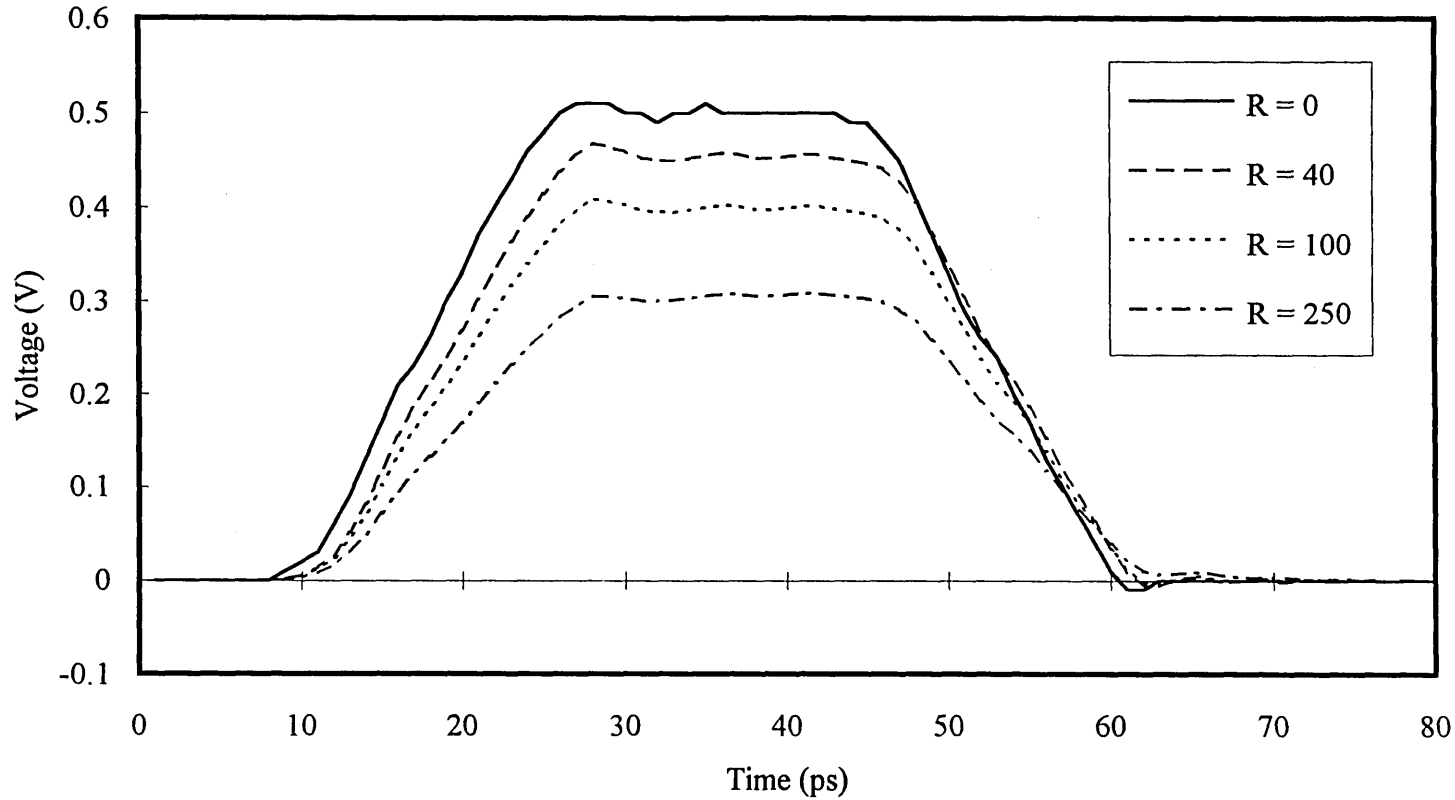

Figure 5.23 : Graph of varying R_i for $Z_0 = 200\Omega$.

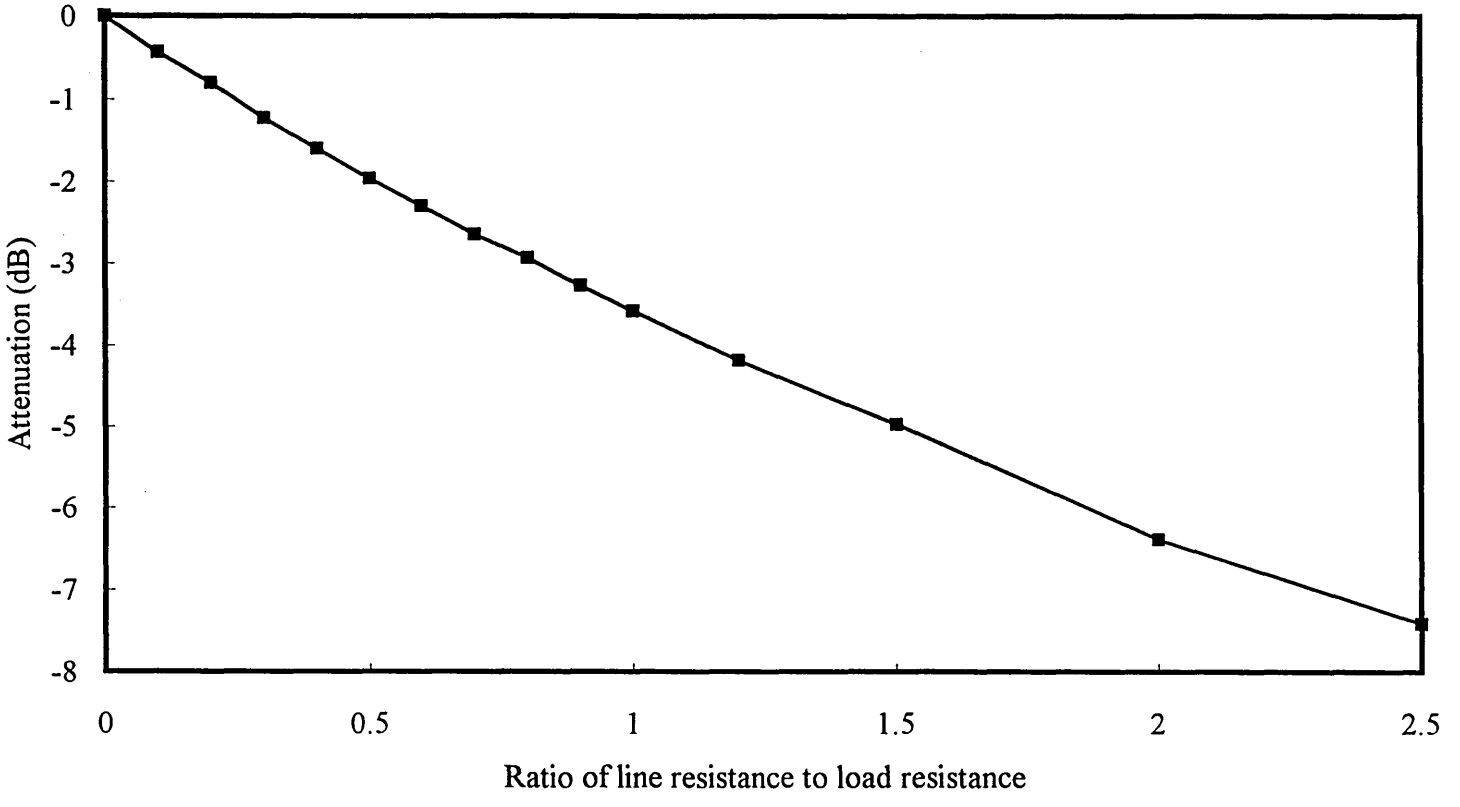

Figure 5.24 : Graph of attenuation versus the load ratio.

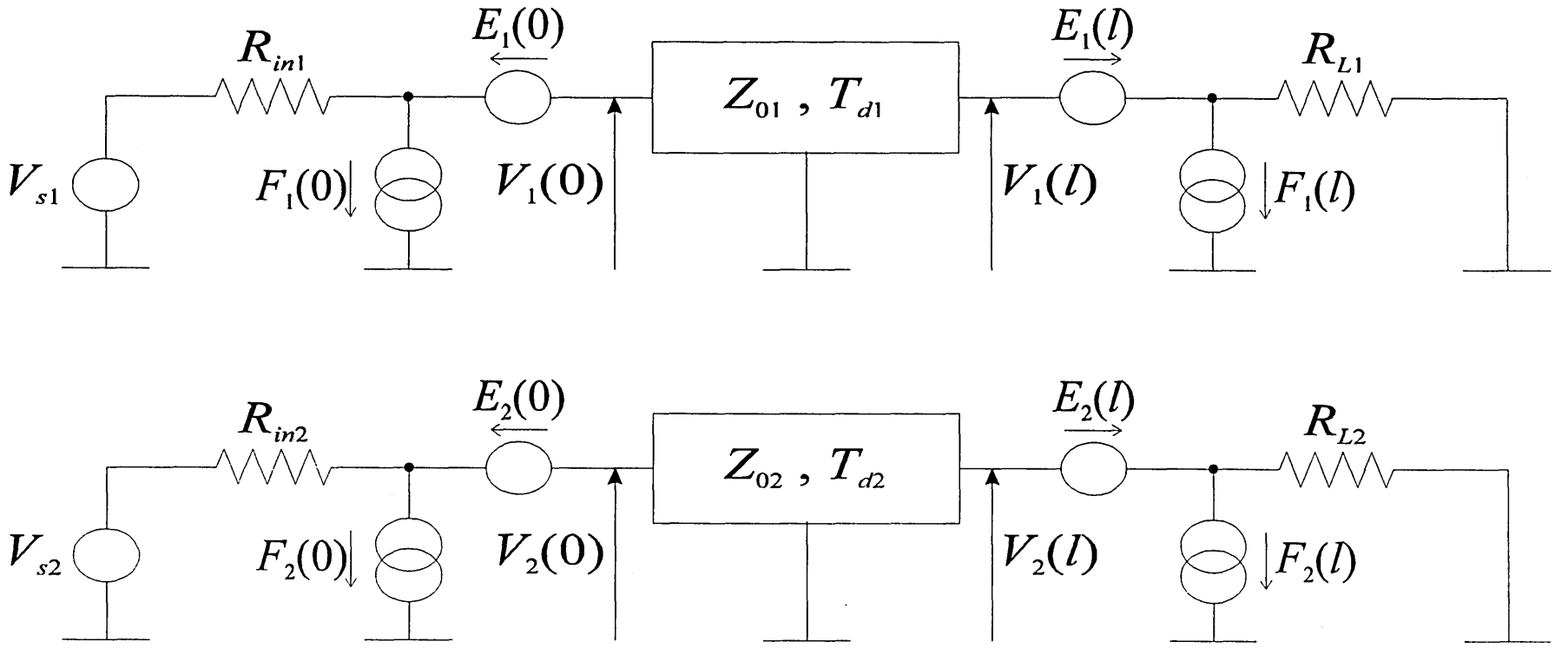

Figure 5.25 : Configuration used for simulating a pair of microstrip lines.

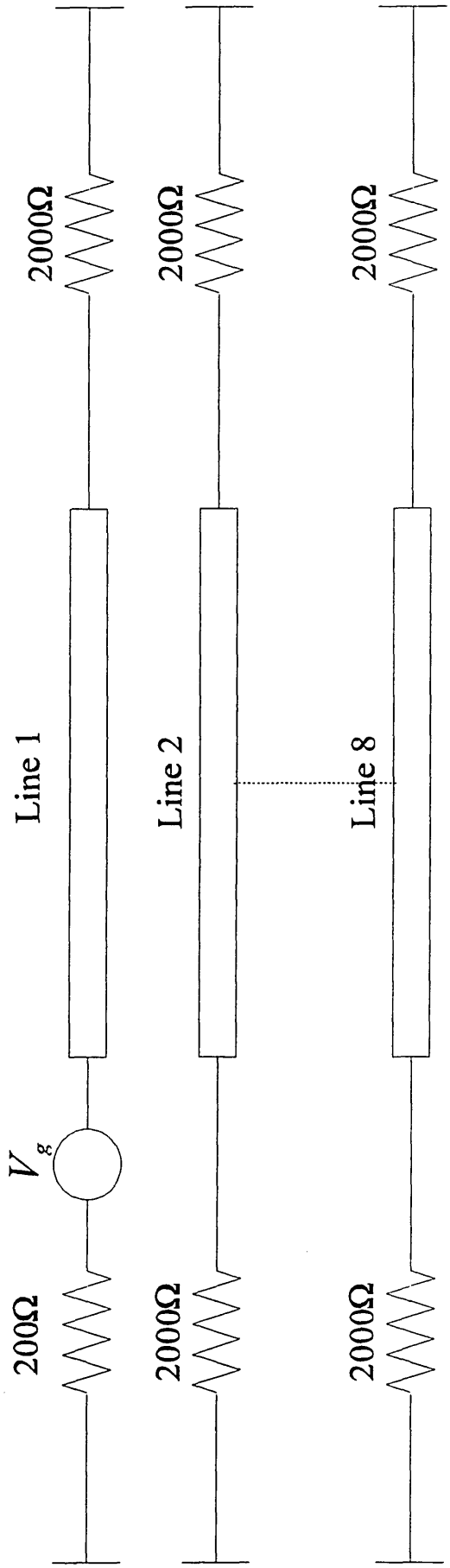

Figure 5.26 : Operating configuration of the eight line bus.

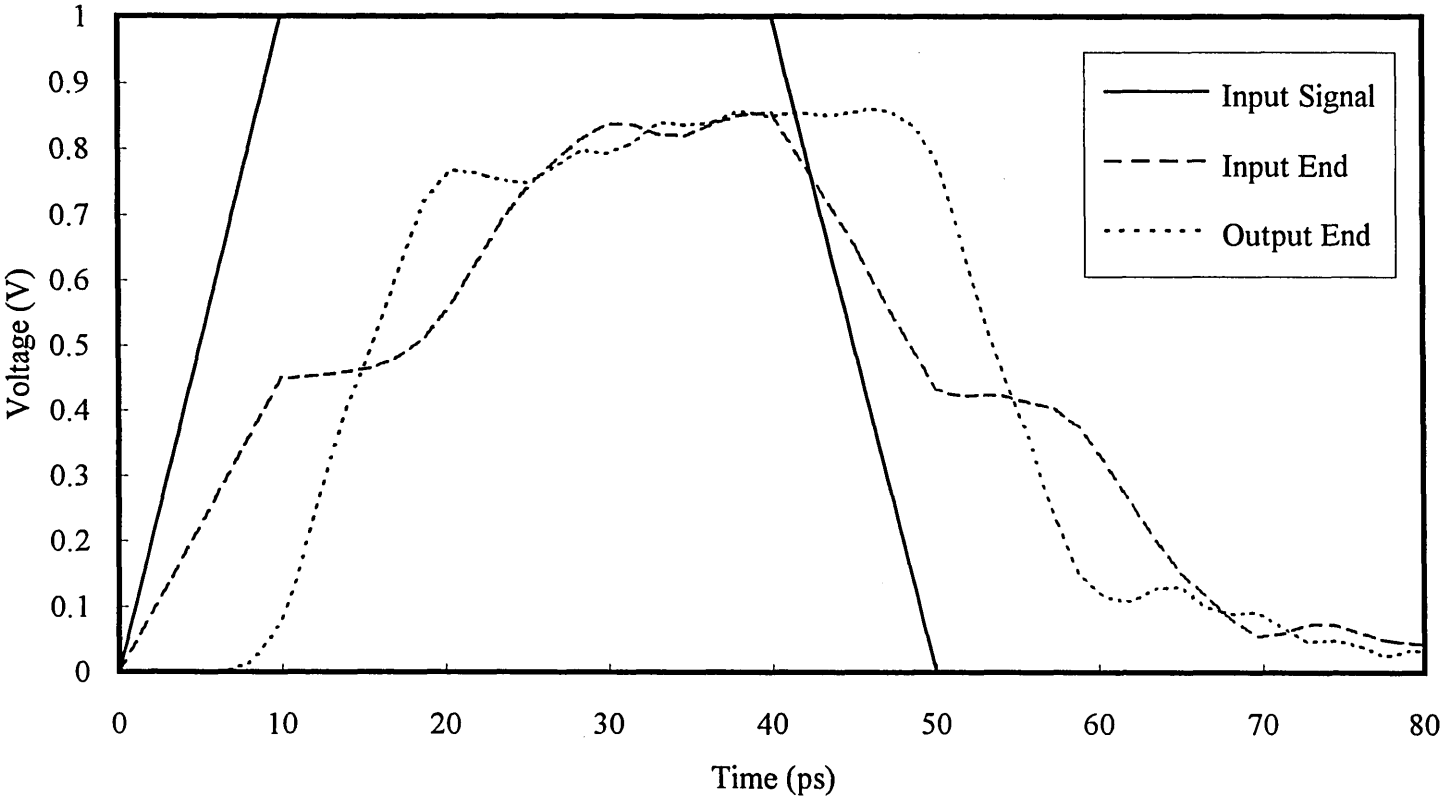

Figure 5.27 : Voltage waveforms present at both ends of line 1.

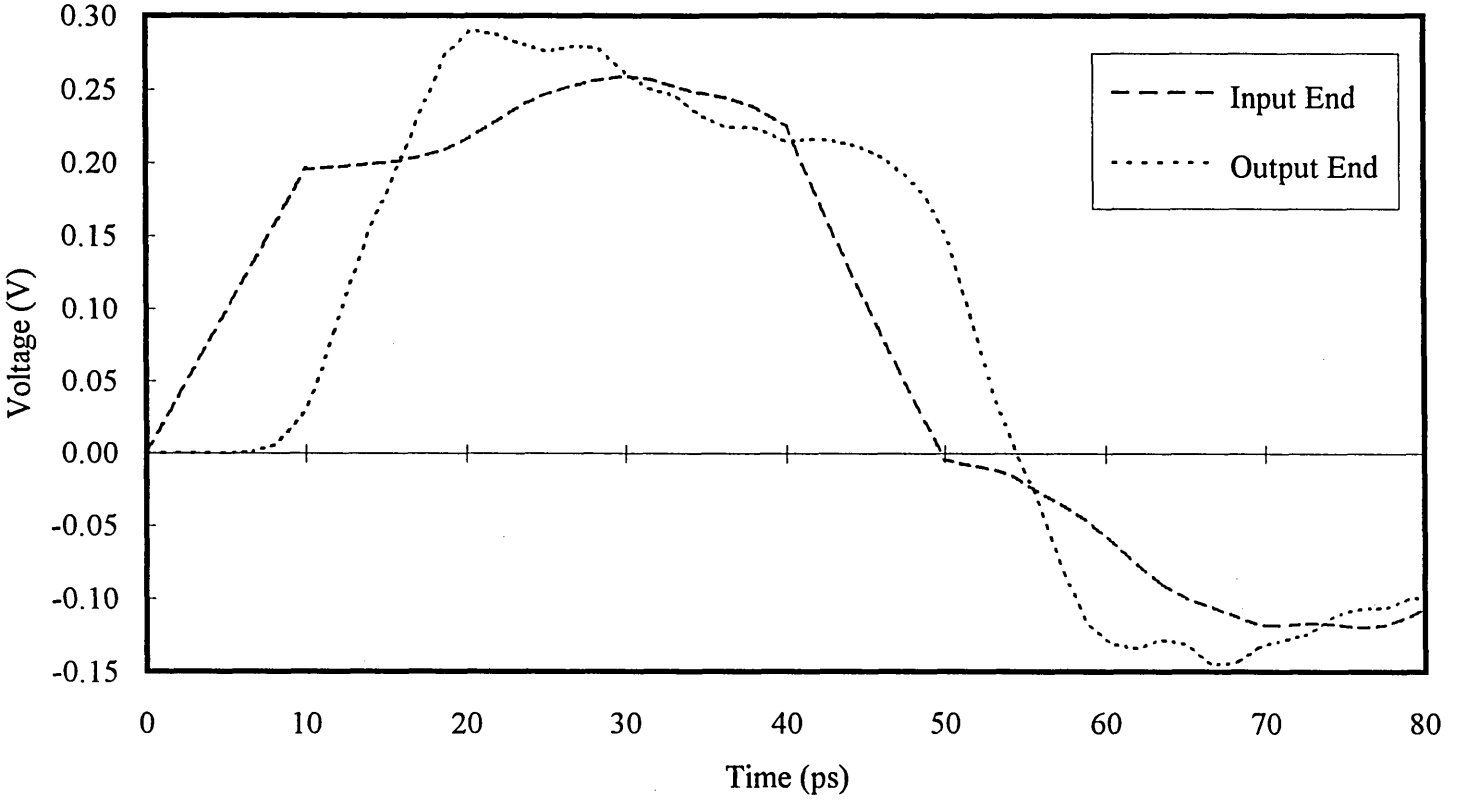

Figure 5.28 : Voltage waveforms present at both ends of line 2.

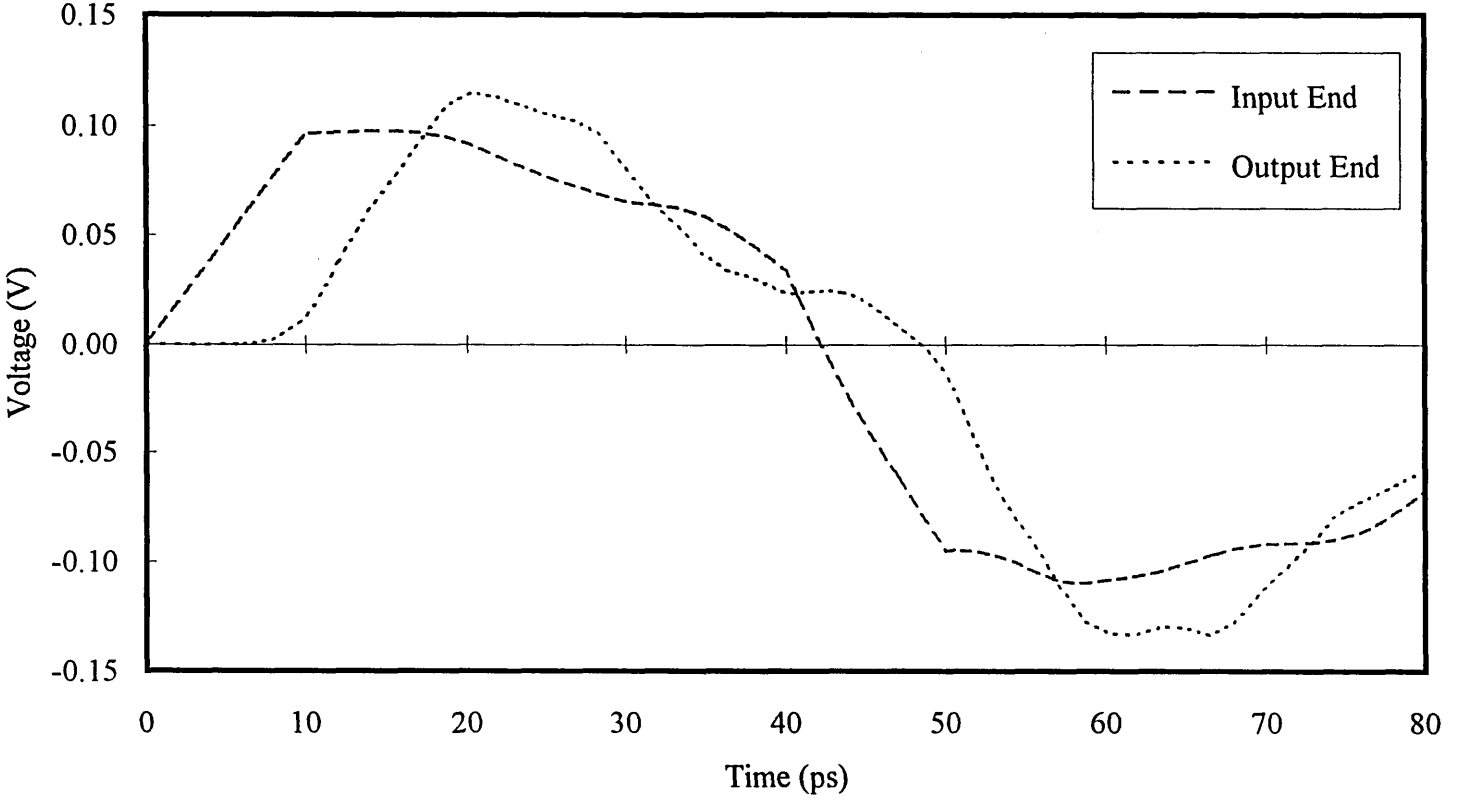

Figure 5.29 : Voltage waveforms present at both ends of line 3.

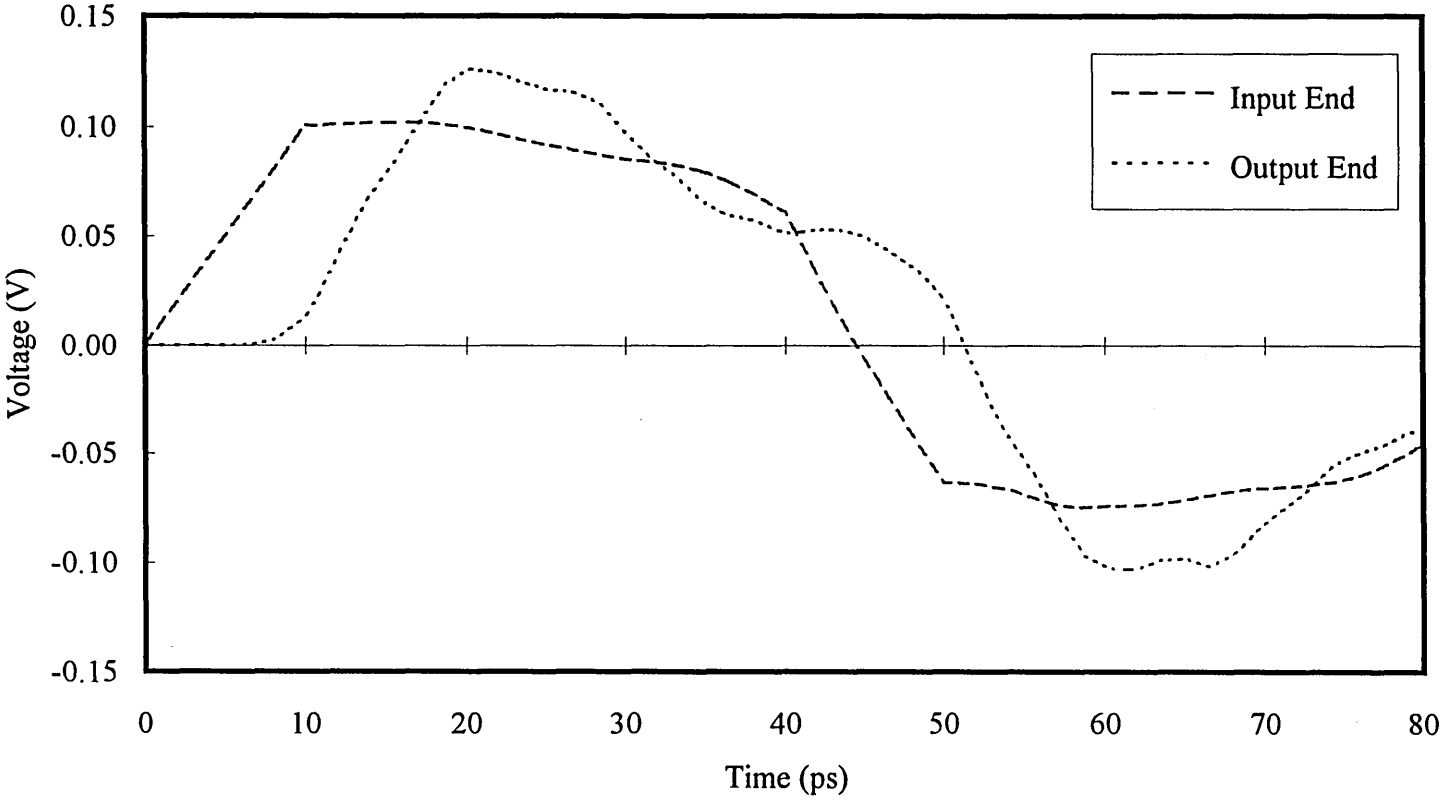

Figure 5.30 : Voltage waveforms present at both ends of line 4.

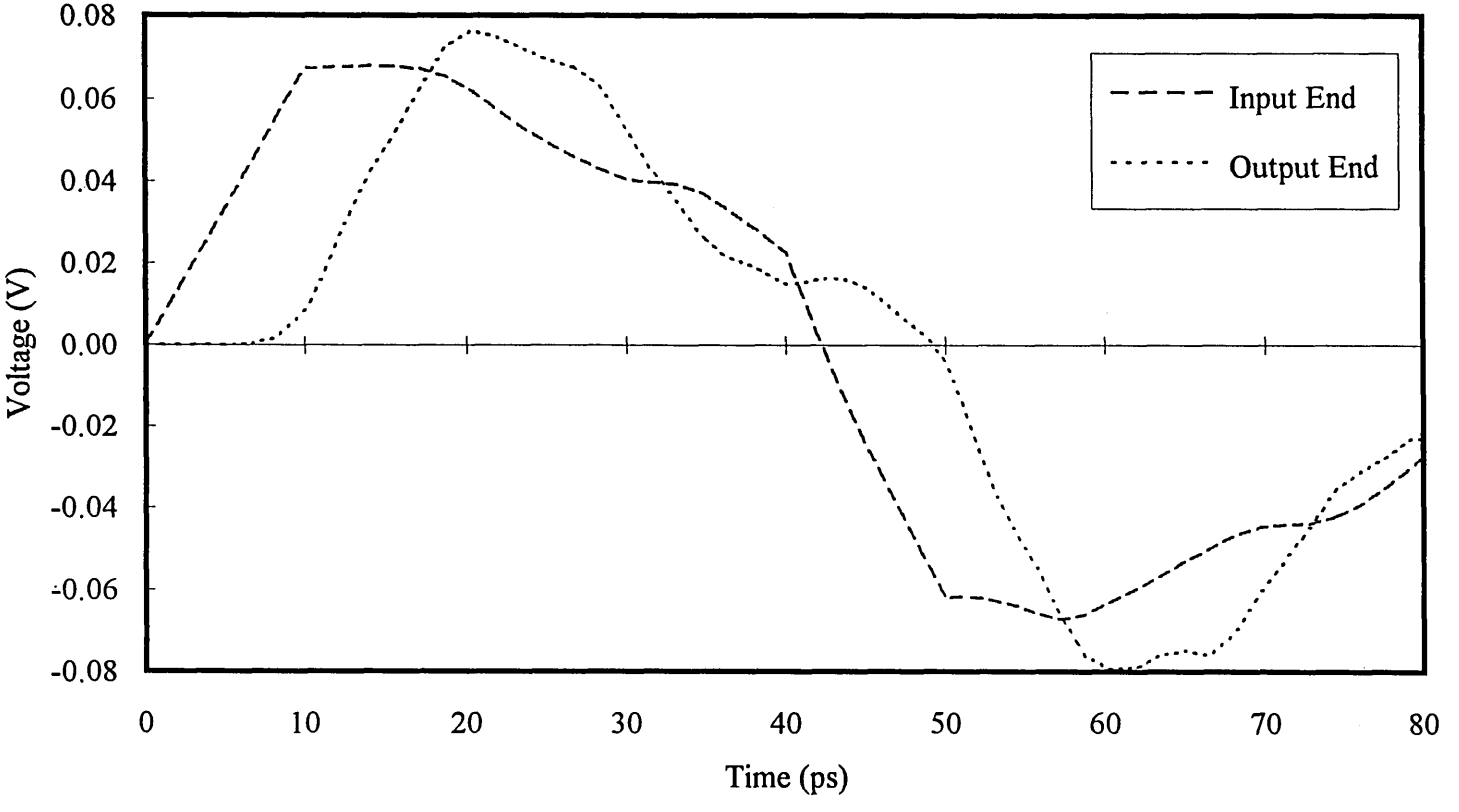

Figure 5.31 : Voltage waveforms present at both ends of line 5.

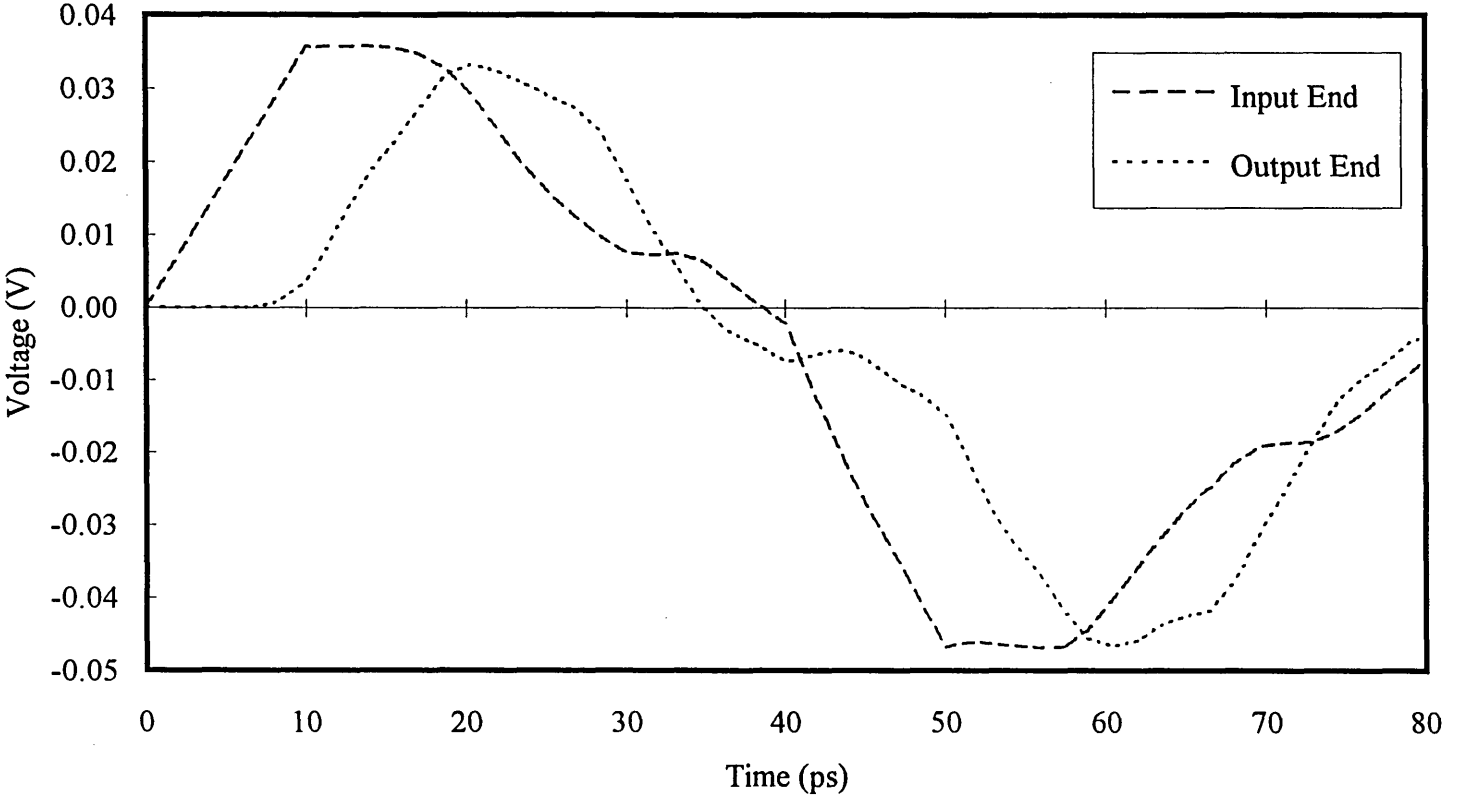

Figure 5.32 : Voltage waveforms present at both ends of line 6.

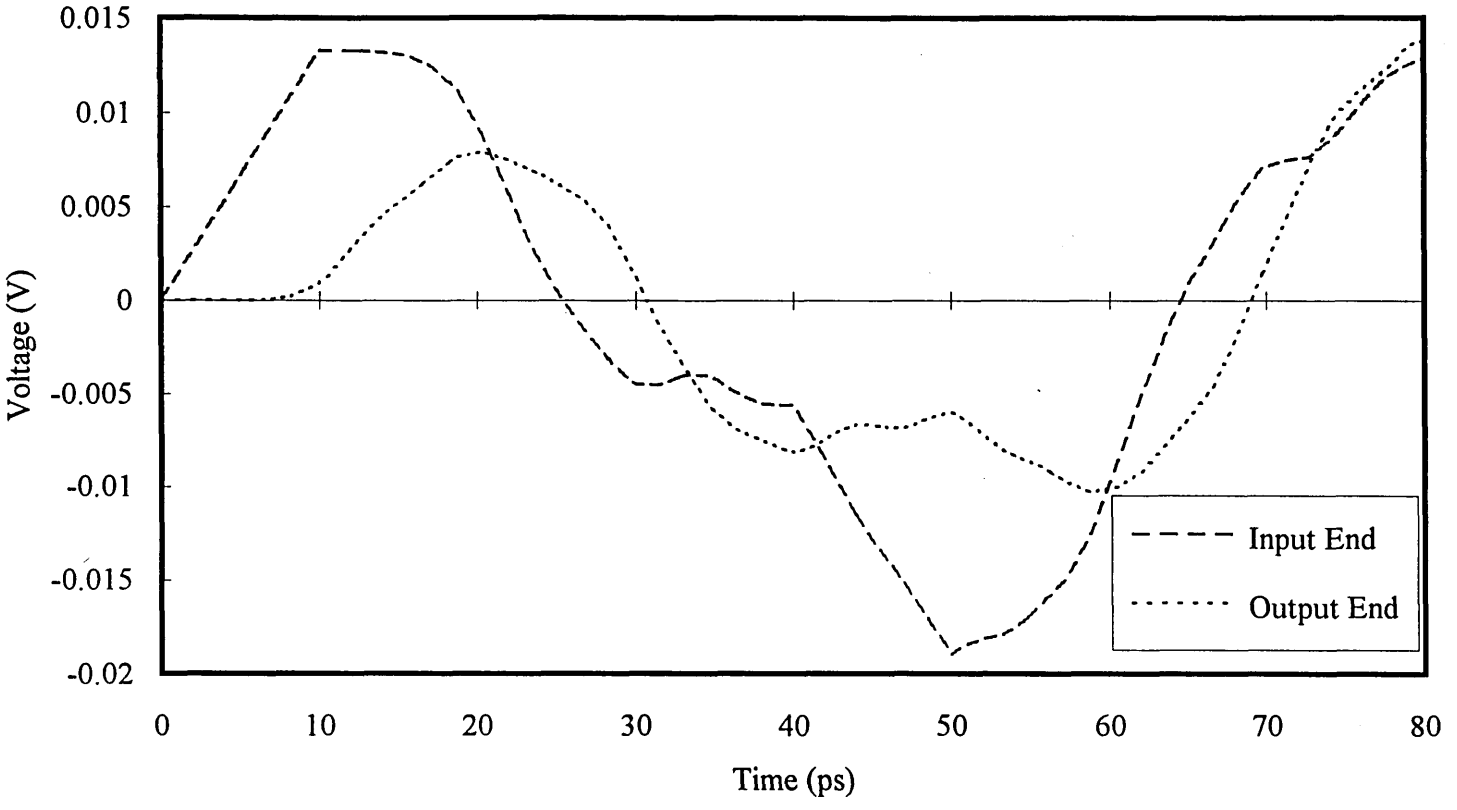

Figure 5.33 : Voltage waveforms present at both ends of line 7.

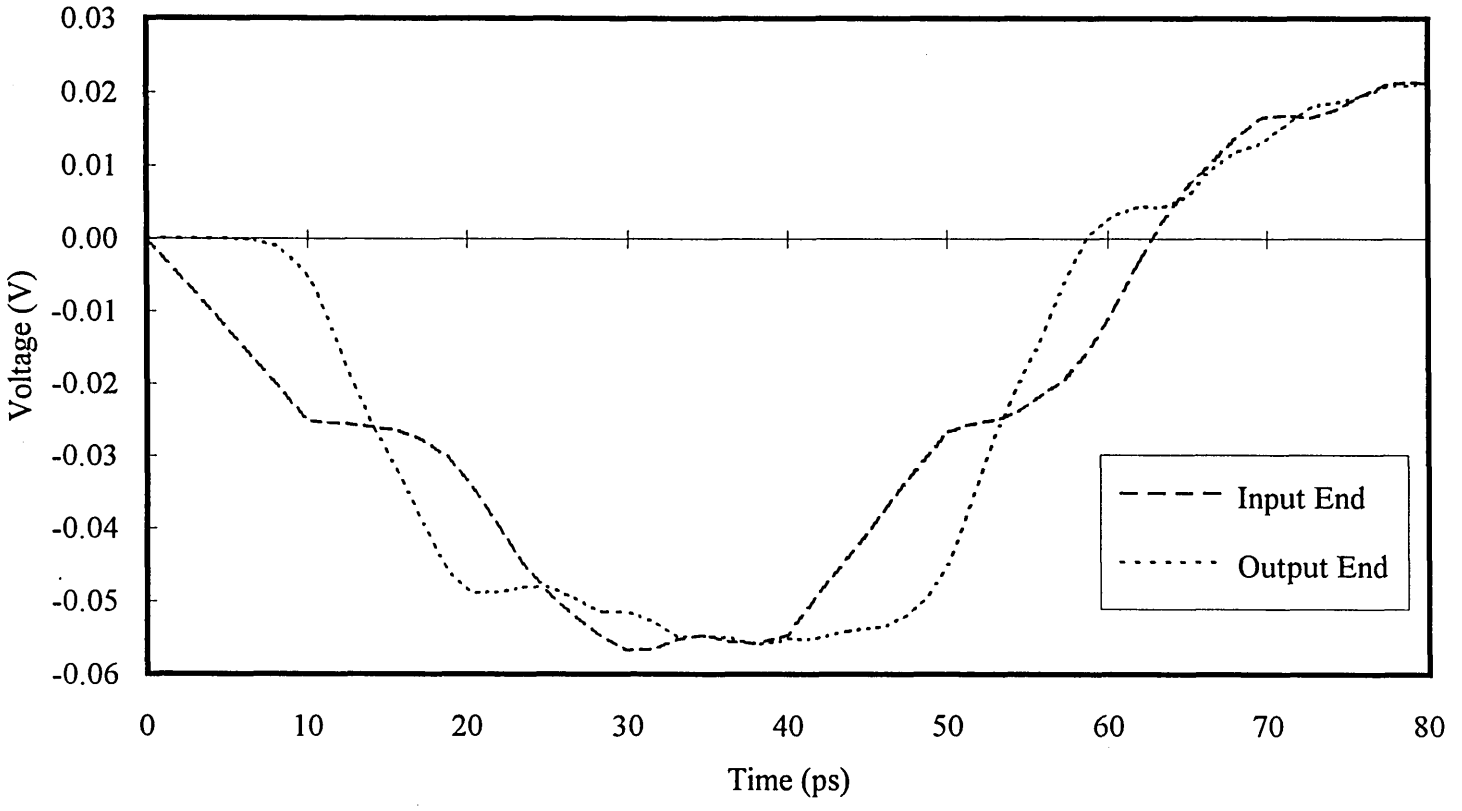

Figure 5.34 : Voltage waveforms present at both ends of line 8.

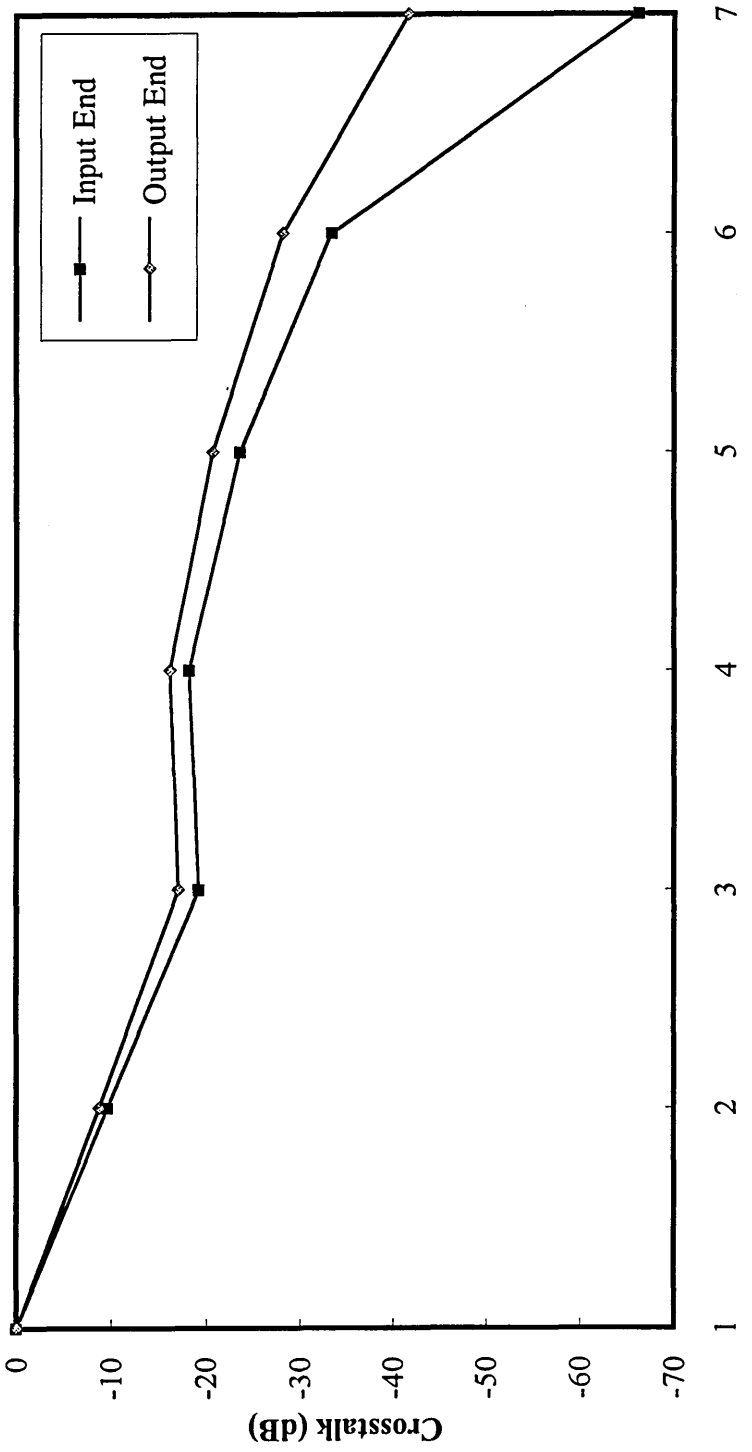

Figure 5.35 : Graph of crosstalk versus line no. for pulse input on line 1 only.

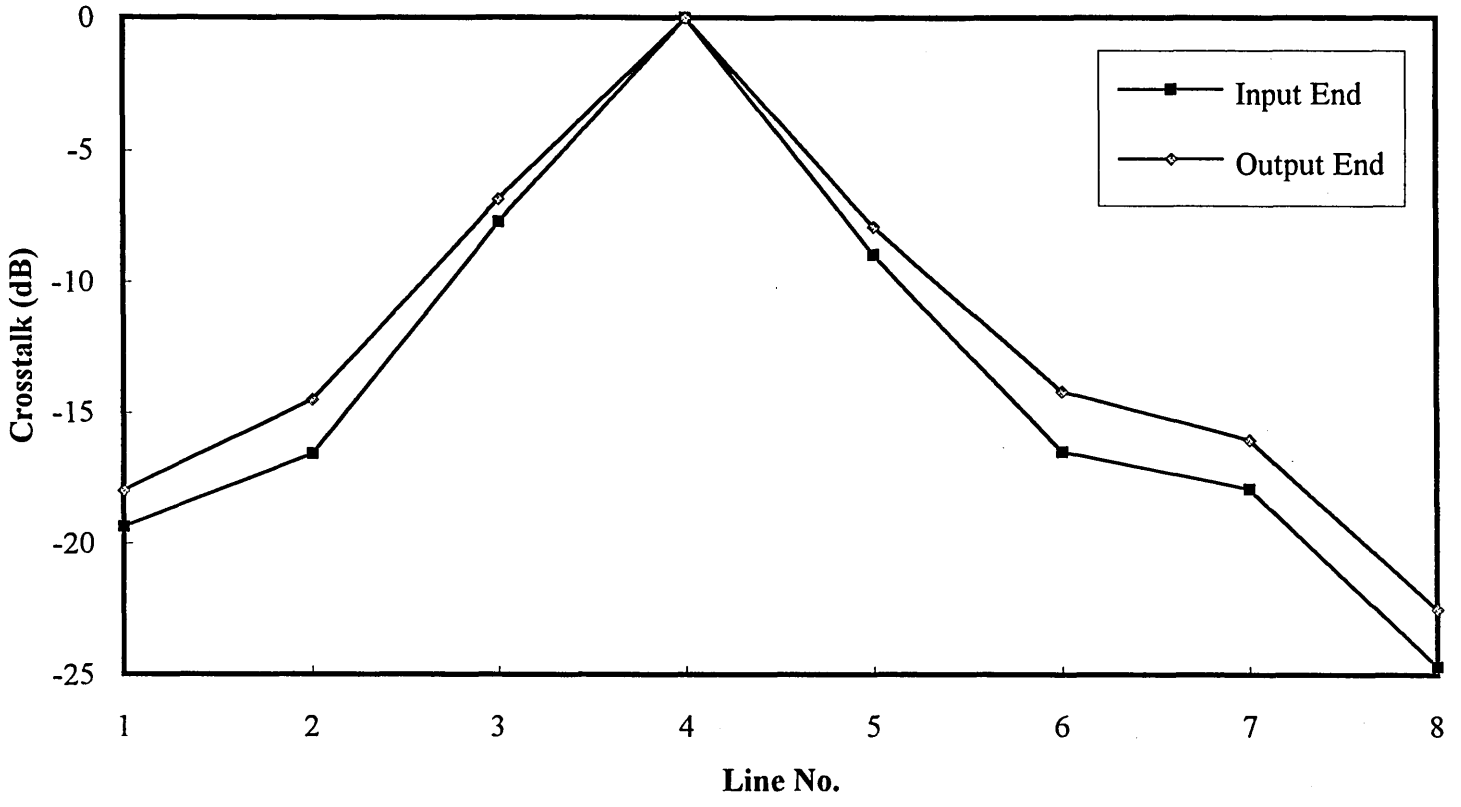

Figure 5.36 : Graph of crosstalk versus line no. for pulse input on line 4 only.

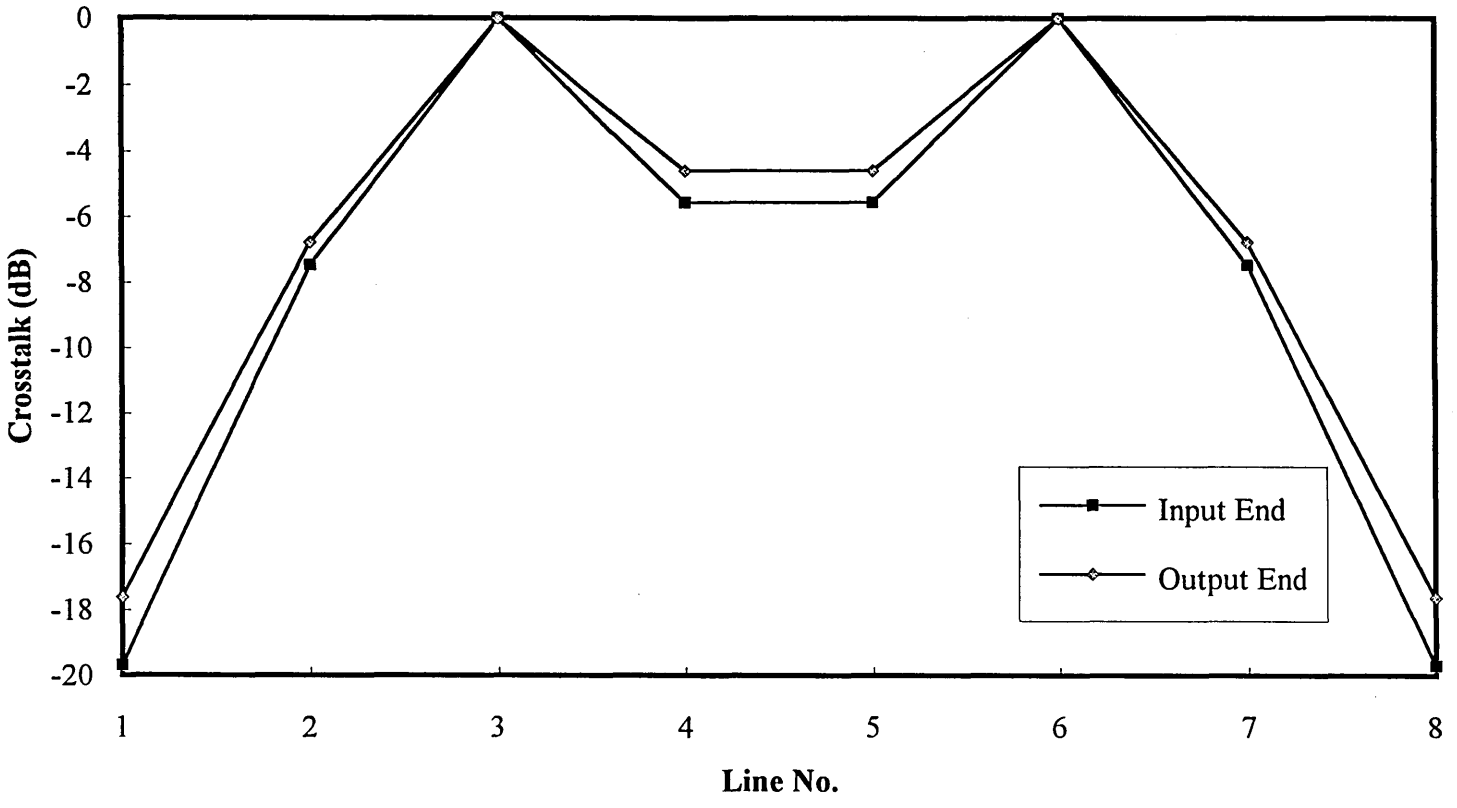

Figure 5.37 : Graph of crosstalk versus line no. for pulse input on lines 3 and 6.

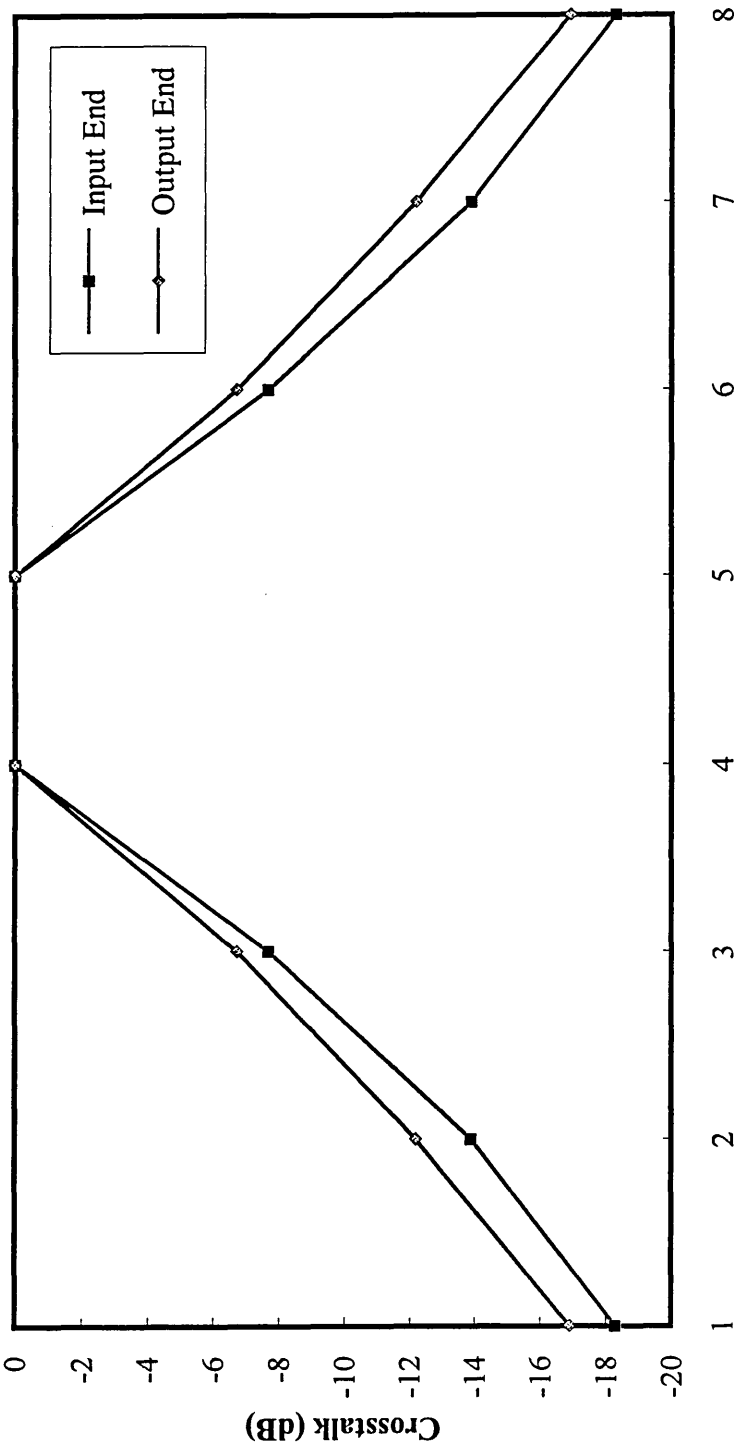

Figure 5.38 : Graph of crosstalk versus line no. for pulse input on lines 4 and 5.

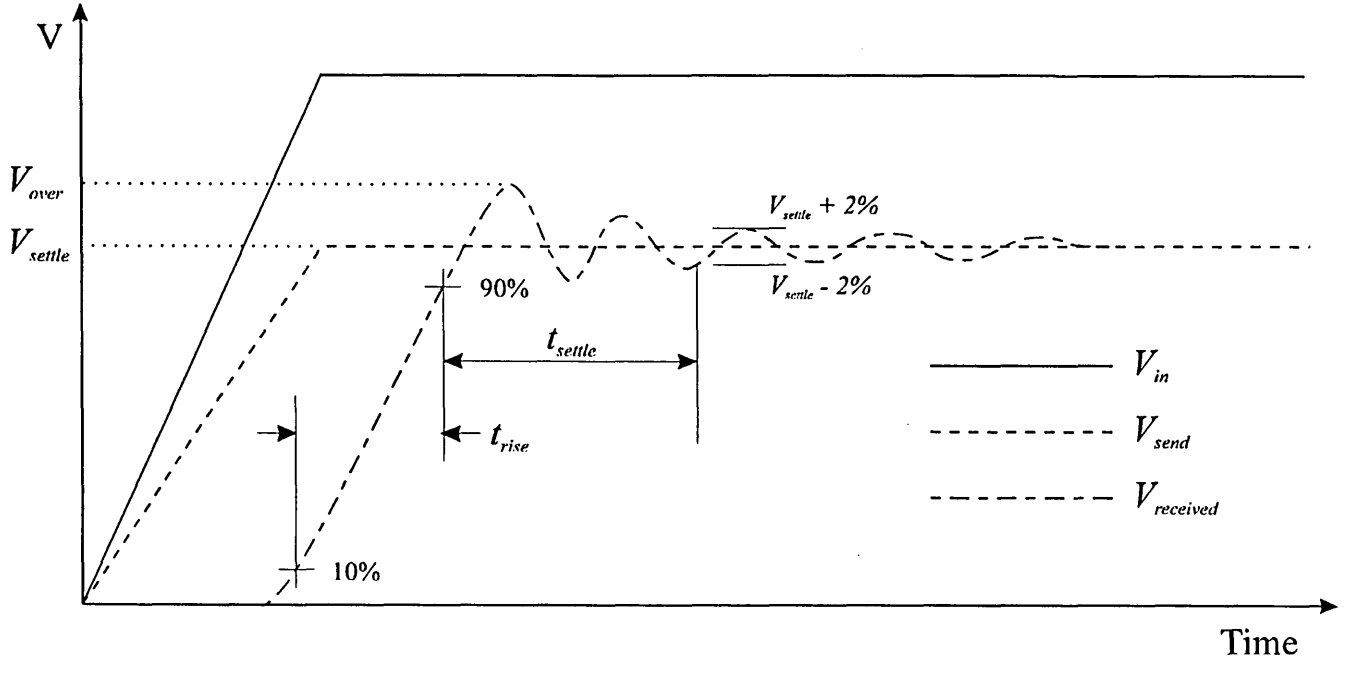

Figure 5.39 : Diagram of risetime parameters

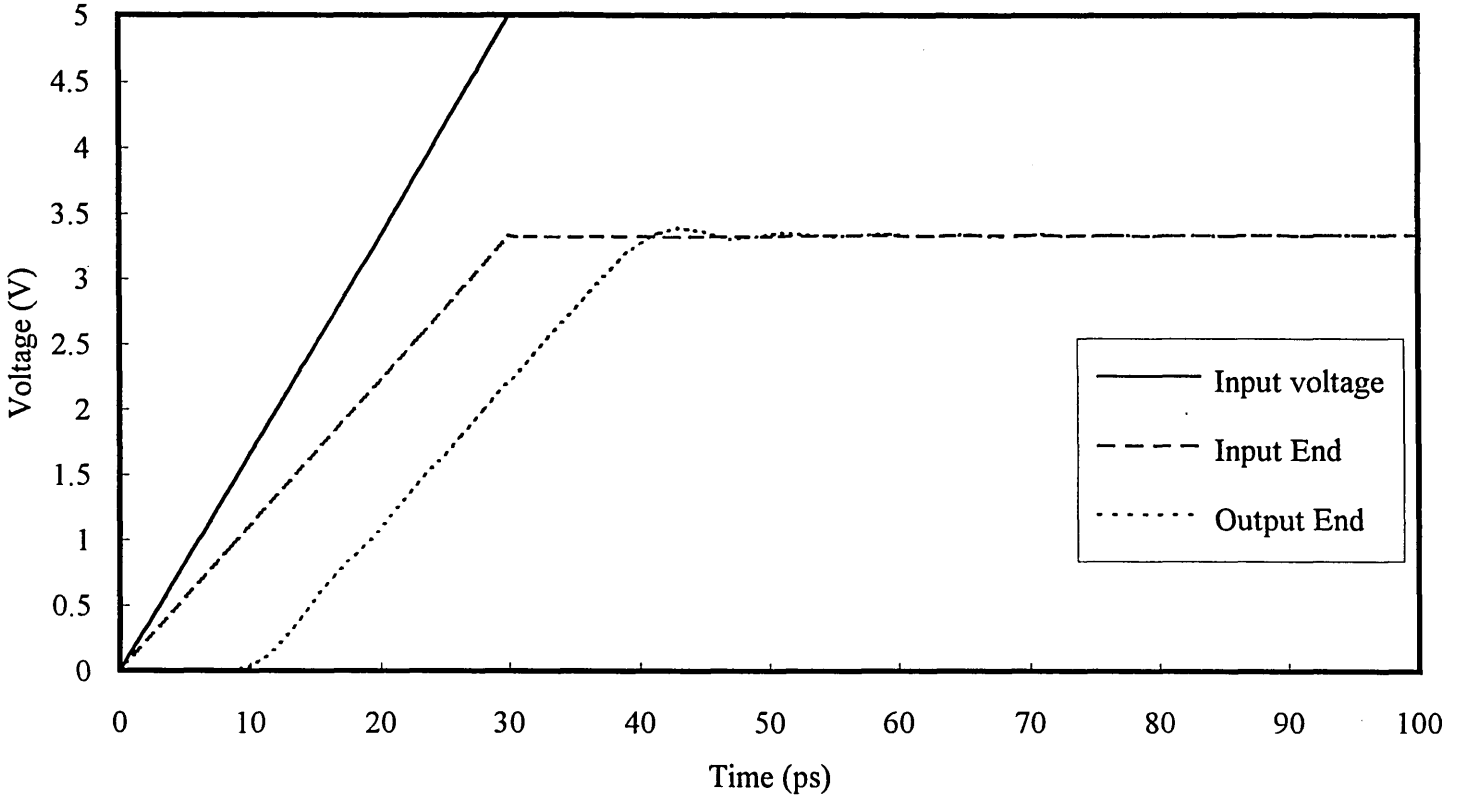

Figure 5.40 : 30ps risetime

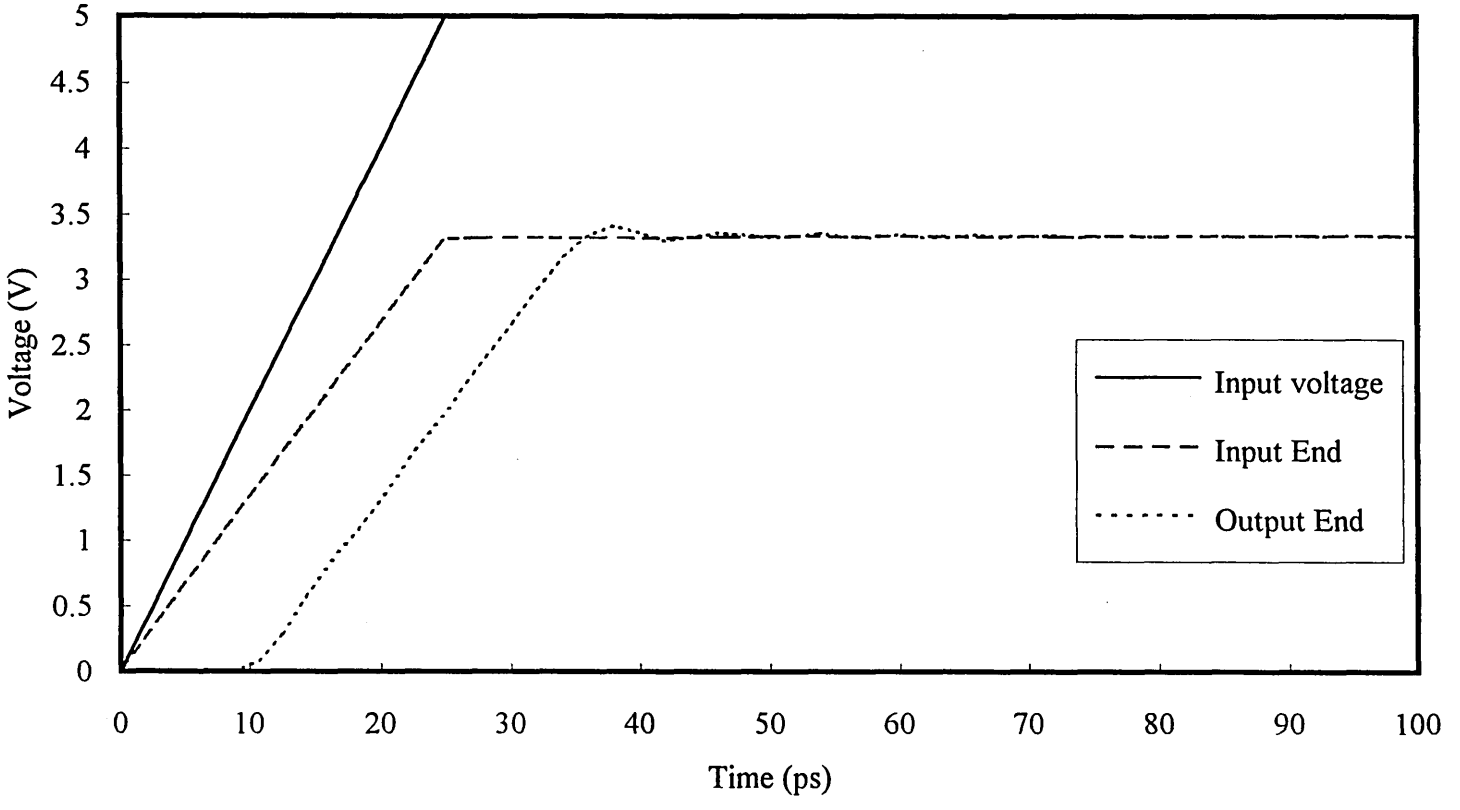

Figure 5.41 : 25ps risetime

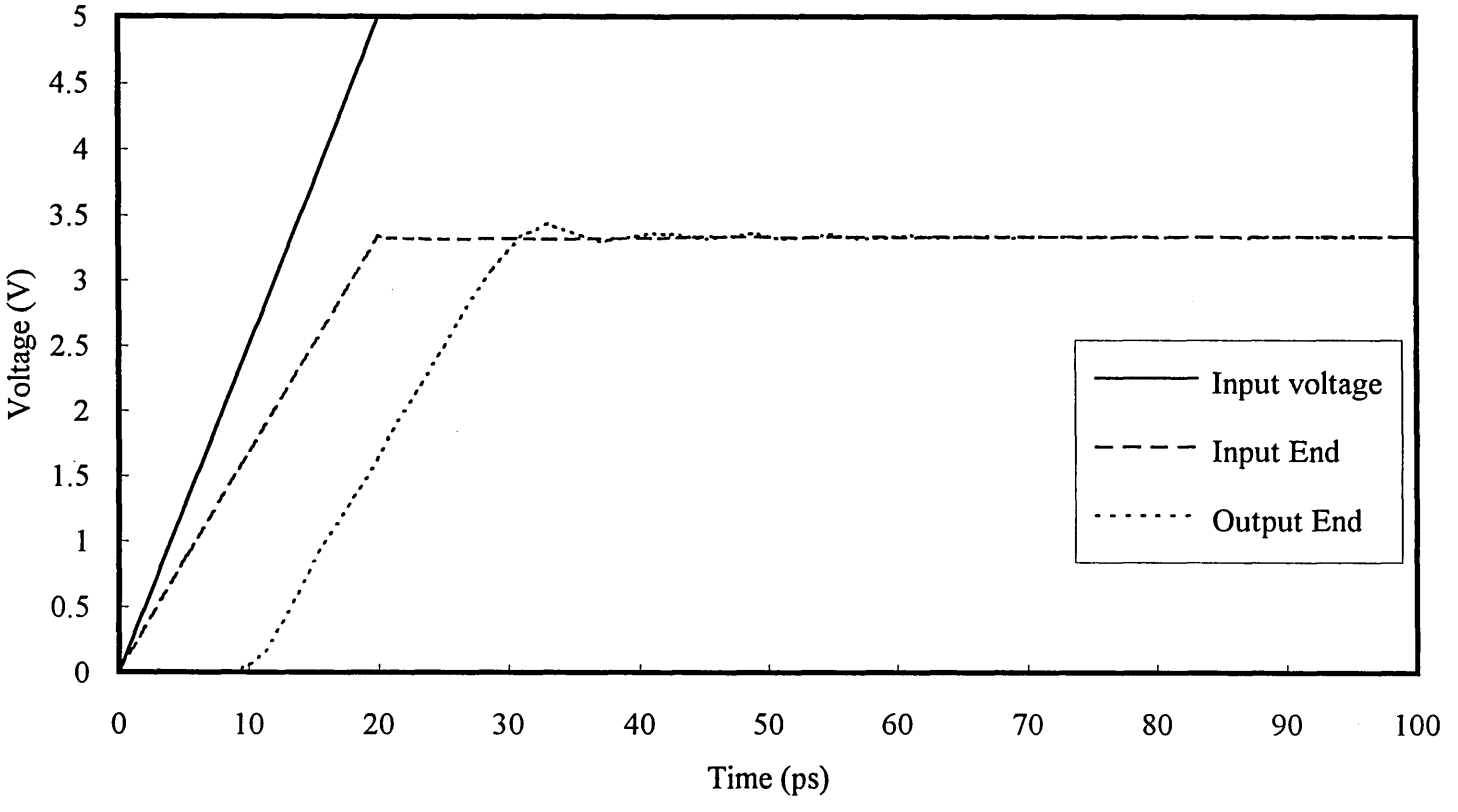

Figure 5.42 : 20ps risetime

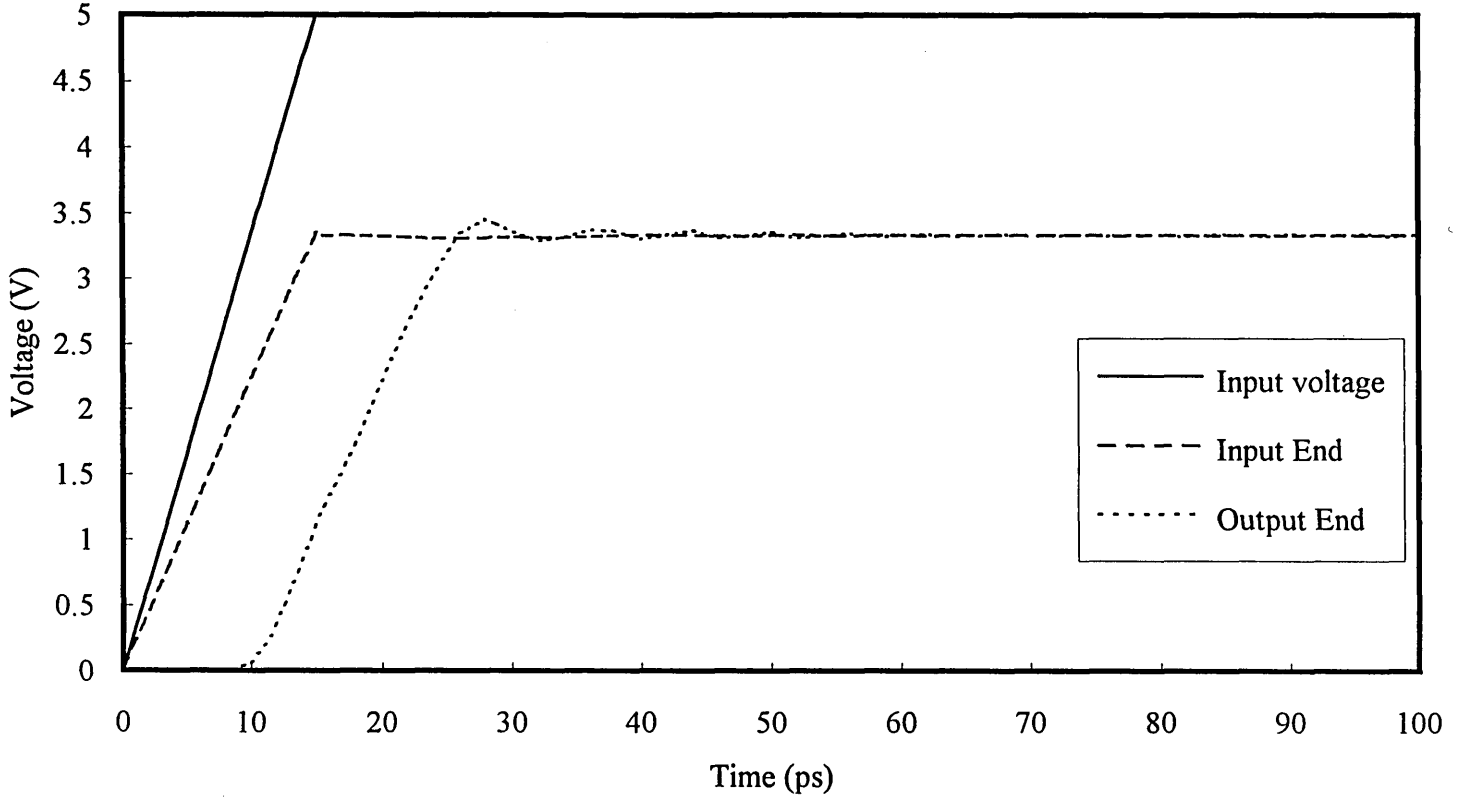

Figure 5.43 : 15ps risetime

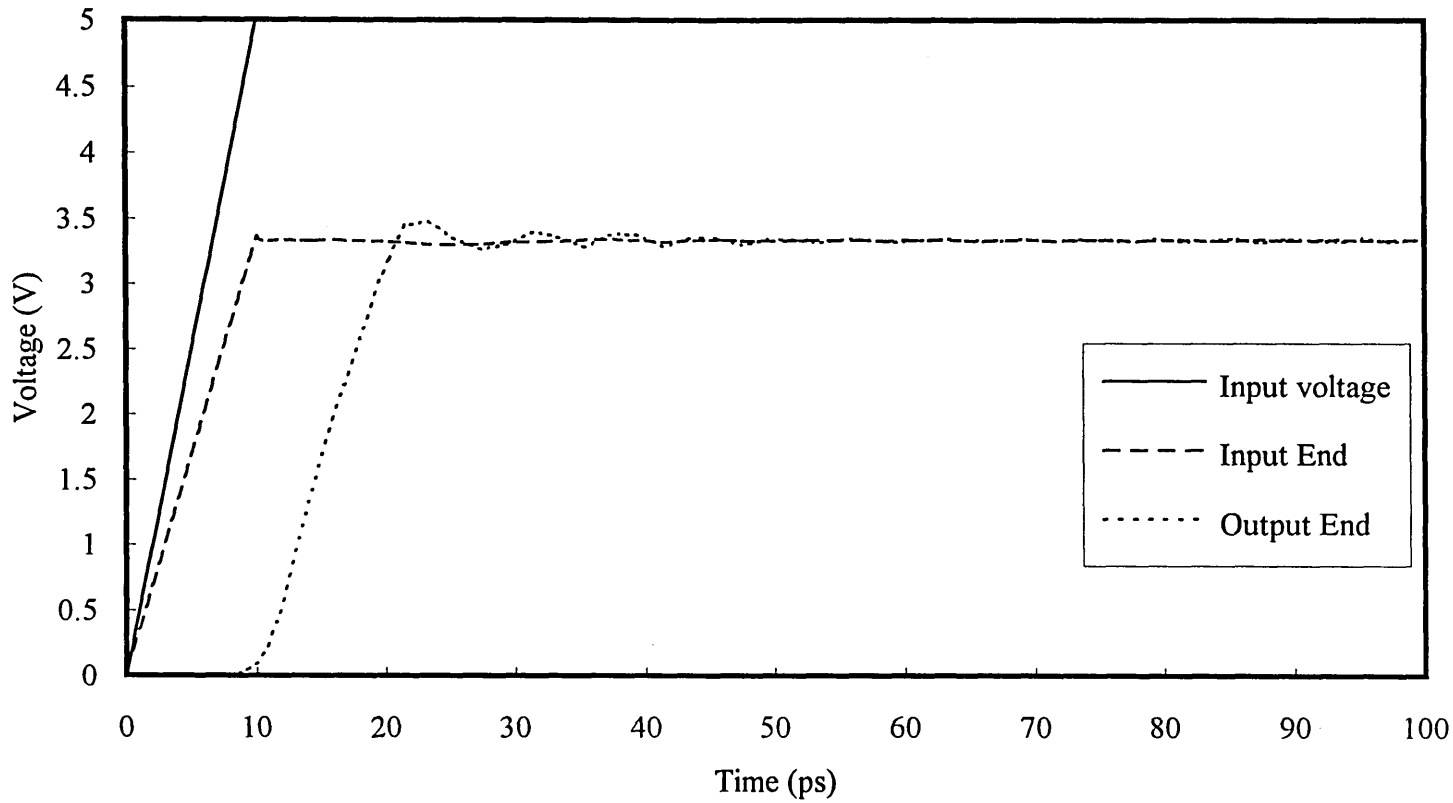

Figure 5.44 : 10ps risetime

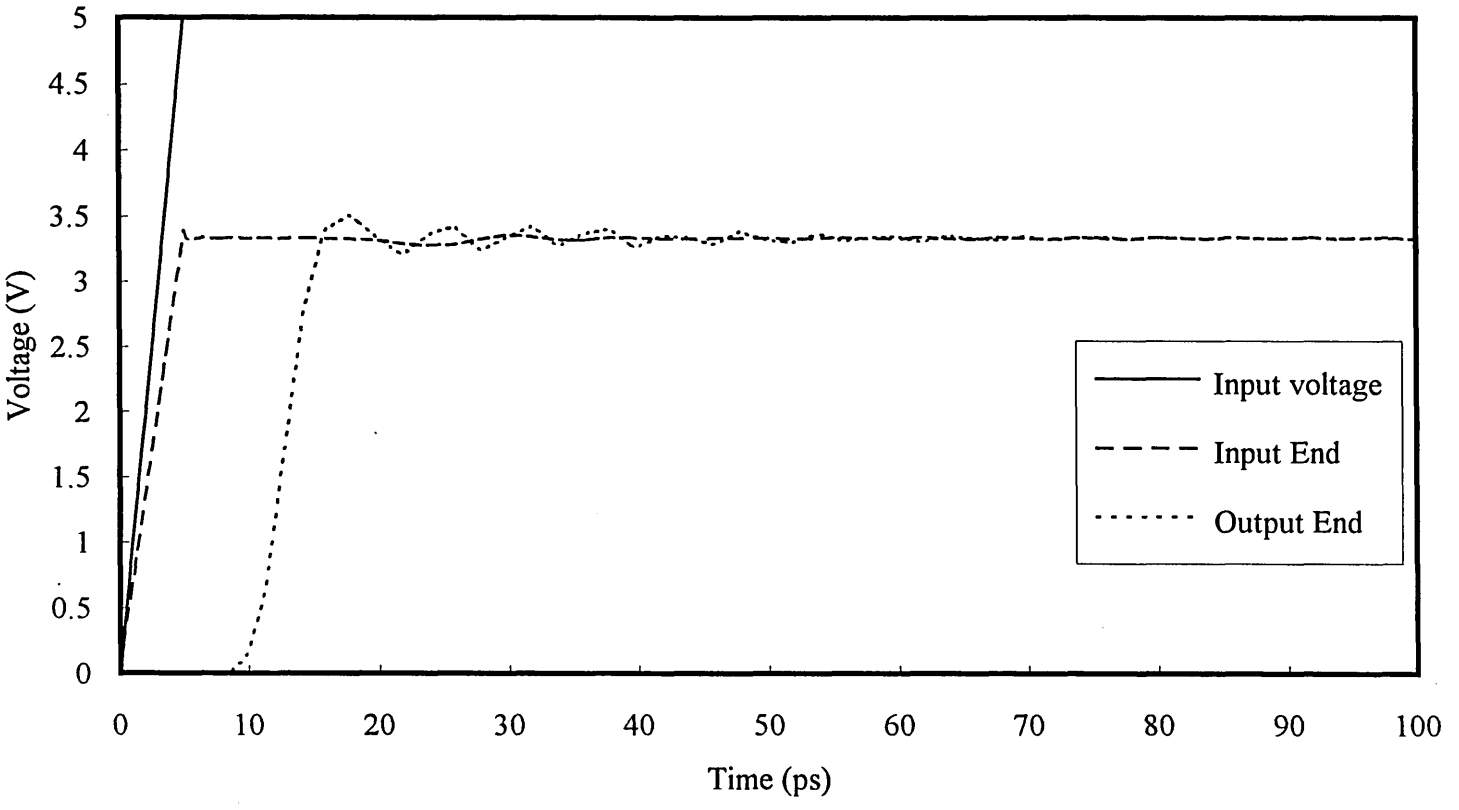

Figure 5.45 : 5ps risetime

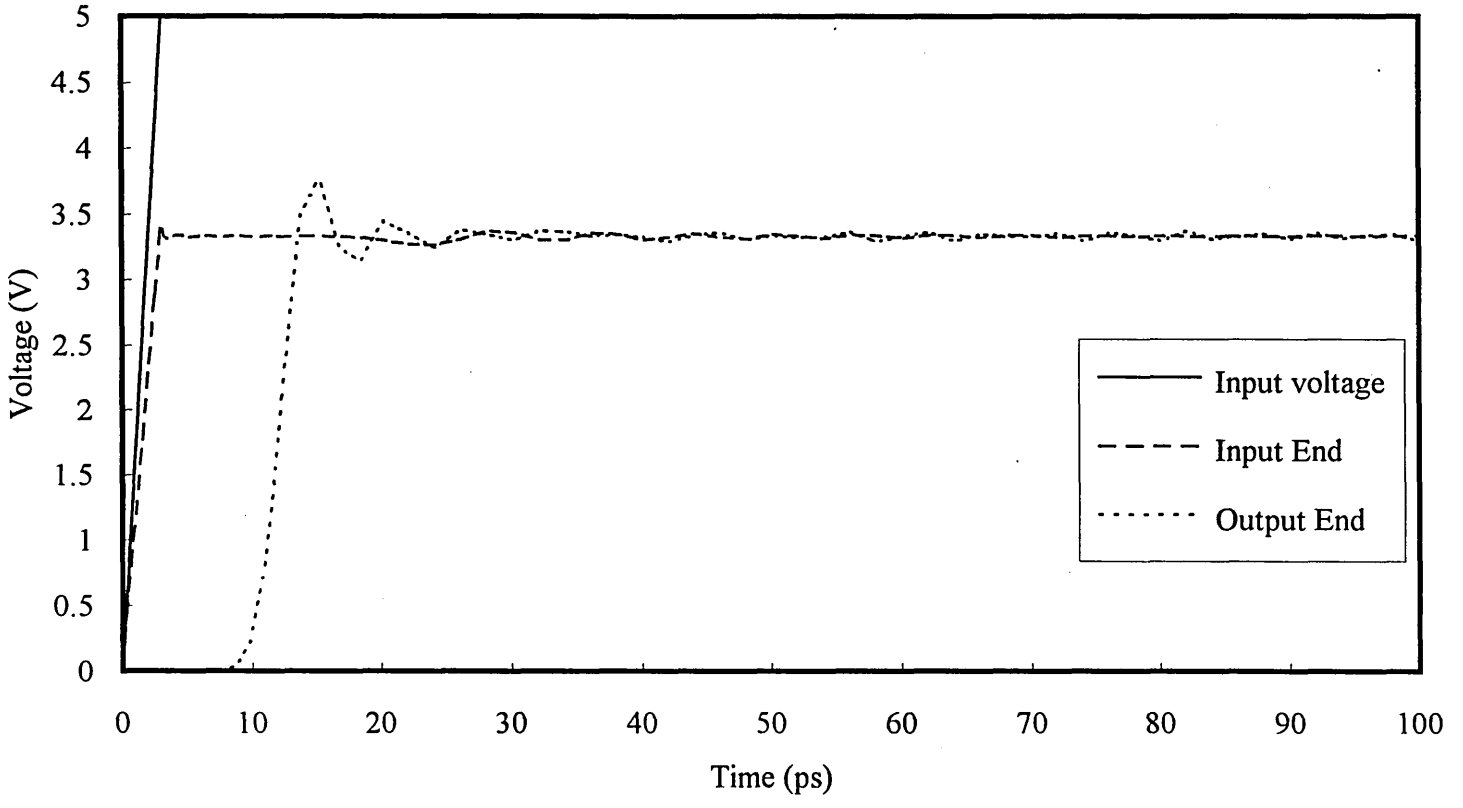

Figure 5.46 : 3ps risetime

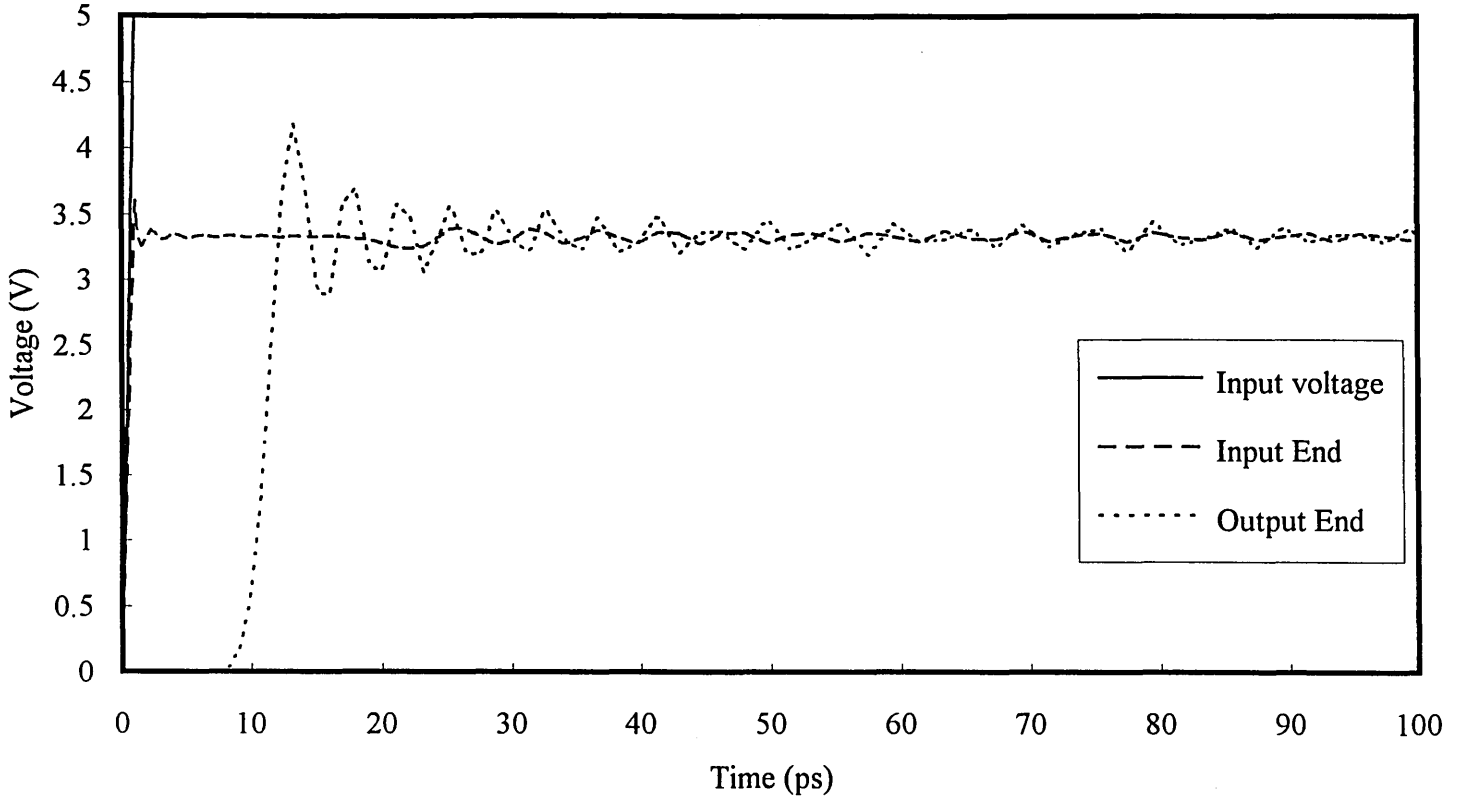

Figure 5.47 : 1ps risetime

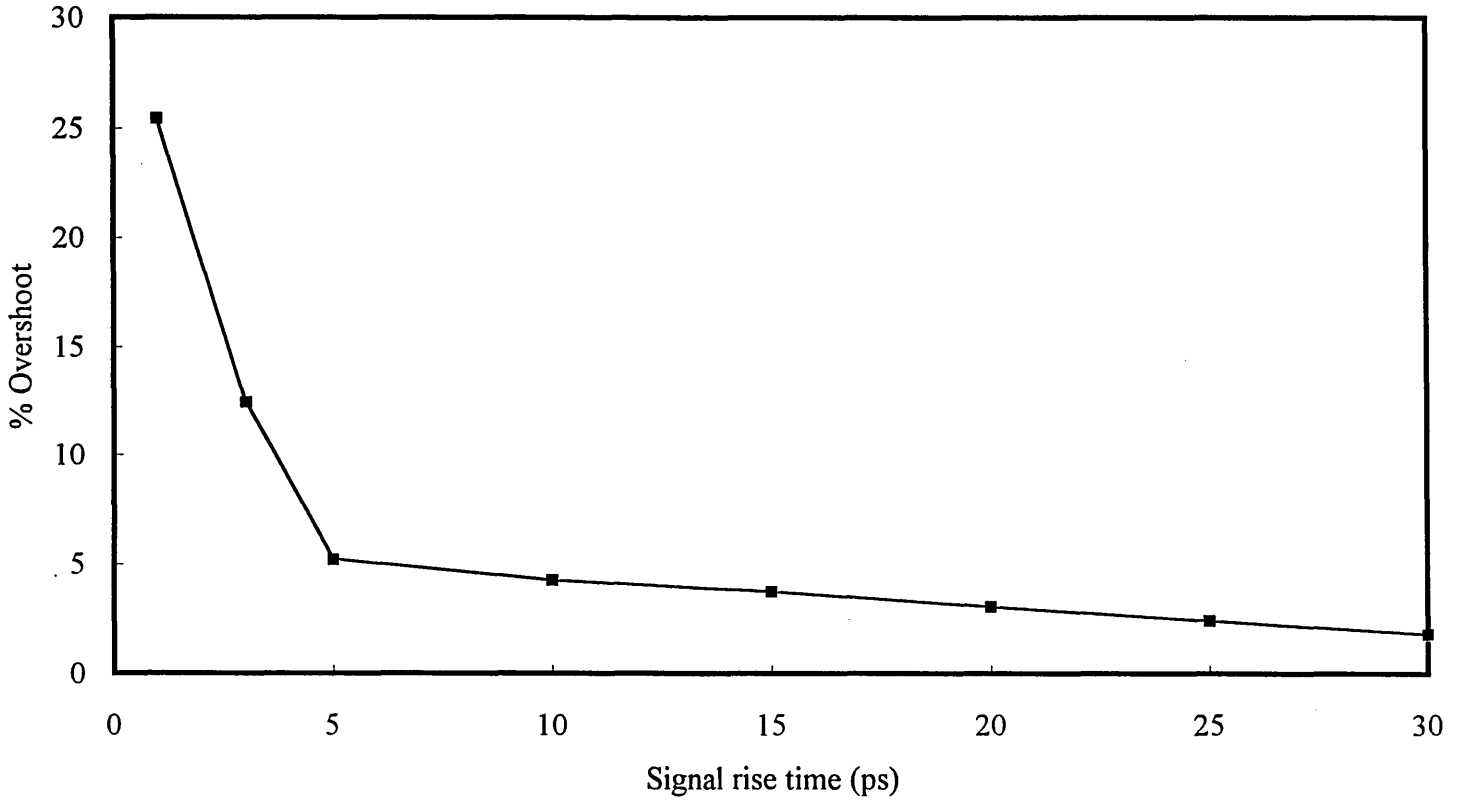

Figure 5.48 : Signal percentage overshoot against risetime.

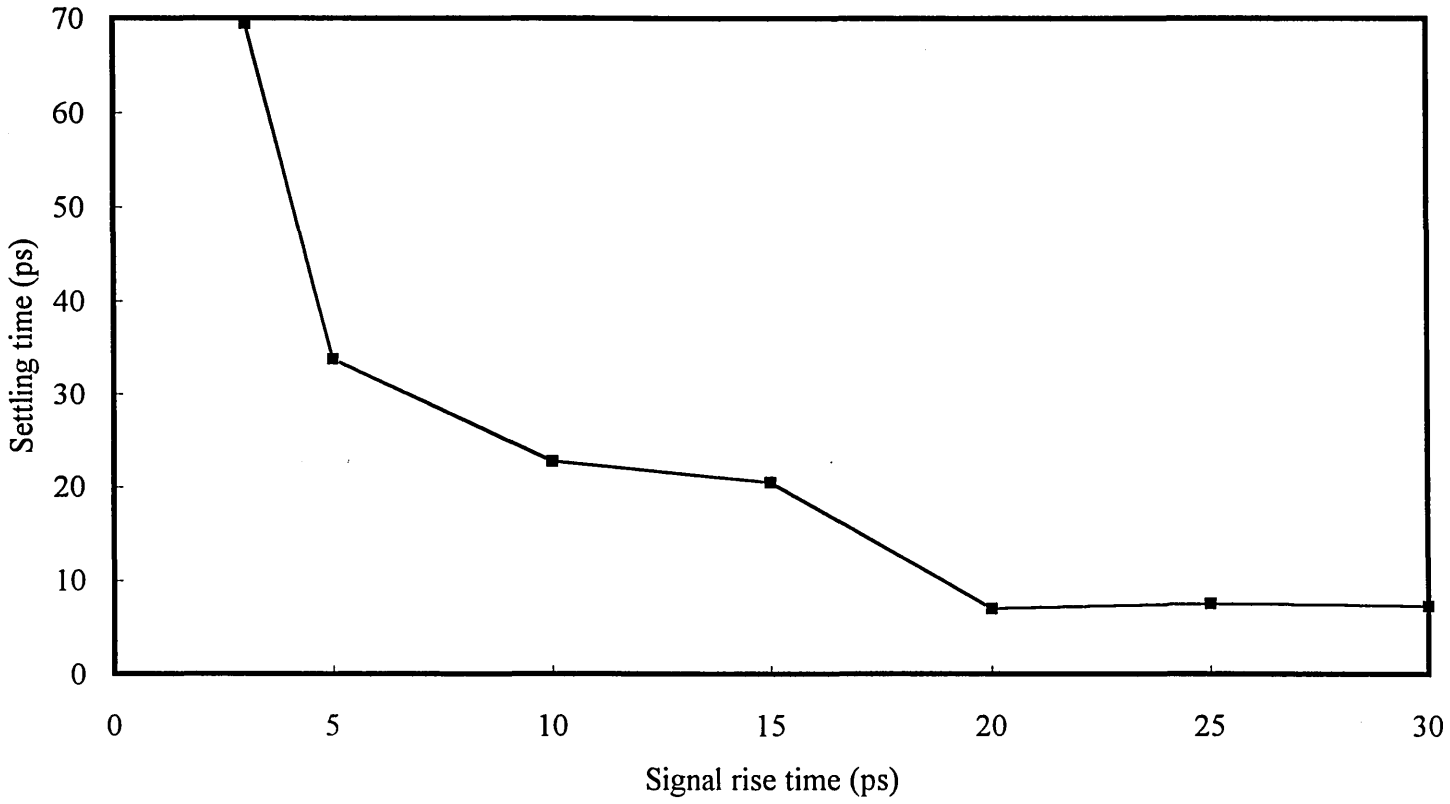

Figure 5.49 : signal settling time against risetime.

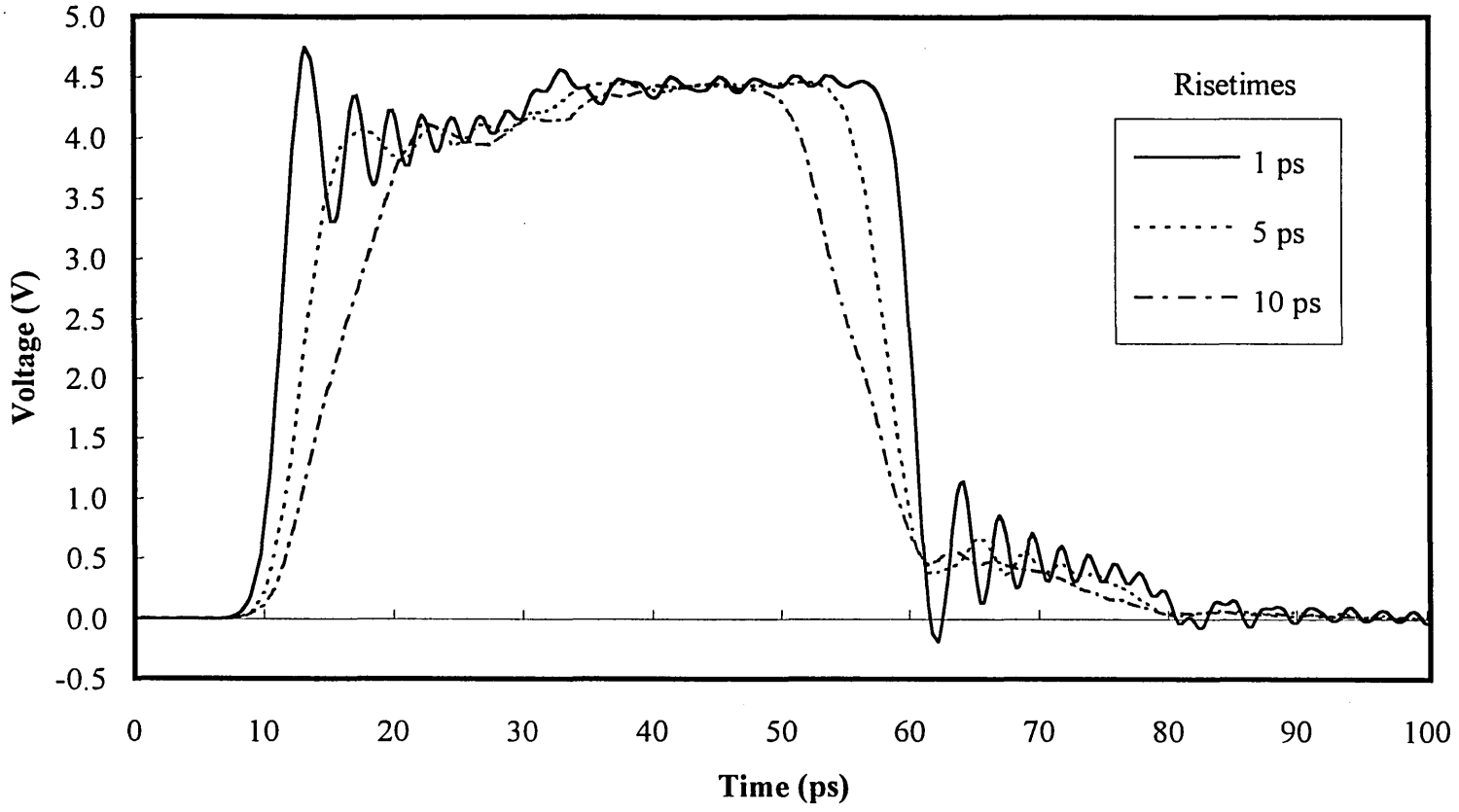

Figure 5.50 : Output signals for pulses of varying risetime where $Z_0 = 166\Omega$, $T_d = 10ps$, $R_{in} = 200\Omega$, $R_L = 2000\Omega$ and a pulse width of 50ps.

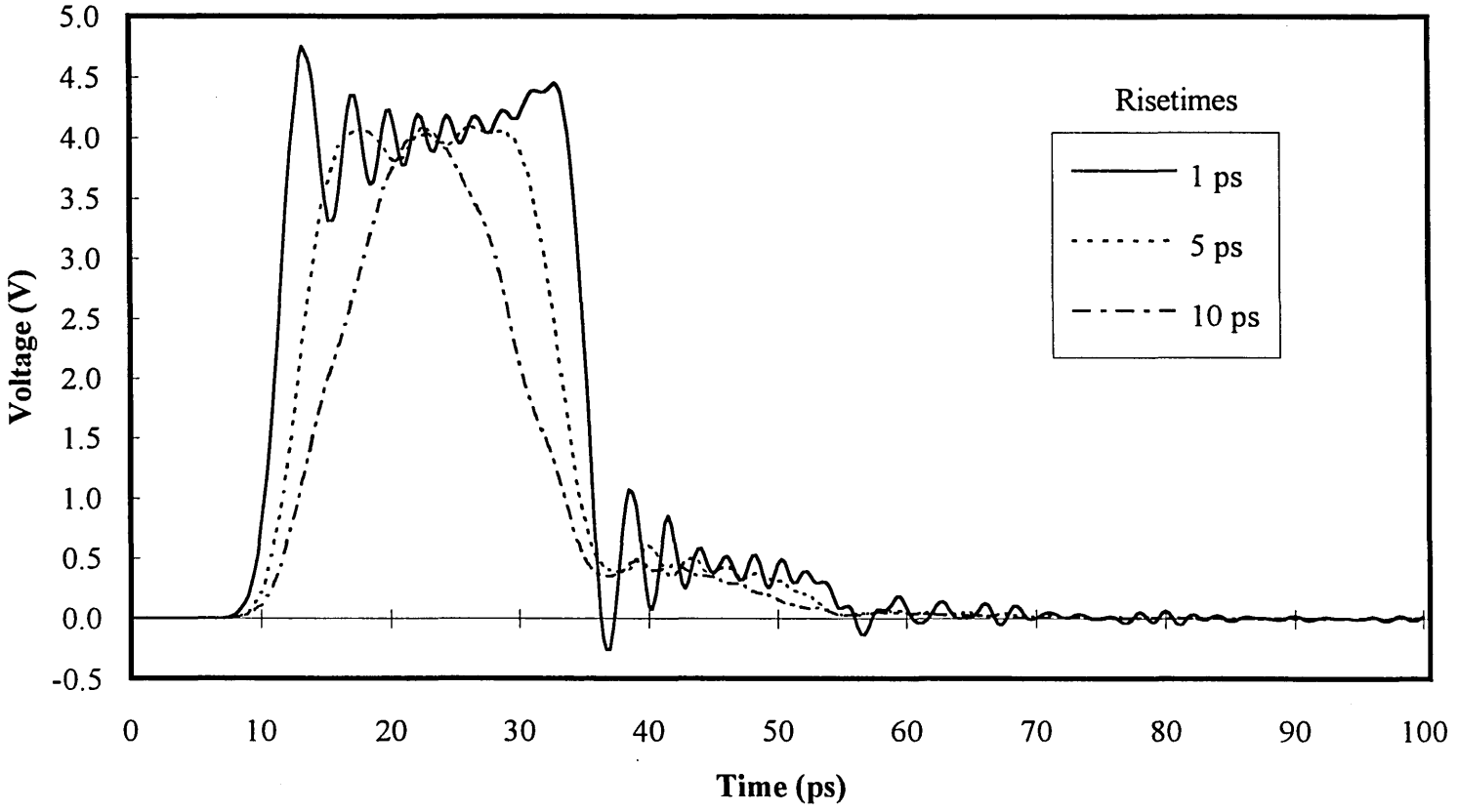

Figure 5.51 : Output signals for pulses of varying risetime where $Z_0 = 166\Omega$, $T_d = 10ps$, $R_{in} = 200\Omega$, $R_L = 2000\Omega$ and a pulse width of 25ps.

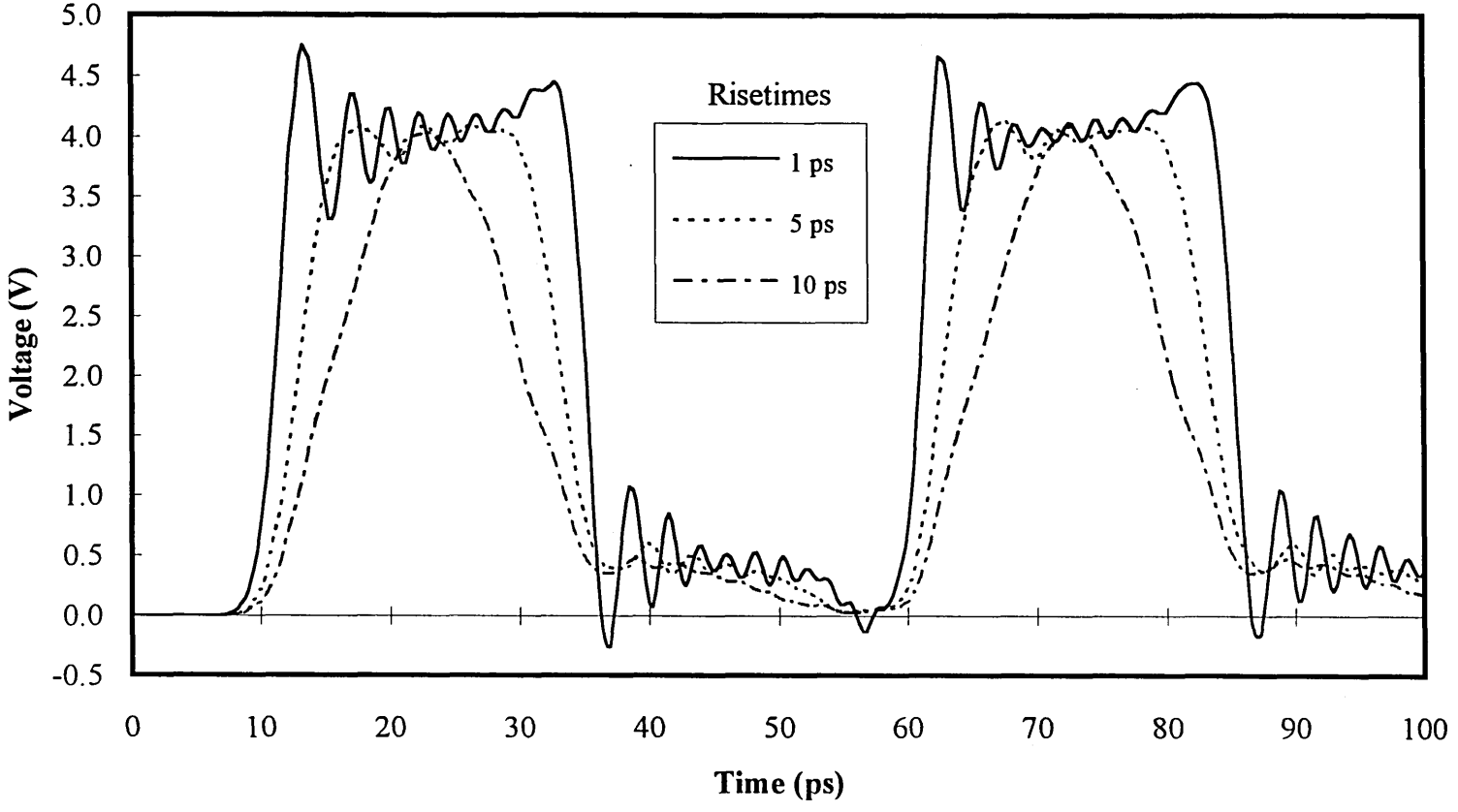

Figure 5.52 : Output signals for a pair of pulses of varying risetime where $Z_0 = 166\Omega$, $T_d = 10ps$, $R_{in} = 200\Omega$, $R_L = 2000\Omega$ and a pulse width of 25ps.

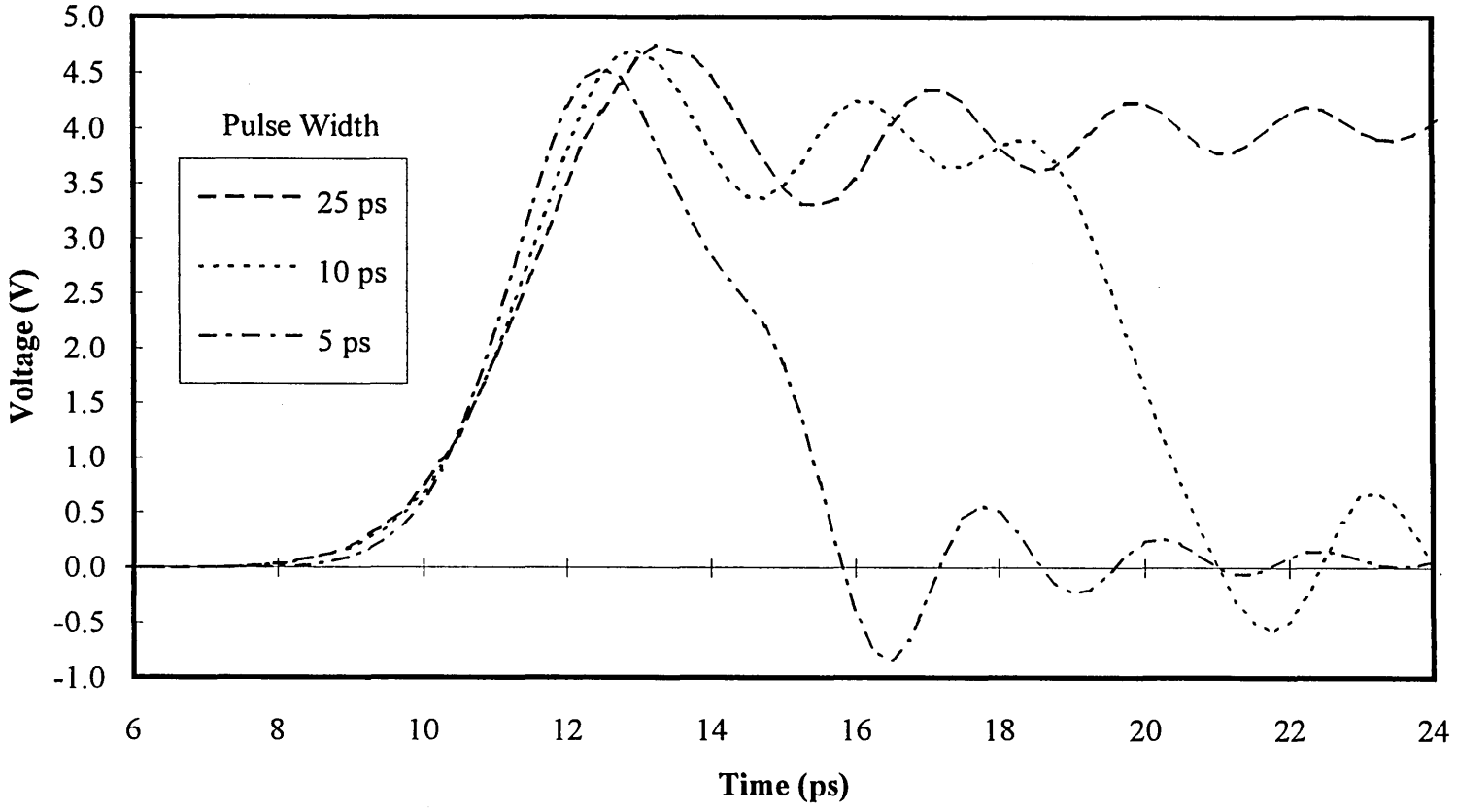

Figure 5.53 : Output signals for various pulses of 1ps risetime where $Z_0 = 166\Omega$, $T_d = 10ps$, $R_{in} = 200\Omega$, $R_L = 2000\Omega$

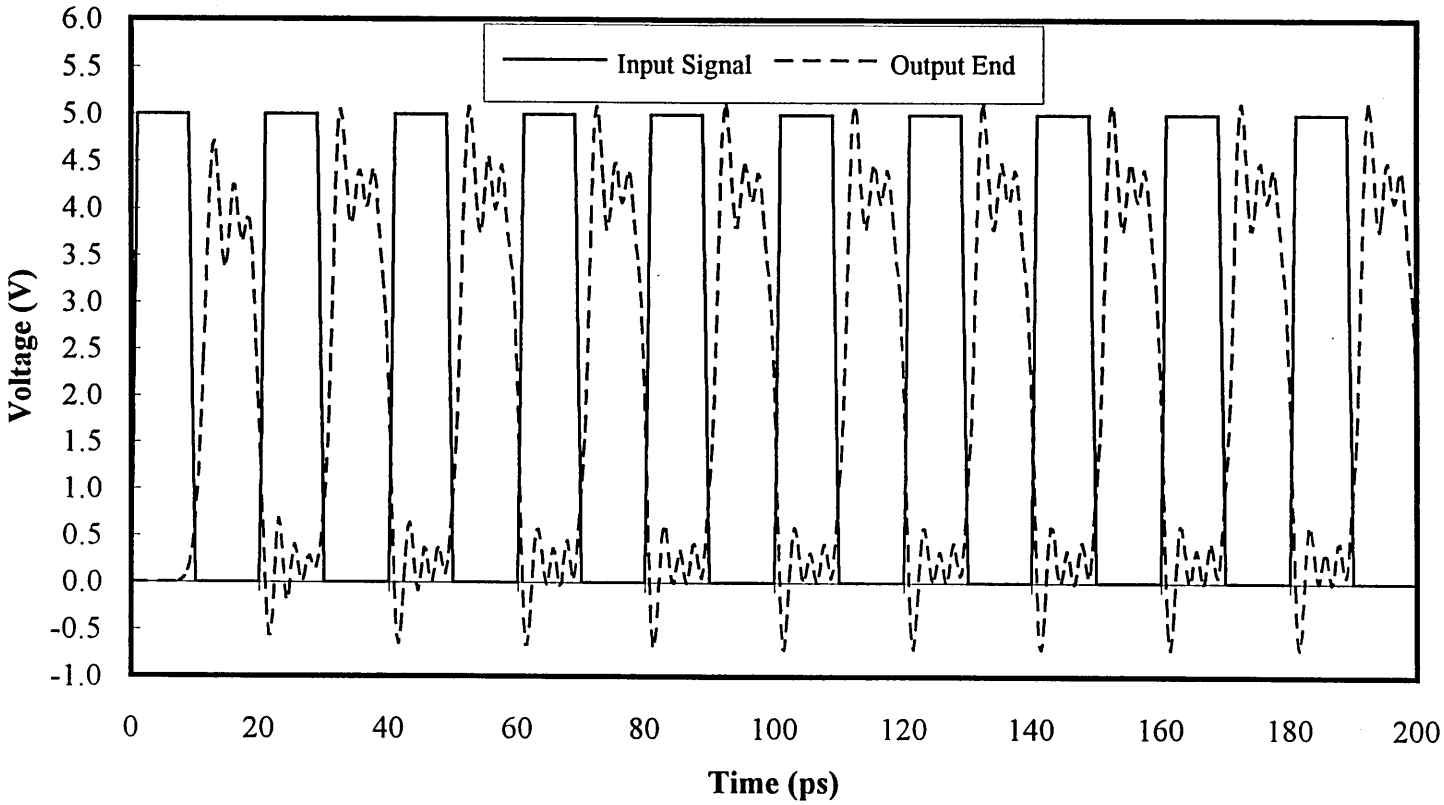

Figure 5.54 : Input and received signals for a pulse train where $Z_0 = 166\Omega$, $T_d = 10ps$, $R_{in} = 200\Omega$, $R_L = 2000\Omega$ and a pulse width of 10ps and a rise and full time of 1ps

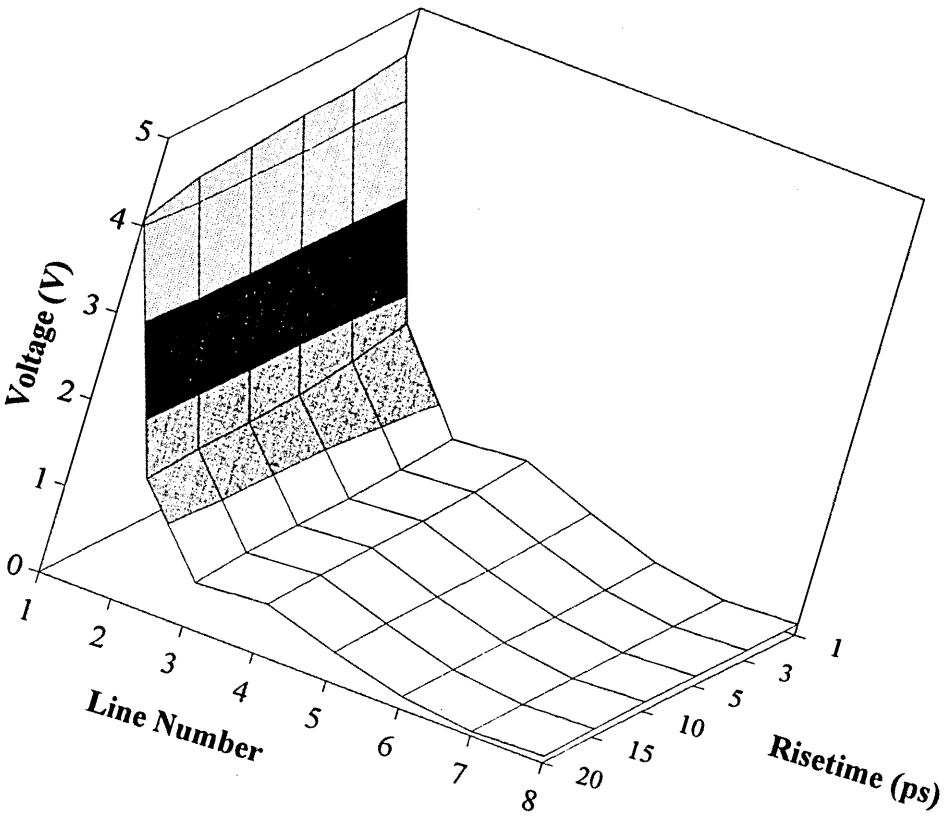

Figure 5.55 : 3D peak voltage plot of risetime against line number for line 1 activated only.

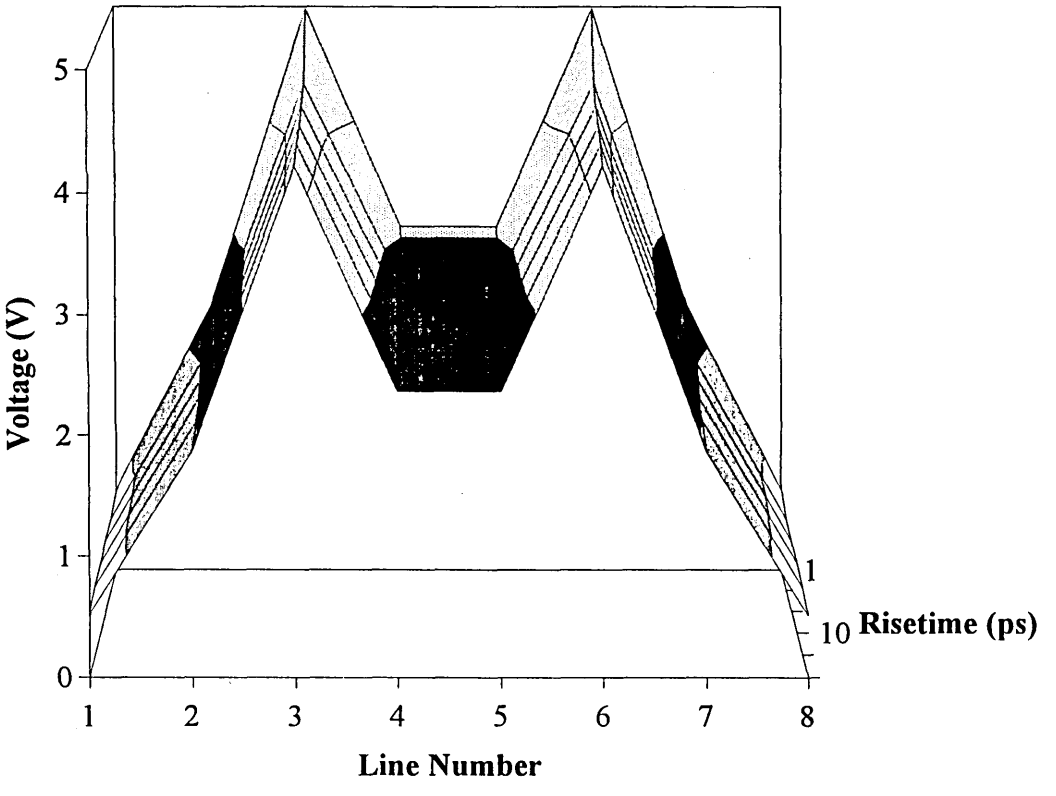

Figure 5.56 : 3D peak voltage plot of risetime versus line number for lines 3 and 6 activated.

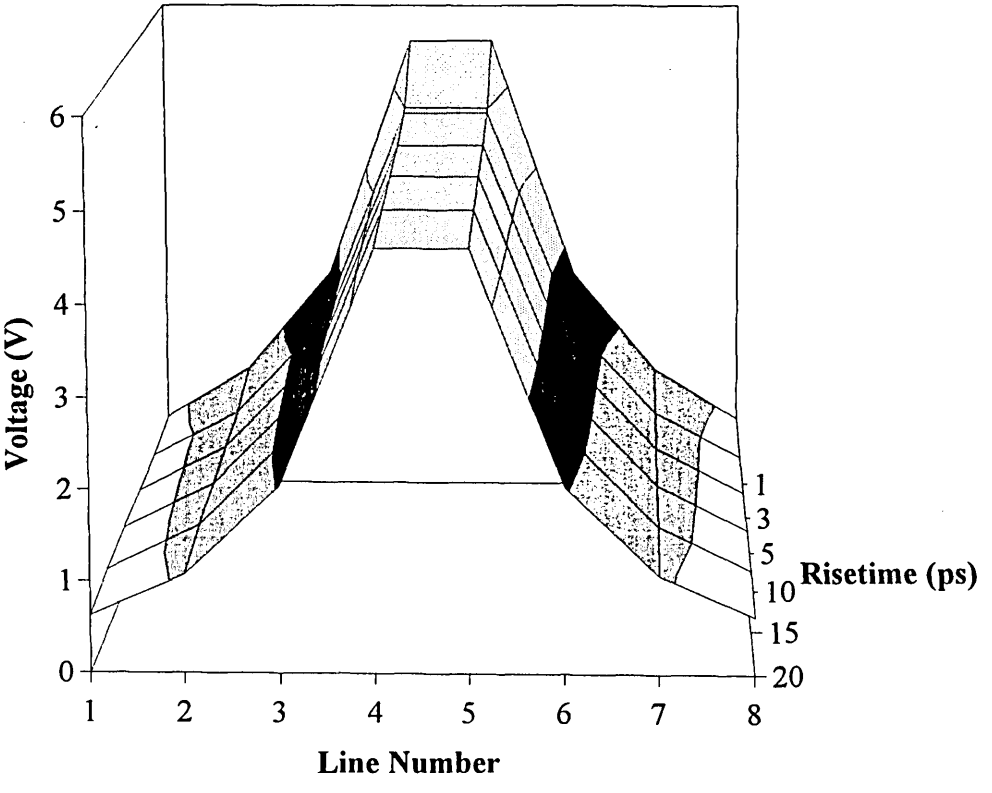

Figure 5.57 : 3D peak voltage plot of risetime against line number for lines 4 and 5 activated.

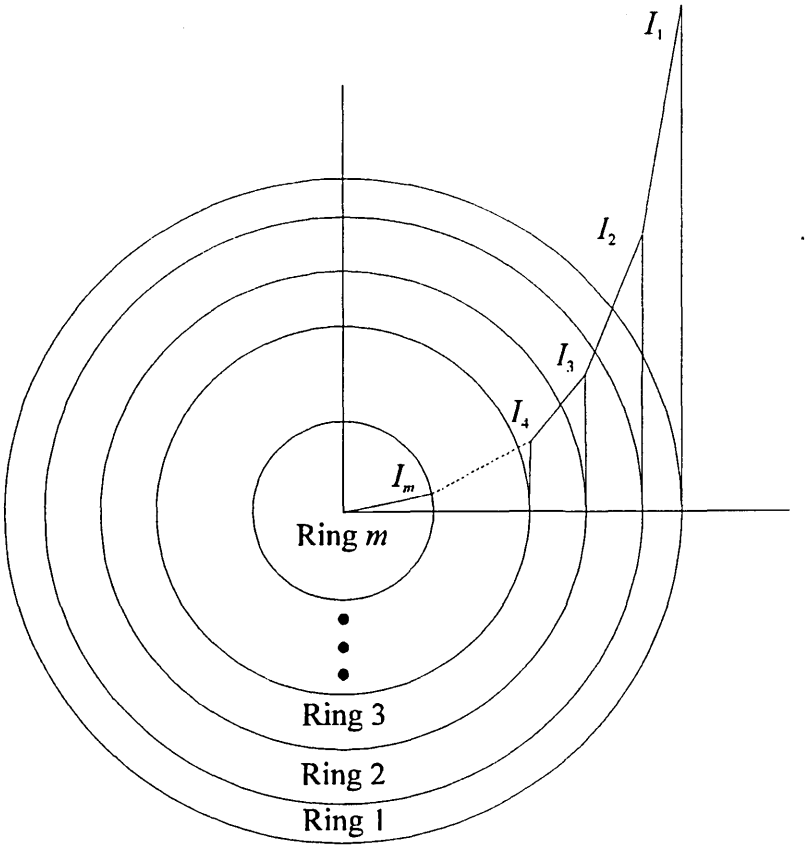

Figure 5.58 : Current distribution diagram for a circular conductor.

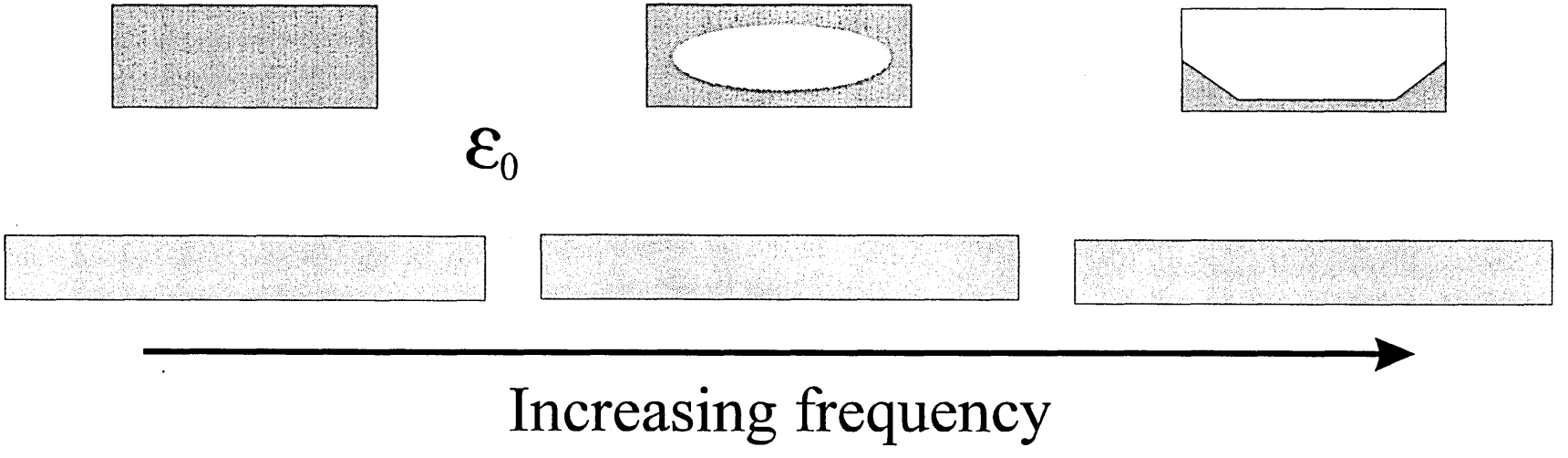

Figure 5.59 : Change of current density inside a microstrip line with increasing frequency.

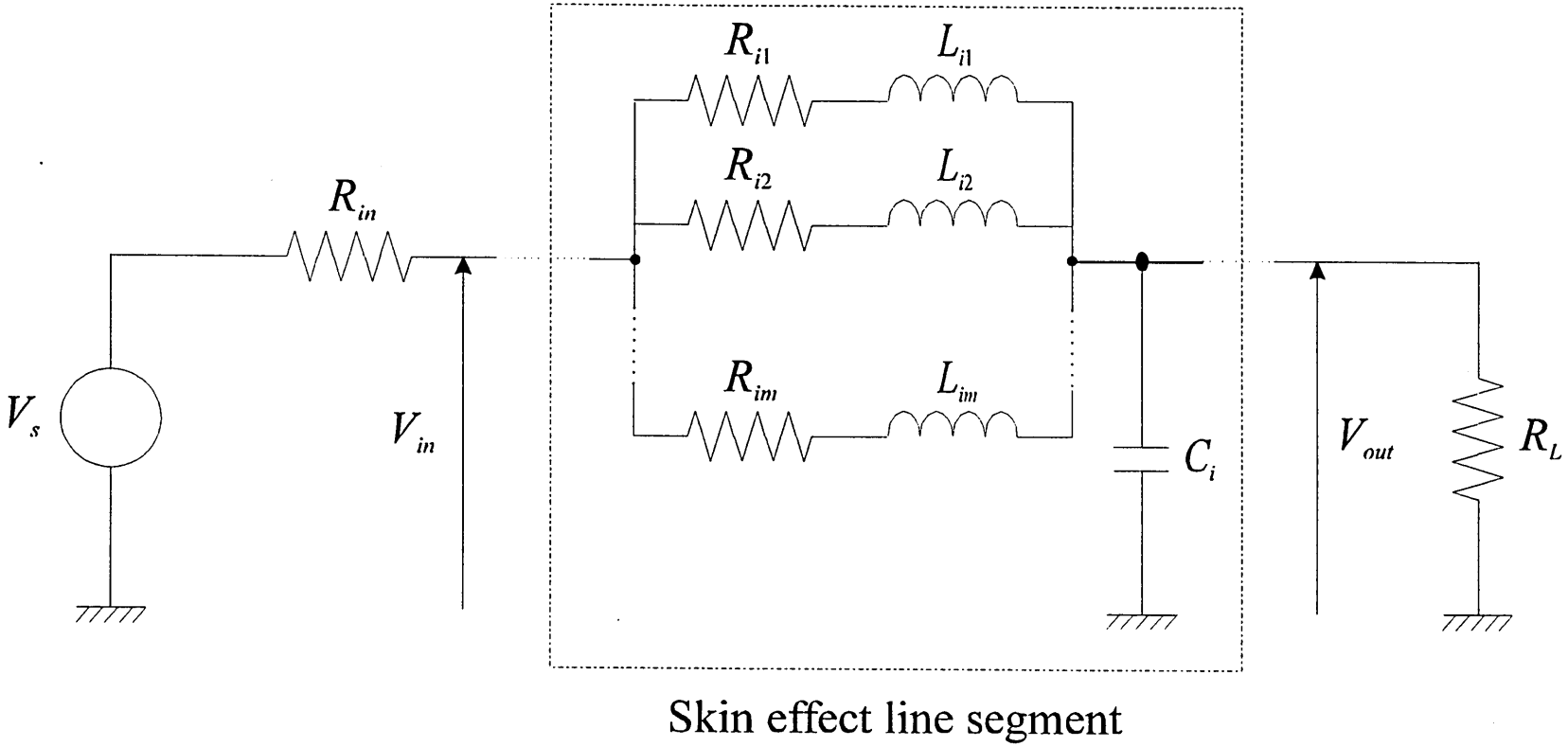

Figure 5.60 : Equivalent circuit model for simulating the skin effect

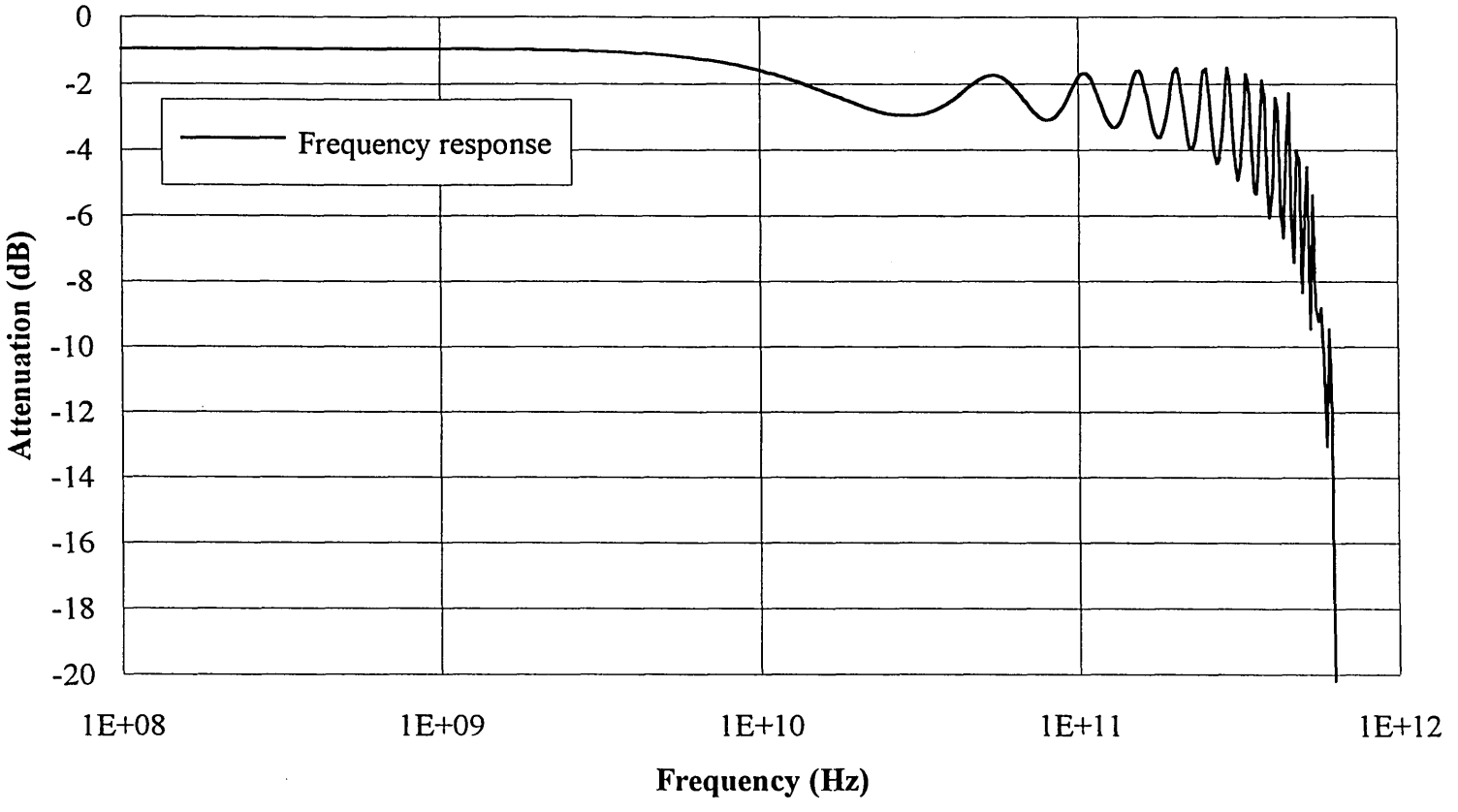

Figure 5.61 : Frequency response for the lossy line model.

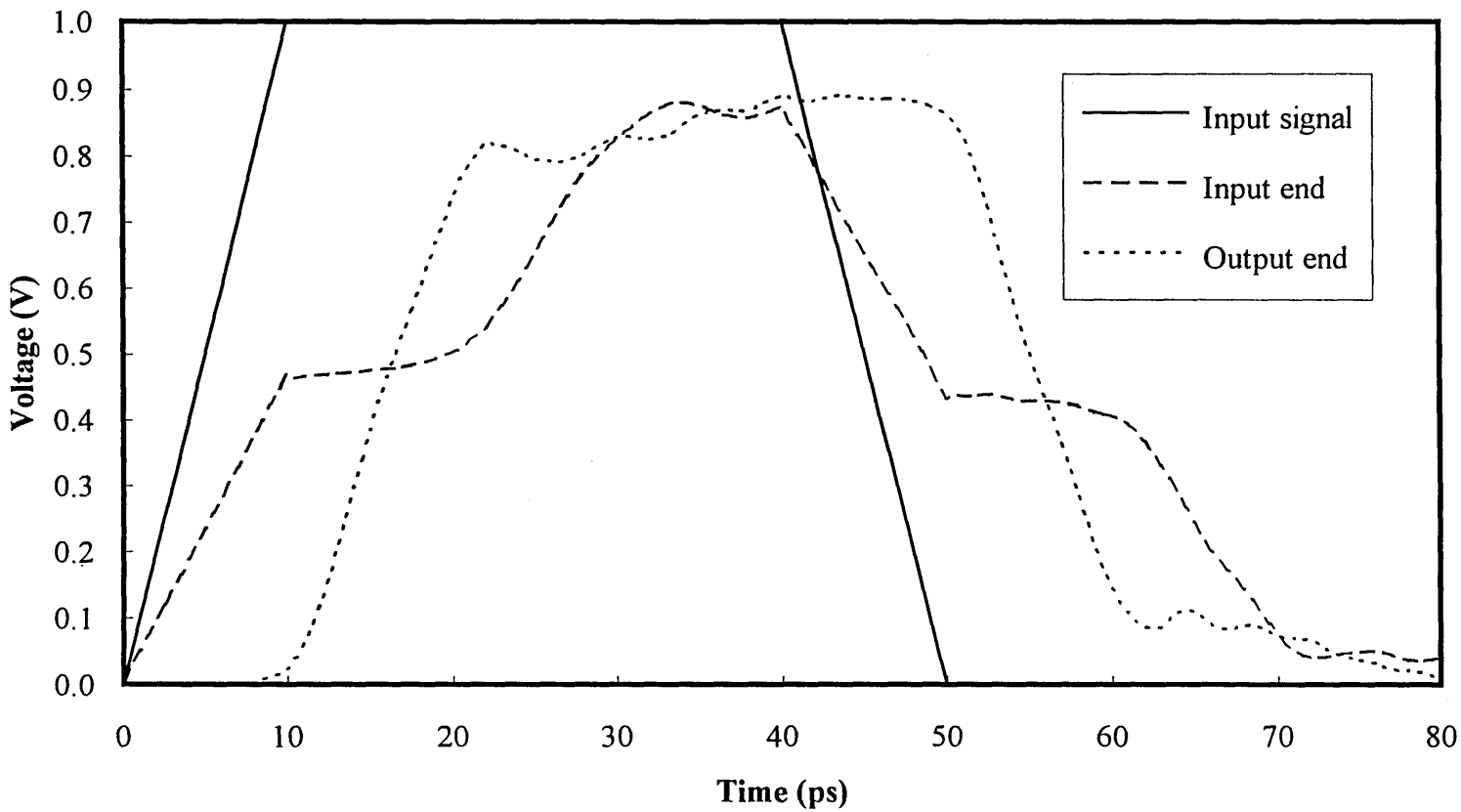

Figure 5.62 : Transient response for the lossy line model.

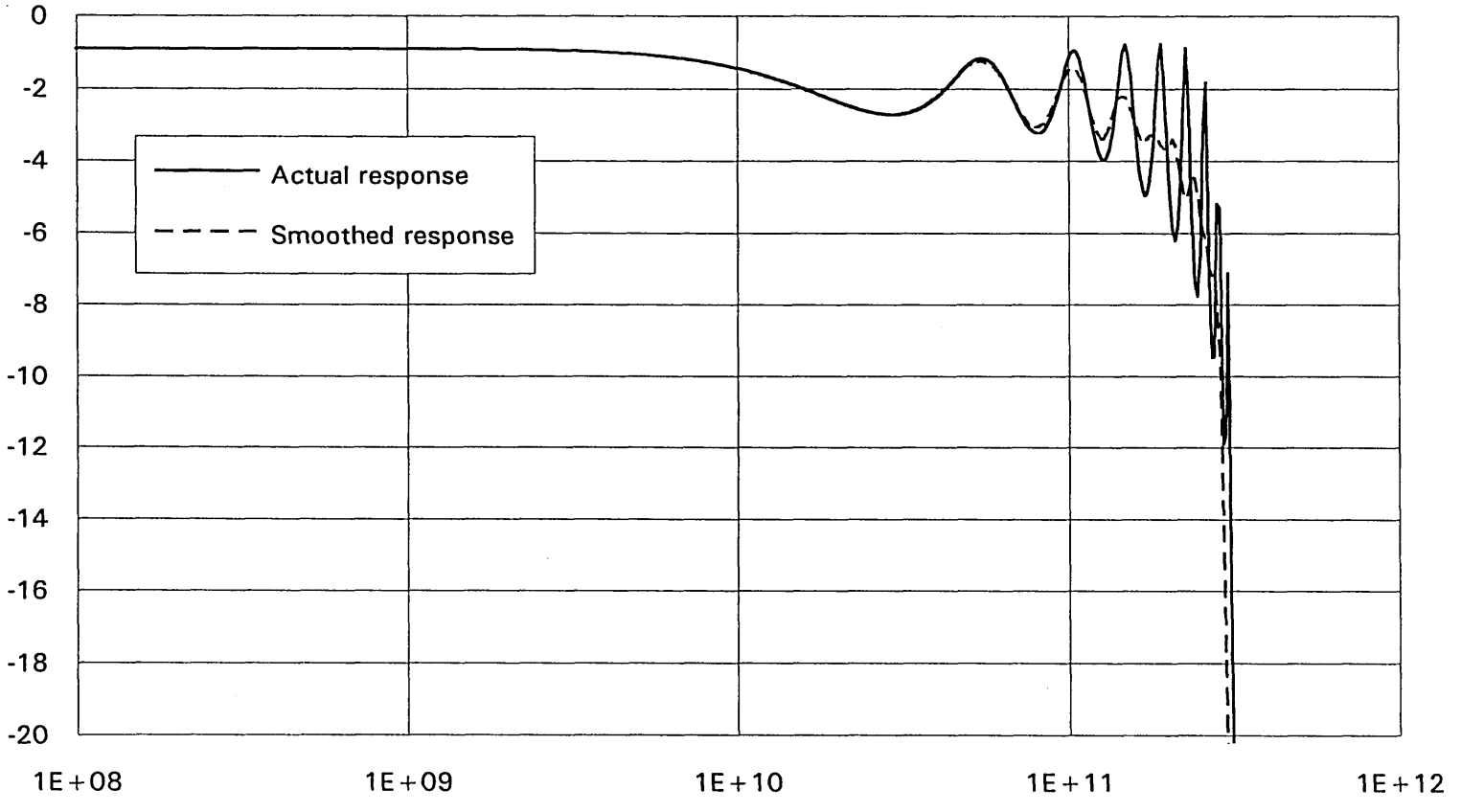

Figure 5.63 : Bode plot 10 sections in series, and 10 sections in parallel.

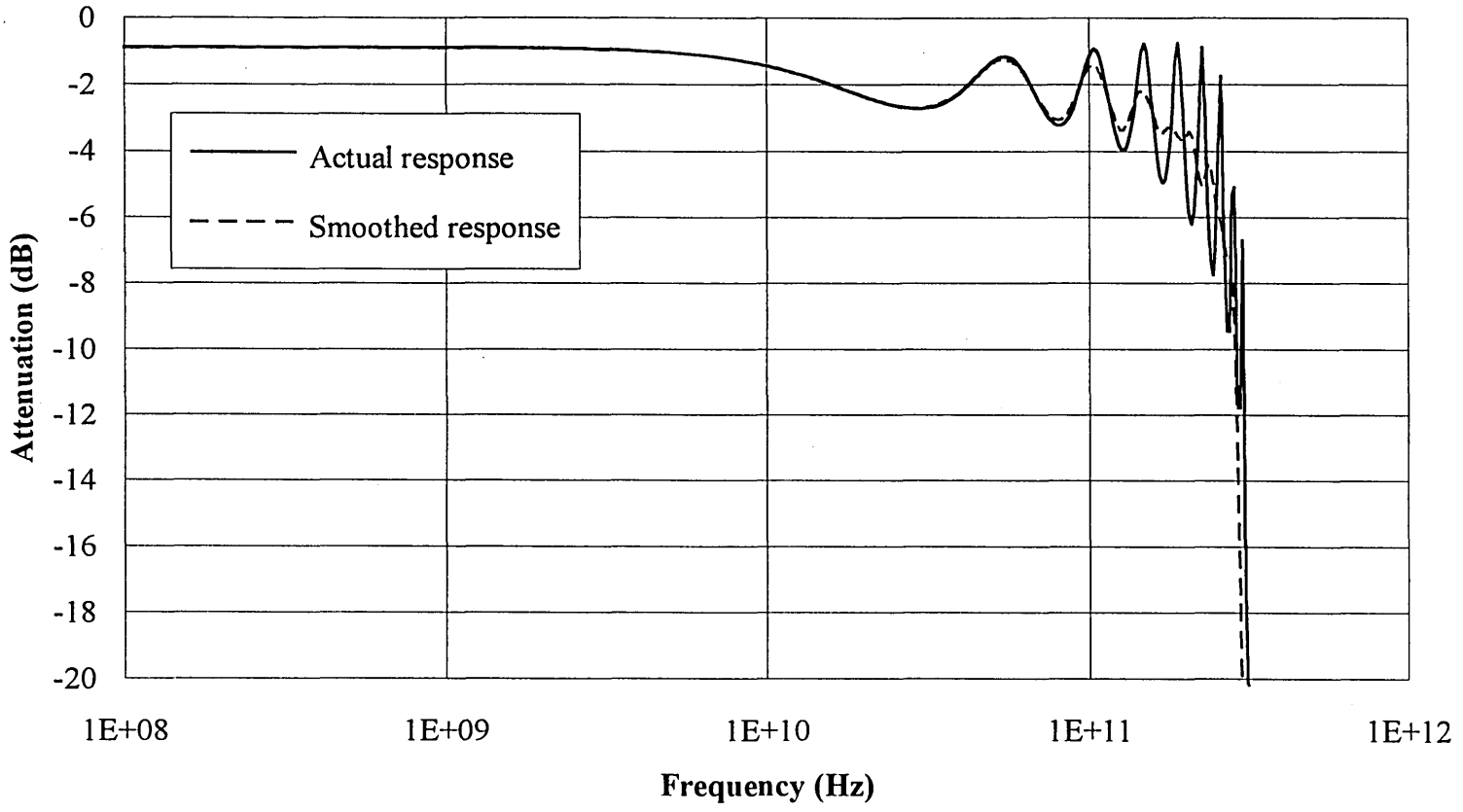

Figure 5.64 : Bode plot for 10 sections in series, and 20 sections in parallel.

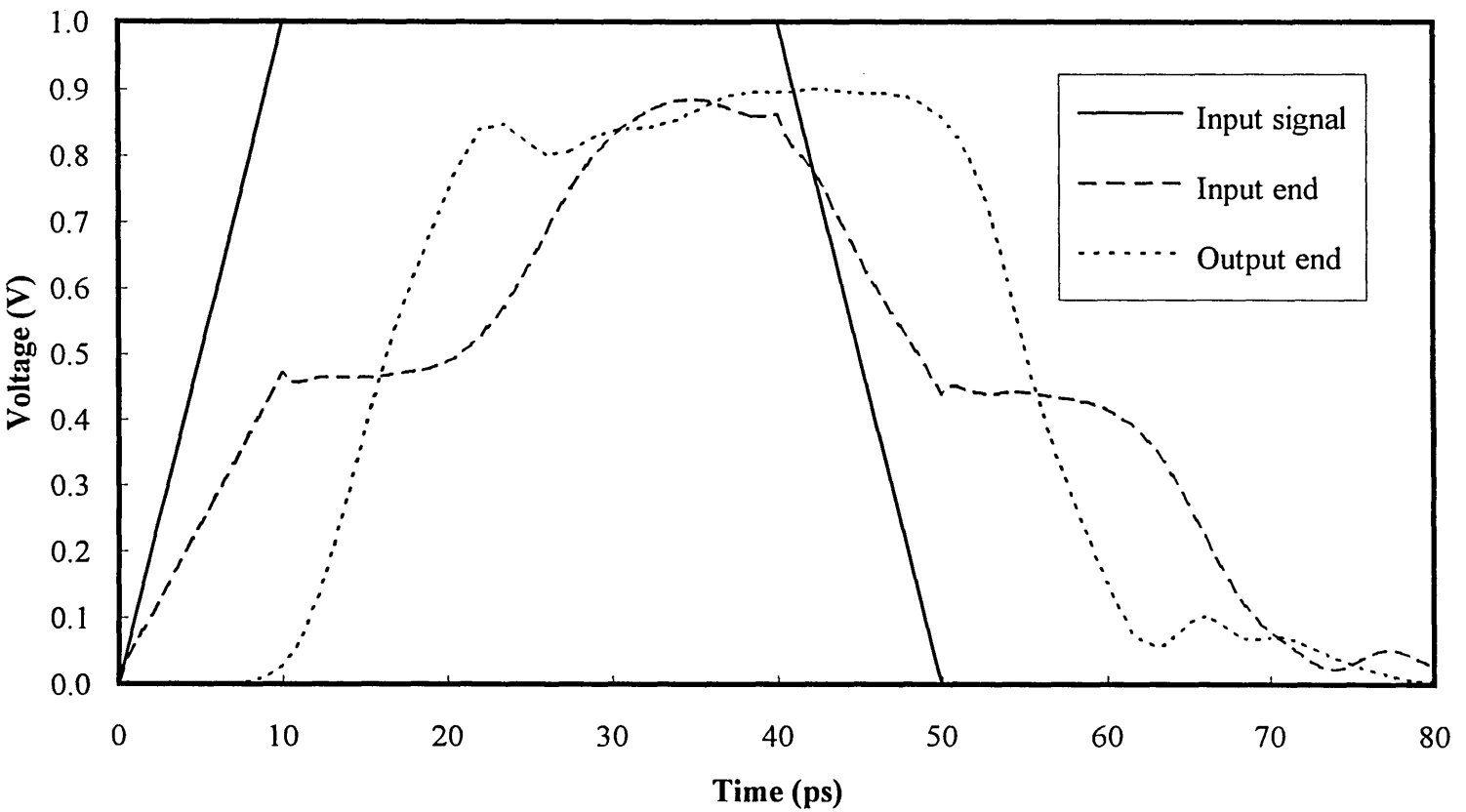

Figure 5.65 : Transient response for the skin effect model.

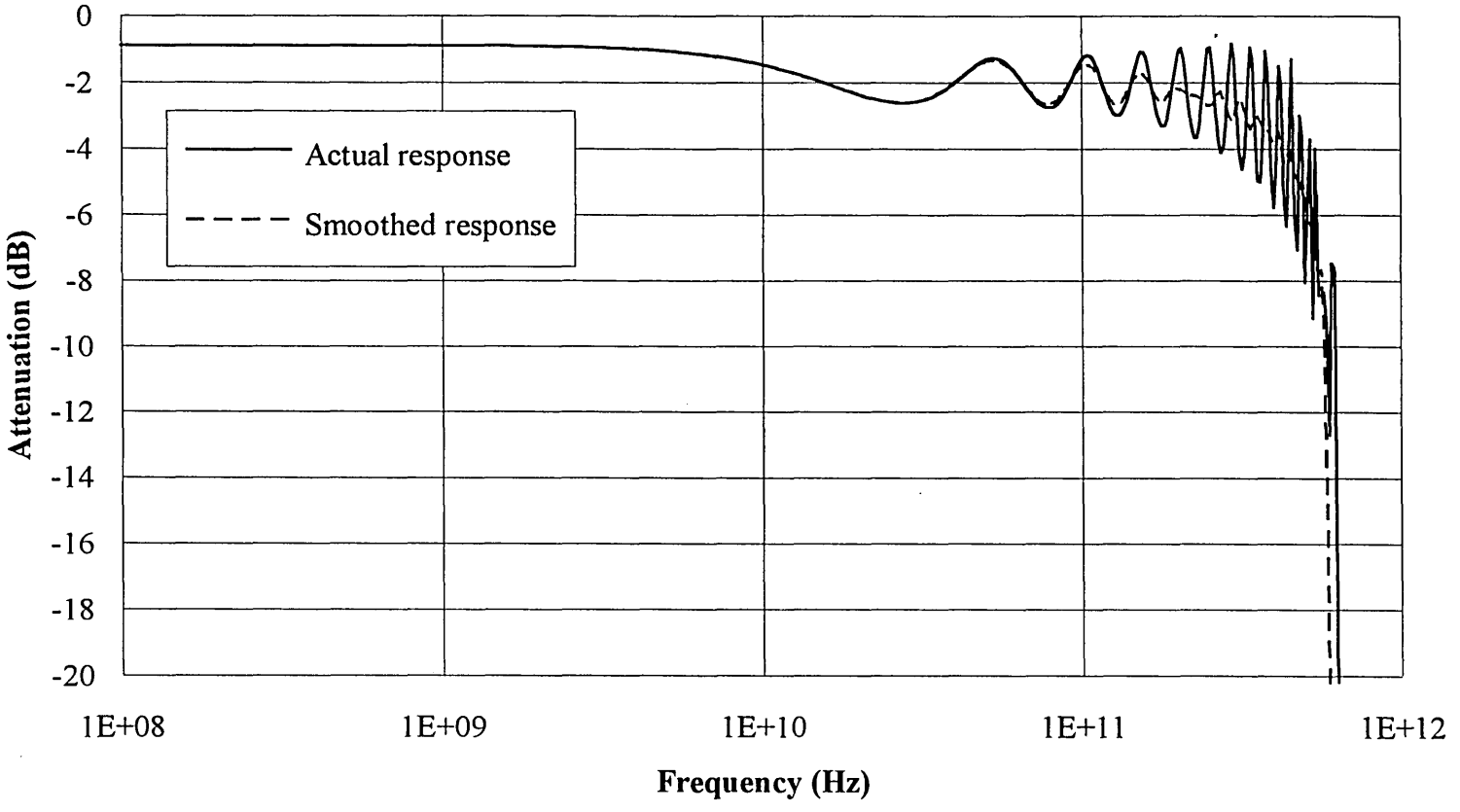

Figure 5.66 : Bode plot for 20 sections in series, and 10 sections in parallel.

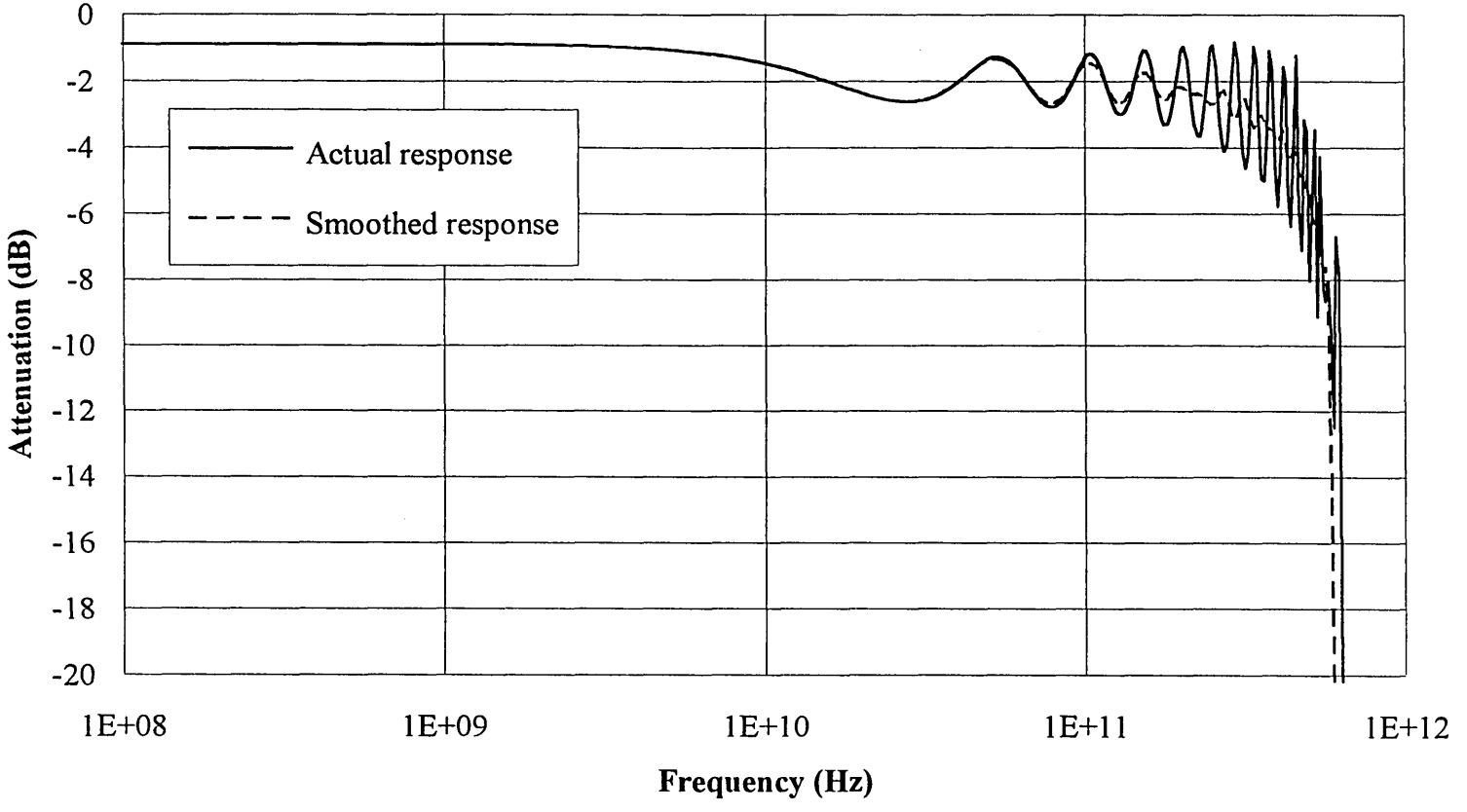

Figure 5.67 : Bode plot for 20 sections in series, and 20 sections in parallel.

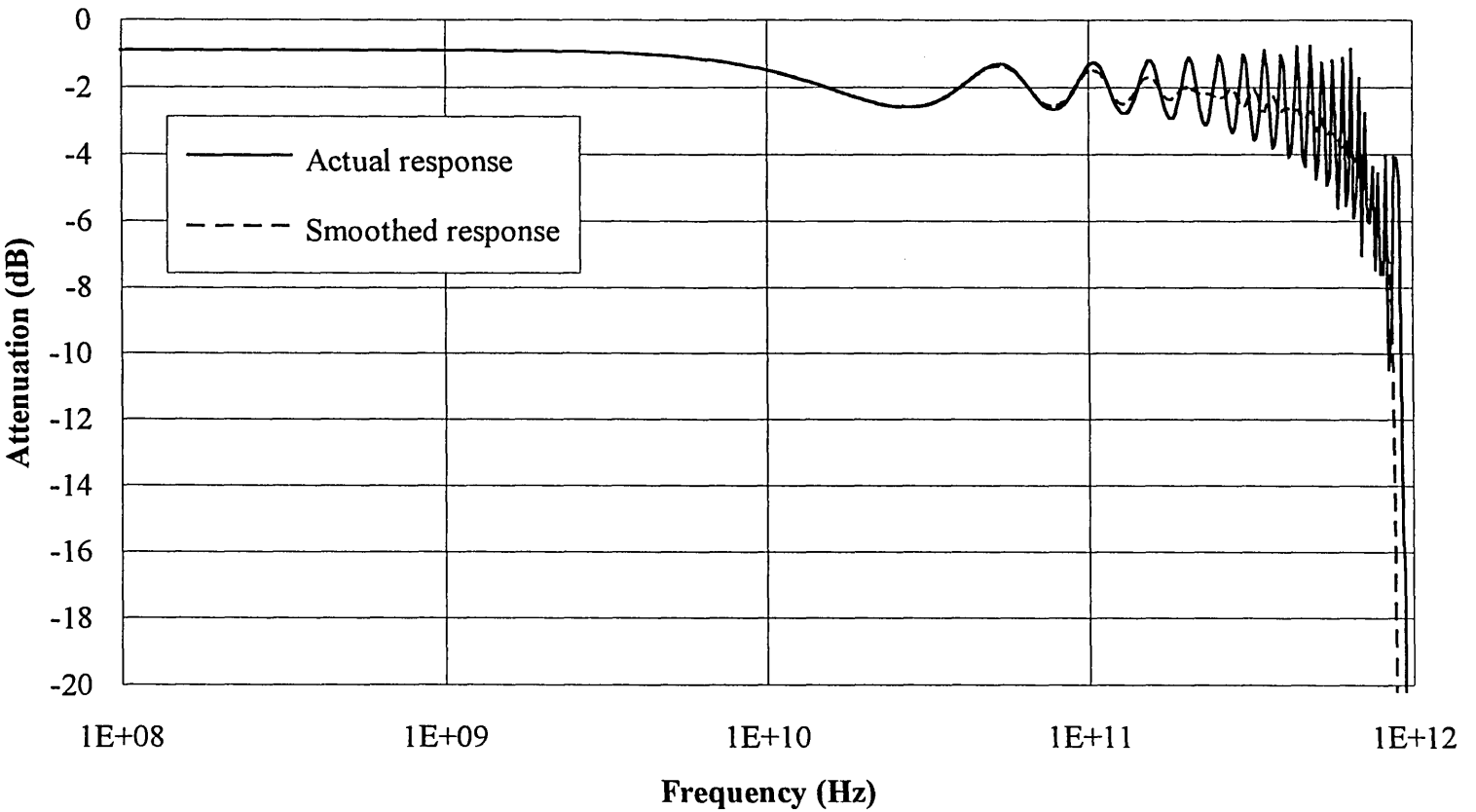

Figure 5.68 : Bode plot for 30 sections in series, and 10 sections in parallel.

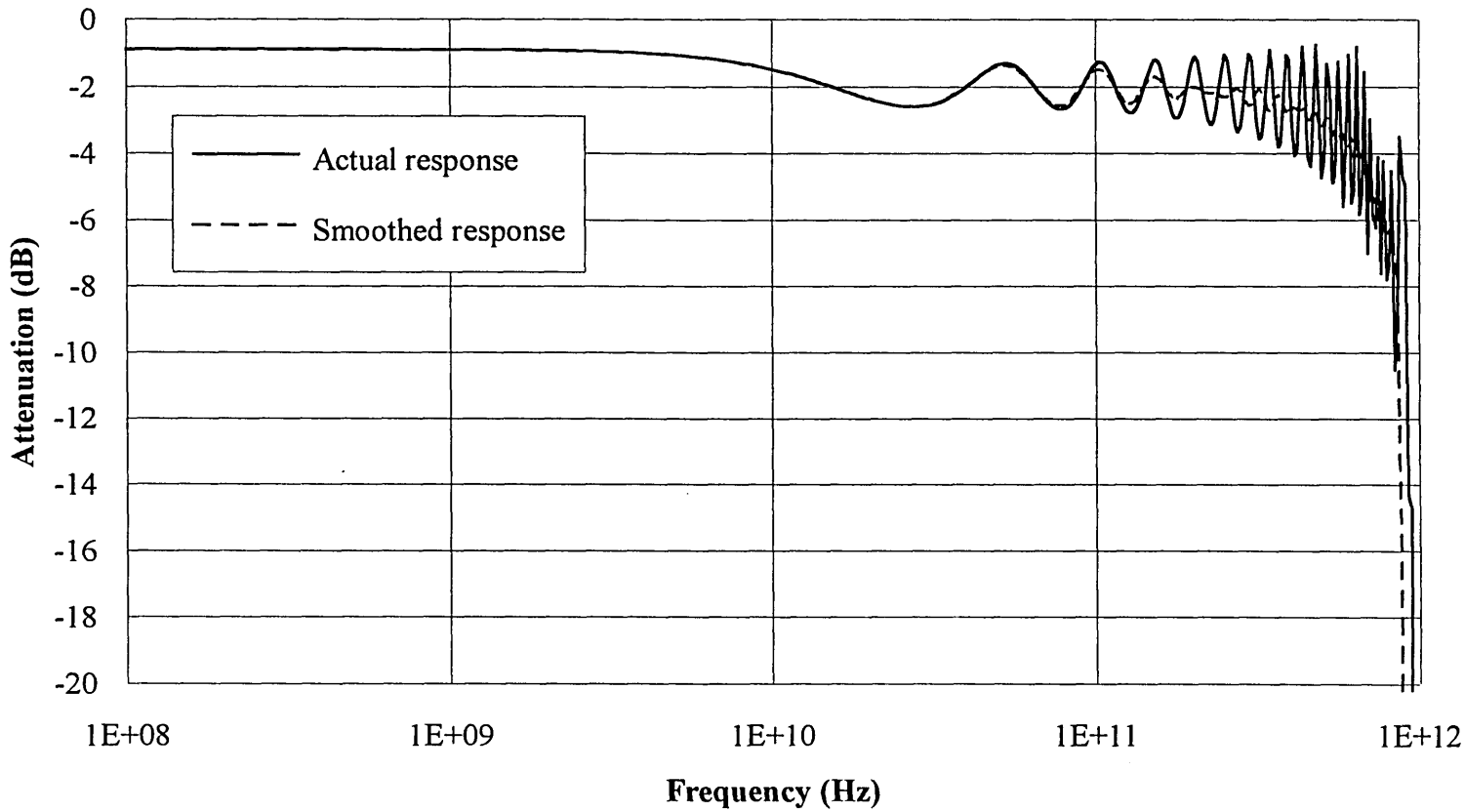

Figure 5.69 : Bode plot for 30 sections in series, and 20 sections in parallel.

Chapter 6

Mathematica Calculations

Chapter 6

Mathematica Calculations

6.1.2 : Effect of the inclusion of line thickness

The expressions for impedance of a single line taking the thickness, t, of the line into account are given by equations (3.22)-(3.27). Figure 6.2 shows how the impedance of a single microstrip line varies with the W/h ratio, for a finite line thickness (t/h = 0.1), for various values of effective dielectric constant, ε_r. The shape of the curves in figure 6.2 are found to be very similar to those in figure 6.1. However the values of calculated impedance are now found to be lower (c.f. figure 6.1) due to the inclusion of line thickness.

The results obtained for the impedance by varying the ratio of line thickness to width, t/h, for varying W/h ratios are depicted in figure 6.3. For small values of W/h ratio (e.g. W/h = 0.1 and W/h = 0.5) the impedance is found to decrease as the t/W ratio is increased (approximately from 215Ω to 175Ω and 100Ω to 85Ω, respectively). However for larger values of W/h ratio (i.e. W/h > 0.5; where the impedance is low, e.g. < 30Ω), changes in the ratio of t/W has little or no effect upon the impedance.

The above findings are seen to be consistent with previously published work (Wheeler 1965, Kaupp 1967, Gunston and Weale 1969, Silvester 1968, Stinehelfer 1968, Yamashita and Mittra 1968, Schneider 1969, John and Arlett 1974, Kumar *et al* 1976, Ross and Howes 1976, Bahl and Garg 1977).

In the paper by Chilo and Arnaud (1984), from which the example of the eight line logic bus is taken (outlined in chapter 1), they have calculated the impedance of one single line on its own, with the given geometry (er = 12, t = 0.3μm, W = 2μm, h = 400μm), to be 166Ω. Using the above outlined method the impedance for this single line is 167Ω giving confirmation as to the suitability of this method.

6.2 : Coupled Microstrip Line Pair

Equations (3.15)-(3.21) give the formulae for computing the impedance of a pair of microstrip lines, where the even and odd mode capacitances for the lines are given by equations (3.5) and (3.10) respectively. In this section the effect of changing the geometric parameters upon the even and odd mode, capacitances and impedances are studied, as well as their effect upon the overall impedance of a pair of parallel coupled lines.

6.2.1 : Even mode capacitance

The even mode capacitance for a pair of parallel microstrip lines may be calculated using equations (3.5)-(3.9). Figures 6.4 and 6.5 show how the even mode impedance for two parallel microstrip lines varies with W/h ratio for three different values of W/S ratios; for W/h between 0.1 to 1 and 1 to 10 respectively. These graphs demonstrate that changing the ratio of W/S does not have much effect upon the even mode capacitance, whereas the capacitance increases rapidly as the W/h ratio is increased. Figure 6.6 displays how the even mode capacitance alters with changes in the W/S ratio for various values of W/h ratio. The ratio of W/h is found to be the most important factor in the determination of the even mode capacitance of a microstrip line.

6.2.2 : Odd mode capacitance

Equations (3.10)-(3.14) may be used to calculate the odd mode capacitance for a pair of coupled lines. Figure 6.7 displays how the odd mode capacitance changes in relation to variations in the W/h ratio, for different values of W/S ratio. As the ratio of W/h is increased from 0.1 the capacitance falls slightly. However for $W/h > 0.3$ the capacitance starts to increase, rising very sharply in the region where $W/h > 2$. For $0.1 \leq W/h \leq 2$, as

the *W/S* ratio is increased so the capacitance also increases. Where *W/h* > 2 the calculated capacitances for all values of *W/S* ratio are almost exactly the same.

Figure 6.8 depicts the variation in impedance as the *W/S* ratio is altered for different values of *W/h*. Increases in the value of the *W/S* ratio causes an increase in the value of the capacitance calculated, but is not as significant as changes in the *W/h* ratio. Therefore the most important factor concerning the odd mode capacitance is the ratio of line width to height above the ground plane.

6.2.3 : Even mode impedance

Figure 6.9 shows how the even mode impedance of the line, calculated using equation (3.19), decreases as the ratio of *W/h* is increased, for varyious values of *W/S*. For the region *W/h* < 2 the impedance increases with *W/S* ratio, but above this little or no difference is seen for changes in the *W/S* ratio.

Figure 6.10 shows how the even mode impedance changes with *W/S* ratio, for different values of *W/h* ratio. For *W/h* = 5 there is negligible change in the impedance calculate, but as the *W/h* is decreased so the changes in *W/S* have more effect upon the impedance, where there is an increase in impedance with *W/S* and flattening a of the curve as *W/S* tends towards 10.

6.2.4 : Odd mode impedance

The odd mode impedance for a pair of microstrip lines is calculated using equation (3.20). It is depicted in figure 6.11 how as the *W/h* ratio is increased from 0.1 the impedance also starts to rise. However, when *W/h* > 0.2 the impedance starts to fall with further increases in *W/h*. As *W/S* is increased, so the impedance falls, but for the region

where $W/h > 3$ changes in W/S have little or no effect upon the value of the odd mode impedance.

Figure 6.12 displays a graph of W/S ratio versus odd mode impedance for varying values of W/h ratio. For a value of $W/h = 5$, changes in the ratio of W/S have little or no effect upon the value of the calculated impedance. However as W/h is decreased, so the impedance is also found to increase.

6.2.5 : Impedance calculations

The characteristic impedance, Z_0, of a pair of parallel microstrip lines of equal width, can be calculated from equation (3.21). Figure 6.13 shows how the impedance of a pair of parallel microstrip lines is affected by changes in the ratio of line width to height above ground plane, W/h, for varying values of W/S. The impedance of the pair of lines is found to decrease as the ratio of W/h is increased. For the region where $W/h > 2$, the effect of changing the ratio of W/S has a negligible effect upon the impedance. Where $W/h < 2$ the impedance is found to decrease as W/S is increased.

The above results show how the design of a microstrip with a particular required characteristic impedance is a compromise between the different parameters of line width, W, height above ground plane, h, and separation between the lines, S.

6.3 : *n* Coupled Lines

The generalisation of the method for n coupled lines, introduces its very own unique problems. One of these is that the calculation of the eigenvalues and eigenvectors is not a trivial calculation, and the second problem being the calculation of the inverse of a matrix. For matrices larger than 3×3, Mathematica may introduce errors which are then

propagated rapidly through to the final evaluation of the characteristic impedance and propagation delay. This is due to nature of the how these matrices are calculated, which may therefore be considered to be ill-defined by Mathematica. Due to this problem, calculation of the impedance and time delay for the example of the eight line logic bus (outlined in chapter 1) will not be attempted.

For the above reasons, some examples of a three line bus (Belahrach 1990) will be used to evaluate the generalised method outlined in chapter 3. Figure 6.15 shows a schematic representation of three parallel microstrip lines, with the geometric parameters given in table 6.1, where $\varepsilon_r = 9$. Using equations (3.31)-(3.49) all the physical properties of the set of three lines can be calculated, from this set of geometrical parameters.

6.3.1 : Three coupled lines

Equations (3.32)-(3.36) are used for the calculation of all the elements contained in the per-unit length matrix, **C**. All the matrix elements calculated for the 4 different structures, are given in table 6.2. The per-unit length inductance matrix elements, $L_{i,j}$, calculated from equation (3.37) are given in table 6.3. These results are found to be consistent with previously published work (Belahrach 1990).

Diagonalisation of the PUL inductance matrix, **L**, and the PUL capacitance matrix, **C**, to $\mathbf{L}_d$ and $\mathbf{C}_d$, is accomplished using equations (3.41) and (3.42) respectively. Using these diagonalised matrices the characteristic impedances, Z_{di}, for each line can be calculated from equation (3.49), with the results for the each individual structure given in table 6.4. These results are consistent in there form with those obtained by Chilo and Arnaud (1984) for an eight line bus structure. The time delay per metre matrix, $\mathbf{T}_d$, is calculated using equation (3.48), with results of the calculation for each structure given in table 6.5. These are also found to be consistent with previously published work (Chang 1970, Chilo and Arnaud 1984).

6.3.2 : SPICE transient analysis

Having calculated the characteristic impedances and time delays for each of the three line bus examples, it is possible to use these parameters to construct an equivalent circuit model, as developed in Chapter 5, and use the SPICE program to simulate the behaviour of such a three line microstrip structure. Figure 6.16 shows the operating configuration for the three line microstrip structures (outlined in table 6.1), where the component values used in the terminating networks are given in table 6.6.

Figures 6.17-6.20 show the input and output signals seen on lines 2 and 3 for the transient analysis of structures 1 to 4 respectively. A step function of 1V is input into the centre of the three lines, having a rise time of 600ps. Upon investigation it is found that there is very little difference between the transient analysis results obtained for each of the four structures. The shape of the voltage waveforms are found to be almost identical, with some small change in the magnitude of the voltage levels. This would suggest that the particular changes to the geometry, in the given coupled microstrip line examples (Belahrach 1990), do not have a significant affect upon the transient performance of such a bus.

6.4 : Summary

This chapter illustrates the use of the program developed (appendix A) in Mathematica for calculating the impedance, and other parameters appertaining to parallel microstrip lines.

The effect of changes to the geometrical and physical parameters of a single microstrip line, upon the impedance is studied, and these results are found to be consistent with all

previous investigations.

A pair of parallel coupled microstrip lines is then investigated, in order to study the effect that changes in geometry have upon, the odd and even mode capacitances and impedances, and the characteristic impedance of the pair of lines. These results are also found to be consistent with previous work on coupled microstrip line pairs.

A set of four, three coupled line microstrip interconnection buses are studied. The characteristic impedances of each line and the associated propagation delays are then calculated. The parameters are then used to construct SPICE equivalent circuits, for which transient analyses are carried out. The results obtained are seen to be consistent with all previous work conducted on coupled three line structures.

Structure No.	W (μm)	S (μm)	t (μm)	h (μm)
1	405±10	285±10	16±2	1060±20
2	425±10	260±10	16±2	1060±20
3	405±10	210±10	16±2	1060±20
4	300±10	200±10	16±2	1060±20

Table 6.1 : Geometric parameters of four different three line microstrip configurations.

Structure No.	$C_{1,1}$ (pF/m)	$C_{2,2}$ (pF/m)	$C_{1,2}$ (pF/m)	$C_{1,3}$ (pF/m)
1	137.4	161.0	-31.4	-7.8
2	142.0	167.1	-33.5	-8.4
3	146.6	173.8	-37.8	-10.6
4	138.5	163.6	-37.7	-12.5

Table 6.2 : Capacitance coefficients for the four example structures.

Structure No.	$L_{1,1}$ (nH/m)	$L_{2,2}$ (nH/m)	$L_{1,2}$ (nH/m)	$L_{1,3}$ (nH/m)
1	451.2	401.7	95.2	45.7
2	439.1	390.2	96.6	47.7
3	430.8	382.6	104.7	56.6
4	459.9	411.4	117.2	68.7

Table 6.3 : Inductance coefficients of the four example structures.

Structure No.	Z_1 (Ω)	Z_2 (Ω)	Z_3 (Ω)
1	47.3	213.7	253.2
2	42.1	169.2	215.9
3	39.4	158.9	214.4
4	42.1	187.3	248.7

Table 6.4 : Characteristic impedance values calculated for the example structures.

Structure No.	T_{d1} (ns/m)	T_{d2} (ns/m)	T_{d3} (ns/m)
1	7.68	7.69	7.61
2	7.68	7.69	7.63
3	7.67	7.69	7.61
4	7.69	7.74	7.50

Table 6.5 : Propagation time values calculated for the example structures.

Structure No.	$R_0\,(\Omega)$	$R_1\,(\Omega)$	$R_2\,(\Omega)$
1	75	47	82
2	75	43	82
3	75	47	82
4	91	56	75

Table 6.6 : Terminal resistances for the three line microstrip simulation circuit.

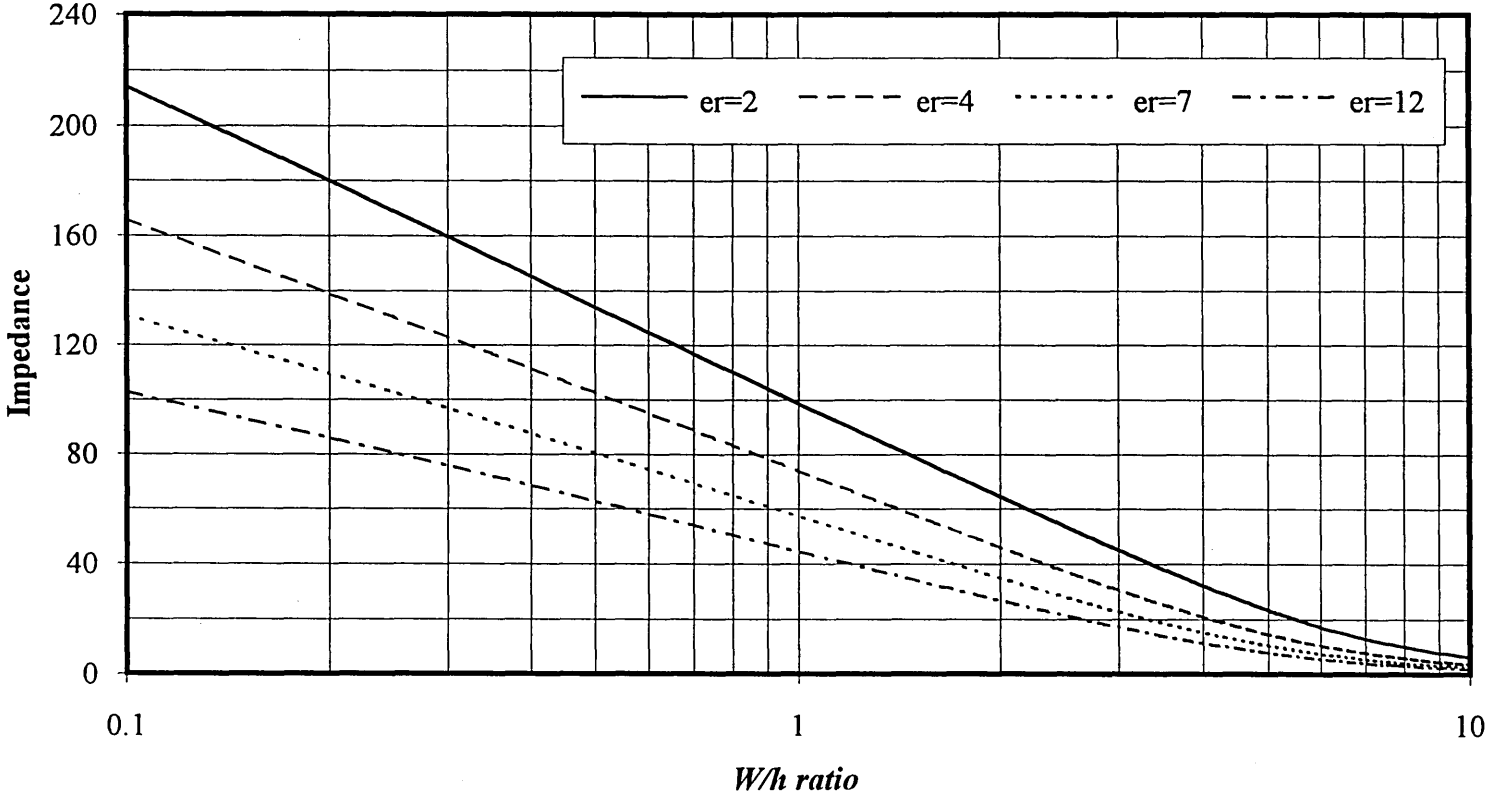

Figure 6.1 : Variation of impedance with W/h ratio for various values of ε_r, and t=0 for a single microstrip line.

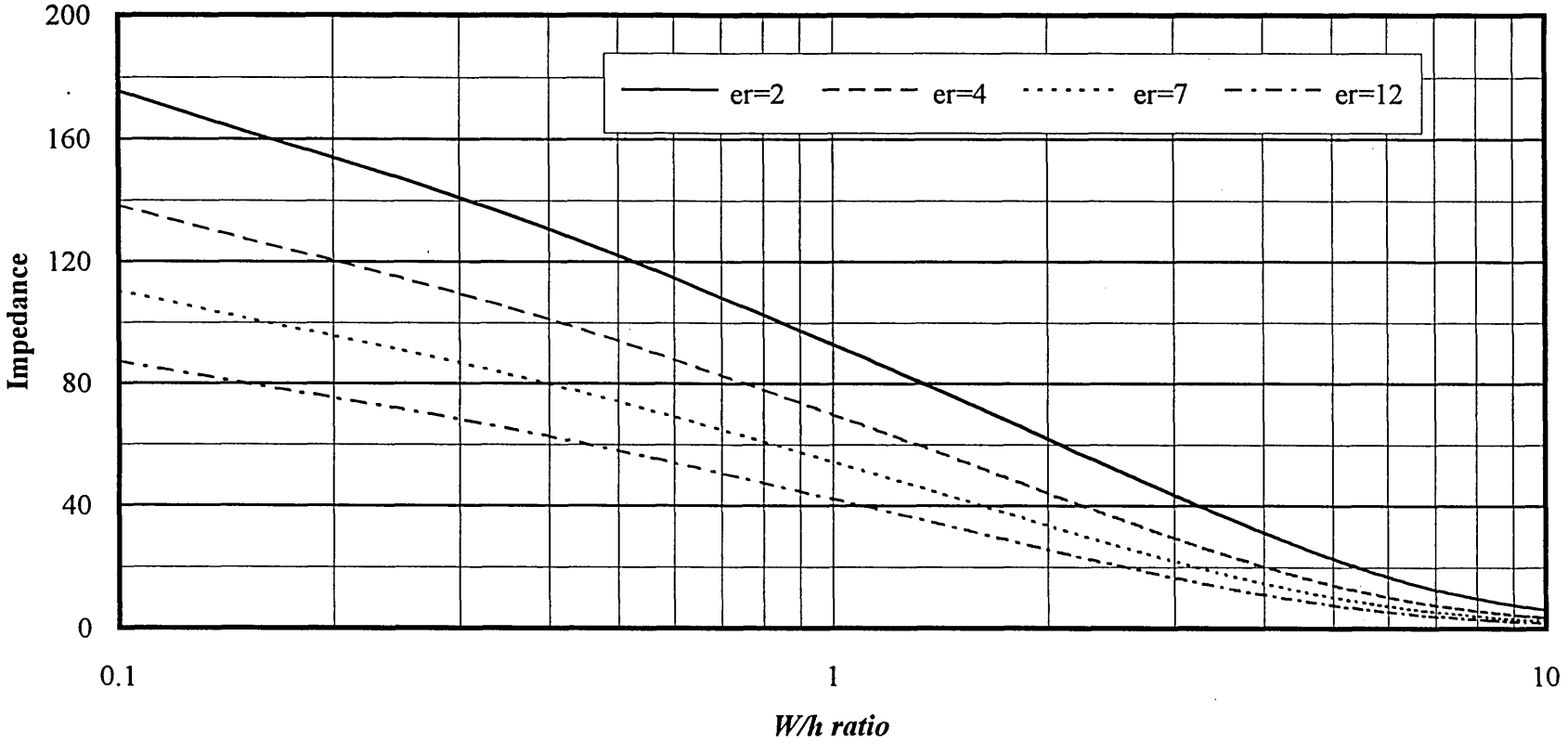

Figure 6.2 : Variation of impedance with W/h ratio for t/h = 0.1 for a single microstrip line.

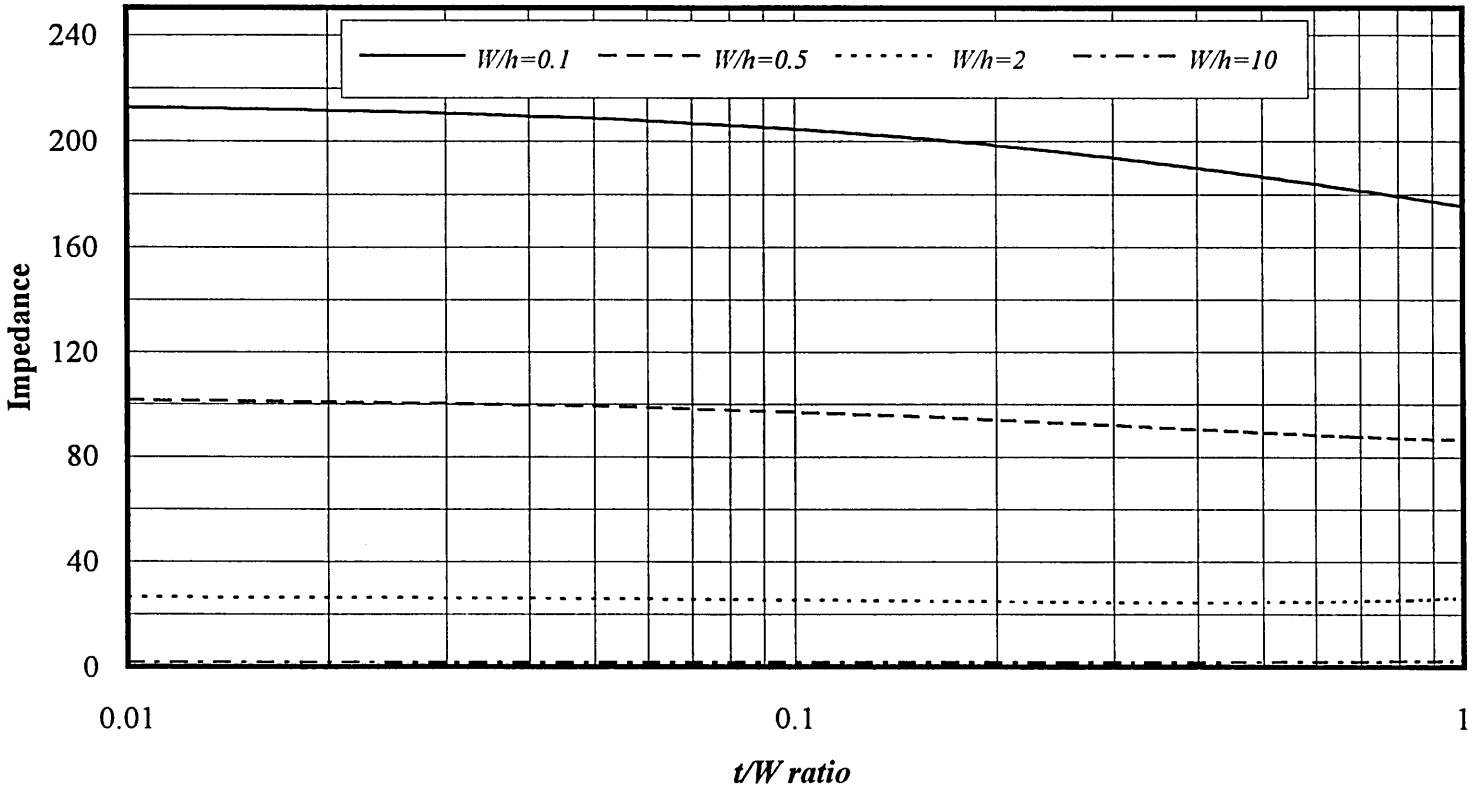

Figure 6.3 :Variation of t/W ratio for various values of W/h ratio for a single microstrip line.

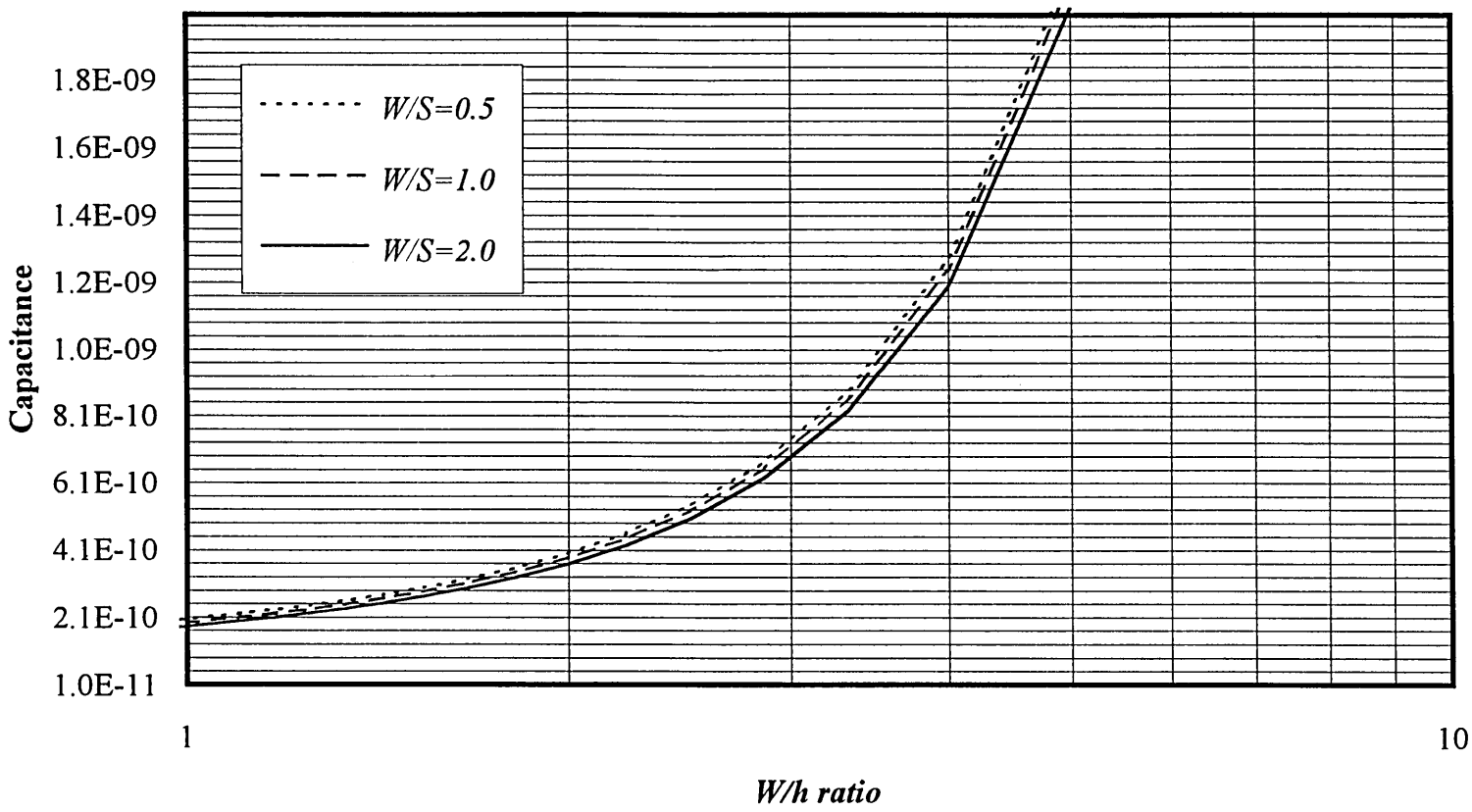

Figure 6.4 : Even mode capacitance versus W/h ratio for varying W/S ratios for a coupled microstrip pair.

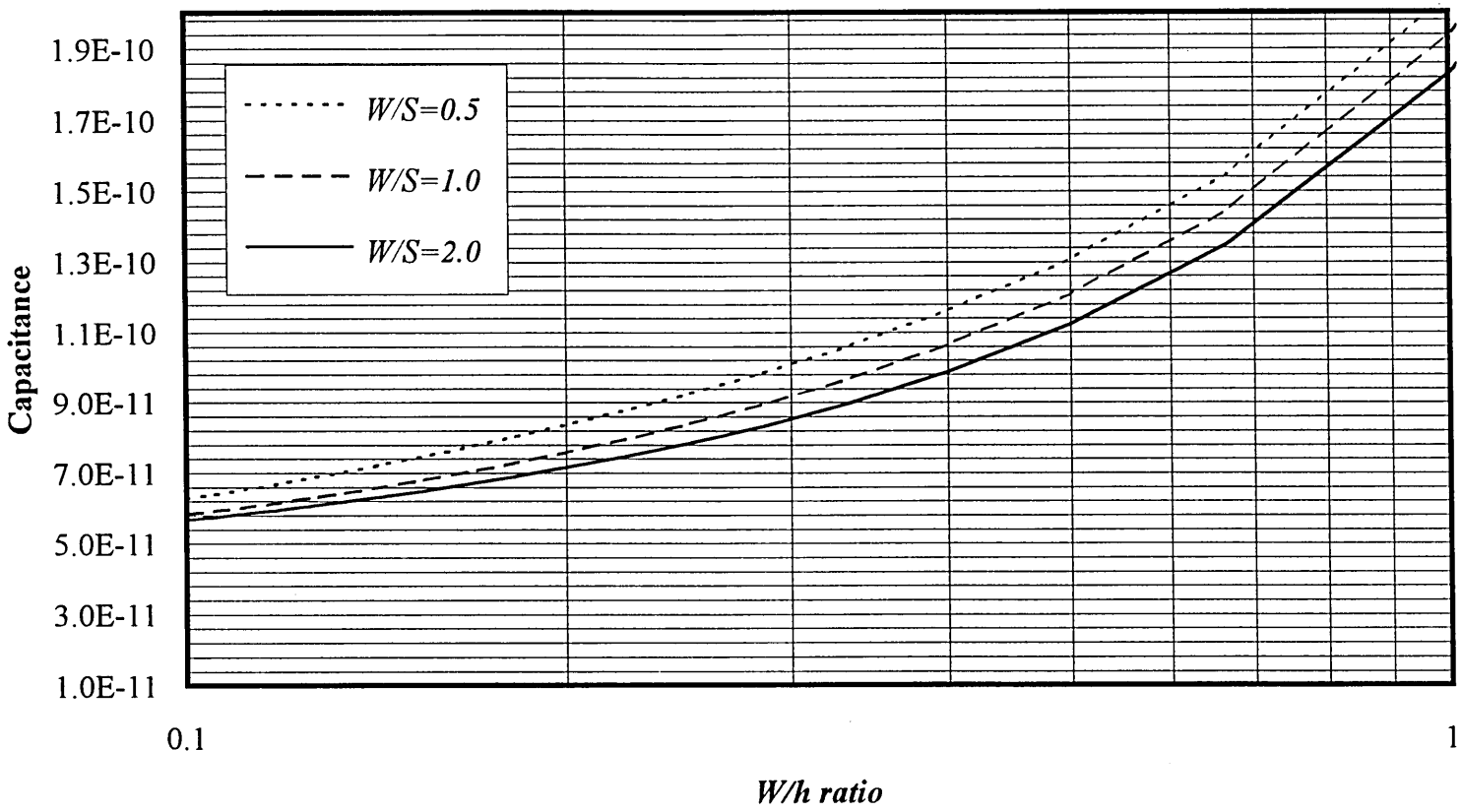

Figure 6.5 : Even mode capacitance versus W/h ratio for varying W/S ratios for a coupled microstrip pair.

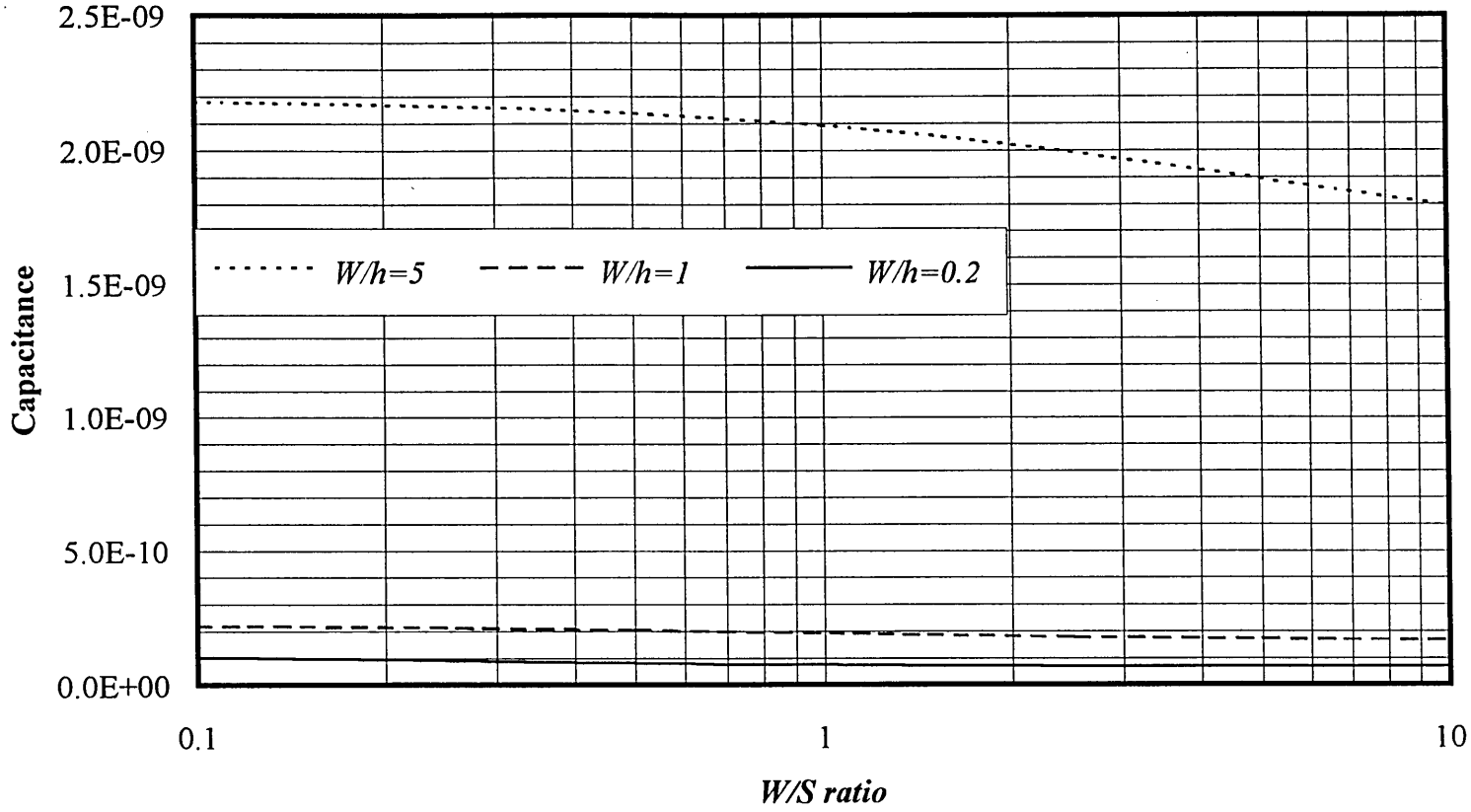

Figure 6.6 : Even mode capacitance versus W/S ratio for varying W/h ratio for a coupled microstrip pair.

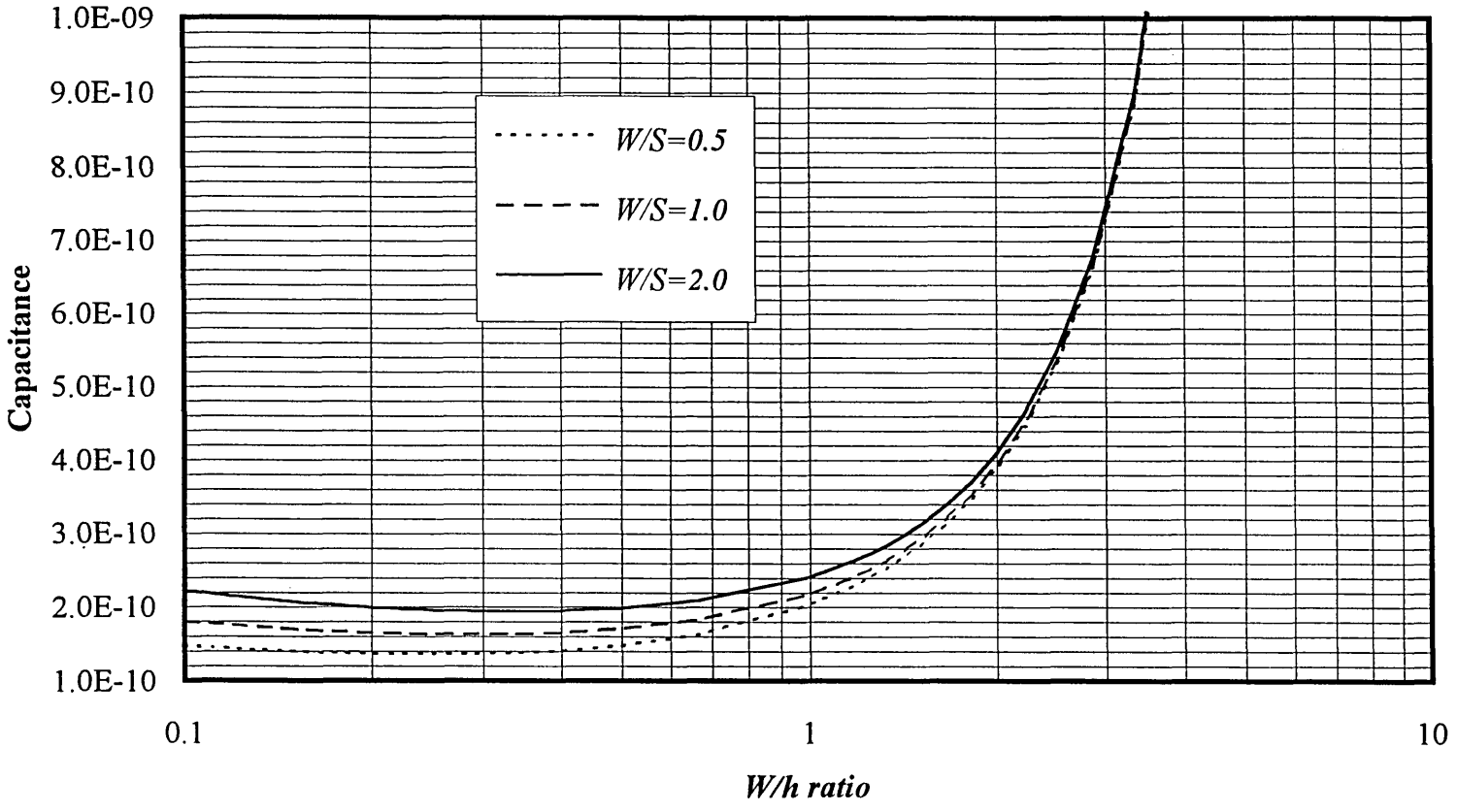

Figure 6.7 : Odd mode capacitance versus W/h ratio for varying W/S ratios for a coupled microstrip pair.

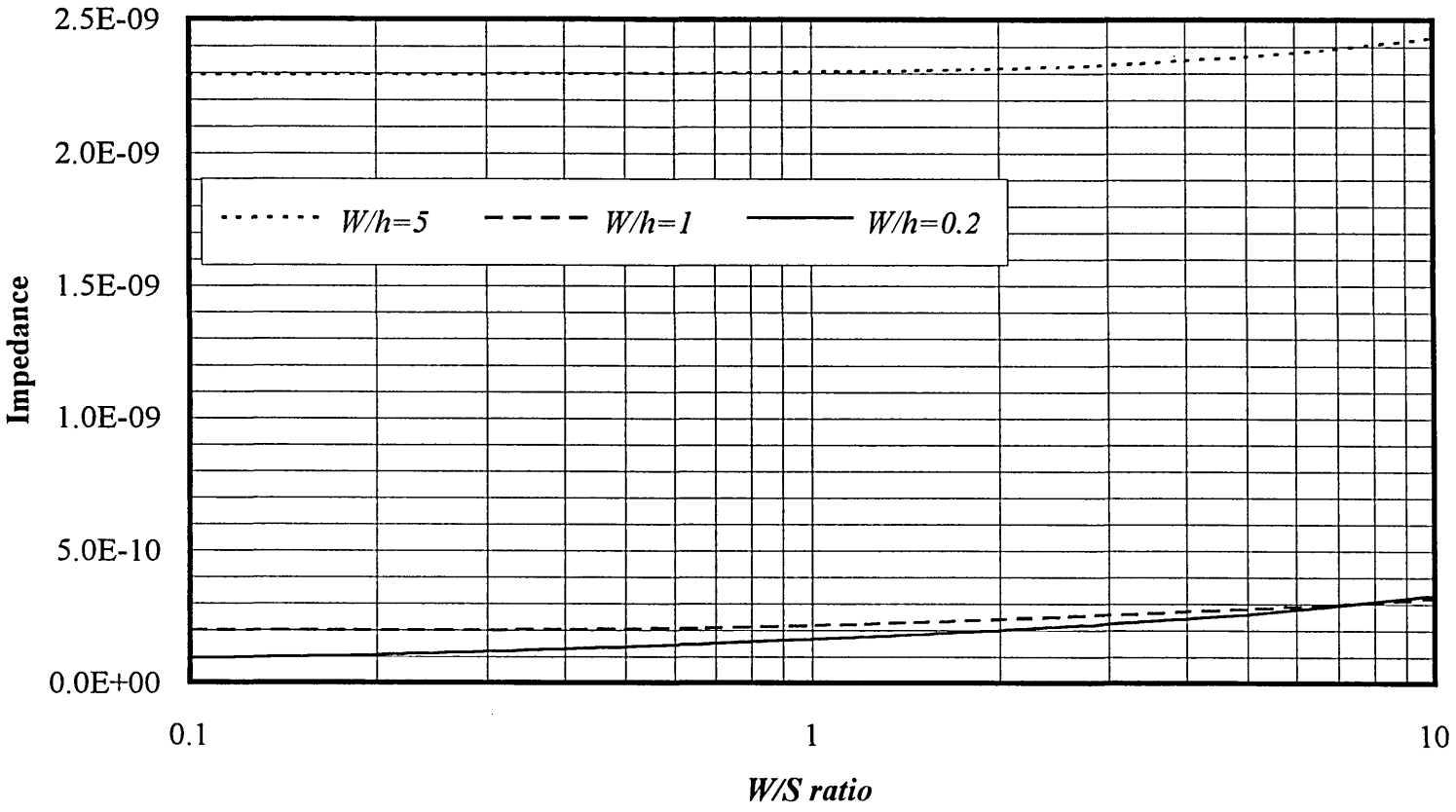

Figure 6.8 : Odd mode capacitance versus W/S ratio for varying W/h ratio for a coupled microstrip pair.

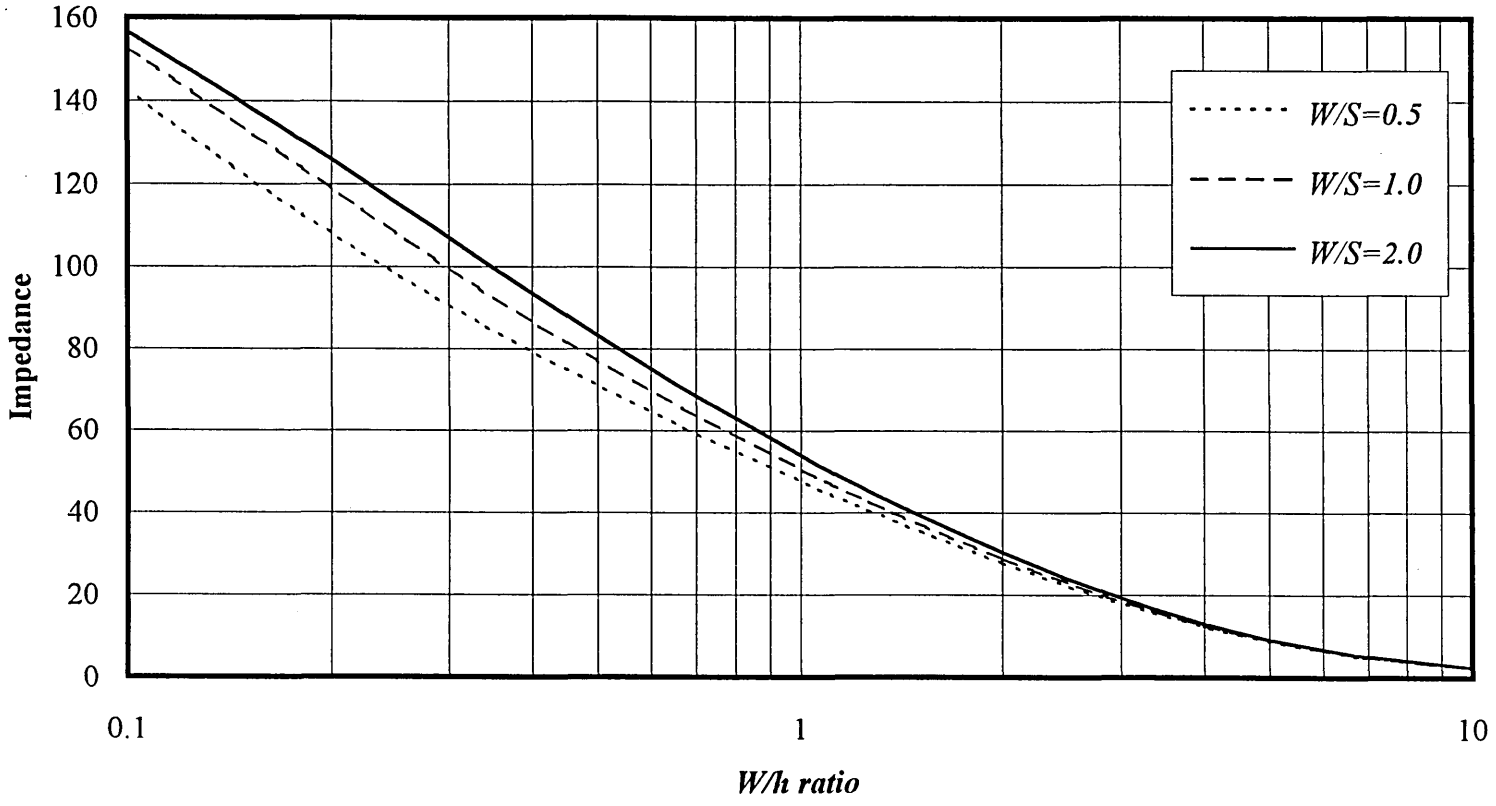

Figure 6.9 : Even mode impedance versus W/h ratio for varying W/S ratios for a coupled microstrip pair.

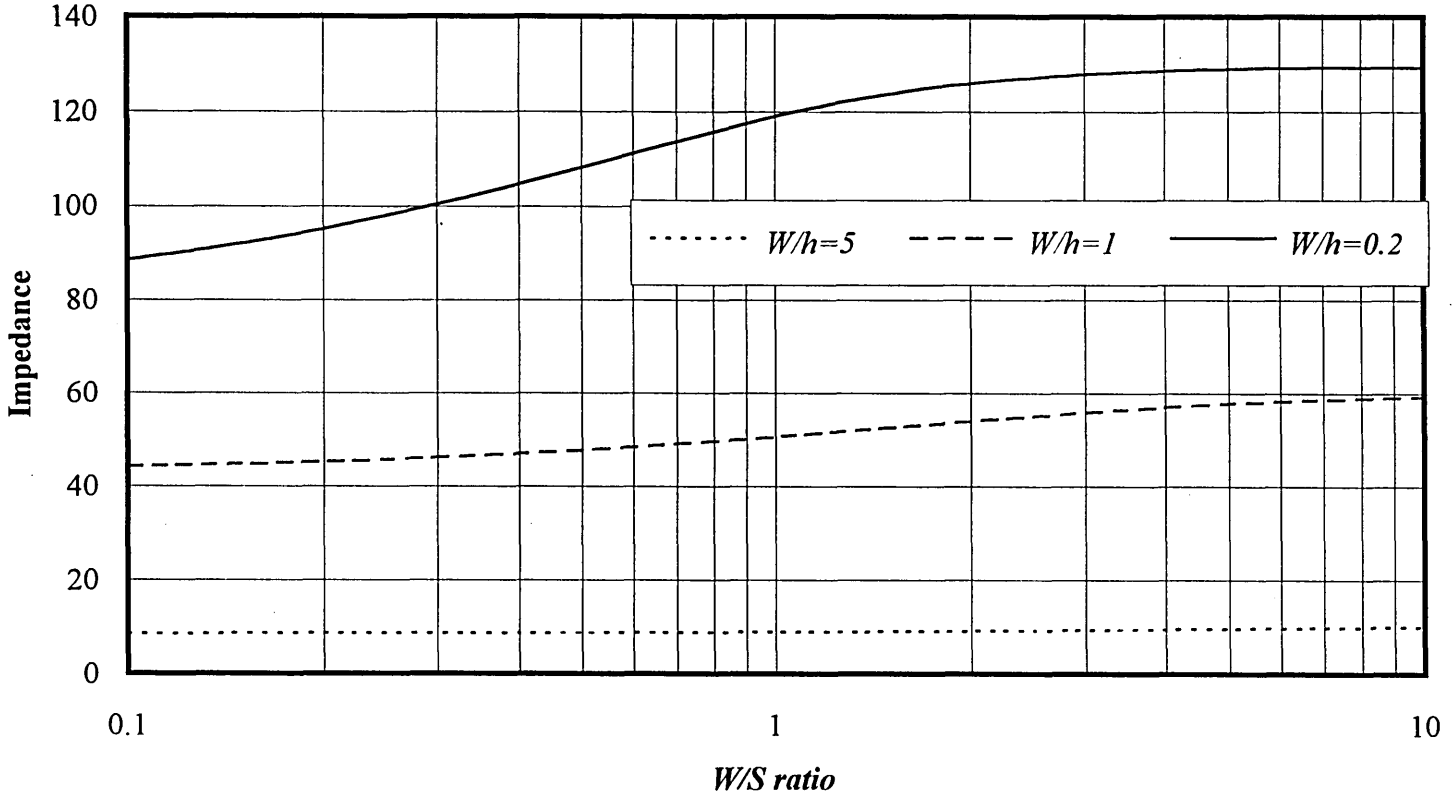

Figure 6.10 : Even mode impedance versus W/S ratio for varying W/h ratios for a coupled microstrip pair.

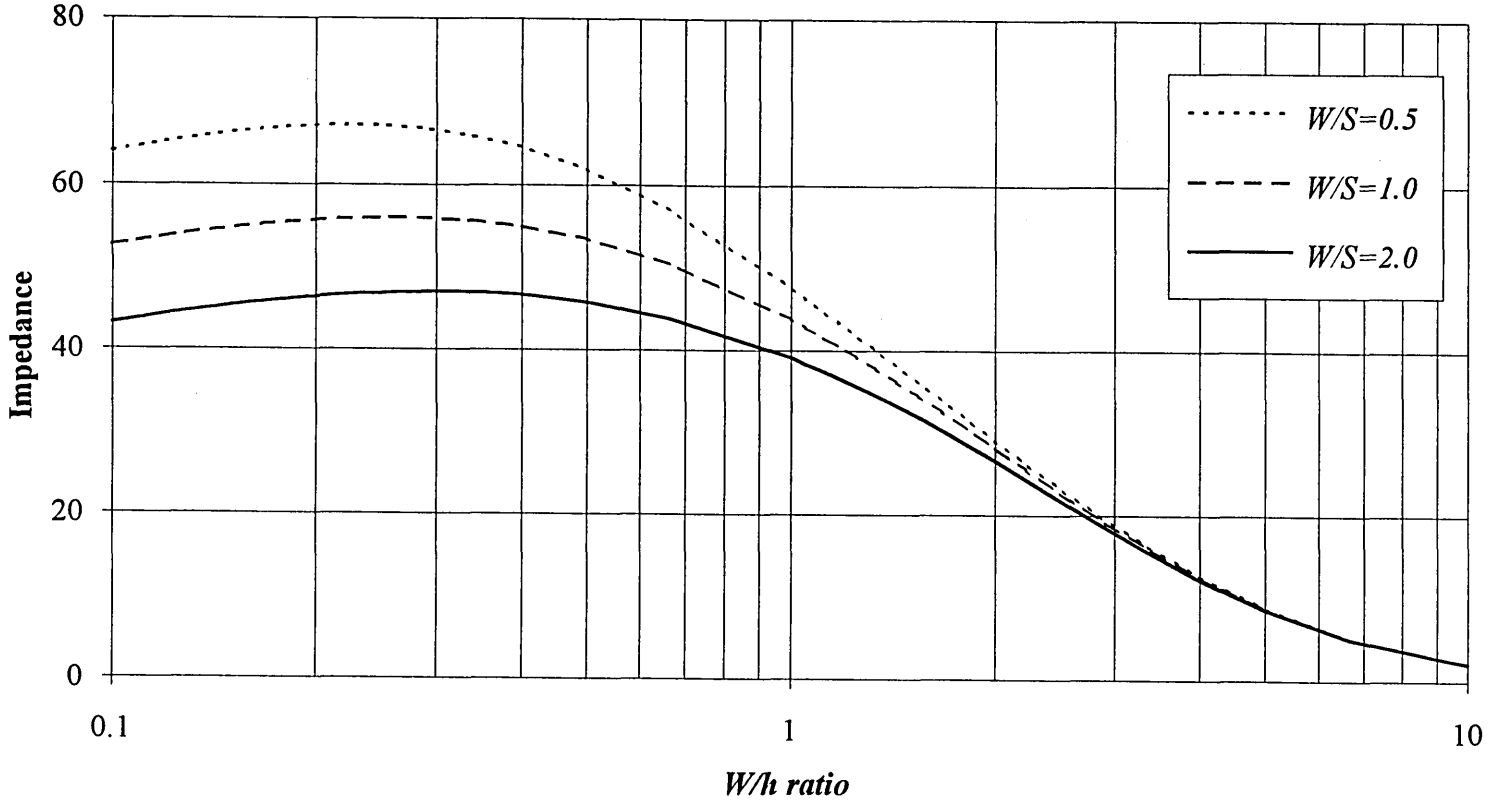

Figure 6.11 : Odd mode impedance versus W/h ratio for varying W/S ratios for a coupled microstrip pair.

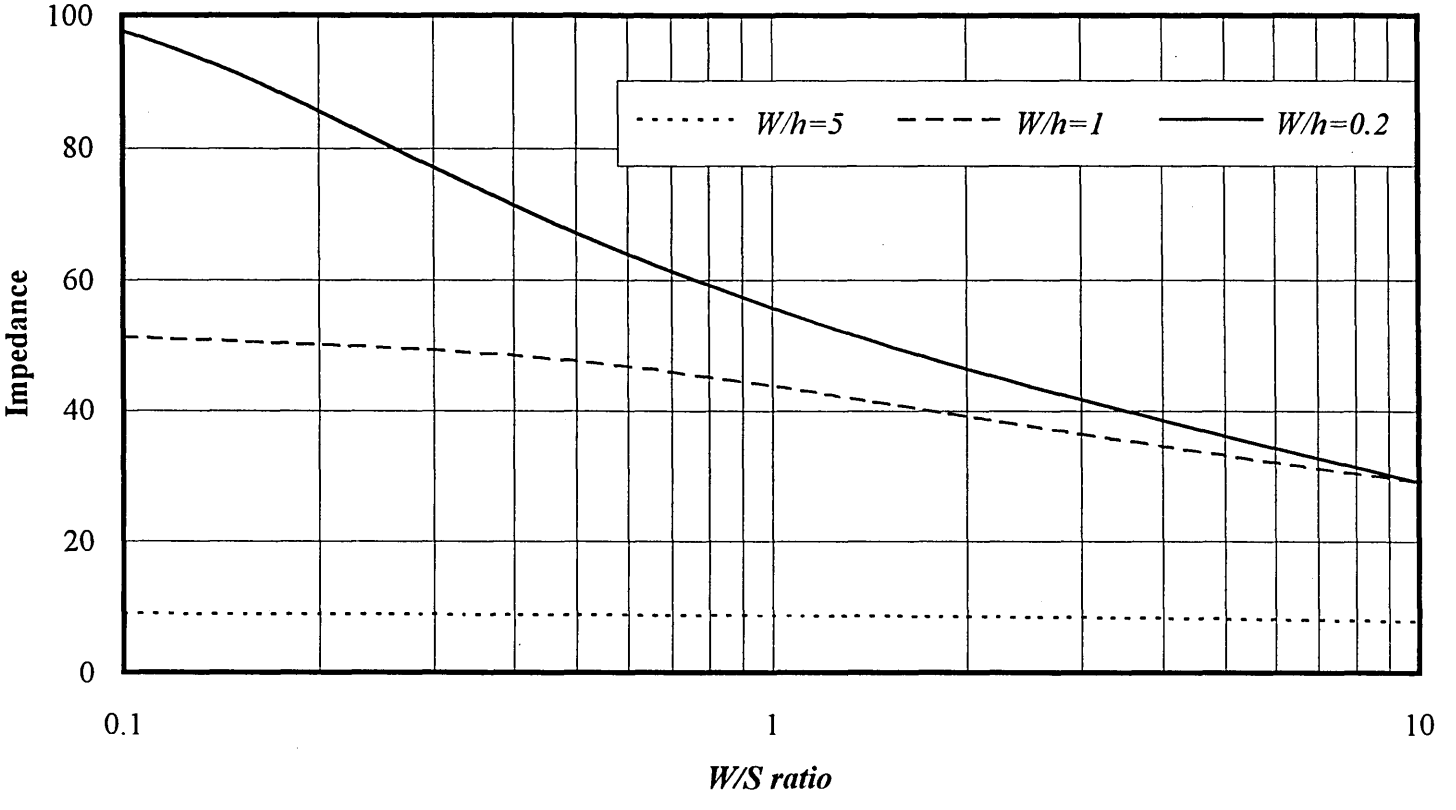

Figure 6.12 : Odd mode impedance versus W/S ratio for varying W/h ratios for a coupled microstrip pair.

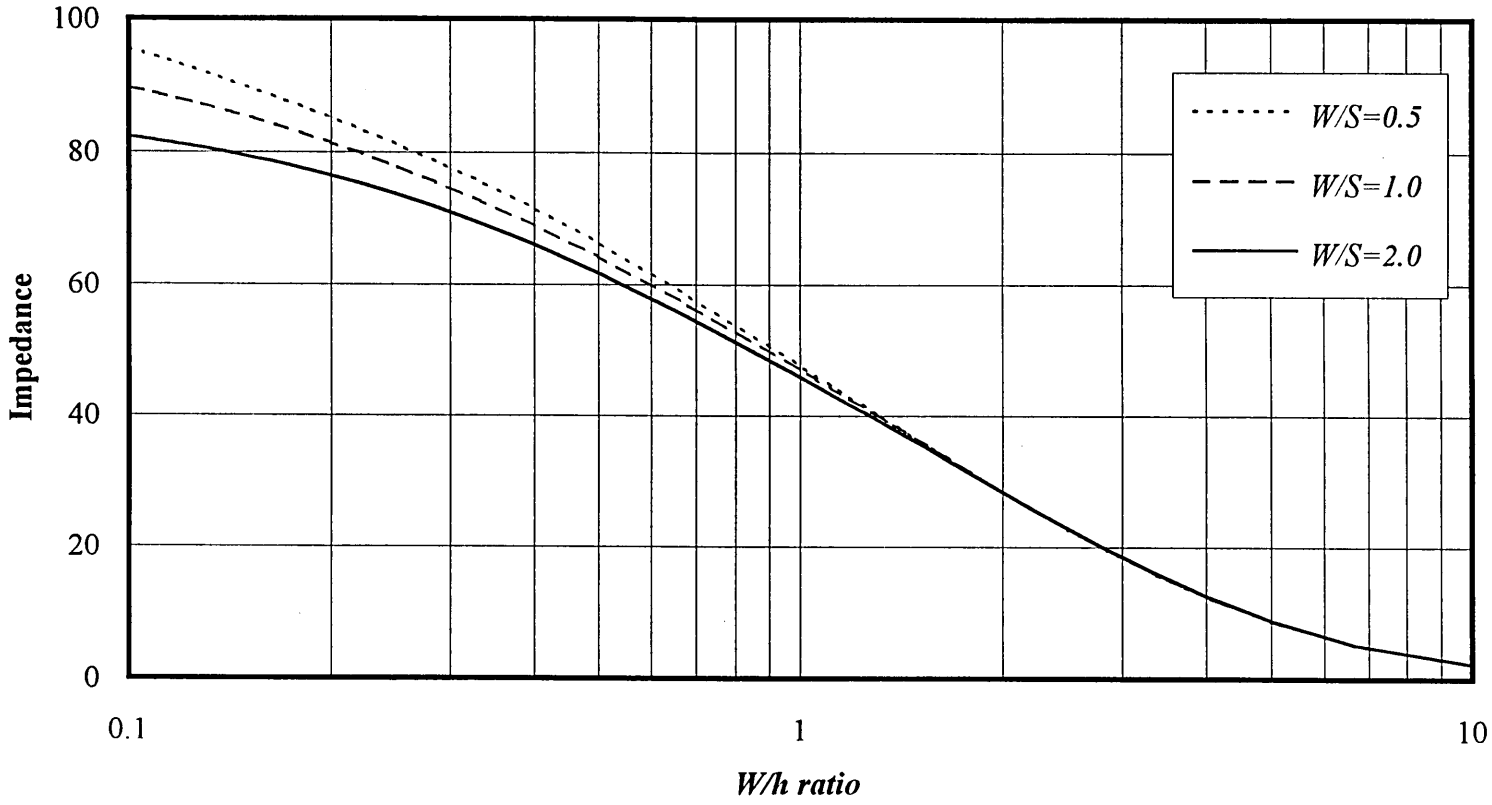

Figure 6.13 : Impedance versus W/h ratio for varying W/S ratios for a coupled microstrip pair.

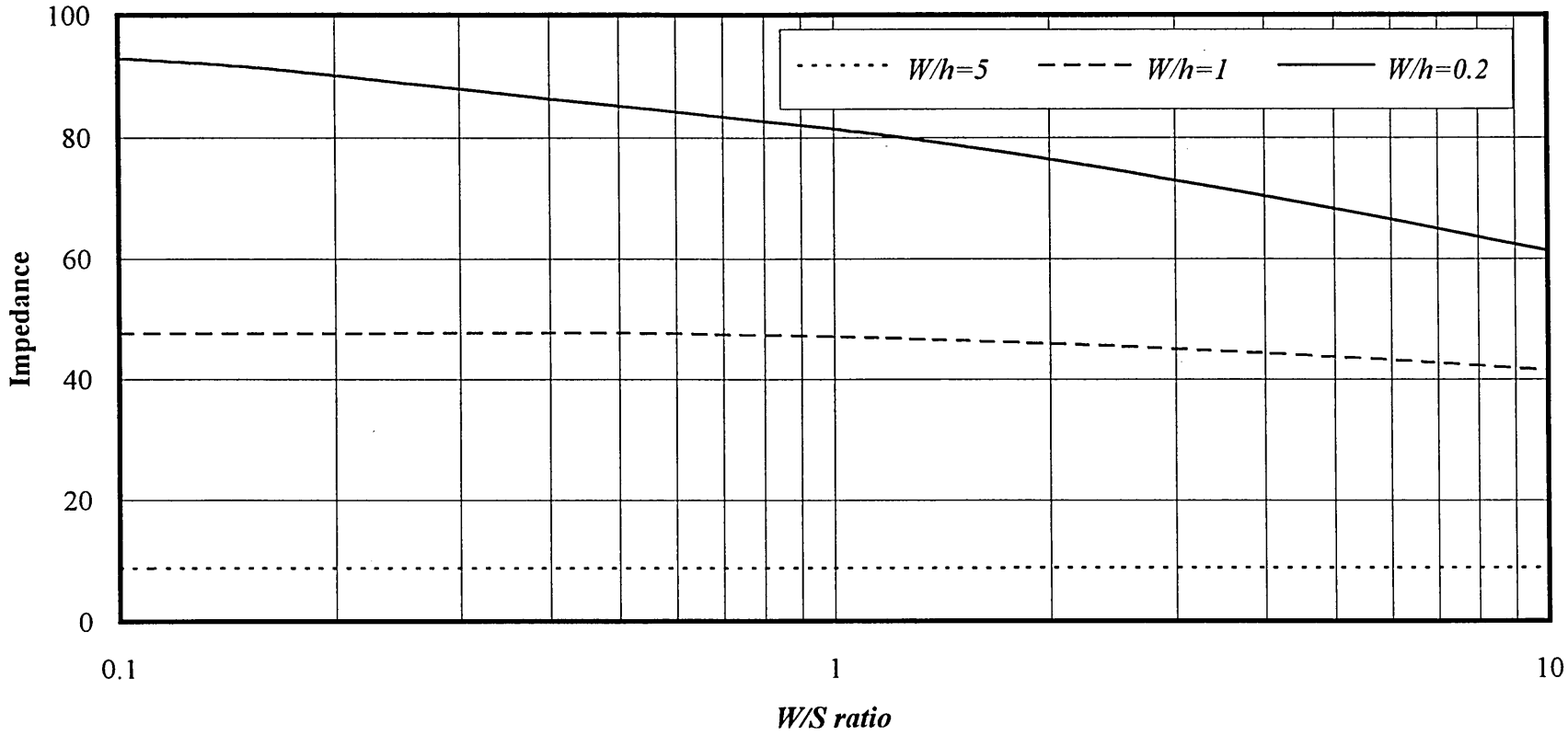

Figure 6.14 : Impedance versus W/S ratio for varying W/h ratios for a coupled microstrip pair.

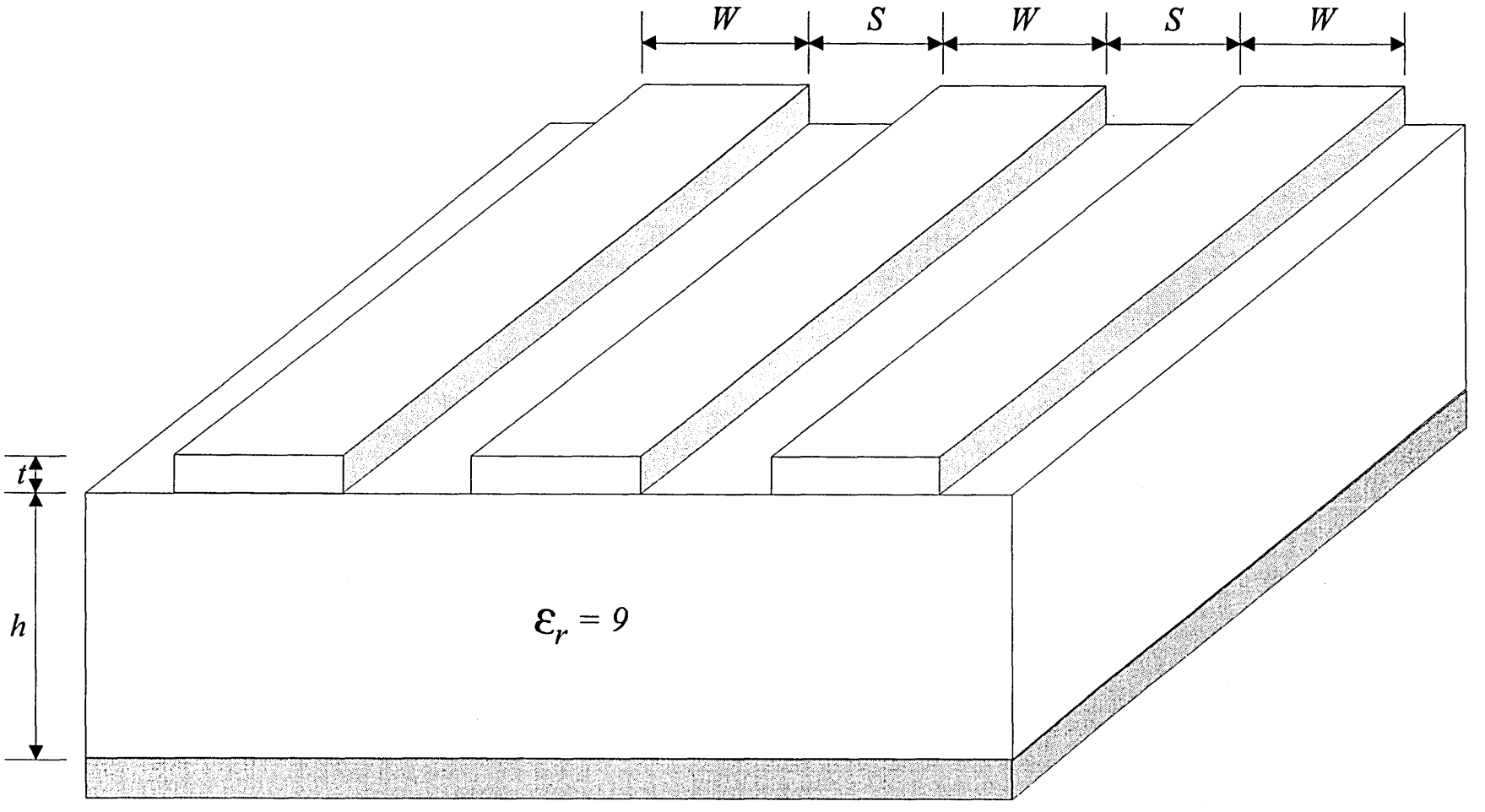

Figure 6.15 : Schematic representation of three parallel microstrip lines.

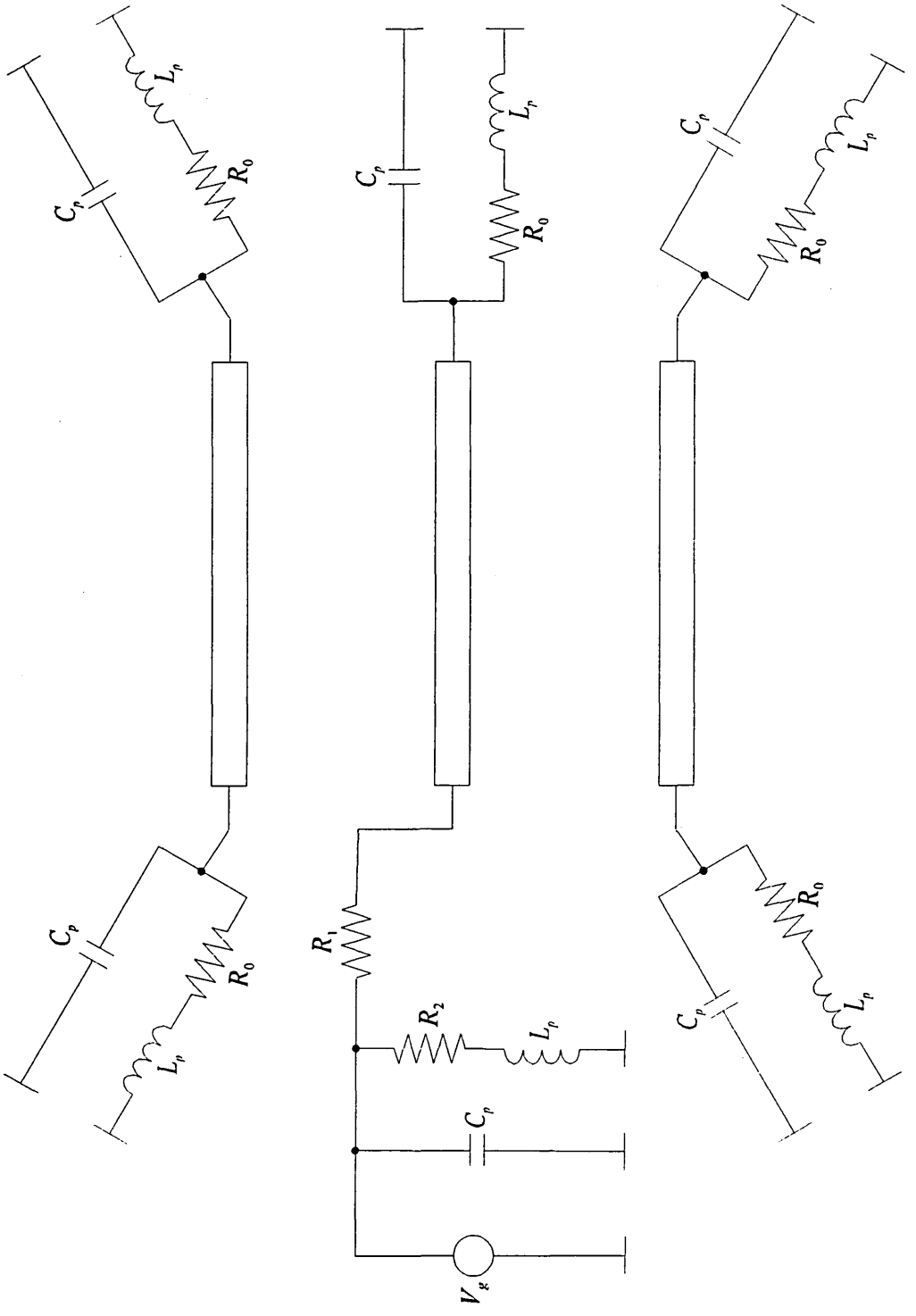

Figure 6.16 : Configuration used for the simulation of the three line microstrip examples.

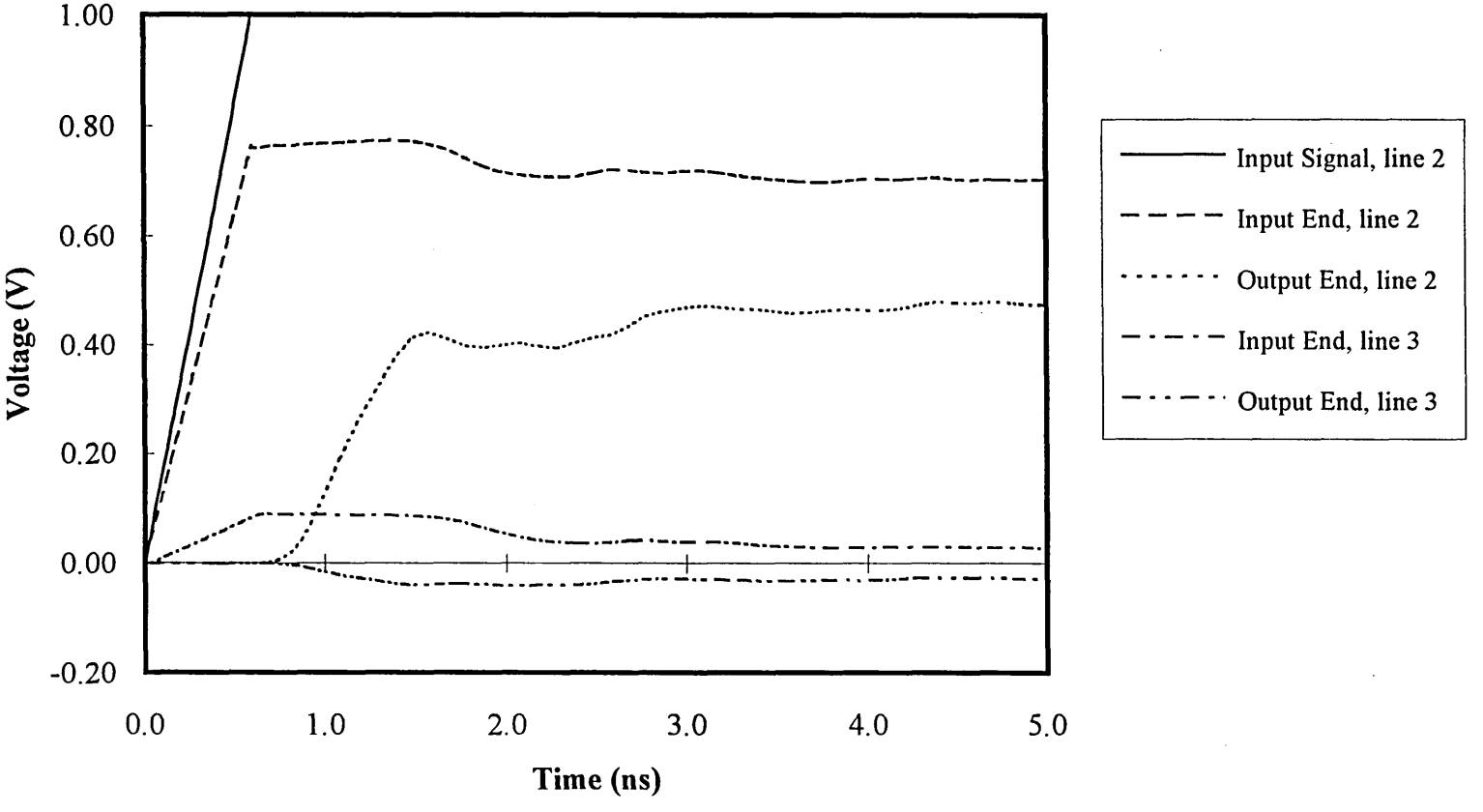

Figure 6.17 : Input and output signals on lines 2 and 3, for three line structure 1.

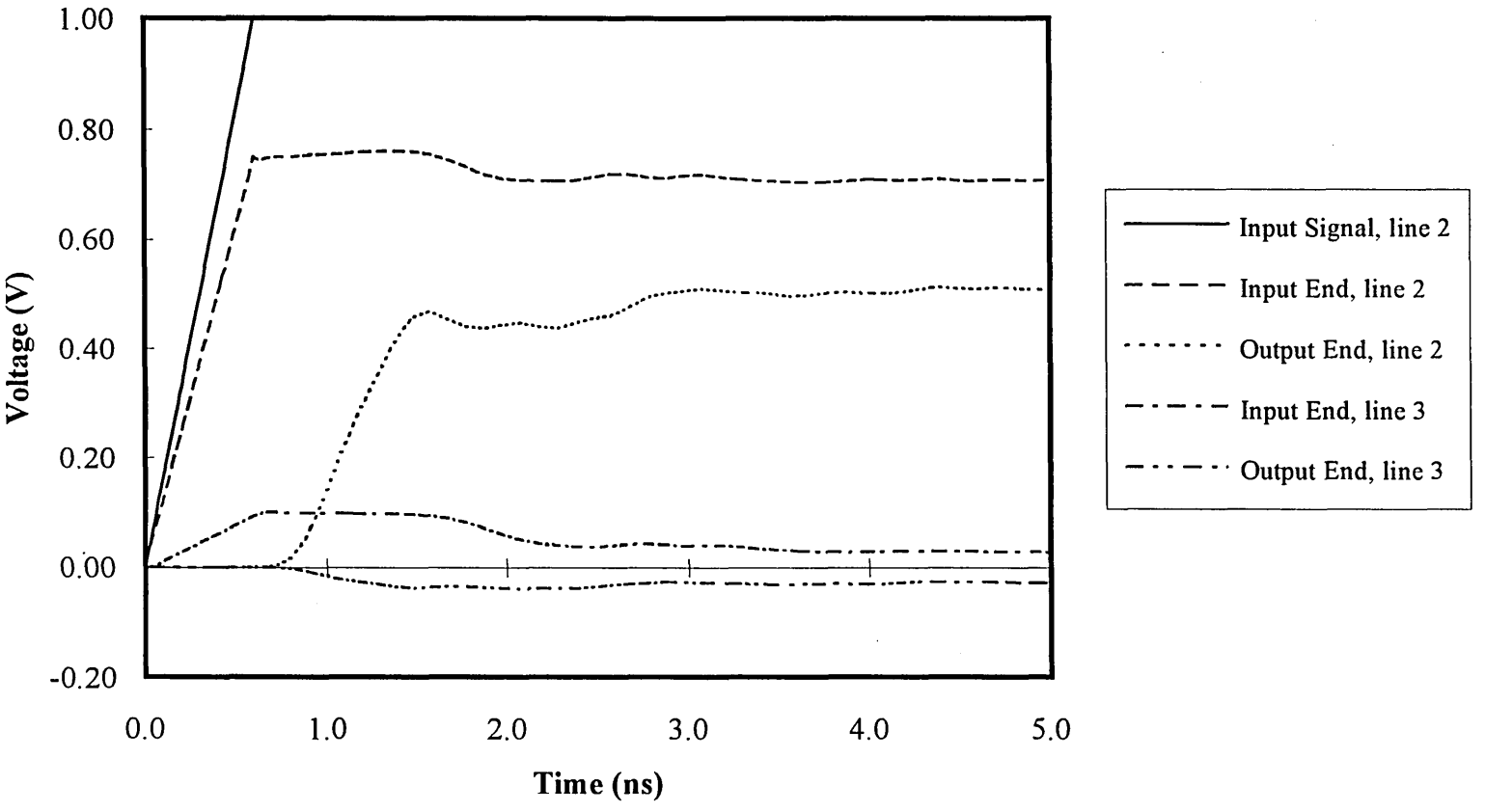

Figure 6.18 : Input and output signals on lines 2 and 3, for three line structure 2.

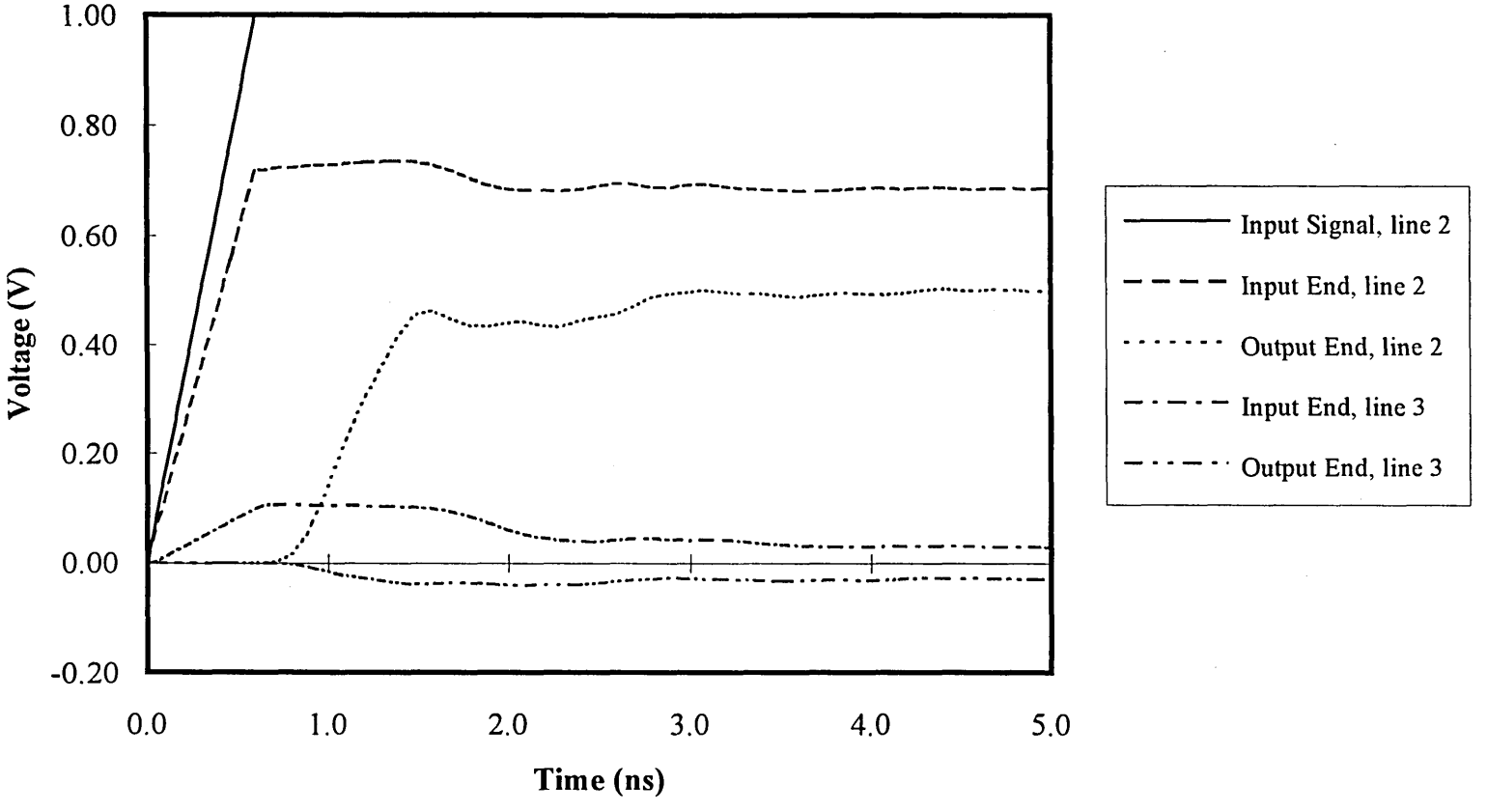

Figure 6.19 : Input and output signals on lines 2 and 3, for three line structure 3.

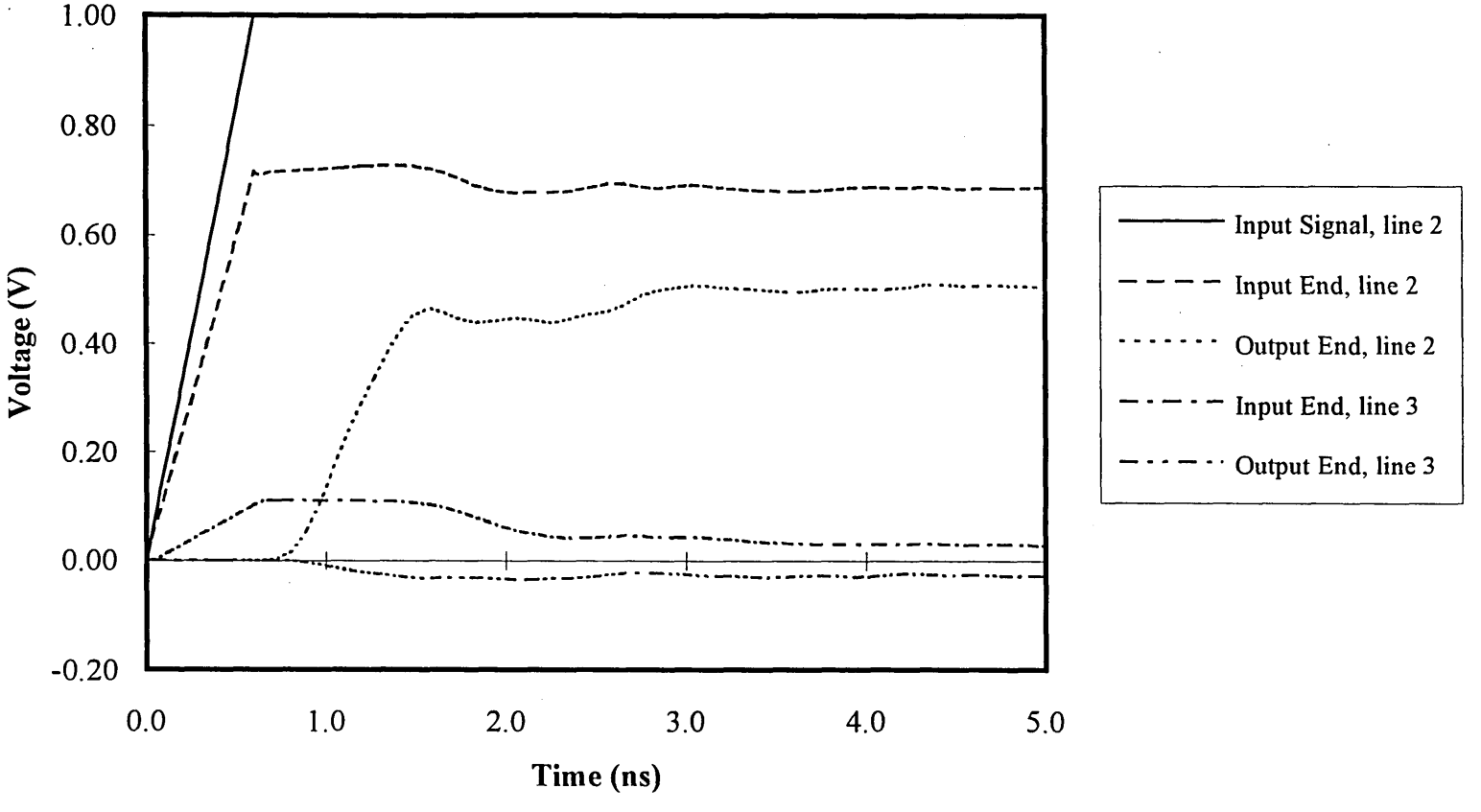

Figure 6.20 : Input and output signals on lines 2 and 3, for three line structure 4.

7.0 : Concluding Remarks

The work undertaken in this thesis provides the fundamental design and simulation tools required by a high-speed integrated circuit designer for taking the effects of on-chip interconnections into account.

The development of the quasi-distributed equivalent circuit model, and its implementation into the SPICE circuit simulator has been illustrated. This equivalent circuit model is then used for the simulation of lossless transmission lines. A modification is made to the circuit to allow the simulation of lossy transmission lines.

The time domain transient simulations undertaken demonstrate the importance of choosing the correct input and load impedances, in order to minimise the distortion inherent when unmatched loads are used. The effect of attenuation due to series line resistance (much greater in high-density integrated circuits) of a lossy transmission line is investigated, showing it to be independent of the impedance of the line.

A time domain study of crosstalk between the interconnection lines on high-speed digital circuits using the SPICE circuit simulator is presented for the example of the eight line bus. This analysis shows that for the case of two activated lines, an increase in crosstalk is seen on the lines between them, but little or no change is seen on the other lines, when compared to the case of a single activated line. This is due to a shielding effect caused by the activated lines, such that an activated line will cause little or no effect upon lines the other side of a second activated line. It is found that this crosstalk can be the possible cause of logic errors and is therefore a very important factor to be considered when designing a coupled microstrip line structure.

The lossy line model is then used to investigate the effect that the risetime of a signal travelling along it, has upon the received signal. This is accomplished using a step input with varying risetimes and pulses with varying risetime and width. These results show

that as the risetime is decreased so the level of ringing and distortion increases. This increase in distortion with decrease in risetime is due to an associated increase in the settling time and thus the shorter the pulse width the greater the pulse deformation. This sets an effective limit on the risetime and width of the signals which can be transmitted along the microstrip line. However the apparent ringing seen in the results may be due to convergence problems within the SPICE circuit simulator, and may not be as significant in the practical case.

A study of the effect of risetime upon coupling is also carried out and reveals that under certain conditions (very fast risetimes) an error in logic may be induced. This is because as the risetime is decreased so the initial peak overshoot increases and therefore the associated increase in the voltage level induced on other lines may be higher than the threshold voltage of the logic device, and thus an error in logic would become apparent. The risetime is therefore a very important factor which must be considered by the high-speed IC designer, to ensure that the circuit will perform without logic errors being induced when using the required signal speeds.

An equivalent circuit model for simulating the skin effect is developed, and used to investigate the frequency response of the line. It is however found that SPICE does not provide a set of satisfactory results and changing the number of sections used in the simulation alters the cut-off frequency. This is due to the nature of way in which SPICE sets up the mathematical equations used for analysing such a circuit, and does not allow proper convergence of the frequency response which also causes spikes to be seen in the response curve.

The program developed in Mathematica for calculating the impedance, and other parameters appertaining to parallel microstrip lines is used to evaluate the method developed for calculating the impedance of n coupled microstrip lines. This method provides the high-speed integrated circuit designer an easy and simple method of calculating the impedance, time delays and transformation network parameters for any

given set of n coupled microstrip lines.

The effect of changing the geometrical and physical parameters of a single microstrip line, upon the impedance is studied, and the results are found to be consistent with all previous investigations. A pair of parallel coupled microstrip lines is then investigated, in order to study the effect that changes in geometry have upon, the odd and even mode capacitances and impedances, and the characteristic impedance of the pair of lines.

A set of four, three coupled line microstrip interconnection lines are studied. The characteristic impedances of each line and the associated propagation delays are calculated. It is seen that the impedance of lines increases with distance in moving across the three line structure. This is due to the matrix calculations producing a set of eigenmodes, which take the coupling parameters into account and are therefore not the true measured values of impedance. The parameters are then used to construct SPICE equivalent circuits, for which transient analyses are carried out. The results obtained are seen to be consistent with all previous work conducted on coupled three line structures, and give good verification of both the Mathematica program and the SPICE equivalent circuit model.

The calculation of the parameters for structures with more than 3 parallel lines has not been found possible due to Mathematica not being able to provide accurate results for the eigenvectors and the inverse of larger matrices. This problem is due to larger matrices being ill-defined, not allowing the correct calculation of their inverse and eigenvalues. Therefore all the calculations have been restricted to 3 coupled line structures.

If a designer is required to investigate the performance of a coupled 3 line system using the methods developed in this thesis, the geometrical parameters and the dielectric constant of the substrate must be known. This data can then be entered into the developed Mathematica program which produces a set of impedance and time delay

values for each line and a matrix containing the coupling coefficients. These can then be entered into the FORTRAN program which produces a file containing the SPICE equivalent circuit model. This model then allows the designer to be able to run a series of simulations upon the set of coupled lines, and thus be able to characterise their behaviour.

7.1 : Possible Further Work

Further possible work which may be undertaken, is the improvement of the skin effect equivalent circuit model, such that a proper AC analysis can be performed, so that the cut-off frequency is independent of the number of sections used to simulate the line. Another area for further research would be to find a viable and stable method with which to accurately calculate the eigenvectors and the inverse of large matrices (i.e. greater than 3×3). This would allow the calculation of the properties for coupled microstrip lines where there are more than 3 lines in parallel.

The further investigation into calculating the impedance and time delay for nonuniform lines (e.g. tapered), multilevel structures (e.g. vias) and lines containing discontinuities, such as bends, stepped line structures and line intersections, would be extremely useful extra tools for the designer of a high-speed IC. The further development of the equivalent SPICE circuit models to implement these structures would also be necessary.

Another research project which would compliment the work undertaken in this thesis, is the fabrication and testing of coupled microstrip line structures, allowing the direct comparison of the modelling techniques to be made against practical measurements.

1. BAHL, I. J. and GARG, R., 1977, 'Simple and accurate formulas for a microstrip with finite strip thickness', IEEE Proc., Vol. 65, pp. 1611-1612.

2. BALABAN, P., 1973, 'Calculation of the capacitance coefficients of planar conductors on a dielectric surface', *IEEE Trans.*, **CT-20**, pp. 725-731.

3. BANZHAF, W., 1989, Computer-aided circuit analysis using SPICE, Prentice Hall, Englewood Cliffs, N. J.

4. BELAHRACH, H., 1990, Caractérisation electrique des interconnexions en technologies hybrides multicouches : modélisation numérique (2D et 3D) et simulation temporelle, Thèse de Doctorat, Université de Bordeaux I.

5. BENEDEK, P., 1976, 'Capacitances of a planar multiconductor configuration on a dielectric substrate by a mixed order finite-element method', *IEEE Trans.*, **CAS-23**, pp. 279-284.

6. BLAKE, R., 1993, Basic electronic communication, West Publishing Co., St. Paul, MN.

7. BLOOD, JR, W. R., 1988, MECL system design handbook, Motorola Inc.

8. BRANIN, JR, F. H., 1967, 'Transient analysis of lossless transmission lines', *Proc. IEEE.*, **Vol. 55.**, pp. 2012-2013.

9. BRENAN, P. A. and RUEHLI, A. E., 1978, 'Time-domain skin-effect model using resistors and lossless transmission lines', *IBM Tech. Discl. Bulletin.*, **Vol. 21**, pp. 2162-2163.

10. BRYANT, T. G. and WEISS, J. A., 1968, 'Parameters of microstrip transmission lines and of coupled pairs of microstrip lines', *IEEE Trans.*, **MTT-16**, pp. 1021-1027.

11. CALVEZ, L. and LE BIHAN, J., 1986, 'Coefficient algorithms for time domain response of skin effect lossy coaxial cables with arbitrary resistive terminations', *IEEE Trans.*, **CAS-33**, pp. 915-920.

12. CASES, M. and QUINN, D. M., 1980, 'Transient response of uniformly distributed RLC transmission lines', *IEEE Trans.*, **CAS-27**, pp. 200-207.

13. CHANG, F. Y., 1970, 'Transient analysis of lossless coupled transmission lines in a nonhomogeneous dielectric medium', *IEEE Trans.*, **MTT-18**, pp. 616-626.

14. CHANG, F. Y., 1990, 'Waveform relaxation analysis of RLCG transmission lines', *IEEE Trans.*, **CAS-37**, pp. 1394-1415.

15. CHANG, F. Y., 1991, 'Waveform relaxation analysis of nonuniform lossy transmission lines characterized with frequency-dependent parameters', *IEEE Trans.*, **CAS-38**, pp. 1484-1500.

16. CHEN, Z. and GAO, B., 1989, 'Deterministic approach to full-wave analysis of discontinuities in MIC's using the method of lines', *IEEE Trans.*, **MTT-37**, pp. 606-611.

17. CHEN, L. and LI, S., 1991, 'The new method of time-domain analysis of planar transmission line with discontinuity', *Int. J. Infrared and Millim. Waves.*, **Vol. 12.**, pp. 1315-1320.

18. CHENG, K. K. M. and EVERARD, J. K. A., 1991, 'Accurate formulas for efficient calculation of the characteristic impedance of microstrip line', *IEEE Trans.*, **MTT-39**, pp. 1658-1661.

19. CHILO, J. and ARNAUD, T., 1984, 'Coupling effects in the time domain for an interconnecting bus in high speed GaAs logic circuits', *IEEE Trans.*, **ED-31**, pp. 347-352.

20. CHOWDHURY, S. *ET AL*, 1992, 'A transmission line simulator for high-speed interconnects', *IEEE Trans.*, **CAS-II-39**, pp. 201-211.

21. COEN, S., 1975, 'A note on Green's function for microstrip', *IEEE Trans.*, **MTT-33**, pp. 591-593.

22. COLLIN, R. E., 1960, Field theory of guided waves, McGraw Hill, NY.

23. CROZAT, P., ZOUNON, A. and ADDE, R., 1988, 'Condition of modal analysis in time domain of lossy coupled lines', *Electronics Letters*, **Vol. 24**, pp. 1289-1290.

24. DEUTSCH, A. *ET AL*, 1990, 'High-speed signal propagation on lossy transmission lines', *IBM J. Res. Develop.*, **Vol. 34**, pp. 601-615.

25. DHAENE, T. and DE ZUTTER, D., 1992, 'Extended thevenin models for transient analysis of non-uniform dispersive lossy multiconductor transmission lines', *IEEE Int. Symp. Circuits and Syst.*, pp. 1772-1775.

26. DJORDJEVIC, A. R. and SARKAR, T. K., 1994, 'Closed-form formulas for frequency-dependent resistance and inductance per unit length of microstrip transmission lines', *IEEE Trans.*, **MTT-42**, pp. 241-248.

27. DJORDJEVIC, A. R., SARKAR, T. K. and HARRINGTON, R. F., 1987, 'Time-domain response of multiconductor transmission lines', *Proc. IEEE*, **Vol. 75**, pp. 743-764

28. DOMMEL, H. W., 1969, 'Digital computer solution of electromagnetic transients in single and multiphase networks', *IEEE Trans.*, **PAS-88**, pp.388-399.

29. DUFFIN, W. J., 1965, Electricity and magnetism, McGraw-Hill, London.

30. FAIRCHILD, 1987, Fairchild advanced CMOS technology logic data book, Fairchild semiconductor corporation, Milan.

31. FARRAR, A. and ADAMS, A. T., 1970, 'Characteristic impedance of microstrip by the method of moments', *IEEE Trans.*, **MTT-17**, pp. 65-66.

32. FARRAR, A. and ADAMS, A. T., 1971, 'Computation of lumped microstrip capacities by matrix methods - rectangular sections and end effects', *IEEE Trans.*, **MTT-18**, pp. 495-497.

33. GAO, D. S., YANG, A. T. and KANG, S. M., 1990, 'Modeling and simulation of interconnection delays and crosstalks in high speed integrated circuits', *IEEE Trans.*, **CAS-37**, pp. 1-9.

34. CHEN, Z. and GAO, B., 1989, 'Deterministic approach to full-wave analysis of discontinuities in MIC's using the method of lines', *IEEE Trans.*, **MTT-37**, pp. 606-611.

35. GILB, J. P. and BALANIS, C.A., 1990, 'Transient analysis of distortion and coupling in lossy coupled microstrips', *IEEE Trans.*, **MTT-S Digest**, pp. 641-644.

36. GLADWELL, G. M. L. and COEN, S., 1975, 'A chebyshev approximation method for microstrip problems', *IEEE Trans.*, **MTT-23**, pp. 865-870.

37. GORDON, C., 1992, 'Time-domain simulation of multiconductor transmission lines with frequency-dependent losses', *IEEE Intl. Conf. on Computer Design* : VLSI in Comp. and Proc., pp. 222-228.

38. GRIFFITH, R. and NAKHLA, M., 1990, 'A new method for the time-domain analysis of lossy coupled transmission lines', *IEEE Trans.*, **MTT-S Digest**, pp. 645-647.

39. GROUDIS, A. J., 1979, 'Transient analysis of uniform resistive transmission lines in a homogeneous medium', *IBM J. Res. Develop.*, **Vol. 23**, pp. 675-681.

40. GROUDIS, A. J. and CHANG, C. S., 1981, 'Coupled lossy transmission line characterisation and simulation', *IBM J. Res. Develop.*, **Vol. 25**, pp. 25-41.

41. GUNSTON, M. A. R. and WEALE, J. R., 1969, 'Variation of microstrip impedance with strip thickness', *Electronics Letters*, **Vol. 5**, pp. 697-698.

42. GUPTA, K. C., GARG, R. and BAHL, I. J., 1979, Microstrip Lines and Slotlines, Artech House, Dedham, MA : USA.

43. HAMMERSTAD, E. O., 1975, 'Equations for microstrip circuit design', *Proc. European Microwave Conf.*, pp. 268-272.

44. HARMS, P. H. and MITTRA, R., 1993, 'Equivalent circuits for multiconductor microstrip bend discontinuities', *IEEE Trans.*, **MTT-41**, pp. 62-69.

45. HASEGAWA, H. and SEKI, S., 1984, 'Analysis of interconnection delay on very high-speed LSI/VLSI chips using an MIS microstrip line model', *IEEE Trans.*, **MTT-32**, pp. 1721-1727.

46. HILL, Y. M., RECKORD, N. O. and WINNER, D. R., 1969, 'A general method for obtaining impedance and coupling characteristics of practical microstrip and triplate transmission line configurations', *IBM J. Res. Develop.*, **Vol. 13**, pp. 314-322.

47. HO, C. W., 1973, 'Theory and computer aided analysis of lossless transmission lines', *IBM J. Res. Develop.*, **Vol. 17**, pp. 249-255.

48. HUANG, W. X. and WING, O., 1991, 'Spice models and pulse distortion characterization of bent interconnect lines', *Int. J. Hybrid Microelectronics*, **Vol. 14**, pp. 151-160.

49. HWANG, L. and TURLIK, I., 1992, 'A review of the skin effect as applied to thin film interconnections', *IEEE Trans.*, **CHMT-15**, pp. 42-55.

50. ISHIMARU, A., 1991, Electromagnetic wave propagation, radiation, and

scattering, Prentice Hall, Englewood Cliffs, NJ.

51. JOHN, S. and ARLETT, P., 1974, 'Simple method for the calculation of the characteristic impedance of microstrip', *Electronics Letters*, **Vol. 10**, pp. 188-190.

52. KAMMLER, D. W., 1968, 'Calculation of characteristic admittances and coupling coefficients for strip transmission lines', *IEEE Trans.*, **MTT-16**, pp. 925-937.

53. KAUPP, H. R., 1967, 'Characteristics of microstrip transmission lines', *IEEE Trans.*, **EC-16**, pp. 185-193.

54. KRAGE, M. K. and HADDAD, G. I., 1970, 'Characteristics of coupled microstrip transmission lines-I: coupled mode formulation of inhomogeneous lines', *IEEE Trans.*, **MTT-18**, pp. 217-222.

55. KRAGE, M. K. and HADDAD, G. I., 1972, 'Frequency-dependent characteristics of microstrip transmission lines', *IEEE Trans.*, **MTT-20**, pp. 678-688.

56. KUMAR, A. et al, 1976, 'A method for the calculation of the characteristic impedance of microstrip', *Int. J. Electronics*, **Vol. 40**, pp. 45-47.

57. LIAO, J. C., PALUSINSKI, O. A. and PRINCE J. L., 1990, 'Computation of transients in lossy VLSI packaging interconnections', *IEEE Trans. Comp., hybrids, manuf., Technol.*, **Vol. 13**, pp. 833-838.

58. LONG, S. I. and BUTNER, S. E., 1990, Gallium arsenide digital integrated circuit design, McGraw Hill.

59. MAEDER, R., 1991, Programming in Mathematica, Addison Wesley, Redwood City, CA.

60. MAGNUSSON, P. C., 1970, Transmission lines and wave propagation, Newton, MA: Allyn and Bacon.

61. MAO, J. -F. and LI, Z. -F., 1991, 'Analysis of time response of nonuniformly coupled multiconductor transmission lines with frequency-dependent losses', *Electronics Letters*, **Vol. 27**, pp. 1941-1943.

62. MILLER, G. M., 1983, Modern electrical communication, Prentice Hall,

Englewood Cliffs, NJ.

63. NAHMAN, N. S. and HOLT, D. R., 1972, 'Transient analysis of coaxial cables using the skin effect approximation A + B$\sqrt{s}$', *IEEE Trans.*, **CT-19**, pp. 443-451.

64. NAM, S., LING, H. and ITOH, T., 1989, 'Characterization of uniform microstrip line and its discontinuities using the time-domain method of lines', *IEEE Trans.*, **MTT-37**, pp. 2051-2057.

65. OH, K. S. and SCHUTT-AINE, 1993, 'Transient analysis of coupled, tapered transmission lines with arbitrary nonlinear terminations', *IEEE Trans.*, **MTT-41**, pp. 268-273.

66. ORHANOVIC, N., TRIPATHI, V. K. and WANG, P., 1990, 'Time domain simulation of uniform and nonuniform multiconductor lossy lines by the method of characteristics', *IEEE Trans.*, **MTT-S Digest**, pp. 1191-1194.

67. OWYANG, G. H. and WU, T. T., 1958, 'The approximate parameters of slotlines and their complement', *IRE Trans.*, **AP-6**, pp. 49-55.

68. PALUSINSKI, O. A. and LEE, A., 1989, 'Analysis of transients in nonuniform and uniform multiconductor transmission lines', *IEEE Trans.*, **MTT-37**, pp. 127-138.

69. PARKER, B. H., RAY, A. K. and GHASSEMLOOY, Z., 1994, 'Crosstalk in the interconnection bus for a high-speed digital logic circuit', *Int. J. Electronics*, **Vol. 76**, pp. 265-269.

70. PATEL, P. D., 1971, 'Calculation of capacitance coefficients for a system of irregular finite conductors on a dielectric sheet', *IEEE Trans.*, **MTT-19**, pp. 862-869.

71. PAUL, C. R., 1973, 'On uniform multimode transmission lines', *IEEE Trans.*, **MTT-21**, pp. 556-558.

72. PAUL, C. R., 1975, 'Useful matrix chain parameter identities for the analysis of multiconductor transmission lines', *IEEE Trans.*, **MTT-23**, pp. 756-760.

73. PEASE, M. C., 1965, Methods of matrix algebra, Academic Press, London.

74. PUCEL, R. A., MASSE, D. J. and HARTWIG, C. P., 1968, 'Losses in

microstrip', *IEEE Trans.*, **MTT-16**, pp. 342-350.

75. QIAN, Y. and YAMASHITA, E., 1993, 'Characterization of picosecond pulse crosstalk between coupled microstrip lines with arbitrary conductor width', *IEEE Trans.*, **MTT-41**, pp. 1011-1016.

76. RASHID, M. H., 1990, Spice for circuits and electronics using PSpice, Prentice Hall, Englewood Cliffs, N. J.

77. RICKAYZEN, G., 1980, Green's functions and condensed matter, Academic Press, London.

78. ROMEO, F. and SANTOMAURO, M., 1987, 'Time domain simulation of n coupled transmission lines', *IEEE Trans.*, **MTT-35**, pp. 131-136.

79. ROSS, R. F. G. and HOWES, M. J., 1976, 'Simple formulas for microstrip lines', *Electronics Letters*, **Vol. 12**, p. 410.

80. RUEHLI, A. E., 1979, 'Survey of computer aided electrical analysis of integrated circuit interconnections', *IBM J. Res. Develop.*, **Vol. 23**, pp. 626-639.

81. SABBAN, A. and GUPTA, K. C., 1992, 'A planar-lumped model for coupled microstrip lines and discontinuities', *IEEE Trans.*, **MTT-40**, pp. 245-252.

82. SATO, R. and CRISTAL, E. G., 1970, 'Simplified analysis of coupled transmission-line networks', *IEEE Trans.*, **MTT-18**, pp. 122-131.

83. SCHNEIDER, M. V., 1969, 'Microstrip lines for microwave integrated circuits', *Bell System Technical Journal*, **Vol. 48**, pp. 1421-1444.

84. SCHREYER, T. A., NISHI, Y., and SARASWAT, K. C., 1988, 'Simulation and measurement of picosecond step responses in VLSI interconnections', Int. Electron. Devices Meeting Tech. Digest, pp. 344-347.

85. SCHUTT-AINE, J. E., 1992, 'Transient analysis of nonuniform transmission lines', *IEEE Trans.*, **CAS-I-39**, pp. 378-385.

86. SCHUTT-AINE, J. E., and MITTRA, R., 1985, 'Analysis of pulse propagation in coupled transmission lines', *IEEE Trans.*, **CAS-32**, pp. 1214-1219.

87. SCHUTT-AINE, J. E., and MITTRA, R., 1988, 'Scattering parameter transient analysis of transmission lines loaded with nonlinear terminations', *IEEE Trans.*, **MTT-36**, pp. 529-535.

88. SCHUTT-AINE, J. E., and MITTRA, R., 1989, 'Nonlinear transient analysis of coupled transmission lines', *IEEE Trans.*, **CAS-36**, pp. 959-966.

89. SEKI, S. and HASEGAWA, H., 1984, 'Analysis of crosstalk in very high-speed LSI/VLSI's using a coupled multiconductor MIS microstrip line model', *IEEE Trans.*, **MTT-32**, pp. 1715-1720.

90. SILVESTER, P., 1968, 'TEM wave properties of microstrip transmission lines', *IEE Proc.*, **Vol. 115**, pp. 43-48.

91. SILVESTER, P. and BENEDEK, P., 1972(a), 'Equivalent capacitances of microstrip open circuits', *IEEE Trans.*, **MTT-20**, pp. 511-516.

92. SILVESTER, P. and BENEDEK, P., 1972(b), 'Electrostatics of the microstrip - revisited', *IEEE Trans.*, **MTT-20**, pp. 756-758.

93. SINNEMA, W., 1979, Electronic transmission technology, lines, waves and antennas, Prentice Hall, Englewood Cliffs, NJ.

94. SON, J-H. *ET AL*, 1993, 'Picosecond pulse propagation on coplanar striplines fabricated on lossy semiconductor substrates: modeling and experiments', *IEEE Trans.*, **MTT-41**, pp. 1574-1579.

95. STINEHELFER, H. E., 1968, 'An accurate calculation of uniform microstrip transmission lines', *IEEE Trans.*, **MTT-16**, pp. 439-444.

96. SUSSMAN-FORT, S. E. and HANTGAN, J. C., 1988, 'SPICE implementation of lossy transmission line and Schottky diode models', *IEEE Trans.*, **MTT-36**, pp. 153-155.

97. SCHWARTZ, H. A., RUTISCHAUSER, H. and STIEFEL, E., Numerical analysis of symmetric matrices, Prentice Hall, Englewood Cliffs, NJ.

98. TRIPATHI, V. K. and BUCOLO, R. J., 1987, 'Analysis and modeling of multilevel parallel and crossing interconnection lines', *IEEE Trans.*, **ED-34**, pp. 650-658.

99. TRIPATHI, V. K. and RETTIG, J. B., 1985, 'A SPICE model for multiple coupled microstrips and other transmission lines', *IEEE Trans.*, **MTT-33**, pp. 1513-1518.

100. VAN DEVENTER, T. E., KATEHI, L. P. B. and CANGELLARIS, A. C., 1994,

'Analysis of conductor losses in high-speed interconnects', *IEEE Trans.*, **MTT-42**, pp. 78-83.

101. VU DINH, T., CABON, B. and CHILO, J., 1990(a), 'New skin-effect equivalent circuit', *Electronics Letters*, **Vol. 26**, pp. 1582-1584.

102. VU DINH, T., CABON, B. and CHILO, J., 1990(b), 'Time domain analysis of skin effect on lossy interconnections', *Electronics Letters*, **Vol. 26**, pp. 2057-2058.

103. VU DINH, T., CABON, B. and CHILO, J., 1991, 'Equivalent circuit modelling of lossy coupled lines using spice software', *Electronics Letters*, **Vol. 27**, pp. 710-712.

104. VU DINH, T., CABON, B. and CHILO, J., 1992, 'Modelling the capacitance of microstrip line using spice', *Electronics Letters*, **Vol. 28**, pp. 194-196.

105. WEEKS, W. T., 1970, 'Calculation of coefficients of capacitance of multiconductor transmission lines in the presence of a dielectric interface', *IEEE Trans.*, **MTT-18**, pp. 35-43.

106. WEEKS, W. T., 1973, 'Algorithms for ASTAP - A network-analysis program', *IEEE Trans.*, **CT-20**, pp. 628-634.

107. WEEKS, W. T., WU, L. L., MCALLISTER, M. F. and SINGH, A., !979, 'Resistive and inductive skin effect in rectangular conductors', *IBM J. Res. Develop.*, **Vol. 23**, pp. 652-660.

108. WHEELER, H. A., 1942, 'Formulas for the skin effect', *Proc. I.R.E*, **Vol. 40**, pp. 412-424.

109. WHEELER, H. A., 1965, 'Transmission line properties of parallel strips separated.by a dielectric sheet', *IEEE Trans.*, **MTT-13**, pp. 172-185.

110. WIRTH, K. -H., 1990, 'New model for time domain simulation of lossy coupled lines', *Electronics Letters*, **Vol. 26**, pp. 1723-1725.

111. WLODARCZYK, W. and BESCH, V., 1990, 'Skin effect losses of interconnect lines in frequency and time domain', *Electronics Letters*, **Vol. 26**, pp. 1237-1238.

112. WOLFRAM, S., 1991, Mathematica a system for doing mathematics by computer, Addison Wesley.

113. YAMASHITA, E. and MITTRA, R., 1968, 'Variational method for the analysis of microstrip lines', *IEEE Trans.*, **MTT-16**, pp. 251-256.

114. YAMASHITA, E., 1968, 'Variational method for the analysis of microstrip-like transmission lines', *IEEE Trans.*, **MTT-16**, pp. 529-535.

115. YANG, Y. E., KONG, J. A. and GU, Q., 1985, 'Time domain perturbational analysis of nonuniformly coupled transmission lines', *IEEE Trans.*, **MTT-33**, pp. 1120-1130.

116. YAUN, H., LIN, Y. and CHIANG, S., 1982, 'Properties of interconnection on silicon, sapphire and semi-insulating gallium arsenide substrates', *IEEE Trans.*, **ED-29**, pp. 639-644.

117. YEN, C., FAZARINC, Z. and WHEELER, R. L., 1982, 'Time domain skin effect model for transient analysis of lossy transmission lines', *Proc. IEEE*, **Vol. 70**, pp. 750-757.

118. ZHANG, Q., LUM, S. and NAKHLA, M. S., 1992, 'Minimization of delay and crosstalk in high-speed VLSI interconnects', *IEEE Trans.*, **MTT-40**, pp. 1555-1563.

119. ZHENG, J. X. and CHANG, D. C., 1990, 'Numerical modelling of chamfered bends and other microstrip junctions of general shap in MMICS', *IEEE Trans.*, **MTT-S Digest**, pp. 709-712.

120. ZYSMAN, G. I. and JOHNSON, A. K., 1969, 'Coupled transmission line networks in an inhomogeneous dielectric medium', *IEEE Trans.*, **MTT-17**, pp. 753-759.

Appendix A

Program Listing for Mathematica Calculations

```
Off[General::spell]
Off[General::spell1]
Off[Set::setraw]
Off[SetDelayed::write]

BeginPackage["Impedance`"]

Zom::usage = "Zom[Er,t,w,h]
        w is width of line
        h is height of line above ground plane
        t is thickness of line
        er is relative dielectric constant of substrate
        Calculate the impedance of a single microstrip line
        with the above parameters."

Z0::usage = "Z0[Er,t,w,h,s]
        w is width of line
        h is height of line above ground plane
        t is thickness of line
        s is the separation between the lines
        er is relative dielectric constant of substrate
        Calculate the impedance of a pair of microstrip lines
        with the above parameters."

Tline::usage = "Tline[Er,t,w,h,s,totln]
        w is width of the lines
        h is height of the lines above the ground plane
        t is thickness of the lines
        s is the separation between adjacent lines
        er is relative dielectric constant of substrate
        totln is the total number of lines
        s, w, and t are the same for all lines
        Calculates the time delay and impedance of a set of
        linen microstrip lines with the above parameters and also
        returns the transformation network control parameters."

Carray::usage = "Carray[Er,t,w,h,s,totln]
        w is width of the lines
        h is height of the lines above the ground plane
        t is thickness of the lines
```

```
        s is the separation between adjacent lines
        er is relative dielectric constant of substrate
        totln is the total number of lines
        s, w, and t are the same for all lines"

Begin["`Private`"]

E0 = 8.854188*10^-12
mu0 = 12.566371*10^-7

MakeRuleConditional[var_, rhs_, condition_] :=
        (var := rhs /; condition)      (* Assigns var = rhs if condition is true *)

CalcC[er_, t_, w_, h_] :=
        Module[ {c},
                c = (er - 1)*t / 4.6 / Sqrt[w/h] / h;
        c
        ]       (* Correction factor for the effective dielectric *)

We[t_, w_, h_] :=
        Module[ {we},
                MakeRuleConditional[we,
                        w+1.25/N[Pi]*t*(1+Log[4*N[Pi]*w/t]),
                        w/h <= 1/(2*N[Pi])];
                MakeRuleConditional[we,
                        w+1.25/N[Pi]*t*(1+Log[2*h/t]),
                        w/h > 1/(2*N[Pi])];
        we
        ]     (* Calculates the effective width of a microstrip line *)

CalcF[w_, h_] :=
        Module[ {conf},
                MakeRuleConditional[conf,
                        1/Sqrt[1+12h/w],
                        w/h <= 1];
                MakeRuleConditional[conf,
                        1/Sqrt[1+12h/w]+0.04(1-w/h)^2,
                        w/h > 1];
        conf
        ]       (* Another correction term for the effective dielectric *)
```

```
Ere[Er_, t_, w_, h_] :=
        Module[ {ere, c, conf},
                conf = CalcF[w,h];
                c = CalcC[Er,t,w,h];
                ere = (Er+1)/2+conf*(w/h)*(Er-1)/2-c;
        ere
        ]       (* Calculates the effective dielectric constant of the substrate and lines *)

Zom[Er_, t_, w_, h_] :=
        Module[ {zom, we, ere},
                we = We[t,w,h];
                ere = Ere[Er,t,w,h];
                MakeRuleConditional[zom,
                        60/Sqrt[ere]*Log[8*h/we+0.25*we/h],
                        w/h <= 1];
                MakeRuleConditional[zom,
                        120*N[Pi]/(Sqrt[ere]*(we/h+1.393+0.667*Log[we/h+1.444])),
                        w/h > 1];
        N[zom]
        ]       (* Calculates the impedance of a single microstrip lines with the given
parameters *)

Cp[Er_, w_, h_] :=
        Module[ {cp},
                cp = E0*Er*w/h;
        cp
        ]       (* Line to ground plane capacitance *)

Cf[Er_, t_, w_, h_] :=
        Module[ {cf, cp, zom, clight, ere},
                ere = Ere[Er, t, w, h];
                clight = 299792458;
                cp = Cp[Er, w, h];
                zom = Zom[Er, t, w, h];
                cf = (Sqrt[ere]/clight/zom - cp)/2;
        cf
        ]       (* Fringe capacitance for the outside of the lines *)

CalcA[w_, h_] :=
```

```
        Module[ {A},
                A = Exp[-0.1*Exp[2.33-2.53*w/h]];
        A
        ]

Cfpri[Er_, t_, w_, h_, s_] :=
        Module[ {cfpri, ere, cf, A},
                ere = Ere[Er, t ,w, h];
                cf = Cf[Er, t, w, h];
                A = CalcA[w, h];
                cfpri = cf*Sqrt[Er/ere]/(1+A*h/s*Tanh[10*s/h]);
        cfpri
        ]       (* Fringe capacitance between the lines *)

Cgd[Er_, t_, w_, h_, s_] :=
        Module[ {cgd, cf},
                cf = Cf[Er, t, w, h];
                cgd = E0*Er*Log[Coth[N[Pi]*s/4/h]]/N[Pi]
                    + 0.65*cf*(0.02/(s/h)*Sqrt[Er]+(1-1/(Er*Er)));
        cgd
        ]       (* Gap capacitance through the dielectric interface *)

Cga[w_, h_, s_] :=
        Module[ {k, kpri, cga},
                k = (s/h)/(s/h + 2*w/h);
                kpri = Sqrt[1-k*k];
                cga = E0*EllipticK[kpri]/EllipticK[k]/2;
        cga
        ]       (* Gap capacitance through the air interface *)

Cgt[t_, s_] :=
        Module[ {cgt},
                cgt = 2*E0*t/s;
        cgt
        ]       (* Capacitance due to the thickness of the line *)

Cm[Er_, t_, w_, h_, s_] :=
        Module[ {cgd, cga, cgt, cfpri, cm},
                cgd = Cgd[Er, t, w, h, s];
                cga = Cga[w, h, s];
```

```
            cgt = Cgt[t, s];
            cfpri = Cfpri[Er, t, w, h, s];
            cm = N[(cgd + cga + cgt - cfpri)/2];
        cm
        ](* Calculates the mutual capacitance beween two lines *)

Ci0[Er_, t_, w_, h_] :=
        Module[ {ci0, cp, cf},
            cf = Cf[Er, t, w, h];
            cp = Cp[Er, w, h];
            ci0 = cp + 2*cf;
        ci0
        ](* Calculates the total capacitance of a single line *)

Carray[Er_, t_, w_, h_, s_, totln_] :=
        Module[ {ctemp, ctemp2, diff, seff, carray, i, j},
            Do[
                ctemp = 0;
                Do[If [!(i === j),
                    {diff = Abs[N[i-j]];
                    seff = diff * (s + w) - w;
                    ctemp2 = Cm[Er, t, w, h, seff];
                    carray[i,j] = N[- ctemp2];
                    ctemp = N[ctemp + ctemp2]}
                ],
                {j, 1, totln}
                ];
                carray[i,i] = N[Ci0[Er, t, w, h] + ctemp],
            {i, 1, totln}
            ];
        Array[carray, {totln, totln}]
        ]       (* Constructs the capacitance per unit length matrix
                  for the given dielectric and line dimensions *)

Tline[Er_, t_, w_, h_, s_, totln_] :=
        Module[ {L, LC, Mv, Cd, Ld, Wd, Zd, CE0},
            CE0 = Carray[1, t, w, h, s, totln];
                (* Capacitance Matrix without dielectric substrate *)
            L = E0 * mu0 * Inverse[CE0];
                (* Inductance per unit length matrix *)
```

```
            CEr = Carray[Er, t, w, h, s, totln];
                (* Capacitance per unit length matrix *)
            LC = L . CEr;
            Mv = Transpose[Eigenvectors[LC]];
                (* Transformation matrix obtained from right eigenvectors of
                LC matrix *)
            Cd = Transpose[Mv].CEr.Mv;
                (* Diagonalised capacitance matrix *)
            Ld = Inverse[Mv].L.Transpose[Inverse[Mv]];
                (* Diagonalised inductance matrix *)
            Wd = Sqrt[Abs[Ld.Cd]];
                (* Time delay matrix *)
            Zd = Sqrt[Abs[Ld.Cd]].Inverse[Cd];
                (* Impedance matrix *)
        Print[CEr];
        Print[L];
        {Mv, Wd, Zd}
        ] (* Calculates the time delay, impedance and transformation network *)

Codd[Er_, t_, w_, h_, s_] :=
        Module[ {codd, cf, cp, cgd, cga, cgt},
            cf = Cf[Er, t, w, h];
            cp = Cp[Er, w, h];
            cgd = Cgd[Er, t, w, h, s];
            cga = Cga[w, h, s];
            cgt = Cgt[t, s];
            codd = cf + cp + cgd + cga + cgt;
        N[codd]
        ]    (* Odd mode capacitance of the lines *)

Ceven[Er_, t_, w_, h_, s_] :=
        Module[ {ceven, cf, cfpri, cp},
            cp = Cp[Er, w, h];
            cf = Cf[Er, t, w, h];
            cfpri = Cfpri[Er, t, w, h, s];
            ceven = cp + cf + cfpri;
        N[ceven]
        ]    (* Even mode capacitance of the lines *)

Zoe[Er_, t_, w_, h_, s_] :=
```

```
        Module[ {zoe, cea, ceer},
                cea = Ceven[1, t, w, h, s];
                ceer = Ceven[Er, t, w, h, s];
                zoe = Sqrt[mu0*E0/cea/ceer];
        N[zoe]
        ]     (* Even mode impedance of the lines *)

Zoo[Er_, t_, w_, h_, s_] :=
        Module[ {zoo, coa, coer},
                coa = Codd[1, t, w, h, s];
                coer = Codd[Er, t, w, h, s];
                zoo = Sqrt[mu0*E0/coa/coer];
        N[zoo]
        ]     (* Odd mode impedance of the lines *)

Z0[Er_, t_, w_, h_, s_] :=
        Module[ {z0, zoe, zoo},
                zoe = Zoe[Er, t, w ,h, s];
                zoo = Zoo[Er, t, w, h ,s];
                z0 = Sqrt[zoe*zoo];
        N[z0]
        ]     (* Overall impedance of the pair of lines *)

EndPackage[]
```

Appendix B

Listing of Fortran Program for SPICE Equivalent Circuit Setup.

```
      Program Transnetwork

************************************************************************
***   Given the number of lines, n (user input), the user inputs the following
***         information:
***
***         i)    The number of RLC sections to be used in the simulation.
***         ii)   The impedance, Z0, of each line.
***         iii)  The time delay, Td, of each line.
***         iv)   The series resistance of the lines.
***         v)    The name of a file into which the SPICE compatible output is the
***                     be written.
***
************************************************************************
***   The following information is then calculated by the program:
***
***         i)    The value of the capacitor to be used in each RLC section.
***         ii)   The value of the inductor to be used in each RLC section.
***         iii)  The value of the resistor to be used in each RLC section.
***         iv)   The eigenvalues of the Toeplitz matrix.
***         v)    The right eigenvector matrix from the Toeplitz matrix.
***         vi)   From the eigenvector matrix the transformation network
***                     parameters are calculated.
***
************************************************************************
***   The following information is then written into the output file, which can then be
***         used for input in the SPICE circuit simulator.
***
***         i)    RLC subcircuit for each line.
***         ii)   Transmission line subcircuit for each line consisting of
***                     the RLC subcircuits.
***         iii)  Circuit containing the transmission lines and the transformation
***                     networks for the implementation of crosstalk.
***
************************************************************************
      Implicit Double Precision (A-H,O-Z)

      Dimension r_mu(10), phi(10,10), gamma(10), r_mat(10,10),

     +          u(10,10)
```

```
      Character*150  ctemp

      Integer    i, j, n, nsec, chanfile, itemp

      Parameter (pi = 3.141592654)

*************************************************************************
***   Description of the variables:
***
***   r_mu          :-    Contains the eigenvalues of the Toeplitz matrix.
***   phi           :-    Contains the eigenvectors from the Toeplitz matrix.
***   gamma         :-    Holds the normalising factor for the network parameters.
***   r_mat         :-    Temporary matrix used in calculating the network
***                             parameters.
***   u             :-    Holds the transformation network parameters.
***   n             :-    The number of lines in the simulation.
***   nsec          :-    The number of RLC sections in each line.
***   chanfile      :-    The channel number used for the output file.
***
*************************************************************************
***
***   Get the number of lines
***
      Print *, 'Input number of coupled lines:'

      n = 0

***
***   The number of lines must be between 2 and 8
***
      Do While ((n .lt. 2) .or. (n .gt. 8))

            Read *, n

      End Do

***
***   Set output channel for file to 1
***
```

```
      chanfile = 1

***
***   Open the output file
***
      Call Openfile(chanfile)


***
***   Get the number of RLC sections to be used in each line.
***
      Print *, 'Input number of sections for each line:'

      nsec = 0

***
***   Number of sections must be between 5 and 100.
***
      Do While ((nsec .lt. 5) .or. (nsec .gt. 100))

            Read *, nsec

      End Do

***
***   This loop sets up the RLC and transmission line subcircuits for each line.
***
      Do i = 1,n

***
***   Get impedance of line i.
***
            Print *, 'Input Z0 for line ', i

            Read *, zimp

***
***   Get time delay of each line.
***
            Print *, 'Input T0 for line ', i
```

```
            Read *, tdel

***
***     Calculate of the time delay of a single RLC section.
***
            tdel = tdel / nsec

***
***     Capacitor for the RLC section.
***
            r_ctran = tdel / zimp

***
***     Inductor for the RLC section.
***
            r_ltran = tdel * zimp

***
***     Resistor for the RLC section.
***
            r_rtran = zimp / (nsec * 5)

***
***     Write out the RLC subcircuit.
***
            write (chanfile, 1000) i

            write (chanfile, 1010) i, r_rtran

            write (chanfile, 1020) i, r_ctran

            write (chanfile, 1030) i, r_ltran

            write (chanfile, 1040) i

***
***     Format statements for the RLC subcircuit.
***
1000    Format ('.subckt RLC',i2.2,' 1 3')
```

```
1010   Format ('rtran',i2.2, ' 2 3 ', e14.6)

1020   Format ('ctran',i2.2, ' 2 0 ', e14.6)

1030   Format ('ltran',i2.2, ' 1 2 ', e14.6)

1040   Format ('.ends RLC',i2.2)


***
***    Write out the transmission line subcircuit.
***
               write (chanfile, 1100) i, (nsec+1)

               Do j = 1,nsec

                     write (chanfile, 1110) i, j, j, j+1, i

               End Do

               write (chanfile, 1120) i

***
***    Format statements for the transmission line subcircuit.
***
1100   Format ('.subckt Tranml',i2.2,' 1 ',i3)

1110   Format ('x',i2.2,i2.2,1x,i2,1x,i2,' RLC',i2.2)

1120   Format ('.ends Tranml',i2.2)

       End Do
***
***    End of subcircuit loop
***


***
***    Calculate the eigenvalues of the Toeplitz matrix.
***
```

```
      Do i = 1,n

            r_mu(i) = -2 * COS(i * pi / (n + 1))

      End Do

***
***   Calculate the eigenvectors for the Toeplitz matrix.
***
      Do i = 1,n

            phi(i,1) = 1

            phi(i,2) = r_mu(i)

            Do j = 3,n

                  phi(i,j) = r_mu(i) * phi(i,j-1) - phi(i,j-2)

            End Do

      End Do

***
***   Calculate the normalisation factor for the eigenvector matrix.
***
      Do i = 1,n

            total = 0

            Do j = 1,n

                  total = total + phi(i,j)**2

            End Do

            gamma(i) = SQRT(total)

      End Do
```

```
***
***     Normalise the eigenvector matrix.
***
        Do i = 1,n

            Do j = 1,n

                r_mat(i,j) = phi(j,i) / gamma(j)

                u(i,j) = r_mat(i,j)

                If (i .eq. j) Then

                    u(i,j) = u(i,j) - 1

                End If

            End Do

        End Do


        Print *, 'mu            gamma'

        Do i = 1,n

            print *, r_mu(i), gamma(i)

        End Do

        Print *,' '

        Print *, 'Matrix M'

        Do i = 1,n

            Write (*, 100) (r_mat(i,j), j = 1,n)

        End Do
```

```
      Print *, 'Matrix U'

      Do i = 1,n

            Write (*, 100) (u(i,j), j = 1,n)

      End Do

100   Format (10(f6.3))


      Do i = 1,n

            Write (chanfile,110) i

            Write (chanfile,120) i, i, i, '2000'

            Write (chanfile,130) i, i, i, n

            Write (chanfile,132) (j, j = 1,n)

            Write (ctemp,134) (u(i,j), j = 1,n)

            Call Linesplit(ctemp,chanfile)

            Write (chanfile,140) '0', i, i, '04', i, '03'

            Write (chanfile,150) i, i, n

            Write (chanfile,152) ('v0sen',j, j=1,n)

            Write (ctemp,134) (u(i,j), j = 1,n)

            Call Linesplit(ctemp,chanfile)

            Write (chanfile,160) i, i, '04', i, '05', i

            Write (chanfile,180) i, i, n

            Write (chanfile,152) ('vlsen',j, j=1,n)
```

```
            Write (ctemp,134) (u(i,j), j = 1,n)

            Call Linesplit(ctemp,chanfile)

            Write (chanfile,140) 'l', i, i, '05', i, '06'

            Write (chanfile,190) i, i, i, n

            Write (chanfile,192) (j, j = 1,n)

            Write (ctemp,134) (u(i,j), j = 1,n)

            Call Linesplit(ctemp,chanfile)

            Write (chanfile,170) i, i

        End Do


        Write (chanfile,200)


        Do i = 1,n

            Write (chanfile,210) i, i

        End Do


        Write (chanfile,220)


110     Format ('*'/'* Transformation network for line ',i2.2)

120     Format ('Rin',i2.2,1x,i2,'01',1x,i2,'02',1x,a8)

130     Format ('e0s',i2.2,1x,i2,'02',1x,i2,'03',1x,'Poly(',i2.2,')')

132     Format ('+',10(1x,i2,'04',1x,'0'))
```

```
134     Format ('0 ',10(e14.6))

140     Format ('V',a1,'sen',i2.2,2(1x,i2,a2),1x,'0')

150     Format ('f0s',i2.2,1x,'0',1x,i2,'02',1x,'Poly(',i2.2,')')

152     Format ('+',10(1x,a5,i2.2))

160     Format ('xline',i2.2,2(1x,i2,a2),1x,'tranml',i2.2)

170     Format ('Rload',i2.2,1x,i2,'07 0 2000')

180     Format ('fls',i2.2,1x,'0',1x,i2,'07',1x,'Poly(',i2.2,')')

190     Format ('els',i2.2,1x,i2,'07',1x,i2,'06',1x,'Poly(',i2.2,')')

192     Format ('+',10(1x,i2,'05',1x,'0'))

200     Format ('.tran 1p 80p')

210     Format ('.plot tran v(',i2.2,'02) v(',i2.2,'07)')

220     Format ('.end')


        Call Closefile(chanfile)

        End


**********************************************************************
        Subroutine Linesplit(ctemp,chanfile)

        Character*150   ctemp

        Integer     i, itemp, chanfile, lend, pend
```

```
      pend = LEN(ctemp)
      Call Find_Locc(ctemp,pend,1)
      i = 1
      Do While (i .lt. pend)
            lend = MIN0(i + 69,pend)
            If (lend .lt. pend) Then
                  Call Find_Locc(ctemp,lend,0)
            End If
            Write (chanfile,'(a2,a)') '+ ',ctemp(i:lend)
            i = lend
      End Do

      Return
      End

**********************************************************************
      Subroutine Find_Locc(String,Pos,Type)
      Character*150   String
      Integer    Pos, Type, itemp
      itemp = Pos
```

```
      Do While (INDEX(String(pos:itemp),' ') .eq. Type)

            pos = pos - 1

      End Do

      Return


      End

*********************************************************************
      Subroutine Openfile(chanfile)


      Character*20    filename

      Integer     chanfile


      Print *, 'Input Name of output file:'

      Read (5,'(a20)') filename

      Open (unit = chanfile, file = filename, status = 'NEW')

      Print *, ' '

      Print *, 'Openned file :  ',filename

      Return

      End


*********************************************************************
      Subroutine Closefile(Chanfile)
```

INT. J. ELECTRONICS, 1994, VOL. 76, NO. 2, 265–269

Crosstalk in the interconnection bus for a high-speed digital logic circuit

B. H. PARKER†, A. K. RAY† and Z. GHASSEMLOOY†

A quasi-distributed circuit model using RLC 'T' elements is implemented on SPICE to simulate the crosstalk in an interconnection bus on high-speed logic circuits. Logic functions for the lines lying in an intervening space between the pulse-activated lines are found to be affected more than the outside lines.

1. Introduction

The study of crosstalk between the interconnection lines on high-speed digital circuits is important because this phenomenon may lead to the distortion of desired logic functions. The purpose of this article is to present the results of modelling work on crosstalk between the neighbouring lines. On-chip interconnects in high-speed digital circuits are regarded as being transmission lines. For n coupled lossy lines, the TEM analysis is given in terms of a set of coupled equations connecting $(n \times n)$ symmetric $[L]$ and $[C]$ matrices to $(n \times 1)$ voltage $[V]$ and current $[I]$ vectors (Chang 1970). The problem can be solved numerically (Yang *et al.* 1985) or with the help of an equivalent circuit model (Tripathi 1987, Wirth 1990). For the present purpose, a quasi-distributed circuit model using a series of RLC 'T' elements for each line is implemented on the SPICE package to simulate the behaviour of a bus. The choice of RLC 'T' elements is appropriate in view of losses associated with small cross-sectional dimensions of the lines. In an earlier work, lossy transmission lines are individually modelled by a lumped circuit consisting of four time-varying components, namely two resistors and two current sources (Gao *et al.* 1990).

2. Circuit simulation

Figure 1 shows the schematic diagram of an eight-line bus in a high-speed GaAs logic device. Each line is 1 mm long, 2 μm wide and 0·3 μm high. The inter-line

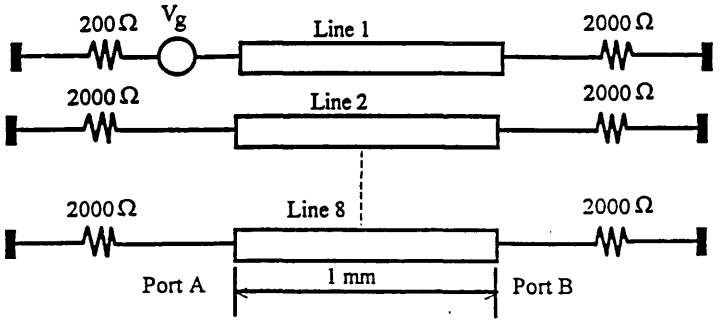

Figure 1. Operating configuration of the eight-line bus. The 200Ω resistor on the first line corresponds to the output impedance of a GaAs gate. Input impedance of these gates is taken to be 2000Ω.

Received 1 July 1993; accepted 14 July 1993.

† Physical Electronics and Fibre-optics Research Group, School of Engineering Information Technology, Sheffield Hallam University, Pond Street, Sheffield S1 1WB, U.K.

separation is taken to be 3 μm. Logic pulses of -1 V and $+5$ V corresponding to ECL and TTL levels, respectively, are input to one or two chosen lines. The duration of logic signals is 50 ps including rise and fall times of 10 ps. The equivalent RLC 'T' circuit is shown in Fig. 2. The circuit i is characterized by the impedance Z_i and the propagation delay T_i in terms of the net values of inductance and capacitance L_i and C_i, respectively:

$$Z_i=\left(\frac{L_i}{C_i}\right)^{1/2} \quad \text{and} \quad T_i=(L_iC_i)^{1/2} \tag{1}$$

Values of L_i and C_i are generally found from the dimensions of lines and the dielectric constant, and also from the coupling factors. The loss in the circuit i occurs due to the total resistance

$$R_{0i}=\sum_n R_{in}$$

where n is the number of sections used for a given simulation.

Using values of the characteristics of the eigenmodes $[Z]$ and $[T]$ for an eight-line bus with similar geometries and dimensions (Chilo and Arnaud 1984), a Fortran program is developed to calculate values of individual components L_{in}, C_{in} and R_{in} using (1). These values are then stored in an input file for the SPICE package. For the implementation of crosstalk, the transformation network is described by means of voltage-controlled voltage sources (VCVS) $E_i(x)$ and current-controlled current sources (CCCS) $F_i(x)$ as shown in Fig. 2. The controlling parameters for each $E_i(x)$ and $F_i(x)$ can be calculated by using the following set of equations:

$$E_i(x)=\sum_{j=1}^{8} M_{ij}V_j(x)-V_i(x) \tag{2}$$

$$F_i(x)=\sum_{j=1}^{8} M_{ij}I_j(x)-I_i(x) \tag{3}$$

where summation extends over all lines. Assuming the coupling to be between adjacent lines only and to be independent of line length and impedance, the matrix elements M_{ij} are calculated according to a simplified model (Romeo and Santo-

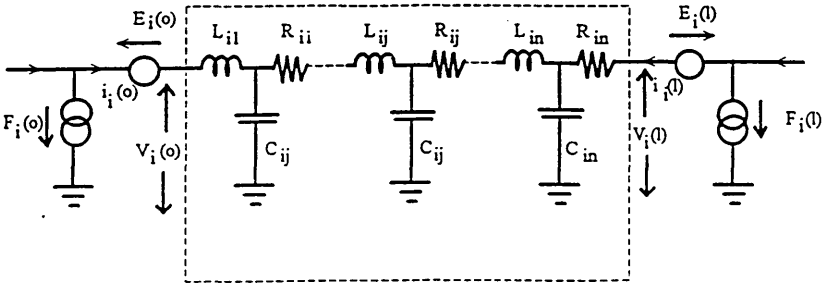

Figure 2. Lossy transmission line circuit model using a series of RLC 'T' elements and the associated transformation network for the line i of the bus.

mauro 1987). The transform network depends upon the number of coupled lines but not on their electrical parameters.

3. Results

The simulation is initially run using ten sections of the RLC 'T' circuits for each line, passing a 1 V logic pulse along the first line with the other seven lines inactivated. It is seen that the use of unmatched loads results in severe distortion of the transmitted signal due to the reflected waveform. The line capacitance causes a slight ripple in the output signal, with the series resistance bringing about a small amount of attenuation. The induced signals on the nearest neighbouring lines are often large enough to introduce possible errors in logic level. The simulation is also repeated by using twenty and fifty sections for each line. Although no significant changes in the waveforms have been noticed, the overall simulation time increases from three minutes for ten sections to six minutes for fifty sections.

If V_i is the voltage at time t on an inactivated line i, the crosstalk (ξ) in dB at a particular position on the line is defined as:

$$\xi = 20 \log_{10} [V_i(t)/V_a(t)] \tag{4}$$

where V_a is the voltage on the activated line at the same time t. In our present investigations, ξ is calculated at both input and output ends at the time $t = 25$ ps corresponding to the mid-point of the logic pulse. A group of three curves in Fig. 3 illustrates the crosstalk between adjacent lines under different operating conditions. As shown in Fig. 3 (*a*) the crosstalk decays gradually in a non-linear fashion with increasing distance from the activated lines. When signals are applied to the third and sixth lines, large crosstalk is observed for the fourth and fifth lines due to the superposition effect (Fig. 3 (*b*)). The value in the order of 6 dB at their input ends is approximately 2 dB higher than those for the second and seventh lines. Referring to Fig. 3 (*c*), the crosstalk for line 3 remains at almost the same level whether line 4 is activated on its own or along with line 5. When the voltage pulse input is increased to 5 V, voltage levels of transmitted and reflected waveforms are found to be now much higher than before but their essential features remain the same, implying that the effect on crosstalk is independent of ECL and TTL inputs. Further analysis shows that with the use of the second ground plane at a distance of 5 μm above the bus, the decrease in crosstalk is not significant enough to compensate for associated increases in signal distortions.

4. Concluding remarks

A time domain study of crosstalk between the interconnection lines on high-speed digital circuits using the SPICE circuit simulator has been presented. This analysis shows that for the case of two activated lines, an increase in crosstalk is seen on the lines between them, but little or no change in crosstalk is seen on the other lines, when compared to the case of a single line. Our results are seen to be consistent with those obtained from previous work. The network used in the present simulation consists of a simple transformation network that can be constructed separately from the transmission lines. Alterations in line impedance can be made without requiring the transformation network to be altered.

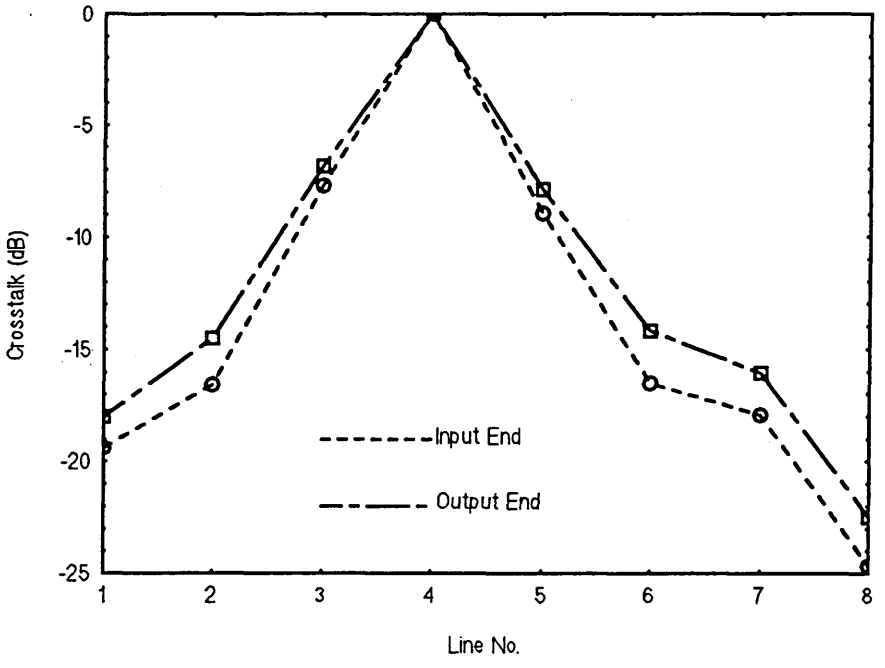
0
-5
-10
-15
-20
-25
Crosstalk (dB)
Input End
Output End
1
2
3
4
5
6
7
8
Line No.

3(*a*)

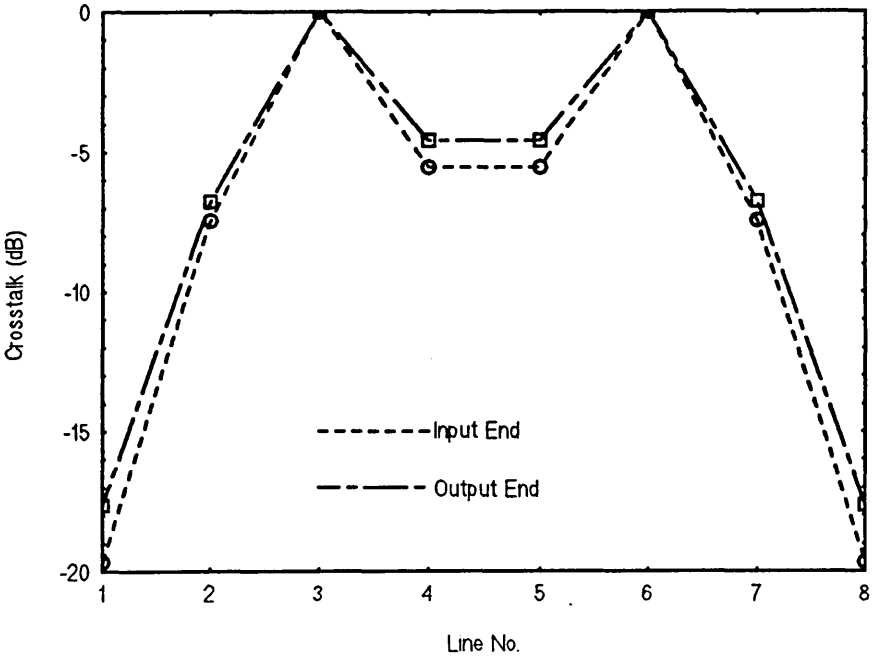
0
-5
-10
-15
-20
Crosstalk (dB)
Input End
Output End
1
2
3
4
5
6
7
8
Line No.

3(*b*)

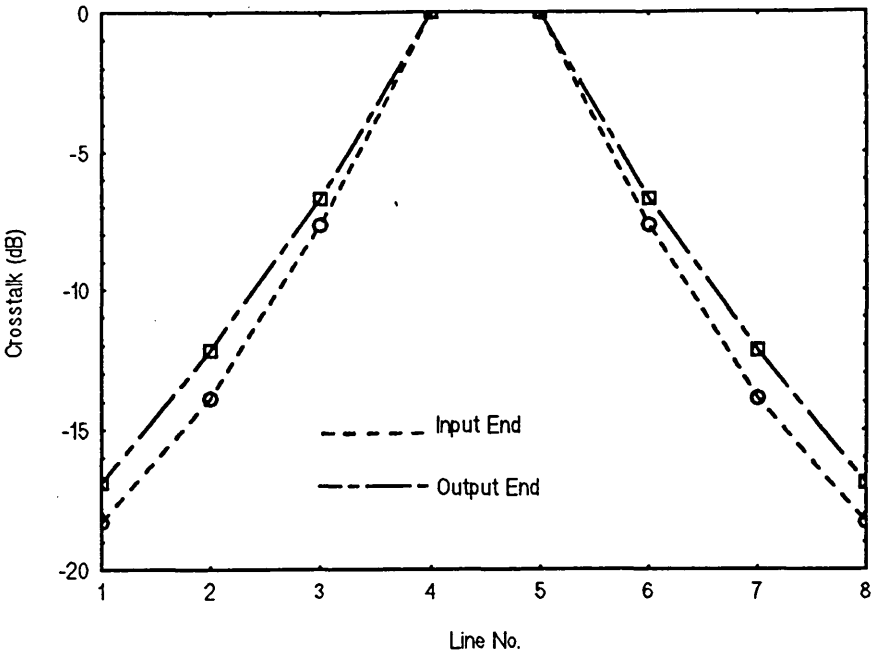

(*c*)

Figure 3. Crosstalk versus line number, for input signals applied on (*a*) line 4, (*b*) lines 3 and 6 and (*c*) lines 4 and 5.

Acknowledgments

The authors acknowledge the support received from the Science and Engineering Research Council for this work. Thanks are due to Professor C. A. Hogarth and Dr C. Johnson of Brunel University and Coventry University, respectively, for fruitful discussions.

References

Chang, F. Y., 1970, Transient analysis of lossless coupled transmission lines in a nonhomogeneous dielectric medium. *IEEE Transactions on Microwave Theory and Techniques*, **18**, 616–626.

Chilo, J., and Arnaud, T., 1984, Coupling effects in the time domain for an interconnecting bus in high-speed GaAs logic circuits. *IEEE Transactions on Electron Devices*, **31**, 347–352.

Gao, D. S., Yang, A. T., and Kang, S. M., 1990, Modelling and simulation of interconnection delays and crosstalks in high-speed integrated circuits. *IEEE Transactions on Circuits and Systems*, **37**, 1–9.

Romeo, F., and Santomauro, M., 1987, Time-domain simulation of *n* coupled transmission lines. *IEEE Transactions on Microwave Theory and Techniques*, **35**, 131–136.

Tripathi, V. K., 1987, Analysis and modeling of multilevel parallel and crossing interconnection lines. *IEEE Transactions on Electron Devices*, **34**, 650–658.

Wirth, K. H., 1990, New model for time domain simulation of lossy coupled lines. *Electronics Letters*, **26**, 1723–1725.

Yang, Y.-C. E., Kong, J. A., and Gu, Q., 1985, Time-domain perturbational analysis of nonuniformly coupled transmission lines. *IEEE Transactions on Microwave Theory and Techniques*, **33**, 1120–1130.